分类号：X131　　单位代码：10422
密　级：　　学　　号：200911927

山东大学
SHANDONG UNIVERSITY

博士学位论文

Dissertation for Doctoral Degree

论文题目：黄河三角洲地区大气颗粒物理化特性研究

Physicochemical characteristics of atmospheric particle in Yellow River Delta of China

作　者　姓　名　袁琦
培　养　单　位　环境研究院
专　业　名　称　环境科学
指　导　教　师　王　韬　教授
合　作　导　师　王文兴　院士

2015 年 5 月 27 日

原 创 性 声 明

本人郑重声明：所呈交的学位论文，是本人在导师的指导下，独立进行研究所取得的成果。除文中已经注明引用的内容外，本论文不包含任何其他个人或集体已经发表或撰写过的科研成果。对本文的研究作出重要贡献的个人和集体，均已在文中以明确方式标明。本声明的法律责任由本人承担。

论文作者签名：袁琦　　日　期：2015.5.27

关于学位论文使用授权的声明

本人同意学校保留或向国家有关部门或机构送交论文的印刷件和电子版，允许论文被查阅和借阅；本人授权山东大学可以将本学位论文的全部或部分内容编入有关数据库进行检索，可以采用影印、缩印或其他复制手段保存论文和汇编本学位论文。

(保密论文在解密后应遵守此规定)

论文作者签名：袁琦　导师签名：王静　日　期：2015.5.27

目录

Contents

摘要

大气颗粒物是我国目前最主要的空气污染物之一，对人类健康、能见度、气候和空气质量等都有重要的影响，而颗粒物的理化性质是这些相关研究的重要理论基础。目前对我国大气颗粒物污染最严重地区之一--环渤海地区的区域背景点的相关研究还相对缺乏。本研究选取了环渤海地区区域背景点之一-黄河三角洲自然保护区开展了大气颗粒物理化特性的相关研究，并重点分析了雾霾天气下颗粒物的污染特征及气团传输对当地颗粒物污染的影响。

本研究采用在线观测与离线分析相结合的方法于 2011 年 4 月至 2012 年 1 月对环渤海地区区域背景点-黄河三角洲自然保护区的大气颗粒物理化性质进行了为期四个月的综合观测，主要研究了不同季节和不同天气下 $PM_{2.5}$ 中水溶性离子污染特征、颗粒物数浓度及粒径分布特征、单颗粒类型及混合状态。并利用后推气流轨迹法和主成分分析法对黄河三角洲地区颗粒物污染的来源进行了分析，得到如下有意义的结果：

黄河三角洲地区观测期间年均总水溶性离子浓度为 49.72 $\mu g/m^3$，其中 SO_4^{2-}、NO_3^-和 NH_4^+是黄河三角洲地区 $PM_{2.5}$ 中最主要的水溶性成分，年均浓度分别为 22.48 $\mu g/m^3$、12.77 $\mu g/m^3$、11.21 $\mu g/m^3$，三者浓度总和占总水溶性离子的 93.6%，且三种离子质量浓度远高于美国、日本和韩国的城市及郊区站点，与国内一些大城市相当，说明黄河三角洲地区面临严重的二次无机气溶胶污染。夏季硫酸盐的转化率（SOR）远高于其它三个季节，导致夏季 SO_4^{2-}浓度最高。太阳辐射、O_3 浓度以及边界高度的变化是影响 SO_4^{2-}日变化的主要因素，而太阳辐射、温度以及边界层高度的变化是影响 NO_3^-日变化的主要因素。黄河三角洲地区冬季酸性颗粒物的比重最高，约有 62.4%的颗粒物是酸性颗粒物，其中 32.1%的颗粒物为强酸性颗粒物。后推气流轨迹分析发现来自山东省内及京津冀的短距离输送气团对黄河三角洲地区的离子贡献率最高。利用主因子分析对黄河三角洲地区 $PM_{2.5}$ 的来源进行解析，结果显示燃料燃烧、二次生成及扬尘和土壤是影响当地 $PM_{2.5}$ 水溶性离子的主要因素。

黄河三角洲地区观测期间 5-10000 nm 粒径范围内总颗粒物平均数浓度为

12838 #/cm^3，春季数浓度最高，冬季最低。气溶胶中爱根模态颗粒物数浓度最高，全年平均占总颗粒物数浓度的 60.7%，其次为积聚模态（25.2%）和凝结核模态（14.1%）。凝结核模态颗粒物在春季和夏季数浓度最高，爱根模态颗粒物则是在春季和秋季数浓度最高，积聚模态颗粒物秋季数浓度最高。在观测期间，共有 26 天发生了新颗粒物生成事件（New particle formatin，NPF），约占总观测时间的 22%。颗粒物的平均成核速率为 6.6 #/(cm^3·s)，颗粒物的平均增长速率为 5.3 nm/h，NPF 事件对凝结核模态和爱根模态颗粒物数浓度日变化有明显影响。风速越高，爱根模态和积聚模态颗粒物数浓度越低，且颗粒物粒径分布的峰值偏向小粒径，偏南风时颗粒物的数浓度要高于偏北风时。南部及东部短距离传输的气团具有更高数浓度的颗粒物，平均为 14903 #/cm^3，而北部长距离传输的气团的颗粒物数浓度较低，平均为 11462 #/cm^3。北部长距离传输的气团的颗粒物粒径分布均为单峰分布，峰值均在爱根模态，而南部和东部短距离传输的气团粒径分布曲线在更大粒径位置（100 nm 附近）出现峰值。

通过透射电镜及能谱分析相结合的方法研究了不同天气条件下单个气溶胶颗粒，根据它们的形貌和成分可以分为以下 9 大类：矿物颗粒、富钾颗粒、富钠/镁颗粒、金属/飞灰颗粒、钙盐颗粒、富硫颗粒、烟尘颗粒、有机颗粒和海盐颗粒。雾霾天气颗粒物老化程度明显，通过长距离输送的雾霾颗粒会通过有机和无机的气态凝结（包括在颗粒物表面的非均相反应）和物理凝聚而发生老化现象。雾霾天颗粒物的混合程度强烈，且多从外部混合转变为内部混合。在雾霾天可溶性的硫酸盐和富钾颗粒趋向于与难熔的新鲜排放的颗粒物包括烟尘颗粒、金属/飞灰颗粒、有机颗粒和矿物颗粒等发生融合。在沙尘暴发生前、发生中和发生后不同时期的颗粒物类型、含量及成分的不同，这表明不同类型颗粒物的混合以及沙尘矿物颗粒与酸性气体的非均相反应取决于气象因素和混合的过程。富硫颗粒是本研究含量最丰富的颗粒，约占颗粒物总数的 86.8%，500 nm 以上粒径段的富硫颗粒数量在雾霾天明显增加。雾天中大部分颗粒是以雾滴形式存在，雾滴有利于硫酸铵颗粒的增大，同时颗粒物之间强烈的混合作用增加了雾霾天富硫颗粒的粒径。

本论文研究结果显示黄河三角洲背景地区存在较严重的大气颗粒物污染，这更反应了当前我国空气污染的区域性和复杂性，气团传输已成为影响城市间、区

域间空气质量的重要因素之一，未来应进一步加强对背景地区颗粒物理化性质的研究，从而为我国制定有效的颗粒物污染的控制对策提供重要的理论依据。

关键词：黄河三角洲地区、水溶性离子、颗粒物数浓度及粒径分布、单颗粒混合状态、雾霾

ABSTRACT

Atmospheric particulate matter is one of the major air pollutants in our country at present, which has serious damage to human health, visibility, climate, and air quality.The physical and chemical properties of particles play a very important role in these processes. Therefore, scholars at home and abroad are paying more attention to the particle contribution and influence to air pollution ofthe Bohai sea rim region.However, understanding chemical and physical properties of aerosol particles in aged air masses after long-range transport from urban areas are rather limitedin the background areas.

In this study, one regional background site was selectedin Yellow River Delta (YRD) nature reserve and adopts the online observation and offline analysis methodto investigatethe physical and chemical properties of atmospheric aerosols.The field study was conducted from April 2011 to January 2012over a period of four months comprehensive observation. This study mainly involved the characteristics of water-soluble ions in $PM_{2.5}$, particle number concentrations and size distributions, single particle mixing statein different seasons and different weather.Possible pollution sources and transports were evaluated using the backward trajectories cluster method and principal component analysis method.

The results showed that the annual average total water soluble ion concentration was 49.72 $\mu g/m^3$ and SO_4^{2-}、NO_3^- and NH_4^+ were the dominant ionic species (constituting 93.6% of the total ionic mass) with their annual average concentrations of 22.48 $\mu g/m^3$, 12.77 $\mu g/m^3$ and 11.21 $\mu g/m^3$, respectively.These three ion concentrations were generally lower than those observed in major cities in China but higher than other rural and nature reserve sites, indicating that the Yellow River delta facing serious secondary mineral aerosol pollution. Ion concentrations exhibited significantly seasonal variations, and maximum values were observed in summer. Solar radiation、O_3 concentrations and temperature are the main factors influencing the daily variation of SO_4^{2-} and NO_3^-. About 62.4% of the total

particleswereacidicand 32.1% of the particles were strongly acidic. Backward air trajectory analysis found that the short distances air masses from Shandong province and Beijing-Tianjin-Hebei cities clusterhad the highest ions contribution to the Yellow River Delta. Principal component analysis results showed that combustion, secondaryaerosol and dust were the main sources of the local aerosol water-soluble ions.

The annual average total particle (5-10000 nm) number concentration was 12838 #/cm^3, while the concentration was highest in spring and lowest in winter.Aitken mode particles had the highest proportion (60.7%) of the total particle, followed by the accumulation mode (25.2%) and nucleation mode (14.1%). Nucleation mode particles had higher number concentrations in spring and summer, while Aitken mode particles had higher number concentrations in spring and autumn. The mean growth and formation rates were calculated as 5.3 nm/h and 6.6 #/(cm^3·s), respectively.Obviously diurnal variations were observed during the new particle formation (NPF) periods, suggesting that NPF events had significant effect on the daily variation of particle number concentrations.With increasing wind speed, the Aitken and accumulation mode particle numbers decreased obviously, and the particle sizes were reduced.Higher particle number concentrations (14903 #/cm^3) were associated with southern and eastern air masses, and smaller diameter peaks were associated with northern air masses.

In this study, aerosol particles were classified into nine particle types using transmission electron microscopy (TEM) and energy dispersive X-Ray (EDX): mineral, K-rich, Na/Mg-rich, metal/fly ash, $CaSO_4$/$Ca(NO_3)_2$, S-rich, soot, organic matter, and NaCl particle. Particles in HF days aged through organic and inorganic gaseous condensate (including the heterogeneous reaction on the surface of the particulate matter) and physical coagulation during transport. Particles mixed intensively in HF days with increase of number fraction of the internally mixed particles but a decrease of externally mixed primary particles. Soluble sulfates and K-rich particles tend to aggregate with refractory fine particles including soot, metal/fly ash, organic, and mineral particles. Individual particle analyses clearly

showed significant difference in particle abundance and compositions before, during, and after the dust storm, indicating that mixtures of various particles and heterogeneous reactions of dust mineral particles with acidic gases depended on the meteorological conditions. S-rich particles were the most abundant particles content in this study, accounts for about 86.8% of the total particulate matter. The number concentrations of larger S-rich particles (>500 nm) increased significantly in HF days. Most of the fog particle existed in the form of dropletsanddroplets were beneficial to the growth of S-rich particles and the strong particle mixing action could enlarge the S-rich particle sizes.

This paper made comprehensively study of the regional background sites of the Bohai sea rim region——the Yellow River delta nature reserve.The physical and chemical properties of atmospheric particulates were investigated to provideeffective supplement for the research on air pollution in China.The results showed that the Yellow River Deltasufferedserious air pollution, which reflected the regional and complexity of current air pollution in our country.Air mass transport has become an important influencing factor onthe regional air quality.Further study on the physical and chemical properties of particulate matter inbackground region should be enhanced in future, which could provide an important theoretical basis for control countermeasures of particulate matter pollution.

Keyword: Yellow River Delta Nature Reserve; Water soluble ion; Particle number size distribution; Individual particle mixing statement; Haze-fog

第一章 绪论

1.1 研究背景

气溶胶是指液体或固体微粒均匀的分散在气体中形成的相对稳定的悬浮体系，分散在气体中的液体或固体微粒通常称为颗粒物[1]。大气中颗粒物的形状不规则，有球状、片状、柱状等，目前最常用的是用空气动力学直径（Dp）来描述颗粒物的粒径，也就是将实际的颗粒物粒径换算成具有相同空气动力学特性的等效直径（或等当量直径），具体是指某一种类的粒子不论其形状、大小和密度如何，如果它在空气中的沉降速度与一种密度为1的球型粒子的沉降速度一样时，则这种球型粒子的直径即为该种粒子的空气动力学直径。根据颗粒物粒径的大小可以将颗粒物分为三种：细颗粒物（$PM_{2.5}$，粒径小于2.5 μm的颗粒物）、可吸入颗粒物（PM_{10}，粒径小于10 μm的颗粒物）和总悬浮颗粒物（TSP，粒径小于100 μm的所有悬浮颗粒物总称）。美国国家环保署（EPA）于1997年颁布并于2006年修订了环境空气质量标准，标准规定美国$PM_{2.5}$年均浓度限值为15 μg/m^3，日均浓度限值为35 μg/m^3。我国也在1996年颁布并于2012年修订了新的《环境空气质量标准》(GB3095-2012)，一级标准规定$PM_{2.5}$年均浓度限值为15 μg/m^3，日均浓度限值为35 μg/m^3，二级标准规定$PM_{2.5}$年均浓度限值为35 μg/m^3，日均浓度限值为75 μg/m^3。颗粒物从形成途径可以分为一次颗粒物和二次颗粒物。一次颗粒物是自然源或者人为源直接排放到环境空气中的颗粒物。自然源主要包括土壤、岩石风化、地面扬尘、植物释放、海洋飞沫和火山喷发等自然因素释放的颗粒物，人为源主要是工业、农业活动、交通以及化石燃料的燃烧等人为因素释放的颗粒物[2]。二次颗粒物是指由气态前体污染物（如SO_2、NO_x、PAHs等）通过大气化学反应而生成的二次颗粒物[3-5]。

大气中颗粒物的来源广泛，对环境和人类的影响也很广泛。颗粒物可以影响人类健康、能见度、气候和空气质量等[6-9]。研究结果表明细颗粒物被吸入人体后可能会导致呼吸系统疾病及心血管疾病，并且死亡率与颗粒物污染水平的高低有着密切联系[10-11]。Kim等人[12]研究发现细颗粒物浓度的升高，特别是细颗粒中硫酸盐、硝酸盐和元素碳浓度的升高对能见度降低有重要影响。颗粒物还可以直

接或间接影响全球的气候变化，如颗粒物通过反射和吸收太阳光从而影响全球的辐射平衡[13]，或者可以作为云凝结核（CCN）影响云的形成，对云雾及降水等过程产生影响[14]等。颗粒物的理化性质在这些过程中起到很重要的作用。水溶性离子是细颗粒物的主要的无机化学组分，特别是NO_3^-、SO_4^{2-}和NH_4^+在降低大气能见度、改变辐射强度、改变地表温度以及影响云形成及湿沉降方面都起到重要的作用[15-19]。细颗粒物的水溶性离子成分还会影响细颗粒物的酸度，通过沉降影响生态系统的健康与稳定[20]。同时颗粒物的粒径大小也是颗粒物的重要性质之一，实验室研究表明，在一定的质量浓度和化学组分的前提下，颗粒物粒径越小所产生的损害健康的效应越大[21]，而颗粒物的凝结成核及长大对于能见度和气候也有重要作用[22]。

中国是世界上最大的煤炭钢铁产国之一，近几十年来煤炭的大量消耗以及机动车的快速增加已经导致二氧化硫和氮氧化物的大量排放[23]。Ohara 等人的研究显示 1980 至 2003 年二十年间我国二氧化硫、氮氧化物、一氧化碳和非甲烷挥发性有机物的排放量分别增加了约 145%、280%、75%和 150%[24]。根据环保部环境统计年报显示，2013 年全年二氧化硫、氮氧化物和烟（粉）尘的排放量分别为 2117.6 万吨、2227.4 万吨和 1278.1 万吨，而环渤海地区是污染物排放量最多的地区（如山东省和河北省）。根据研究显示，中国东部平均地表 $PM_{2.5}$ 浓度是 60-90 $\mu g/m^3$，这是全球最高的区域 $PM_{2.5}$ 浓度之一[25]。由于污染物高强度的排放，环渤海地区过去十年空气污染现象越来越严重，雾霾频繁发生[26-27]。另外，在亚洲季风影响下，环渤海地区人为排放的污染物不仅严重影响当地的空气质量还能影响下风向的国家和地区，比如韩国、日本和北美等地区[28-30]。因此，环渤海地区颗粒物对污染的影响及贡献的研究受到越来越广泛的关注。过去十年间在该地区开展的研究主要是集中于较大城市比如北京、济南、天津等地的气溶胶理化特性[31-34]。但是在环渤海地区区域背景点的研究还相对缺乏[35]，而颗粒物通过不同的传输过程会经历不同的物理化学过程，从而使颗粒物的化学组成以及粒径分布等特征呈现较大的空间差异。因此对环渤海地区区域背景点大气颗粒物理化特性进行观测分析，有利于摸清气团传输对大气颗粒物的影响以及地区污染发生的可能来源，进而全面评估颗粒物的环境效应。

黄河三角洲自然保护区是环渤海地区较典型的湿地自然保护区，人为活动影

响相对较小，一次排放较少，环渤海地区污染较重的地区或城市排放的污染物通过气团传输也许会影响到黄河三角洲地区的空气质量。因此由于它的地理特殊性和环境敏感性，黄河三角洲地区的颗粒物理化性质的研究对于研究整个环渤海地区颗粒物特性及长距离传输机制具有重要意义。

1.2 国内外相关研究现状

1.2.1 颗粒物水溶性离子研究现状

大气颗粒物的主要化学组分有水溶性离子、有机物、土壤尘(或地壳矿物质)、海盐、金属氧化物、氢离子和水等[36]。水溶性离子是大气颗粒物特别是细颗粒物（$PM_{2.5}$）的重要化学组分，水溶性离子组分中阴离子主要是硫酸盐（SO_4^{2-}）、硝酸盐（NO_3^-、NO_2^-）、卤素离子（F^-、Cl^-）；阳离子主要是铵盐(NH_4^+)、碱金属(Na^+、K^+)和碱土金属离子(Mg^{2+}、Ca^{2+})。

其中SO_4^{2-}主要是来自气态前体物SO_2的转化，只有少量是来自一次排放。硫酸盐的转化途径所涉及的化学反应主要有气相和液相两种，其中气相反应主要是SO_2与大气中的OH自由基的反应[37]，液相反应则是SO_2在液滴表面被H_2O_2或者O_3氧化生成，有时金属也会在液相反应中起到催化作用[38-40]。

NO_3^-主要是来自气态前体物NO_x的转化，在昼夜其主要生成途径也不相同。在白天有光照条件下，NO_x被OH自由基氧化生成HNO_3（g），在富氨条件下HNO_3（g）会与NH_3（g）反应形成颗粒态的NH_4NO_3，而该反应受温度影响较大，当温度高于30°C时，大部分硝酸盐以HNO_3（g）形式存在；当温度低于15°C时，大部分的硝酸盐颗粒态的NH_4NO_3形式存在，相对湿度以及氨和硝酸的浓度也对这一平衡有影响，但温度是最主要的影响因素[41]。在夜间硝酸盐则主要是来自N_2O_5水解之后在液相通过H_2O_2和O_3的氧化生成HNO_3[42-43]。

NH_4^+主要来源于NH_3（g）与酸性物质H_2SO_4、HNO_3、HCl等反应生成的铵盐。Cl^-和K^+主要来源于化石燃料、生物质及烟花爆竹等燃烧过程中以及海盐等，Na^+主要来自海盐和土壤等，Mg^{2+}和Ca^{2+}主要来自扬尘及土壤等粗颗粒中。F^-主要来自土壤及工业（如陶瓷、玻璃等）排放。

$PM_{2.5}$中的水溶性离子组分是影响能见度的重要因素之一，而水溶性离子中的硫酸盐和硝酸盐由于具有较高的消光系数，对太阳光容易造成散射，因此是大气中最主要的消光成分之一，其浓度的增加会显著降低大气能见度[44-45]，同时水溶性离子具有吸湿性，在相对湿度比较高的情况下，水溶性离子的吸湿增长特性会加强气溶胶的消光作用，进一步导致能见度的降低[46]。

水溶性离子因为水溶性和吸湿性从而成为云凝结核的主要成分，进而直接影响云的形成，间接影响太阳辐射等。水溶性离子对环境和人体健康也有一定的影响，硫酸盐和硝酸盐是大气中主要的酸性物质之一，直接影响大气降水和云雾水，导致酸雨，由此引起一系列生态和健康问题。因此鉴于水溶性离子对大气环境、人体健康等的重要影响，国内外已经开展了大量的研究工作。

1.2.1.1 欧美地区研究现状

欧美地区对气溶胶研究起步较早，美国EPA在1998年就启动并完成了颗粒物超级站点计划（PM Supersites），在全美国建立起空气质量和气象监测站点的超级网络，如图1-1所示。该计划通过研究开发新型的连续监测技术为研究源排放估算模型、气溶胶的时空分布、大气物理化学过程以及源-受体间关系提供了新的研究方法，这些监测技术涉及到对粗颗粒物[47]、细颗粒物[48-49]和超细颗粒物[50]及其化学成分（离子、有机碳、元素碳等）、颗粒物捕获水、颗粒物密度及粒径分布[51-53]以及单颗粒物的组成[54]等方面进行连续观测。美国在2001年至2005年在纽约还开展了对$PM_{2.5}$监测技术的评估以及$PM_{2.5}$浓度特征的研究项目(PMTACS-NY)，评估了半连续监测仪器与膜采样仪器的监测结果异同，对纽约的城区、郊区以及港口的$PM_{2.5}$化学组成和来源进行了研究，发现硫酸盐在温暖的季节浓度较高，而硝酸盐在春季和冬季浓度较高[55]。

图1-1 美国颗粒物超级站点计划研究区域（http://www.epa.gov/ttn/amtic/supersites.html）

欧洲地区在1979年签订了长距离越境传输空气污染公约（Convention on Long-range Transboundary Air Pollution），之后开展了欧洲空气污染物长距离传输监测与评估合作项目（Co-operative Program for Monitoring and Evaluation of the Long-range Transmission of Air Pollutants in Europe，EMEP），这是针对气溶胶颗粒物最早的大范围综合观测项目，该项目也是为空气污染公约的执行提供科技支撑，最初主要评估大气酸性和富营养化的长距离越境传输，后来则将研究重点转移到地面臭氧的生成，并从1998年起重视颗粒物方面的研究，到2009年已经发展建立起了一个覆盖范围较广的污染物监测站点网络（图1-2）。EMEP已与包括CREATE（Construction, use and delivery of an European aerosol database, http://tarantula.nilu.no/projects/ccc/create/general_info.htm）和GAW（Global Atmosphere Watch，http://www.gaw-wdca.org/）等在内的多个项目开展污染物监测方面的广泛合作，提供了关于气溶胶颗粒物质量、元素、有机碳、水溶性离子以及无机碳的组成等较全面的数据。

1989年-1992年欧共体开展了呼吸健康调查（European communityrespiratory health survey，ECRHS I），2000年6月-2001年11月，欧共体呼吸健康调查二期（ECRHS II）[56]对21个城市的$PM_{2.5}$进行了持续1年多的大气颗粒物综合观测，每个月采集七天的样品。结果发现欧洲不同地区$PM_{2.5}$的质量浓度差别较大，其中冰岛的浓度最低，意大利北部浓度最高。$PM_{2.5}$质量浓度年均值范围为3.7-44.9 μg/m^3，冬季的浓度范围在4.8-69.2 μg/m^{3}之间，明显高于夏季（3.3-23.1 μg/m^3）。

欧洲地区在2002-2003年开展了PAMCHAR计划（the Chemical and Biological Characterization of Ambient Air Coarse, Fine and Ultrafine Particles for Human Health Risk Assessment Project）[57]，在欧洲6个城市背景点对细颗粒物（$PM_{2.5}$）和粗颗粒物（$PM_{2.5-10}$）的质量浓度以及其中的水溶性离子、OC/EC和微量元素进行了为期7周的加强观测，扩展了对粗、细、超细颗粒物化学和毒理学特征的认识。结果发现，$PM_{2.5}$和$PM_{2.5-10}$浓度范围分别为8.3-30 $\mu g/m^3$和5.4-29 $\mu g/m^3$，$PM_{2.5}$的主要化学组分为含碳化合物(28.6-59.7%)、二次无机离子(40%)和海盐(1.1-10%)，湿度高温度低的季节粗粒子和细粒子浓度比值低于1，在湿度低温度高的季节粗粒子和细粒子的浓度比值高于1。

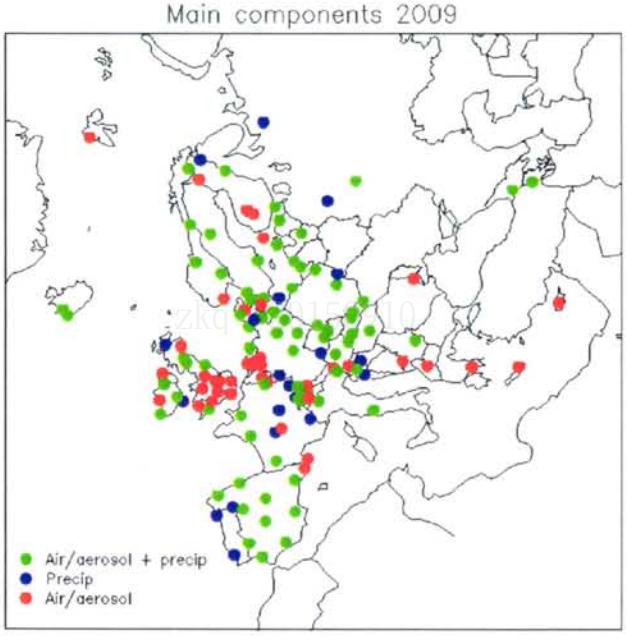

图1-2 2009年EMEP观测网点分布图（来源：http://www.emep.int/）

1.2.1.2 亚洲及我国研究现状

国际大气化学组织（International Global Atmospheric Chemistry Program, IGAC）开展了一系列气溶胶性质实验（Aerosol Characterization Experiments, ACE）[58]，通过融合非现场观测、卫星观测以及模型模拟等手段来降低在评估气溶胶气候效应过程中的不确定性，而其中在亚洲开展的实验项目（ACE-Asia）则主要由两部分组成：一是通过加强观测从而尝试对气溶胶的浓度及性质的时空分布、

气溶胶的演变和存在时间以及气溶胶的辐射效应等方面进行科学的量化，二是通过铺设地面站点网络长期进行非现场或集中观测，从而量化气溶胶的理化性质及光学性质，获取气溶胶的时空变化特征。亚洲区域大气污染研究网络(Asian regional air pollution research network, AIRPET)于2001年至2004年在泰国曼谷、印尼万隆、中国北京、印度金奈、菲律宾马尼拉及越南河内等6个城市开展了对气溶胶污染的观测项目[59]，研究了气溶胶颗粒物在不同城市的时空变化特征，研究结果发现在旱季PM_{10}和$PM_{2.5}$的浓度较高，$PM_{2.5}$主要化学成分为OM、EC、NH_4^+、NO_3^-和SO_4^{2-}，矿物元素含量在PM_{10}中明显升高。

我国对气溶胶颗粒物的研究起步较晚，从20世纪90年代才开始针对$PM_{2.5}$进行综合的观测[60]，并逐渐在较大城市如北京、上海、广州、济南等地开展对$PM_{2.5}$及其化学组分的研究，主要关注质量浓度、时空分布、来源、形成机理以及区域传输等[61-64]。Zhang等[65]总结了北半球37个站点PM_1的化学成分(图1-3)，结果发现PM_1中最主要的化学组分为水溶性离子和有机气溶胶，分别约占总PM_1质量浓度的55%和45%，其中硫酸盐、硝酸盐和铵盐是三种最主要的离子成分；37个监测站点中北京的颗粒物污染最为严重，PM_1质量浓度高达71 $\mu g/m^3$，远高于其他城市及郊区站点。Chan和Yao[66]总结了中国北京、上海、深圳、广州和香港气体污染（SO_2、CO、NO_2、O_3）和颗粒物污染（TSP、PM_{10}、$PM_{2.5}$）的污染特征，发现水溶性离子是我国颗粒物污染的重要组成部分，在这些城市中颗粒物硝酸盐的浓度较高，这可能与机动车排放有密切的相关性。Yang等[67]总结了我国典型地区$PM_{2.5}$及其化学组分的污染状况（如图1-4），结果表明我国北部和西部城市的$PM_{2.5}$质量浓度较高（>100 $\mu g/m^3$），而一些偏远森林地区（如长白山等）$PM_{2.5}$质量浓度较低（<40 $\mu g/m^3$）。东部观测站点的硫酸盐、硝酸盐和铵盐的质量浓度之和占$PM_{2.5}$质量浓度的40%-57%。不同的NO_3^-/SO_4^{2-}质量比表明不同的污染物来源以及当地的能源结构，如广州是以移动源（汽车尾气等）为主，而重庆则是以固定源（燃煤排放等）为主。而从1999年至2008年，北京的NO_3^-/SO_4^{2-}比值呈现增长的趋势，这表明北京的机动车排放对污染的贡献逐年增强。通过上述研究可知，目前对于环渤海地区大气颗粒物理化性质的研究还主要是集中在城市地区，对于区域背景点的研究相对缺乏。

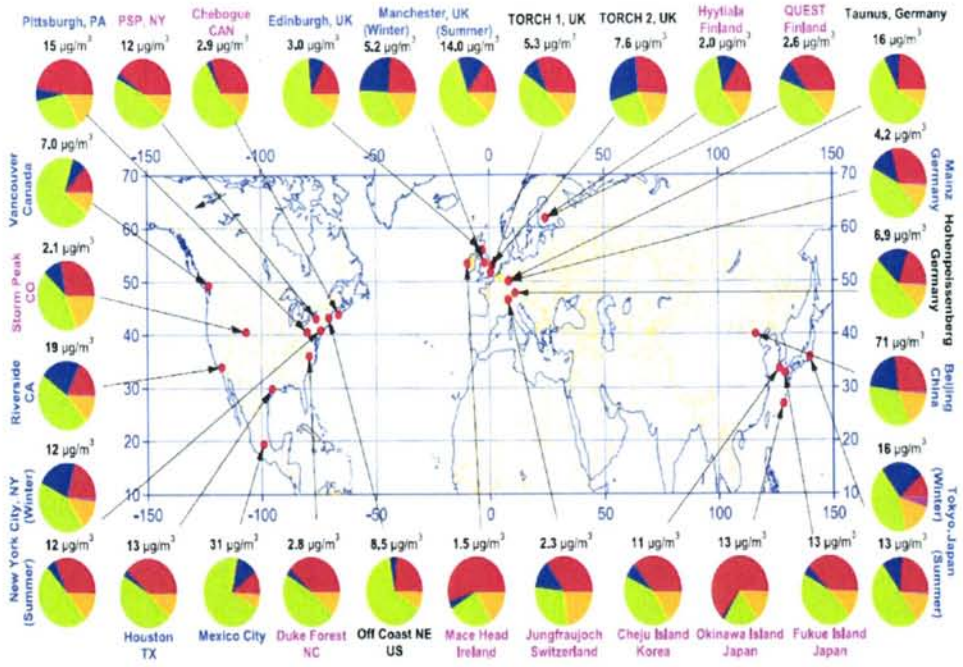

图1-3 北半球各研究站点PM_1组成图谱（饼状图中不同颜色代表不同组分，绿色代表有机物，红色代表硫酸盐，蓝色代表硝酸盐，黄色代表铵盐，紫色代表氯）（Zhang等[65]）

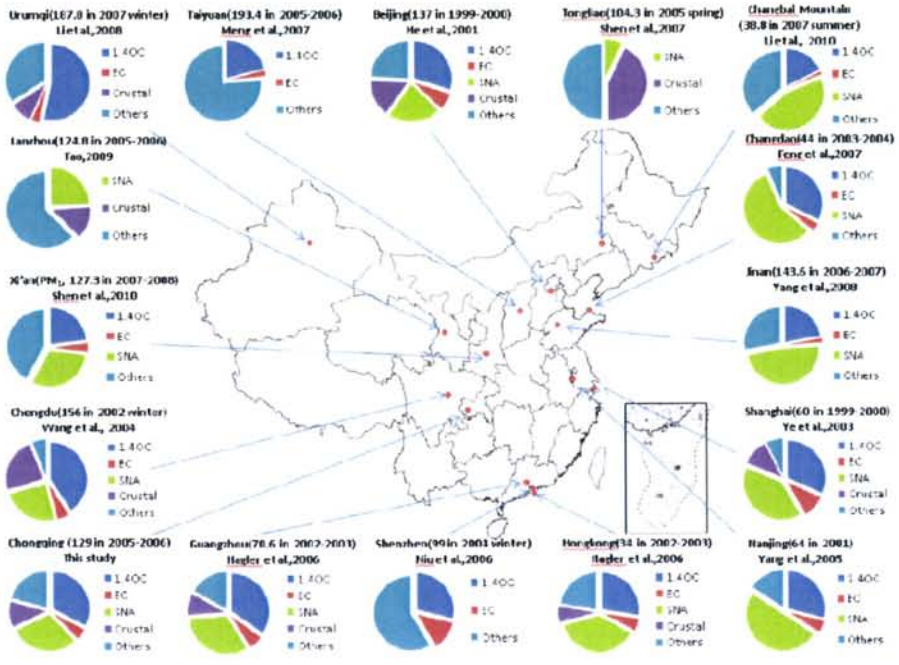

图1-4 中国典型城市及郊区站点$PM_{2.5}$（西安市PM_1）的成分组成图（Yang等[67]）

1.2.1.3 酸度研究

大气颗粒物的酸度是颗粒物重要的理化性质之一，颗粒物酸度可以影响大气的酸沉降，从而对森林、农作物和土壤等生态系统产生重要影响[68]；颗粒物酸度还可以影响大气酸催化反应，从而影响二次有机气溶胶（SOA）的生成[69-70]；长期暴露在强酸性的大气颗粒物环境下，会导致人体的肺病发生几率提高，从而严重危害人体健康[71]。因此加强对大气颗粒物酸度的研究，有助于认清大气颗粒物在酸沉降和大气化学反应中所起的重要作用，加深对大气非均相化学反应机制的认识，并有利于研究控制酸沉降的途径，因此气溶胶酸度的研究受到国内外广大研究者的重视[72-74]。

颗粒物酸度在大气非均相化学反应中扮演重要角色。Yao等[75]通过热动力学模型研究香港地区$PM_{2.5}$的酸度发现$PM_{2.5}$的酸度会影响大气中挥发性和半挥发性反应物及氧化剂在大气气溶胶中的浓度，$HCl(g)/Cl^-$、$HNO_3(g)/NO_3^-$和$NH_3(g)/NH_4^+$在气体和气溶胶中的分配也会受到气溶胶酸度的影响。Keene等[76]研究海盐气溶胶的PH值对S氧化过程的影响时发现，不同的PH条件下S的氧化途径以及氧化剂均不同，PH值越低，海盐气溶胶中S通过氧化成$H_2SO_4(g)$而去除的比例越高。Jang等[77]通过烟雾箱实验研究发现大气气溶胶酸性表面的存在可以潜在的增加SOA数倍的量，Tanner等[78]通过实验室研究也发现在酸性气溶胶浓度越高的时间和地点有机气溶胶的浓度也会越高，这也反映了颗粒物酸度与SOA的生成有紧密联系。

不同地区颗粒物酸度也具有显著差异。Ren等[79]分析中国北方和南方50个城市及背景站点的颗粒物样品的酸度特征，结果发现中国北方大部分观测点位的颗粒物酸度都低于南方，这是导致南方酸雨多发的原因之一。颗粒物的酸化主要是由于化石燃料的燃烧排放出的二氧化硫和氮氧化物引起的，其中燃煤燃烧主要释放出二氧化硫，而机动车燃料燃烧是氮氧化物的主要来源。通过对比过去20年的实验结果发现，中国的酸沉降并没有得到有效的控制，而且酸沉降的影响范围也在逐渐扩大，中国北方地区逐渐受到酸沉降的影响。Brook等[80]在1992-1994年对加拿大安大略湖、魁北克省、大西洋沿岸三省和范库弗峰地区的大气细颗粒物的酸度进行了研究，结果表明滨海地区的细颗粒物酸度最高，郊区次之，城区最低。这主要是由于不同地区的NH_3浓度不同，城区具有最高的NH_3浓度，可以较好的

中和气溶胶的酸性。另外滨海地区雾天的发生频率较高，高的湿度有利于SO_2转化为H_2SO_4，从而导致滨海地区气溶胶酸度较高。

颗粒物酸度不仅具有地区差异，也会随颗粒物粒径或者季节的变化而变化。研究结果还发现气溶胶粒径越小，酸度越高，酸度缓冲能力减弱，这表明粒径是颗粒物酸度的主要影响因素。Hazi等[81]研究了纽约郊区的颗粒物酸度的粒径分布，结果表明小于100 nm的超细颗粒物的酸度比细颗粒物其它粒径段的颗粒物酸度高。王玮等[82]对北京沙尘粒子的酸度研究也表明，来源于土壤和沙尘的粗颗粒所含碱性物质较多，从而导致粗粒子的酸度较低。Pathak等[83]研究了香港地区大气细颗粒物的酸度，结果发现夏季细颗粒物酸度最低，而秋季最高，这可能是由于香港地区大气颗粒物受气团长距离传输影响较大，在春夏季气团主要来自海洋，海洋气团的粗颗粒的海盐较多，硫酸盐和硝酸盐较少，而在秋冬季气团主要来自内陆，内陆的气团中硫酸盐和硝酸盐的比例较高，因此秋冬季节的气溶胶酸度较高。

1.2.2 颗粒物数浓度研究现状

除了化学组份外，颗粒物的物理性质特别是粒径分布特征对于气候、人体健康及大气环境也都有重要的影响[84-85]。颗粒物的粒径分布主要涉及到颗粒物的个数浓度、表面积浓度及体积浓度的粒径分布等。1897年Aitken首次研究了大气中超细颗粒物的粒径分布并提出了新颗粒物生成的证据[86]，之后，随着监测手段的发展，对于大气中超细颗粒物的研究逐渐在全球范围内开展起来。国际上按照颗粒物粒径大小可以将颗粒物归类为凝结核模态（nucleation mode，3-20 nm）、爱根模态（Aitken mode，20-100 nm）、积聚模态（accumulation mode，100-1000 nm）和粗粒子模态（coarse mode，>1000 nm）[87]。而一般将小于粒径100nm的颗粒物称为超细颗粒物。

凝结核模态的颗粒物主要来源于气态前体物通过均相反应即气粒转化的新颗粒物生成过程，而汽车尾气的一次排放也可能产生一定量的凝结核模态颗粒物[88]。爱根模态的颗粒物则主要来源于燃料(汽油、柴油等)燃烧以及凝结核模态颗粒物通过凝结、碰并等方式增长而成[89-90]。积聚模态的颗粒物来源于爱根模态颗粒物的增长、燃料燃烧以及沙尘、海盐等机械作用生成的较大颗粒物，而机动车

尾气排放的颗粒物也主要是积聚模态的颗粒物[91]。粗粒子模态的颗粒物主要来源于扬尘、海水飞沫、工厂的机械磨损、植物花粉等机械过程[92]。

1.2.2.1 欧美地区研究现状

当前欧美地区已经有许多知名的研究小组在大气颗粒物个数浓度、粒径分布、新颗粒物生成及增长等方面做出了重要贡献，如美国明尼阿波利斯大学的McMurry小组、美国Brookhaven国家实验室的Weber小组、芬兰赫尔辛基大学的Kulmala小组和芬兰气象中心的Dowd小组、英国伯明翰大学的Harrison小组及Birmili等、德国莱布尼兹对流层研究所Wiedensohler等。以这些小组为中心，世界各地已经组织了很多针对性的观测研究项目，比如ACE-1(2)、TraceP、美国匹斯堡观测项目、芬兰SMEAR及BIOFOR项目等[22]，这些项目已经覆盖欧美及太平洋的主要区域（如图1-5），由此可见欧美发达国家对颗粒物个数浓度及粒径分布的研究已经比较成熟，同时从图中也可以看到在亚洲地区相关研究的开展较少。

Kopanakis等[93]在地中海地区进行了为期一年的观测发现经过污染区域的气团传输可以提高观测点颗粒物的数浓度，冬季凝结核模态的颗粒物数浓度的爆发与新颗粒物生成事件或者当地的取暖燃料燃烧排放有关。Hussein等[94]通过对赫尔辛基主要交通干道的研究发现，交通源是超细颗粒物的主要来源，特别是在白天交通繁忙的时候该现象更加明显，而积聚模态的颗粒物可能主要是来自区域的传输。Kulmala等[95]人研究了不同地区的凝结核模态颗粒物的生成及增长，总体来说，颗粒物增长速率平均处于0.3-20 nm/h，污染越重的区域，颗粒物的增长速率越高，且硫酸气对于颗粒物的增长的作用越明显。Agus等[96]对英国的路边站点研究发现凝结核模态和爱根模态颗粒物与NOx、CO具有显著的线性关系，说明交通排放是凝结核模态和爱根模态颗粒物的重要来源之一。Kerminen和Kulmala[97]研究了超细颗粒物通过均相成核反应成核的速率的影响因素，结果发现前体气溶胶颗粒物的碰并消除是颗粒物成核重要的汇，而不挥发性的二次有机气体的存在往往有利于新鲜成核颗粒物的长大过程。Stainer等[98]对匹兹堡的颗粒物数浓度和粒径分布研究发现，城市站点的颗粒物数浓度远高于郊区站点，成核反应、交通排放和生物质燃烧是影响颗粒物数浓度日变化特征的主要因素。

Laakso等[99]在芬兰的城市及郊区站点观测结果显示积聚模态颗粒物在夏季数浓度最高，冬季最低，凝结核模态和爱根模态颗粒物则是在春秋季最高；城市站点的颗粒物数浓度日变化受交通源的影响较大，郊区站点则主要是受新颗粒物生成事件的影响。

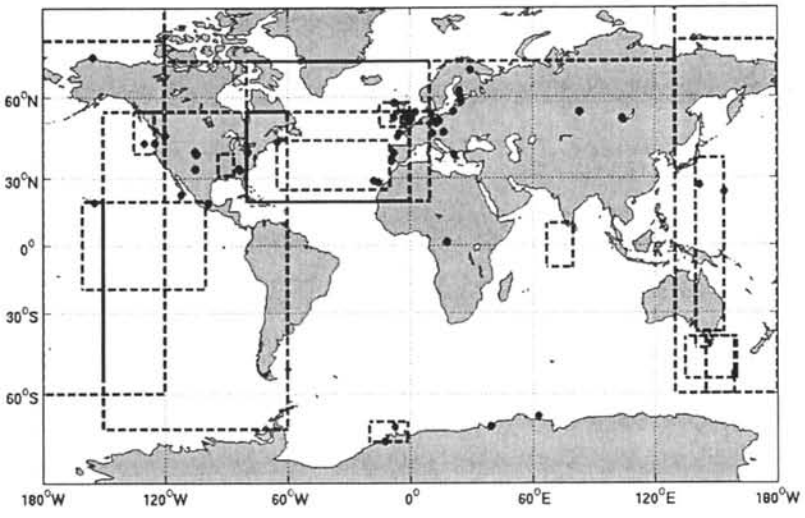

图1-5 全球颗粒物个数浓度及粒径分布主要观测区域（Kulmala,2004[22]）

1.2.2.2 亚洲及我国研究现状

我国针对颗粒物的数浓度及粒径分布等研究最早开始于20世纪80年代在山西太原地区国家八五公关项目中的航空测量[100]。1997年，许黎等[101]在北京开展了对粒径范围为0.3-10 μm的颗粒物数浓度的季节变化、日变化及其与气象因素关系的研究，结果表明颗粒物的数浓度与相对湿度呈现正相关，且风向对数浓度影响较大。胡敏等[102]研究了北京夏季高温高湿及降雨过程对大气颗粒物谱分布的影响，结果发现降雨过后的晴朗干洁天气有利于新粒子(3-20 nm)的生成，生成的新粒子快速长大到50-100 nm。Wu等[103]通过在北京两年的观测发现，风速可以影响不同粒径的颗粒物数浓度，随着风速的提高凝结核模态和粗粒子模态的颗粒物数浓度也随之增加，而爱根模态和积聚模态的颗粒物数浓度则有明显降低。Yue等[104]对广州城市和郊区站点的研究发现，郊区站点的新颗粒物生成事件的发生频率是城市站点的两倍，机动车排放是影响城市站点颗粒物数浓度的重要因素之一，而长距离输送则是郊区站点的主要影响因素。Guo等[105]对香港山地站点的研究发现，新颗粒物生成事件的发生往往伴随着较强的太阳辐射、较高的风

速、较高浓度的SO_2和O_3。Wehner等[106]在北京春季观测发现北京市细颗粒物的数浓度较高，而且新颗粒物生成个例的发生频率也比较高。Liu等[107]在我国珠江三角洲地区也对颗粒物数浓度及粒径分布进行了相关研究，并发现在该地区也有新颗粒物生成现象的发生。Gao等[108]在兰州开展了一系列针对颗粒物数浓度及粒径分布的研究，并观测到新颗粒物生成事件，发现硫酸气是城市地区新颗粒物生成事件发生的重要贡献者之一。Li等[109]研究了上海城区主要道路垂直方向大气气溶胶颗粒物数浓度及粒径分布特征，结果发现在1.5米-20米的垂直范围内随着高度增加，凝结核模态和爱根模态颗粒物的个数浓度下降，粒径分布的峰值从爱根模态偏移到更大的粒径段。牛生杰等[110]曾经利用飞机航测的手段在宁夏地区开展了关于颗粒物粒径分布及云凝结核的相关研究。王玮等[111]也利用飞机航测的手段在华东沿海地区针对大气颗粒物的个数浓度和粒径分布进行了研究。而在中国背景地区开展的相关研究还比较缺乏，Kivekäs等[112]人在青海的瓦里关山对粒径范围为12 nm-570 nm的颗粒物进行了观测研究，发现当地大气颗粒物平均个数浓度约为2030 #/cm^3。

1.2.2.3 颗粒物生成及增长

大气中的颗粒物除了来自一次排放，主要是来自新颗粒物的生成及增长过程，2003年Kulmala在Science上[113]介绍了大气中新颗粒物生成及增长的机理（图1-6所示）。处于分子状态下的气态前体物（如SO_2、NH_3、VOCs等）在特定条件下通过如离子诱导等作用凝结成核形成分子簇，经过颗粒物的增长过程逐渐长大到一定的粒径范围，进一步通过成长过程成长为云凝结核（CCN）。

新颗粒物的生成即成核过程是气体分子凝结成分子簇的过程，也是一个从气态到液态再到固态的变化过程。通过研究发现新颗粒物具有多种生成机制，如硫酸-水二元成核[114]、硫酸-氨-水三元成核[115]、大气有机蒸汽成核[116]、离子诱导成核[117]、卤素元素氧化成核等。新颗粒物生成事件在不同地区大气环境中是普遍发生的现象，如在偏远的北方森林[118]、沿海边界层[119]、重污染的城市地区[95]、以及非常清洁的南北极地区[120]等地区均已观测到新颗粒物生成事件。而新颗粒物生成速率在不同环境下也有明显差异，如在区域成核事件中，边界层内3nm的

颗粒物成核速率范围为0.01-10 #/(cm^3·s)，而在滨海地区以及工业区可以观测到高达10^4-10^5 #/(cm^3·s)的成核速率[22]。

新颗粒物的增长过程是指新鲜排放或者新生成的颗粒物粒径增长变大的过程。颗粒物可以通过以下几种途径增长[121]：成核蒸汽的凝结(Condensation of nucleating vapours)、带电性凝结(Charge-enhanced condensation)、自身碰并凝聚增长(Growth by self-coagulation)、由于其它蒸气的成长(Growth by other vapors)以及多相化学反应(Multi-phase chemical reaction)等。而新颗粒物的增长速率在不同环境下也有明显差异。绝大多数颗粒物的增长速率范围在1-20 nm/h[22]，在某些偏远郊区颗粒物的增长速率可以低至0.1-1 nm/h[122]，在重污染地区则可以观测到高于10 nm/h的增长速率[123]，在森林地区增长速率在1-4 nm/h[124]，超过100 nm/h的增长速率偶尔可以在烟羽和沿海地区观测到[125]。

新颗粒物的生成通常发生在清洁、干燥的白天[126]，而且在不同的季节以及不同的站点，新颗粒物生成事件发生的频率也不一样[127]。Hamed 等[128]在意大利的观测发现，春夏季新颗粒物生成事件发生频率要高于秋冬季，而新颗粒物生成事件发生时往往伴随更高的温度、风速和更强的辐射以及更高浓度的SO_2和O_3。Yue 等[129]在北京观测到了新颗粒物生成事件，并发现硫酸的浓度与新颗粒物生成速率有很好的正相关性，硫酸气的凝结以及硫酸铵的积聚都对颗粒物的增长有重要贡献，而在贫硫的环境下，有机物则是新颗粒物增长的重要贡献因子。Guo 等[130]通过研究发现凝结核模态的颗粒物个数浓度与颗粒物的表面积浓度呈负相关，而且 SO_2 及其二次反应产物可能对颗粒物的生成有一定贡献。Wu 等[131]针对北京市 3 nm~10 μm 粒径范围内的颗粒物个数浓度和粒径分布进行了为期一年的观测，发现在观测期间有大约 40%的观测日发生了新颗粒物生成事件，春季发生频率最高，夏季最低，而且这些事件通常发生在太阳辐射较强且相对湿度较低的情况下。Lee 等[132]在对流层观测到夜间的新颗粒物生成事件，而夜晚空气对流可以将低海拔位置的大量气态前体物带到高海拔处，而高海拔处的温度以及颗粒物表面积都较低，这三个因素的综合有利于夜间对流层新颗粒物的生成。

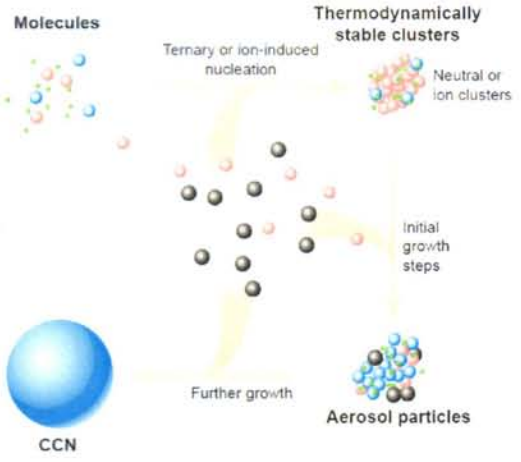

图1-6 颗粒物生成及成长过程示意图（来自Kulmala,2003[113]）

1.2.3 颗粒物单颗粒形貌及混合状态研究现状

当前对气溶胶单颗粒的分析已成为热点，而透射电镜（Transmission electron microscopy, TEM）是分析大气单颗粒理化性质以及混合状态的重要技术之一[133-135]，透射电镜技术可以提供纳米级的单颗粒形貌、成分、混合状态以及结构等颗粒物的重要信息，这对于研究颗粒物对气候、能见度、人体健康等方面的影响具有重要意义[136]。因此国内外学者已经广泛使用透射电镜技术来研究大气中的气溶胶颗粒物[137-140]。

基于颗粒物的形貌特征及成分，可以在纳米到微米的粒径范围内将颗粒物划分为很多种类，如富硫颗粒、金属颗粒、矿物颗粒、烟尘颗粒、有机颗粒等。颗粒物的形貌特征及成分等信息对于研究气溶胶颗粒物的老化过程、颗粒物的光学及吸湿特性等有重要作用[141-142]。

1.2.3.1 欧美地区研究现状

气溶胶单颗粒的研究已在欧美地区广泛开展。Adachi 等[143]人研究发现烟尘颗粒的光学特性很大程度上取决于与烟尘颗粒混合的有机物或硫酸盐的空间位置或者颗粒物的形状，在烟尘颗粒中心位置混合有机物或硫酸盐的颗粒的吸光性强于在外围位置混合的颗粒。Pratt 等[144]研究了垂直空间上单颗粒的混合状态，结果发现在海拔较低的空气中生物质燃烧颗粒、有机碳颗粒和烟尘颗粒主要是内

混硝酸盐和铵盐，而在较高海拔则主要是内混硫酸盐。Laskin 等[145]对有机颗粒的研究发现，有机颗粒和海盐通过水合循环反应而发生混合是有机盐的主要形成途径之一，且混合后能够改变老化颗粒的吸湿性、酸性和光学特性等。Kocbach 等[146]研究发现机动车排放出的颗粒物粒径要明显小于木柴燃烧排放出的颗粒物粒径，机动车排放的含碳颗粒物中主要包含硅和钙等元素，而木柴燃烧产生的含碳颗粒物主要包含钾等元素。Nie 等[147]对芬兰背景地区清洁和污染天气下单颗粒研究发现，当地 0.2-1 μm 粒径范围内最主要的颗粒物类型是硫酸盐颗粒和烟尘颗粒，污染发生时该地区富钙颗粒（Ca-rich particle）比例升高。Li 等[148]对生物质燃烧发生时的单颗粒研究发现，燃烧烟雾中最主要的颗粒物类型是钾盐和有机颗粒，而且大部分颗粒都发生了内混现象，KCl 颗粒主要出现在早期烟雾中，K_2SO_4 和 KNO_3 颗粒则主要出现在后期烟雾中，这说明烟雾中颗粒物老化现象的发生。Kaegi 等[149]对瑞士苏黎世城区的气溶胶单颗粒样品分析发现，富铁颗粒（Fe-rich particle）是交通源排放的标志之一，机动车的发动机可能会直接排放富铁颗粒。

1.2.3.2 亚洲及我国研究现状

近些年亚洲地区也逐渐开始重视气溶胶单颗粒的研究。Okada 等[150]通过在日本和澳洲的观测发现，60%以上的颗粒是富硫颗粒，且富硫颗粒的粒径范围为 0.1-0.5 μm。Ueda 等[151]对日本高山站点的观测发现，超过一半的非水溶性颗粒为烟尘颗粒，烟尘颗粒主要呈现不透明的电子球状的链状聚合体。Geng 等[152]在韩国的观测发现主要的颗粒物类型是含碳颗粒和富硫颗粒，同时气团传输对于颗粒物类型有明显影响。Coz 等[153]人的研究发现新加坡的颗粒物多数为新鲜排放的颗粒物，粒径在 220-460 nm 范围内，马尔代夫则是老化颗粒物占主导，粒径在 130-360 nm 范围内。

我国学者最近十几年也开始广泛利用 TEM、SEM 等技术开展对气溶胶单颗粒的研究[154]，而在环渤海地区的研究主要集中于经济发达的地区和城市[155-156]。Shao 等[157]对室内的 PM_{10} 中单颗粒的理化性质研究表明，烟尘颗粒以及其他未知的细颗粒物对人体细胞的氧化性磨损有重要贡献，从而间接损害人体健康。Zhang 等[158]对山东沿海城市青岛的颗粒物研究分析发现，在细颗粒物和粗颗粒

物中均发现颗粒物内混硫酸盐和硝酸盐的现象，从数浓度来看，内混硫酸盐的颗粒物主要集中于细粒子，内混硝酸盐的颗粒物主要集中于粗粒子。Shi 等[159]利用扫描电镜与 X 射线能谱分析技术对北京不同地区的气溶胶单颗粒样品的粒径分布及形貌特征进行了研究，结果发现在燃煤取暖季节，飞灰颗粒比重明显上升，且北京地区的颗粒物粒径 99%集中于 2.5 μm 以下。Li 和 Shao 等[160]对北京冬季雾天条件下的矿物颗粒研究发现，雾天大部分矿物颗粒被雾滴冲刷去除，在雾天和非雾天矿物颗粒数浓度分别在 0.1-0.3 μm 和 1-2.5 μm 处具有峰值，同时发现在雾天含有大量碱性成分的矿物颗粒特别是富钙颗粒的存在可以有效缓解雾天气溶胶的酸性。

1.2.3.3 颗粒物单颗粒混合状态

在实际大气中颗粒物不同的化学组分往往并不是单独存在的，而常常是混合在一起，颗粒物的混合状态一般可分为内混（internally mixed）和外混（externally mixed），内混一般是指在同一颗粒物内不同物质通过均相及非均相反应而发生的混合现象，外混一般是指不同颗粒之间不同形态的混合。颗粒物的混合现象可以明显改变颗粒物的性质，从而对气候、健康效应等产生重要影响[161-162]。硫酸盐、硝酸盐、铵盐等化学组分是水溶性的，而烟尘和部分有机物等是非水溶性的，两种颗粒物的光学性质也不同，发生混合后会改变颗粒物的吸湿性和光学性质，进而影响颗粒物成为云凝结核的能力并对能见度也会产生一定影响[163]。因此对气溶胶单颗粒混合状态的研究有利于更好地理解气溶胶对气候和健康的影响。

Posfai 等[164]研究发现在海洋对流层中硫酸气溶胶内混烟尘颗粒的现象，飞机排放以及生物质燃烧是烟尘颗粒的主要来源，内混烟尘颗粒的硫酸气溶胶更有效的作为云凝结核影响云的形成等。Moffet 等[165]研究发现日出之后通过光化学反应，烟尘颗粒会与硫酸盐、有机物、硝酸盐等颗粒混合并逐渐老化，而存在内混现象的元素碳的吸光能力比新鲜排放的元素碳强 1.6 倍。Bauer 和 Koch 的研究[166]发现二氧化硫与矿物颗粒的非均相反应有利于硫酸盐的形成，同时硫酸盐与矿物颗粒的混合一方面可以提高矿物颗粒的溶解性，降低矿物颗粒在大气中的停留时间，另一方面可以降低外混硫酸盐的存在，从而降低人为排放的硫酸颗粒的辐射强迫。Li 等[167]对香港大气气溶胶中金属颗粒的研究发现，金属颗粒与酸性

颗粒物的内混现象可以增加金属颗粒的水溶性，从而增加金属颗粒对人体的毒性。

1.2.4 雾霾研究现状

灰霾通常是指由于大气颗粒物对太阳光的吸收和散射作用导致水平能见度低于 10 km，相对湿度小于 80%的现象；雾则是由于小水滴对太阳光的吸收和散射作用导致水平能见度低于 1 km，相对湿度高于 90%的现象；而能见度低于 10 km，相对湿度介于 80%和 90%之间的现象我们称为薄雾[168]。由于有时一天中灰霾、雾和薄雾并不总是单独出现，经常交替发生，因此我们通常将这种空气污染现象称为雾霾。雾霾的发生可以直接影响大气能见度、人体健康以及气候等[169-171]。20 世纪中期发生了震惊世界的五大公害事件，有四个就涉及到空气污染问题：1930 年的比利时马斯河谷烟雾事件、1943 年和 1945 年的美国洛杉矶光化学烟雾事件、1948 年美国多诺拉烟雾事件以及 1952 年的英国伦敦烟雾事件。这些著名的空气污染事件都造成了不同程度的人体疾病和死亡，因此从 19 世纪 70 年代开始，欧美地区国家相继开展了对雾霾相关的研究。

Trijonis 等[172]利用美国西南部 25 年的能见度数据以及 10 年的颗粒物浓度数据分析发现，从 19 世纪 50 年代中期到 70 年代早期美国城市的能见度下降了 10%-30%，通过回归模型显示二次气溶胶（特别是硫酸盐）对能见度的降低起主导作用。Chen 等[173]通过对大西洋中部地区夏季灰霾发生时的 $PM_{2.5}$ 及化学组分研究发现，SO_4^{2-} 在 $PM_{2.5}$ 中比例在灰霾发生时明显升高，说明硫酸盐在灰霾形成中的重要作用。Chan 等[174]研究发现烟尘颗粒与硫酸盐对能见度降低贡献最高，而相对湿度也对能见度降低有一定影响。Nemery 等[175]对马斯河谷烟雾事件的研究发现由于在污染较重地区雾天天气条件下往往伴随高浓度的颗粒物和酸性气体（如 SO_2 和 NO_2 等），因此雾天的发生对敏感人群，特别是老人和儿童以及患有呼吸系统疾病的人群具有直接的健康威胁。

亚洲东部地区，特别是中国的北方城市近年来雾霾现象频繁发生[176-179]，因此针对中国北方地区雾霾的研究也逐渐开展。Li 等[180]在吉林省和辽宁省组织开展了区域性观测实验（EAST-AIRC），对灰霾条件下的颗粒物及气体污染物进行深入研究；Zheng 等[181]参与了 CAREBeijing 项目，重点关注北京的空气质量以及细颗粒物生成事件；Liu 等[182]研究了不同高度气溶胶的性质；这些大型的观测

项目的研究结果都发现长距离输送对华北平原大城市的污染有重要影响。Zhao等[183]研究发现二次气溶胶的形成会显著地影响区域灰霾的，同时较低的风速不利于污染物的扩散，风向也是影响灰霾形成的重要因素。Cheng 等[184]研究发现长江三角洲地区 1980-2000 年这 20 年间能见度从 13.2 km 下降到 10.5 km，细颗粒物在长江三角洲地区灰霾形成中起到关键作用。Ma 等[185]通过飞机航测发现气溶胶污染是我国雾霾形成的重要因素，特别是沙尘颗粒和酸性物质的混合是云凝结核的主要来源之一。Zhang 等[186]研究发现在人口稠密的大城市雾霾发生时空气中的多环芳烃可以增加肺癌的发病几率。Liu 等[187]对北京 2011 年 9 月份的一次区域灰霾事件研究发现反气旋天气条件、一次污染物的排放、边界层高度、长距离传输以及气溶胶的吸湿增长都是影响灰霾形成的主要因素。Huang 等[188]研究发现雾滴可以作为一个微型反应器，有利于一次污染物（如 SO_2 等）转化为二次污染物（如硫酸盐等）。Sun 等[189]对北京雾霾期间的 $PM_{2.5}$ 和 PM_{10} 化学组分研究发现雾霾发生时 $PM_{2.5}$ 中硫酸盐、硝酸盐的质量浓度是非雾霾期间的 10 倍，雾霾期间 $PM_{2.5}$ 主要受气团输送影响，PM_{10} 则主要受局地排放影响。

1.3 本文主要研究内容

本研究基于环保部公益性课题“典型地区大气灰霾特征与控制途径预研究”(201009001)，从 2011 年 4 月到 2012 年 1 月期间，于环渤海地区区域背景点——黄河三角洲国家级自然保护区对大气气溶胶进行综合观测实验，主要分析气溶胶颗粒物的水溶性离子成分、颗粒物数浓度及粒径分布、单个气溶胶颗粒物的成分、粒径、形貌和混合状态等理化特性。主要研究内容如下：

1、分析不同季节水溶性离子的浓度水平和日变化特征，水溶性离子与气态前体物以及气象参数之间的关系，研究气溶胶酸度的季节变化特征，并结合后推气流轨迹法和主因子分析法分析了气溶胶的传输途径和污染物的可能来源，为黄河三角洲地区污染物的形成及来源研究提供科学基础；

2、分析不同季节颗粒物数浓度的粒径分布特征，并研究黄河三角洲地区的新颗粒物生成事件的特征，结合后推气流轨迹法分析了不同路径的气团传输对颗粒物粒径分布的影响；

3、分析春夏两季黄河三角洲地区气溶胶单颗粒的化学成分、粒径大小、形

貌特征和混合状态等理化特性，研究典型天气下（雾霾和沙尘）颗粒物的老化过程，结合后推气流轨迹分析不同路径的气团传输对单颗粒类型的影响；

4、对比雾霾天和清洁天黄河三角洲地区颗粒物理化性质的差异，深入探讨雾霾的形成机制。

1.4 本研究的主要创新点和科学意义

该论文选取环渤海地区区域背景点——黄河三角洲国家级自然保护区对大气气溶胶的理化特性作研究，本研究的创新点主要体现在以下三个方面：

（1）本研究利用在线监测和膜采样相结合的手段，全面研究环渤海地区区域背景点大气颗粒物水溶性离子化学组分、颗粒物数浓度粒径分布及单颗粒形貌特征等理化特性。

（2）本研究以颗粒物理化特性为基础并结合后推气流轨迹法，发现环渤海区域背景点的大气颗粒物污染受山东和京津冀地区气团短距离输送影响显著，未来应加强区域联防联控来解决当地颗粒物污染问题。

（3）本研究发现雾霾天气的颗粒物经历了明显的老化过程，混合程度高，且内部混合占主导，二次转化也是大气细颗粒物的重要来源之一。

目前国内对大气颗粒物理化性质的研究多集中于经济发达、人口密集的城区及其周边近郊地区，对区域背景点的综合观测研究还较少。环渤海地区是我国人口密度最高、经济发展最快的地区之一，而由于环渤海地区独特的地理形势和季风气候，造成该地区的大气污染物难以向外输送，使其成为中国乃至世界范围内大气污染最严重的地区之一。黄河三角洲自然保护区是环渤海地区较典型的湿地自然保护区，人为活动影响相对较小，观测结果显示，黄河三角洲地区受气团区域性长距离传输影响较明显。通过在黄河三角洲自然保护区的综合观测能够弥补典型背景区域的研究空白，通过分析颗粒物的无机水溶性离子组分、数浓度粒径分布及单颗粒形貌和混合状态的差异可以更好的理解区域性污染特征，有利于了解区域性污染相关污染物的来源，摸清环渤海地区区域背景点的的单颗粒的老化过程，有利于更深入的研究区域性污染事件特别是雾霾发生时颗粒物的生成转化机制，从而对未来制定区域性污染控制对策提供有效的数据支持和理论依据。

第二章 观测实验与研究方法

2.1 研究区域概述

黄河三角洲位于环渤海经济区，北部滨临渤海，是京津冀地区与山东半岛的结合点，地处东经 117°15′-119°15′，北纬 36°41′-38°16′之间，地势平坦。黄河三角洲地处中纬度，位于暖温带，背陆面海，受欧亚大陆和太平洋的共同影响，属于暖温带半湿润大陆性季风气候区。

本次观测实验采样点位于黄河三角洲国家级自然保护区一千二管理站(38°03'N, 118°44'E)，黄河三角洲国家级自然保护区位于山东省东营市东北部黄河入海口处，是以保护黄河口湿地生态系统和珍稀濒危鸟类为主体的湿地类型自然保护区，人为活动影响较小。保护区附近无电厂和工业活动，最近的电厂距离采样点西南 58 公里。采样仪器放置在管理站内建筑四楼楼顶平台，距离地面约 15 米。具体采样点位置如图 2-1 所示：

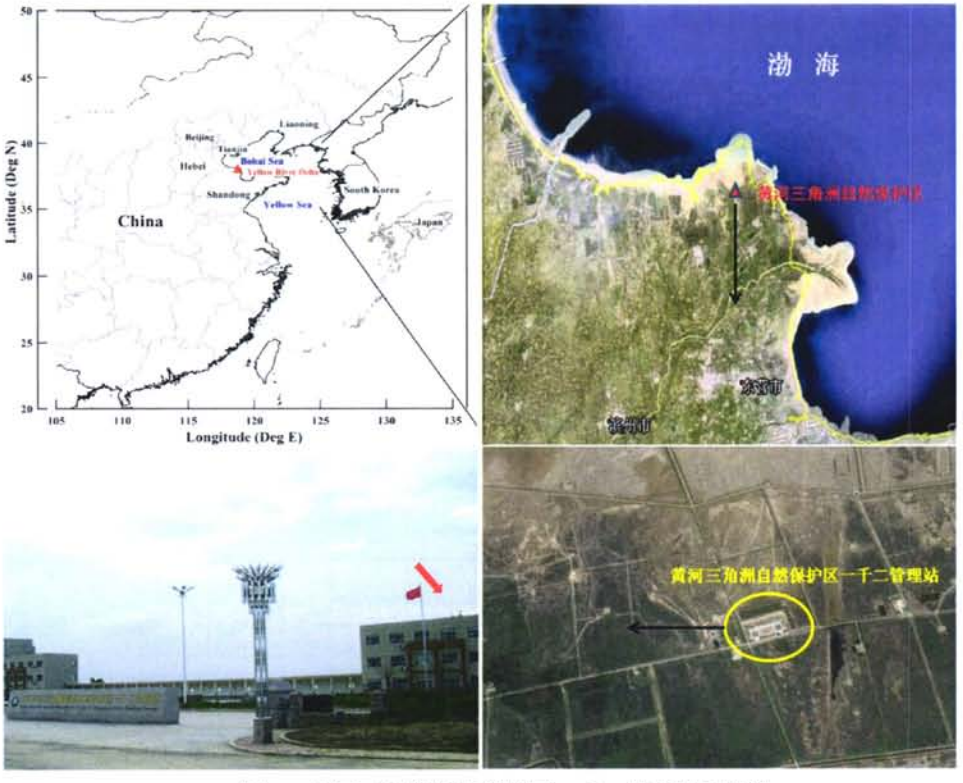

图 2-1 黄河三角洲自然保护区一千二管理站位置图

2.2 观测仪器与质量控制及保证

黄河三角洲大气气溶胶观测实验使用的主要仪器分为离线采样仪器和在线监测仪器，离线采样仪器主要包括美国 Thermo-Anderson 生产的 RAAS2.5-400 四通道 $PM_{2.5}$ 采样器以及 KB-2 型单颗粒采样器；在线监测仪器包括痕量气体分析仪器、$PM_{2.5}$ 在线离子色谱仪（URG9000B）、宽范围气溶胶粒谱仪（WPS）、能见度仪（PWD20，VAISALA）及锦州阳光自动气象站（见表 2-1）。

四通道 $PM_{2.5}$ 采样器主要是采集 $PM_{2.5}$ 膜样品，KB-2 型单颗粒采样器采集透射电镜分析所需的单颗粒样品。主要使用痕量气体分析仪器实时测量气态污染物浓度（O_3，SO_2，NO_y），使用在线离子色谱仪（URG9000B）测量 $PM_{2.5}$ 中水溶性离子浓度（Na^+、NH_4^+、K^+、Mg^{2+}、Ca^{2+}、F^-、Cl^-、NO_2^-、NO_3^-、SO_4^{2-}），使用宽范围气溶胶粒谱仪（WPS）测量不同粒径段颗粒物的数浓度、表面积浓度和体积浓度等，使用锦州阳光自动气象站测量温度（temperature, T）、相对湿度（relative humidity, RH）、风向（wind direction, WD）及风速（wind speed, WS）。

表 2-1 2011 年黄河三角洲地区气溶胶理化性质观测的主要实验仪器

编号	观测仪器	观测分析项目	数据收集/采样频率
1	RAAS2.5-400 四通道 $PM_{2.5}$ 采样器	$PM_{2.5}$	23 h 40 min
2	KB-2 型单颗粒采样器	单颗粒气溶胶	10-100 s
3	Thermo 49C	O_3	1 min
4	Thermo 42CY	NO_y	1 min
5	Thermo 43C	SO_2	1 min
6	URG9000B	Na^+、NH_4^+、K^+、Mg^{2+}、Ca^{2+}、F^-、Cl^-、NO_2^-、NO_3^-、SO_4^{2-}	1 h
7	WPS	气溶胶数浓度粒径分布	8 min
8	能见度仪	能见度	1 min
9	锦州阳光自动气象站	温度、相对湿度、风向、风速	10 min

2.2.1 $PM_{2.5}$膜采样仪器

美国 Thermo-Anderson 生产的 RAAS2.5-400 四通道 $PM_{2.5}$ 采样器共分四个通道，总采样流量为 48 L/min，各通道流量分别为 16.7 L/min、7.3 L/min、7.3 L/min、16.7 L/min，采用切割粒径为 2.5 μm 的旋风切割头。本实验 1-3 通道采用 Quartz 滤膜(Pall 公司)，第 4 通道采用聚四氟乙烯滤膜(Pall 公司)，滤膜孔径均为 1 μm，直径均为 47 mm。采样前 Quartz 滤膜需在马弗炉中 600℃高温下烘烤 2 小时，以消除残留或吸附的有机物影响；聚四氟乙烯滤膜采样前滤膜放置烘箱中在 60℃温度下烘烤 1-2 小时，以剔除杂质防止对采样结果的影响；滤膜在储存及运输过程中均需要避光保存，使用原滤膜盒保存采样后的滤膜，并将滤膜保存在−4℃的冰箱中。采样前后应将滤膜放置在恒温恒湿条件下(T=20±1℃，RH=50%±2%)24 小时，用百万分之一微量电子天平（ME5，Sartorius）对滤膜的重量进行称量。

膜采样过程质量控制和保证：1、采样前、采样期间定期、采样后对仪器的流量进行标定，对采样体积进行校验和修正。2、采样前、采样期间定期、采样后用无水乙醇清洗清洗采样仪器的切割头、采样管路和膜夹。

2.2.2 痕量气体分析仪

本次观测实验使用的 SO_2、O_3 和 NO_y 分析仪均使用美国热电公司(Thermo Electron Corporation)生产的 Model 43C、49C 和 42CY 型气体分析仪（见图 2-2）。二氧化硫分析仪（Model 43C）的原理是空气样品中的 SO_2 分子被 190-230 nm 的脉冲紫外光照射后被激发至激发态，从而发射出波峰为 330 nm 的荧光，利用 SO_2 浓度与荧光强度成正比的关系来测定 SO_2 的浓度。臭氧分析仪（Model 49C）的原理是利用臭氧分子吸收 254 nm 下的紫外光，依据朗伯-比尔定律可以直接根据样品气体对紫外光的吸收度计算样品气体中的臭氧浓度。NO_y 分析仪（Model 42CY）的原理是在采样口处放置钼转化炉，空气样品先经过钼转化炉在 350℃的高温条件下通过氧化钼（MoO）将其中的 NO_y 转化为 NO 后进行测量，而 NO 的测量原理是基于化学发光法，即 NO 与 O_3 反应生成激发态的 NO_2，激发态 NO_2 分子在跃迁回低能态时释放出的非散色性光的光强度与 NO 浓度呈线性关系，来测定 NO 的浓度。该仪器的检出限约为 50 pptv（2 min 测量值），精密度（2σ）

为 4%，不确定性约为 10%。二氧化硫分析仪和 NO_y 分析仪使用美国热电公司生产零气发生器（Model 111）、气体标定仪（Model 146C）以及济南德阳特种气体有限公司生产的瓶装标准气体进行标定，观测期间每隔 3 天对仪器的零点和不同浓度跨度做一次标定，而在每一期的观测实验前后对这些气体仪器进行多点标定对。臭氧分析仪每隔 3 天进行一次零点标定，每一期的观测实验前后使用臭氧标定仪（49C-PS）对仪器进行线性多点标定。

图 2-2 Thermo Electron SO_2、O_3、NO_y 气体分析仪

2.2.3 $PM_{2.5}$ 在线离子色谱仪

水溶性离子分析方法主要有传统的离线膜采样分析法和在线监测分析法。离线膜采样分析法将采集到滤膜上的样品在实验室对水溶性离子经行提取、分析，该方法被广泛应用于水溶性离子分析中。然而该方法忽略了NH_4NO_3的挥发损失[190]以及气态污染物（SO_2、HNO_3和NH_3等）在膜表面的颗粒物吸收[191-192]，从而对分析结果产生影响，同时传统的离线膜采样分析法采样周期长、时间分辨率低，因此无法较好的研究水溶性离子特征及反应机理，而在线监测分析法可以有效的弥补这些缺陷，本次研究就采用半连续的在线监测仪器对$PM_{2.5}$中的水溶性离子组分进行研究。

在线离子采样器采用的型号是美国 URG 公司的 URG9000B，AIM 对于主要的离子(SO_4^{2-}，NO_3^-，NH_4^+，Cl^-和 K^+)的监测结果和传统膜采样之间有很好的相关性(R=0.92-0.97)[31]。如图 2-3 所示，该仪器可分为气溶胶采集、水溶性离子提取和离子分析三部分。空气气流以 3 L/min 的流量经过 $PM_{2.5}$ 旋风切割头切割后将空气空力学直径小于 2.5 μm 的颗粒物抽入仪器内，先经过溶蚀器，溶蚀器中充满了 6 mmol/L 的 H_2O_2 溶液，用来去除 SO_2、NO_x、NH_3 等可能对结果产生影响的气体污染物，此后颗粒物在一个圆柱形玻璃体内与蒸汽发生器产生的水蒸气

相混合，将其中水溶性组分提取，经过螺旋冷凝管冷凝后，气体部分经过旋风分离器经气路通过泵排出，液体部分被收集收集在两个注射器中，每个样品的采样周期为一小时。离子分析采用的是两台 Dionex IC 90 型色谱仪，阴离子使用 Ionpac-AS14A 4×250 mm 分离柱、AMMS300-4 mm 抑制器，阳离子使用 Ionpac-CS12A 4×250 mm 分离柱、CSRS Ultra Ⅱ-4 mm 抑制器，均采用电导检测器。阴离子淋洗液为 3.5 mmol/L Na_2CO_3/1.0 mmol/L $NaHCO_3$，流速 1.2 mL/min;，阳离子淋洗液为 20 mmol/L 甲烷磺酸（MSA），流速 1.0 mL/min。淋洗液配制均使用电阻率为 18.2 MΩ 的超纯水（经 Milipore 纯水机过滤）。检测的无机水溶性离子组分为 F^-、Cl^-、NO_2^-、NO_3^-、SO_4^{2-}、Na^+、NH_4^+、K^+、Mg^{2+}和 Ca^{2+}，最低检出限分别是 0.011、0.022、0.015、0.017、0.084、0.017、0.010、0.090、0.018 和 0.015 μg/m^3。

实验过程中每隔3-4天更换一次淋洗液后配制一系列阴阳离子的标准溶液进行一次标准曲线校正，每天进一针标准溶液保证实验的平行性，以确保仪器数据的准确性和稳定性，标准溶液是由北京国家标准物质中心生产的。标准曲线的准确性是任何实验质控/质保的关键，配一系列阴阳离子标准溶液，在已确定的实验条件下，用标准工作液系列中各组分的峰面积或者峰高与浓度数据作标准曲线，相关系数均在 99.9%以上，证明了该方法的可靠性，可满足定量分析的需要。

配制淋洗液及进标准样品过程中戴无粉手套，以减少对样品的污染；实验所有使用的工具都经过超纯水处理，并在使用前抽样检查。每期实验前后，利用转子流量计检验仪器采样流量并进行校准，实验过程中也定期检查采样流量，每周清洗切割头和采样管路；每两周更换溶蚀器膜，以保证对干扰性气体的高效吸收。

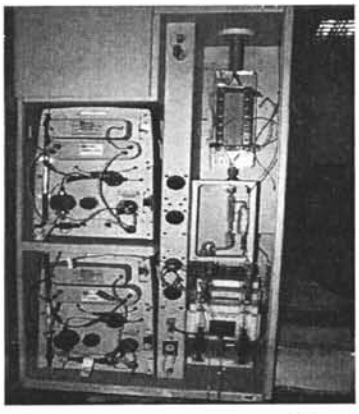

图 2-3 URG-9000B 系统

2.2.4 宽范围气溶胶粒谱仪（WPS）

本研究中测量气溶胶个数浓度及粒径分布的仪器是美国 MSP 公司研制生产的宽范围气溶胶粒谱仪（Wide-range Particle Spectrometer 1000 XP，WPS）（如图 2-4），测定粒径范围是 5 nm-10000 nm，该仪器利用激光气溶胶分光计（Laser Particle Spectrometer，LPS）测量 350 nm-10000 nm 的气溶胶数浓度粒径分布，利用微分动态分析仪（Differential Mobility Analyzer，DMA）与凝结核颗粒物计数器（Condensation Particle Counter，CPC）相结合来测定 5 nm-350 nm 粒径范围的气溶胶数浓度粒径分布。

空气样品以 1.0 L/min 的流量经过气溶胶电荷中和器进入仪器，其中 0.3 L/min 的样品空气进入微分动态分析仪（DMA）对颗粒物进行粒径分级，然后进入凝结核计数器（CPC），0.7 L/min 的样品空气进入激光气溶胶分光计（LPS）。WPS 中采用的微分动态分析仪（DMA）为一圆柱形部件，内部通过施加一个在 0-10000 伏特变化的电场将 5-500 nm 粒径段的颗粒物进行分级。凝结核颗粒物计数器（CPC）则是用来测量被 DMA 粒径分级后的颗粒物个数浓度，CPC 是含有饱和正丁醇蒸汽发生装置的热扩散检测器。空气样品进入 CPC 后，颗粒物先与正丁醇饱和蒸汽混合，再进入到温度为 10 摄氏度的冷凝器中，使颗粒物迅速增大到可以被光学检测器检测到粒径。CPC 部分具有双蓄池设计，可以分别储存工作液体（正丁醇）和冷凝废液。样品进入 CPC 的流量维持在 0.3 L/min，离开时先和 3 L/min 的干净空气混合，再经过仪器尾部排出。激光气溶胶分光计（LPS）是宽角度、单颗粒光学检测器，可用于测量 350 nm-10000 nm 的颗粒物粒径分布。当样品空气以 0.7 L/min 进入 LPS 后，由激光二级管产生激光束（785 nm，5mW）并照射在样品颗粒物上，通过颗粒物的反射作用，激光的反射光被一个散射角度为 20°至 100°球形镜面收集并投射到一个光电倍增管上。光电倍增管的电流脉冲信号转化为电压信号，并被信号放大期检测后输入下一级电路系统，将信号归类整理。

WPS 工作过程中最重要的是 DMA 和 LPS 对颗粒物粒径分离的准确性，因此要定期（一般是 1 年）对其进行校正。仪器校正采用 NIST SRM1691 和 SRM1963 PSL 标准颗粒（平均粒径为 269 nm 和 100.7 nm）。这种标准颗粒为人造橡胶颗粒，以悬浮状态存放在纯水中，标定时使用雾化装置将带有标准颗粒物

的雾水随一定流量的洁净空气打入 DMA 和 LPS，将 DMA 和 LPS 测量的粒径数值与人造颗粒物的真实数值相对比，对 DMA 和 LPS 的参数进行修正。每期实验前后都对 DMA 壳气进出口流量、DMA 采样气进出口流量、LPS 壳气及采样气进口流量等，使用标准流量计进行标定。

图 2-4 宽范围气溶胶粒谱仪（WPS）

2.2.5 气溶胶单颗粒采样器及分析仪器

本次研究使用KB-2型单颗粒采样器，样品以1 L/min的流量经过孔径为0.5 mm的采样头喷嘴，颗粒物样品在冲击器作用下被采集到外边缘为碳的铜膜上（如图2-5），铜膜外径为3 mm。如果假设颗粒物密度为2 g/cm^3，则对于粒径为0.15 μm的颗粒物的采样效率为50%，对于粒径大于0.25 μm的颗粒物的采样效率为100%[193]。采样时间根据当时能见度及污染状况，一般为10 s至100 s不等，每次采样后先通过显微镜观察颗粒物在铜膜中每个网格分布是否均匀，颗粒物数量是否适中，若观察到铜膜有破损或者颗粒物太多，需调整采样时间和采样流量，重新采集，保证之后样品在实验室中的分析。采样结束后样品放置在样品盒中，在恒温（25℃）恒湿（20±3%）的干燥器中保存，避免受到周围空气的影响。

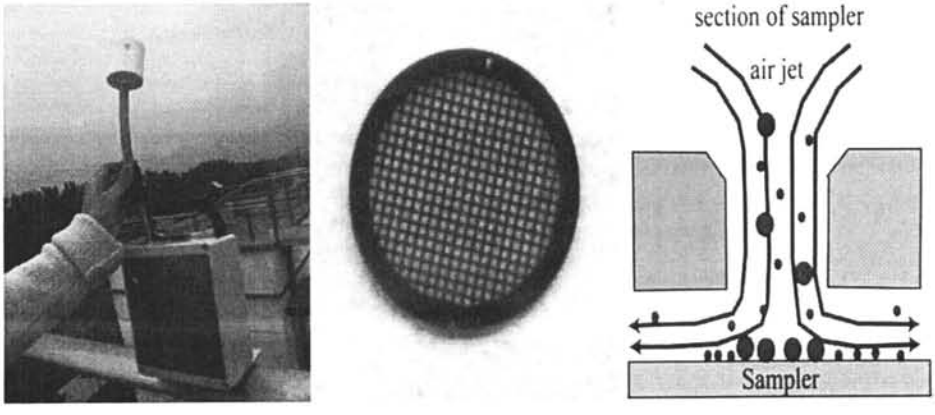

图 2-5 单颗粒采样器、采样铜膜及采样原理图

在实验室中使用透射电镜（Transmission Electron Microscope，简称TEM）（图2-6）放大500-800倍对样品进行分析，其主要原理就是电子束首先经过加速和聚集，然后投射到厚度非常薄的颗粒物样品上，电子与颗粒物样品中的原子发生碰撞然后改变其方向，从而产生立体角度的散射。由于散射角的大小与样品的厚度和密度相关，因此会形成明暗不同的影像，影像通过放大和聚焦之后在成像器件（如荧光屏、胶片、以及感光耦合组件）上显示出来。本研究中透射电子显微镜主要用来观察采集在铜膜上的颗粒物的粒径大小和形貌特征，颗粒物在铜膜中的分布并不均匀，粗颗粒一般处于铜膜中心网格内，而较细的颗粒则位于铜膜边缘的网格内。因此为了能够使分析的样品颗粒更具代表性，一般从中心位置和边缘位置分别选择三到四个网格进行电镜分析。利用X射线能谱仪（EDX）半定量分析颗粒物的元素组成，因为能谱分析会受到铜膜中铜的影响，因此铜不列入我们的研究，另外EDX检测不到N元素，而有机物等颗粒所含的C元素峰值非常强，明显高于铜膜边缘的碳膜所含的C峰，因此可以检测有机物中的C元素。颗粒物的粒径是通过和每一个颗粒物外边界最契合的椭圆的长轴和短轴的算术平均值来表示[194]。

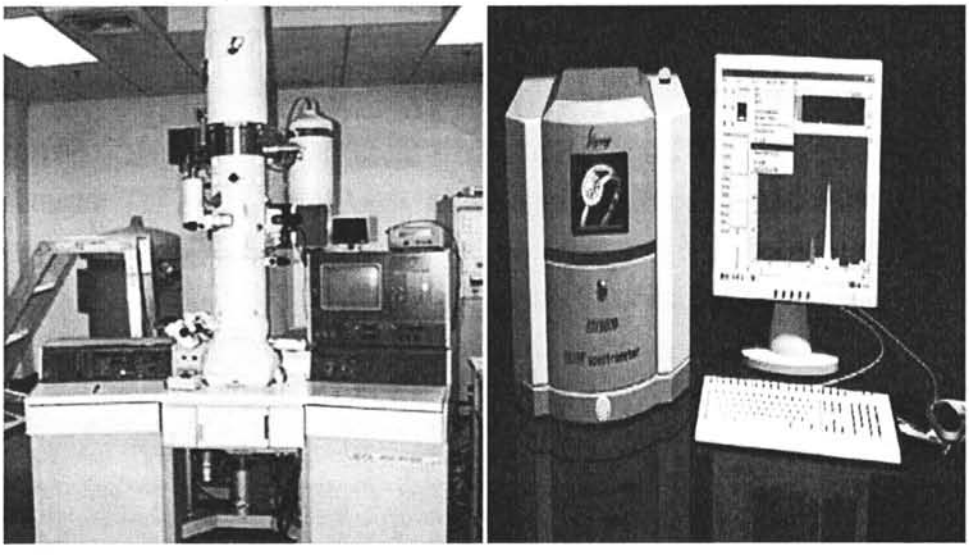

图2-6 透射电子显微镜（TEM）和X射线能谱仪（EDS）

2.2.6 能见度仪（PWD20，VAISALA）

芬兰 VAISALA 公司生产的 PWD20 型前向散射能见度仪(以下简称“能见度

仪")是全自动连续测量大气能见度的光学仪器。它主要是由发射机、控制接收机和处理器三部分构成。能见度仪采用红外管持续放射出中心波长为 875 nm 的一束红外光射入大气中，接收器将特定体积大气（0.1L）的前向散射光汇聚到光电传感器的接受面上，并通过将 PIN 光电二极管检测到的光强度转换为与大气能见度成反比关系的电信号，然后发送到计算机，利用数学模型计算出大气能见度值。它是在 3 个假设的基础上通过散射光强来有效地计算消光系数，即：(1)假定大气是均质的；(2)假定分子的吸收、散射或分子内部交互光学效应为零；(3)假定散射仪测量的散射光强正比于散射系数。仪器的测量范围为 10-20000 m。

图 2-7 VAISALA 公司生产的 PWD20 型能见度仪

2.2.7 自动气象站

采用锦州阳光科技发展有限公司生产的 PC-3 型自动气象站监测系统进行气象参数的收集。PC-3 自动气象站与通用的 PC 电脑配合使用，外接多路温度传感器、湿度传感器、风速风向传感器等。

2.3 研究方法

2.3.1 后推气流轨迹法

后推气流轨迹法是一种可以直观掌握大气中气团或粒子的传输运动轨迹的方法，并在大气综合观测的分析研究中得到非常广泛的应用[195-197]。为了计算后推气流轨迹，本文使用了美国海洋与大气管理局（National Oceanic and Atmospheric Administration，NOAA）空气资源实验室（Air Resources Laboratory，ARL）开发的混合型单粒子拉格朗日综合轨迹模式HYSPLIT（Hybrid Single

Particle Lagrangian Integrated Trajectory Model），版本为4.9，HYSPLIT模式采用的是地形跟随σ坐标系，σ定义为：

$$\sigma = (Z_{top} - Z_{msl}) / (Z_{top} - Z_{gl})$$

这里Z_{top}为模式顶的高度，Z_{gl}为地面高度，Z_{msl}为模式中垂直层次的高度，这里所有的高度都是海拔高度，模式垂直层次的定义使用二次函数：

$$Z_{msl} = aK^2 + bK + c$$

其中a=30，b=−25，c=5，而k为模式由下向上的垂直层次。使用这样函数关系可以保证低层分辨率较高：如第一层约10 m，第二层为75 m，第三层为200 m，...，第20层为11505 m；模式的水平分辨率则是根据输入气象场的水平网格来定义的。该模式支持各种投影坐标系的气象场，如极地投影、麦卡托投影和兰勃特投影等等，模式中使用通用的投影转换子程序[198]。

HYSPLIT模式支持多种坐标系统的气象场，包括压力坐标、σ坐标、压力σ混合坐标等等。模式需要的气象变量至少包括：水平风速（u，v）、气温T、高度Z或压力P，以及地表面压力P_0，相对湿度和垂直速度可选。所有输入的气象场首先根据不同的坐标系转换并插值到模式定义的坐标系统，然后模式进一步进行平流或扩散的计算。

模式中所采用的平流计算方法如下：

首先，若初始时刻粒子或气团中心的位置为P(t)，而经过Δt时间后的第一猜测位置为P′(t + Δt)，则：

$$P'(t + \Delta t) = P(t) + V(P,t) \times \Delta t$$

其中V(P,t)为经过时空插值的t时刻P位置处的速度向量。最后t+Δt时刻粒子或气团中心的最终位置由下式确定：

$$P(t+\Delta t)= P(t)+0.5\times[V(P,t)+V(P',t+\Delta t)]\times\Delta t$$

这种轨迹计算方法得到非常广泛的应用[199]。

关于粒子或气团垂直运动的计算，若输入的气象资料中已经包括了垂直速度场，此时可以直接使用气象资料中的垂直速度来计算垂直运动。如果输入气象资料中没有垂直速度场，可以假定污染物的垂直运动是沿着某一等值面运动而算出新的垂直速度，以代替原始资料中的垂直速度来计算垂直运动路径。假定气团或粒子沿着等η面做垂直运动，则在η面上垂直速度可以表示为：

$$w_\eta = \frac{-\frac{\partial \eta}{\partial t} - u\frac{\partial \eta}{\partial x} - v\frac{\partial \eta}{\partial y}}{\frac{\partial \eta}{\partial z}}$$

该式是由dη/dt=0推导出来的。其中η取为不同的变量即能得到不同类型的气流轨迹，如等压面（Isobaric）轨迹、等σ面（Isosigma）轨迹，等密度面（Isopycnic）轨迹或等熵面（Isentropic）轨迹等等，由于这些轨迹均是沿着某一等值面运动，所以它们又被统称为二维轨迹，以区别于使用实际大气垂直速度计算的三维轨迹。

本研究中将应用该模式计算后推气流轨迹并用于模拟观测期间到达观测点的气团运动路径，从而帮助分析长距离传输对水溶性离子及其它污染物分布的影响。轨迹计算的起点设在采样点黄河三角洲自然保护区(38°03'N, 118°44'E)上空50 m高度处，计算后推三天的轨迹，每一小时计算一条，然后根据轨迹之间在空间分布的相似性，用簇分析手段将这些轨迹分成若干类，簇分析的原则和处理过程在软件使用手册中有详细解释[200]。

2.3.2 主因子分析法

主因子分析（Principal Component Analysis，PCA）是定性研究大气组分的主要来源及控制因素的多元统计分析方法。其基本原理是将污染源看作若干个待求的因子，建立起污染源浓度数据与污染物因子之间的数学模型，再由该数学模型推导出两者之间的关系式，关系式一般为系数矩阵。解算得关系式后，需要对系数矩阵即因子载荷矩阵进行判断，从而判断出观测点的主要污染源的类型及其方差贡献率。本方法基本思想是把实测的多指标即多维向量用少数几个潜在的指标的线性组合来表示。大气污染物通常是来自同一污染源和多个污染源的叠加，并受到温度、湿度、风向风速等气象因素或其他未知因素的影响。主因子分析法就是从实测数据中找到影响污染物浓度的潜在因子，并给予正确的分析和合理的解释。主因子分析主要有两种类型：R型因子分析及Q型因子分析。本研究使用R型因子分析法，R型因子分析模型描述如下：

⑴原始观测变量和变换后的新变量均用x表示，$x = (x_1, x_2, \ldots, x_p)'$是可观测随机向量，均值向量E(x)=0，协方差阵Cov(x)=∑，且协方差阵∑与相关矩阵R相等（只要将变量标准化即可实现）；

(2)$F=(F_1, F_2, \ldots, F_m)'$（m<p）是不可测的向量，其均值向量E(F)=0，协方差矩阵Cov(F) =I，即向量F的各分量是相互独立的;

(3)$e=(e_1, e_2, \ldots, e_p)'$与F相互独立，且E(e)=0，e的协方差阵∑是对角阵，即各分量e之间是相互独立的，则模型：

$x_1 = a_{11}F_1 + a_{12}F_2 + \ldots + a_{1m}F_m + e_1$

$x_2 = a_{21}F_1 + a_{22}F_2 + \ldots + a_{2m}F_m + e_2$

……

$x_p = a_{p1}F_1 + a_{p2}F_2 + \ldots + a_{pm}F_m + e_p$

称为因子分析模型，由于该模型是针对正交因子变量进行的，所以也称为R型正交因子模型。模型的矩阵形式可以归结为：x =AF +*e*.

其中：

$x=(x_1,x_2,\ldots,x_p)'$，$A=\begin{pmatrix} a_{11}a_{12}\cdots a_{1m} \\ a_{21}a_{22}\cdots a_{2m} \\ \cdots\cdots\cdots\cdots \\ a_{p1}a_{p2}\cdots a_{pm} \end{pmatrix}$，$F=(F_1、F_2、\cdots F_m)'$，$e=(e_1, e_2, \cdots, e_p)'$

这里F是x的公共因子或潜因子，e是x的特殊因子，矩阵A是因子载荷矩阵。

2.3.3 酸度计算

由于通常情况下SO_4^{2-}、NO_3^-和NH_4^+三种离子占总水溶性离子的90%以上，占$PM_{2.5}$质量浓度的50%左右，SO_4^{2-}和NO_3^-是$PM_{2.5}$主要的酸性成分，NH_4^+则是$PM_{2.5}$主要的碱性成分，因此颗粒物的酸度可以由这三种离子控制[201]。目前国际上常用的表示酸度的方法有两种：强酸度（strong acidity，H^+_{strong}）和自由酸度（原位酸度，H^+_{air}）。

强酸度是气溶胶颗粒物中水溶性的酸碱离子的综合表征，一般通过计算阴阳离子之差所得的H^+的浓度（单位 nmol/m^3），而自由酸度是在气溶胶饱和液相溶液或者在液相气溶胶中的一些固相颗粒物中存在的自由 H^+的酸度，体现了真实存在的气溶胶中的自由酸酸度，一般利用热力学模型估算获得大气中 H^+的浓度（单位 nmol/m^3）。

2.3.3.1 强酸度（strong acidity，H^+_{strong}）和中和度（Neutralization degree，F）

本研究使用 SO_4^{2-}、NO_3^-和 NH_4^+的小时平均浓度计算 $PM_{2.5}$的强酸度（strong acidity, H^+_{strong}），但是这种方法不适用与粗颗粒（Ca^{2+}和 Mg^{2+}等浓度较高）及有机颗粒比例较高的情况。中和度（Neutralization degree，F）用来表示气溶胶颗粒物中酸性的物质被碱性物质中和的程度，一般用 NH_4^+和$(2\times SO_4^{2-}+NO_3^-)$的摩尔浓度的比值计算，即：$F=[NH_4^+]/(2\times[SO_4^{2-}]+[NO_3^-])$

式中$[NH_4^+]$、$[SO_4^{2-}]$和$[NO_3^-]$分别代表了各自的摩尔浓度（nmol/m^3）。当 F 的比值为 0 时代表没有酸性物质（SO_4^{2-}和 NO_3^-）得到中和，当 F 的比值大于 1 时表示酸性离子被 NH_4^+全部中和。当 0<F<1 时，强酸度 H^+_{strong}浓度可以通过酸碱离子浓度之差来计算，即

$$[H^+]_{strong}=[H^+]+[HSO_4^-]\approx([SO_4^{2-}]+[NO_3^-])-[NH_4^+]$$

2.3.3.2 自由酸度（原位酸度，H^+_{air}）和 pH

自由酸度（原位酸度，H^+_{air}）是指在已知颗粒物离子浓度的前提下，根据热动力学理论，通过计算机模拟得出单个颗粒物本身的酸度情况，本研究采用 AIM-II 模型进行计算(http://www.aim.env.uea.ac.uk/aim/aim.htm)，模型需要输入的参数包括 SO_4^{2-}、NO_3^-、NH_4^+的小时平均浓度、气温、相对湿度、H^+_{strong}，输出的结果包括气溶胶的自由酸度（H^+_{air}）、SO_4^{2-}、NO_3^-、NH_4^+、HSO_4^-和水含量的在空气中的摩尔浓度（mol/m^3）。根据自由 H^+的浓度以及液体的体积可以算出 H^+在液体中的浓度，继而求得 pH 值：

$$pH=-Log[\gamma\times H^+_{air}/(V_{eq}/1000)]$$

式中γ和V_{eq}代表H^+_{air}的活度系数（nmol/m^3）以及液体的体积（cm^3/m^3），需要注意的是液体的存在对于由AIM-II模拟H^+_{air}的方法非常重要，当环境湿度低于颗粒物的风化度（deliquescence Relitive Humidity）时，AIM-II会认为颗粒物是以纯颗粒态的形式存在的，也就不会有H^+_{air}的输出，另外当颗粒物处于完全中和的状态时（即F>1），AIM-II也不会有输出，因此在本研究仅对酸性颗粒物的酸度进行模拟。

2.3.4 颗粒物生成及增长速率

颗粒物的生成速率（Formation Rate，FR）和增长速率（Growth Rate，GR）在Kumala的研究中有过详细的介绍[202]。颗粒物粒径的增长速率用Growth Rate（GR）表示，通常用于衡量颗粒物成核之后颗粒物粒径从纳米级逐渐增大的快慢程度。凝结核模态颗粒物增长速率的计算公式为：

$$GR_{5\text{-}20}=\frac{\Delta dp}{\Delta t}=\frac{dp_2\text{-}dp_1}{t_2\text{-}t_1}$$

在公式中，t_1 和 t_2 代表粒径为 dp_1 和 dp_2 的颗粒物数浓度达到最大时的时间点。5-20 nm 粒径段颗粒物的生成速率($FR_{5\text{-}20}$) 的计算公式如下：

$$FR_{5\text{-}20}=\frac{dN_{5\text{-}20}}{dt}+CoagS_{dp=13nm}\times N_{5\text{-}20}+\frac{GR_{5\text{-}20}\times N_{5\text{-}20}}{15nm}$$

其中$\frac{dN_{5\text{-}20}}{dt}$是指5-20 nm粒径段的新颗粒物净生成速率，公式的第二项$CoagS_{dp=13nm}\times N_{5\text{-}20}$是指因为大颗粒物的碰并而损失的5-20 nm粒径段的新颗粒物，$CoagS_{dp=13nm}$是碰并汇，我们一般使用13 nm 的颗粒物来代表5-20 nm粒径范围内的颗粒物碰并汇(13 nm是5-20 nm的中位值)，公式的第三项$\frac{GR_{5\text{-}20}\times N_{5\text{-}20}}{15nm}$是指由于增长作用而超出5-20nm粒径段的新颗粒物。其中碰并汇计算方法如下：

$$CoagS_{dp=13nm}=\sum_j K_{ij}N_{dpj}$$

N_{dpj}表示粒径j的颗粒物数浓度，K_{ij}为粒径为dp_i和dp_j之间的碰并系数（coagulation coefficient，单位为cm^2/s）。计算方法如下：

$$K_{ij}=\frac{2\pi(D_i+D_j)(dp_i+dp_j)}{\frac{dp_i+dp_j}{dp_i+dp_j+2\left(g_i^2+g_j^2\right)^{\frac{1}{2}}}+\frac{8(D_i+D_j)}{\left(c_i^2+c_j^2\right)^{\frac{1}{2}}(dp_i+dp_j)}}$$

其中D_i和D_j表示粒径为dp_i和dp_j的颗粒物扩散系数，计算方法为：

$$D_i=\frac{kT}{3\pi\mu dp_i}\left(\frac{5+4K_{ni}+6K_{ni}^2+18K_{ni}^3}{5-K_{ni}+(8+\pi)K_{ni}^2}\right)$$

$$K_{ni}=\frac{2\lambda}{dp_i} \qquad g_i=\frac{\left[(dp_i+l_i)^3-\left(dp_i^2+l_i^2\right)^{3/2}\right]}{3dp_i l_i}-dp_i$$

$$l_i=\frac{8D_i}{\pi c_i} \qquad c_i=\left(\frac{8KT}{\pi m_i}\right)^{\frac{1}{2}}$$

其中g_i和l_i的单位为cm，c_i的单位为cm/s，m_i表示粒径为i的颗粒物质量，单位为kg，公式中使用的常数为：温度T=298 K，颗粒物密度ρ=1.0 g/m^3，分子平均自由程λ=6.65e^{-6} cm，空气速度μ=1.83e^{-4} g/(cm·s)，玻尔兹曼常数k=1.38e^{-23}。

第三章 黄河三角洲地区 $PM_{2.5}$ 水溶性离子特征

3.1 $PM_{2.5}$ 水溶性离子时间变化特征

3.1.1 $PM_{2.5}$ 水溶性离子浓度概况

2011年4月至2012年1月在黄河三角洲地区对$PM_{2.5}$中水溶性离子进行了四期在线观测，其中2011年4月26日至2011年5月4日代表春季，2011年7月8日到8月1日代表夏季，2011年10月16日至11月7日代表秋季，2011年12月12日至2012年1月8日代表冬季。图3-1所示为观测期间黄河三角洲地区$PM_{2.5}$中各水溶性离子的时间序列图，从图中可以看出，水溶性离子不同季节浓度变化明显，且在夏秋冬三季有明显的污染物积累过程。不同季节的水溶性离子质量浓度的统计结果如表3-1所示，总水溶性离子质量浓度年平均值为49.72±49.89 μg/m^3，浓度范围为1.17~262.72 μg/m^3。$PM_{2.5}$中水溶性离子质量浓度的高低顺序依次为SO_4^{2-}>NO_3^->NH_4^+>Cl^->Na^+>K^+>NO_2^->Ca^{2+}>Mg^{2+}，年平均质量浓度（±标准偏差）分别为22.48±25.18、12.77±14.49、11.21±11.68、1.31±1.76、0.66±0.54、0.65±0.44、0.33±0.25、0.19±0.39、0.10±0.15 μg/m^3，F^-在观测期间浓度太低，低于仪器的检测限。其中SO_4^{2-}、NO_3^-和NH_4^+平均质量浓度总和为46.52±48.25 μg/m^3，约占总水溶性离子的93.6%，其中SO_4^{2-}是占比最高的水溶性离子，约占总水溶性离子的45.2%，其次为NO_3^-和NH_4^+，Cl^-、NO_2^-、Na^+、K^+、Mg^{2+}和Ca^{2+}浓度之和仅占总水溶性离子的6.4%（如图3-2）。

气溶胶中NO_3^-与SO_4^{2-}的质量浓度比值可以用来表征固定源（如燃煤、石油等）和移动源（如汽车尾气）对大气污染中硫和氮的贡献[203-204]。本研究中观测期间[NO_3^-]/[SO_4^{2-}]质量浓度年平均比值为0.57，其中春季为0.89，夏季为0.40，秋季为0.78，冬季为0.67。该比值略高于国内的济南（0.44）、西安（0.46）和福州（0.41）等[31,205,206]。黄河三角洲地区的比值略高于国内其它城市可能是由于黄河三角洲地区作为沿海地区，相对湿度远高于内陆的济南和西安，较高的相对湿度有利于$PM_{2.5}$硝酸盐的生成。同时也由于黄河三角洲地区所在城市东营的能源结构与其他城市有些不同，东营是我国石油天然气的重要产地，煤炭并不是当

地的主要能源。而本研究的[NO_3^-]/[SO_4^{2-}]质量浓度年平均比值远低于美国加州（6.9）[207]和洛杉矶市区（2）[208]。这说明黄河三角洲地区的固定源对$PM_{2.5}$的贡献更大。从季节变化来看，夏季的NO_3^-与SO_4^{2-}质量浓度比值最低，这可能是由于夏季由于较强的光化学作用硫酸盐的浓度明显高于其他季节，而夏季温度较高，高温会导致硝酸铵的蒸发分解，造成一定的硝酸盐的损失。

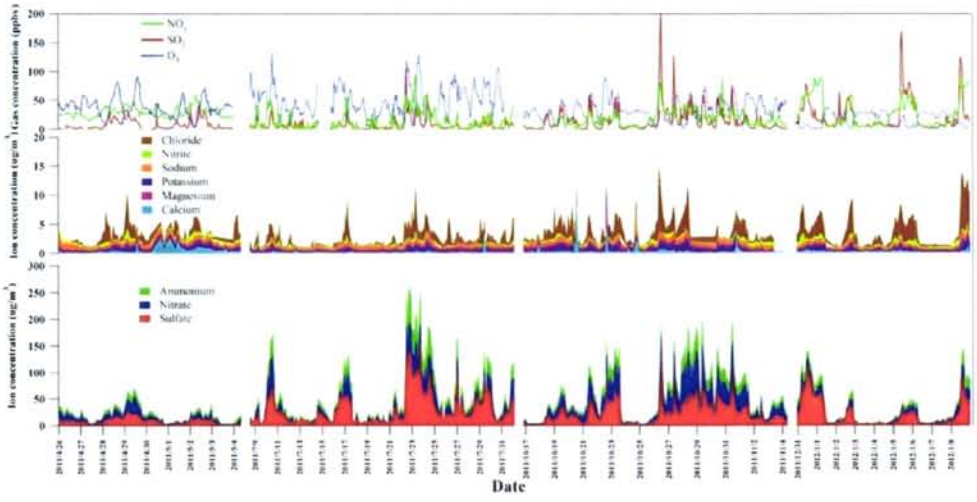

图3-1 黄河三角洲地区观测期间水溶性离子及气态污染物浓度时间变化序列图

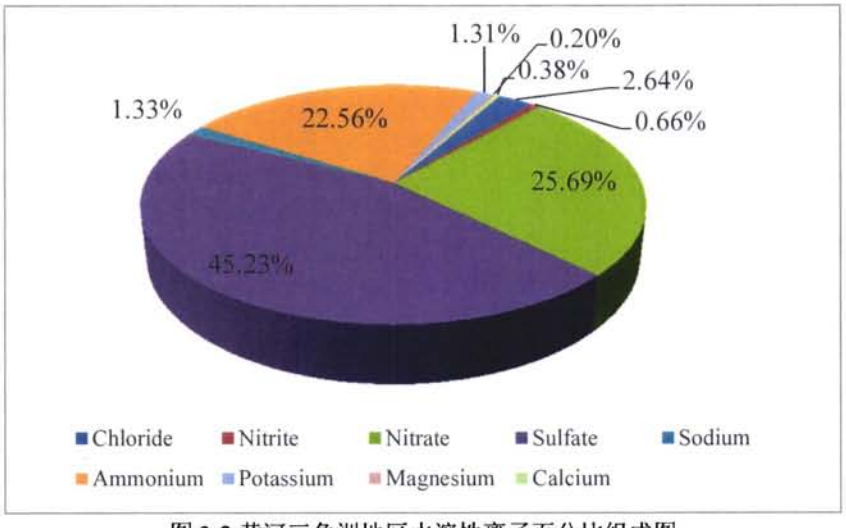

图 3-2 黄河三角洲地区水溶性离子百分比组成图

表3-1 黄河三角洲地区$PM_{2.5}$中水溶性离子在全年四个季节的平均浓度（$\mu g/m^3$）

		Cl^-	NO_2^-	NO_3^-	SO_4^{2-}	Na^+	NH_4^+	K^+	Mg^{2+}	Ca^{2+}	总水溶性离子
春季（N=204）	平均值	1.12	0.40	7.25	8.19	0.75	5.31	0.63	0.14	0.46	24.25
	标准偏差	1.14	0.23	6.26	5.82	0.41	3.55	0.31	0.09	0.54	15.98
	最大值	6.10	1.59	31.95	27.20	5.26	16.19	2.64	0.54	2.55	73.80
	最小值	0.03	0.02	0.66	1.00	0.04	0.40	0.17	0.05	0.03	4.08
夏季（N=567）	平均值	0.91	0.23	12.10	30.32	0.57	15.06	0.54	0.09	0.09	59.91
	标准偏差	1.08	0.16	13.84	30.07	0.17	14.41	0.27	0.03	0.19	57.84
	最大值	7.42	1.12	56.73	153.24	1.31	63.70	1.99	0.29	3.25	262.72
	最小值	0.04	0.02	0.33	2.49	0.14	0.73	0.22	0.04	0.02	5.17
秋季（N=446）	平均值	1.34	0.34	18.72	23.95	0.71	12.03	0.85	0.13	0.13	58.20
	标准偏差	1.56	0.20	17.48	20.76	0.27	10.67	0.47	0.27	0.53	47.73
	最大值	11.28	0.86	77.35	129.27	3.73	48.92	2.32	4.58	8.32	208.60
	最小值	0.03	0.02	0.59	0.82	0.26	0.06	0.12	0.02	0.02	4.47
冬季（N=312）	平均值	2.26	0.42	7.28	19.62	0.70	7.13	0.65	0.05	0.05	38.26
	标准偏差	2.70	0.39	8.11	24.45	1.03	8.26	0.59	0.04	0.13	42.01
	最大值	17.12	4.05	32.35	113.81	17.29	32.61	2.33	0.27	1.27	156.67
	最小值	0.05	0.02	0.03	0.22	0.12	0.34	0.10	0.02	0.03	1.17
年平均（N=1529）	平均值	1.31	0.33	12.77	22.48	0.66	11.21	0.65	0.10	0.19	49.70
	标准偏差	1.76	0.25	14.49	25.18	0.54	11.68	0.44	0.15	0.39	49.89
	最大值	17.12	4.05	77.35	153.24	17.29	63.70	2.64	4.58	8.32	262.72
	最小值	0.03	0.02	0.03	0.22	0.04	0.06	0.10	0.02	0.02	1.17

硫酸盐氧化率（sulfate oxidation rate，SOR）和硝酸盐氧化率（nitrate oxidation rate，NOR）用来反应SO_2和NO_y向硫酸盐和硝酸盐的转化率，计算方法分别为$SOR= SO_4^{2-}/(SO_4^{2-}+SO_2)$、$NOR= NO_3^-/NO_y$。黄河三角洲地区观测期间四季SOR和NOR的值绘于图3-3中，从图中可以看出，四季SOR和NOR的值均大于0.10，说明黄河三角洲地区的SO_4^{2-}和NO_3^-主要是来自SO_2和NOy的氧化[145]。夏季的SOR值最高（0.65），硫酸盐主要通过非均相气粒转化和液相氧化两种途径反应生成，其中非均相气粒转化主要是受温度、太阳辐射强度和OH自由基的影响[209]，而液相氧化主要受相对湿度和氧化剂（H_2O_2和O_3等）有关[210]。夏季高温以及较强的辐射有利于非均相气粒转化，而较高的湿度以及较高的O_3浓度则有利于液相反应，因此夏季的光化学反应较强，从而使硫酸盐的转化率远高于其它三个季节。NOR则是秋季最高（0.57），冬季最低。

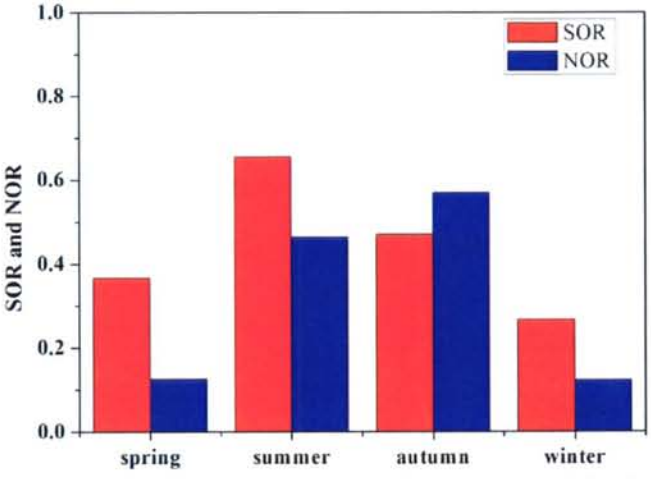

图 3-3 黄河三角洲地区观测期间四季 SOR 和 NOR 变化图

为了解黄河三角洲地区$PM_{2.5}$中水溶性离子的污染状况，将本研究的结果（SO_4^{2-}、NO_3^-和NH_4^+）与国内外其它城市及郊区站点的研究结果进行对比（表3-2）。黄河三角洲地区$PM_{2.5}$中SO_4^{2-}、NO_3^-和NH_4^+的质量浓度仅低于国内的济南和西安以及印度的赖普尔，而远高于美国、日本和韩国的城市及郊区站点，与国内一些大城市相当。说明黄河三角洲地区面临严重的二次无机气溶胶污染，这可能是由于环渤海地区特别是山东省和河北省的一次污染物（如SO_2和NO_x）排放量高(如图3-4所示)，通过气团区域传输和化学反应对黄河三角洲地区的气溶胶化学组分产生较大的影响，同时观测期间特别是夏秋季节雾霾发生频繁，也是导

致水溶性离子浓度较高的原因之一。

表 3-2 黄河三角洲地区与国内外其他站点 $PM_{2.5}$ 中主要水溶性离子 SO_4^{2-}、NO_3^-和 NH_4^+的质量浓度 ($\mu g/m^3$)

Site	Type	Time	Major ions concentrations ($\mu g/m^3$)			References
			NO_3^-	SO_4^{2-}	NH_4^+	
Yellow River Delta	Rural/ coastal	2011-2012	12.77	22.48	11.21	本研究
Jinan, China	Urban	Dec 2007-Oct 2008	15.77	38.33	21.26	Gao et al., 2011[31]
Xi'an, China	Urban	Mar 2006-Mar 2007	16.4	35.6	11.4	Zhang et al., 2011[205]
Guangzhou, China	Urban	Apr 2007	9.5	21.6	7.3	Tao et al., 2009[211]
Beijing, China	Urban	June-August 2011	12.4	9	8	Sun et al., 2012[212]
Shanghai, China	Urban	summer 2010	8.04	16.66	8.75	Zhang et al., 2013[213]
Tianjin,China	Urban	2008	12.0	19.1	6.1	古金霞等, 2013[214]
Taibei Summer	Urban	Aug 2003	1.71	3.47	2.04	Chang et al., 2007[218]
Taibei Winter	Urban	Dec 2003-Jan 2004	3.66	12.01	5.67	
Qingdao, China	Coastal	1997-2000	3.4	11.94	5.79	Hu et al., 2002[215]
Xinken, China	Rural/ coastal	Oct-Nov 2004	7.2	24.1	9.2	Hu et al., 2008[216]
Chongming Island, China	Rural/ coastal	Jun 2006	10.89	23.14	10.28	Li et al.,2010[217]
Jianfengling Nature Reserve, China	Rural/ coastal	Nov 2007	0.13	2.17	0.56	
Saitama City,Japan	Urban	Jan.2010	5.67	2.26	2.22	Kim et al., 2011[220]
Cario, Egypt	Urban	Nov 2004-Mar 2005	6.1	14.2	2.5	Favez et al., 2008[221]
Raipur, India	Urban	Apr 2005-Mar 2006	8.16	46.5	8.76	Verma et al., 2010[222]
Dearborn, USA	Urban	July-Aug 2007	0.81	3.69		Pancras et al.,2013[223]
Brigantine, USA	Rural/ coastal	Nov 2003	1.26	2.27	1.32	Lee et al., 2008[224]
Gwangju,Korea	Rural	Oct.-Nov 2003	2.89	3.86	2.62	Hong et al., 2008[219]

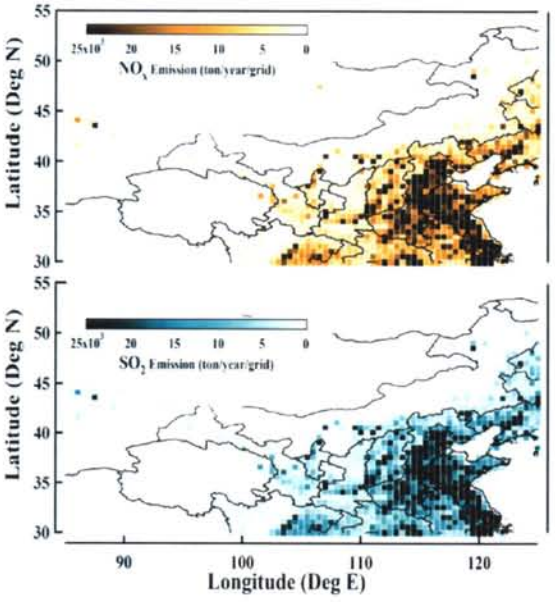

图3-4 中国2006年SO_2 and NO_x排放强度地区分布图[21]

3.1.2 $PM_{2.5}$水溶性离子浓度日变化

对$PM_{2.5}$中主要水溶性离子的质量浓度日变化的研究有助于认识细颗粒物化学组分的浓度变化、气固相化学转化、气团输送及一次排放等过程的关系。图3-5为观测期间四季主要水溶性离子（SO_4^{2-}、NO_3^-和NH_4^+）、气体污染物（SO_2、NO_y和O_3）及主要气象因素（温度、相对湿度）的日变化图。

SO_4^{2-}的质量浓度在夏、秋和冬三个季节均表现出昼高夜低的日变化特征，SO_4^{2-}质量浓度在日出后随着边界层的升高而开始上升，在12:00-13:00左右出现峰值，夏季峰值维持时间最长，一直维持到17:00左右，秋冬季节峰值维持1-2小时，然后随着温度、边界层及太阳辐射强度的降低，SO_4^{2-}浓度也逐渐下降。相关气体污染物SO_2及O_3的浓度也呈现类似的昼夜变化特征。此类日变化特征主要是由于白天随着太阳辐射的增强，光化学氧化反应增强从而产生更多的SO_4^{2-}。夏季SO_4^{2-}峰值持续时间较长也可能与白天高辐射强度条下局地新颗粒物的生成有关[225]。春季SO_4^{2-}变化趋势较为平稳，不同于其它季节，长距离气团输送可能起主导作用,各种污染物浓度昼夜变化不显著。

与冬季相比，NO_3^-在春夏秋三个季节均表现出上午高下午低的日变化特征。秋季NO_3^-质量浓度日出后迅速升高，在9:00左右出现峰值，之后浓度迅速降低，

在下午的 18:00 左右达到最低浓度，夜间 NO_3^-质量浓度又开始缓慢升高。太阳辐射和温度是影响 NO_3^-浓度日变化的主要因素。在细颗粒物中 NO_3^-主要以硝酸铵形式存在，白天随着太阳辐射的增强以及温度的升高，硝酸铵分解生成硝酸气和氨气，导致在正午 12:00 前后 NO_3^-浓度持续降低，而夜间温度降低而相对湿度增大，有利于硝酸气向颗粒态的 NO_3^-转化，从而导致夜间 NO_3^-浓度的升高。

NH_4^+主要是来自于大气中的酸性气体（如 H_2SO_4、HNO_3、HCl、HNO_2）与氨气反应生成的铵盐，因此铵盐存在形式对 NH_4^+的日变化特征有重要影响。在春、夏、秋三个季节，NH_4^+的质量浓度日变化与 SO_4^{2-}、NO_3^-有相似的日变化特征，最大值出现在正午前后，最低值出现在下午。因此 NH_4^+的日变化特征受 SO_4^{2-}和 NO_3^-控制，进一步说明黄河三角洲地区大气细颗粒物中$(NH_4)_2SO_4$和 NH_4NO_3是铵盐重要的存在形式。

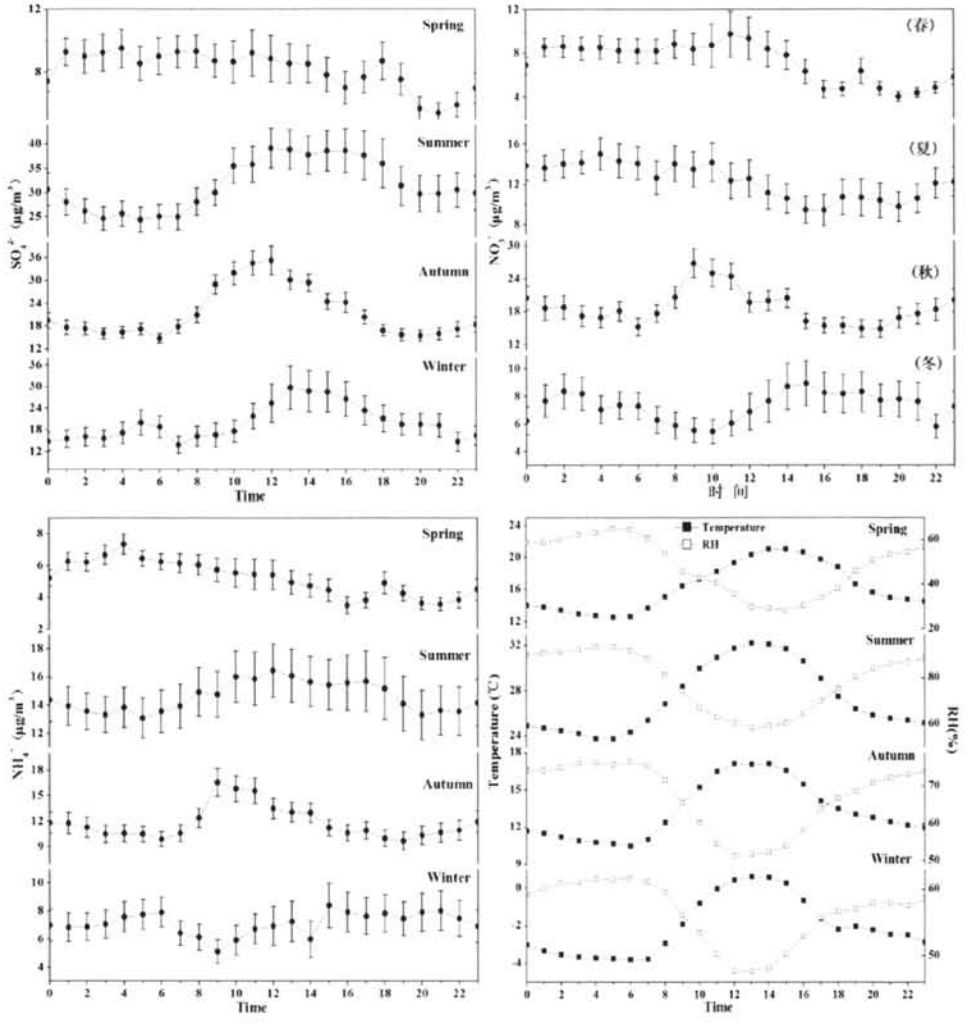

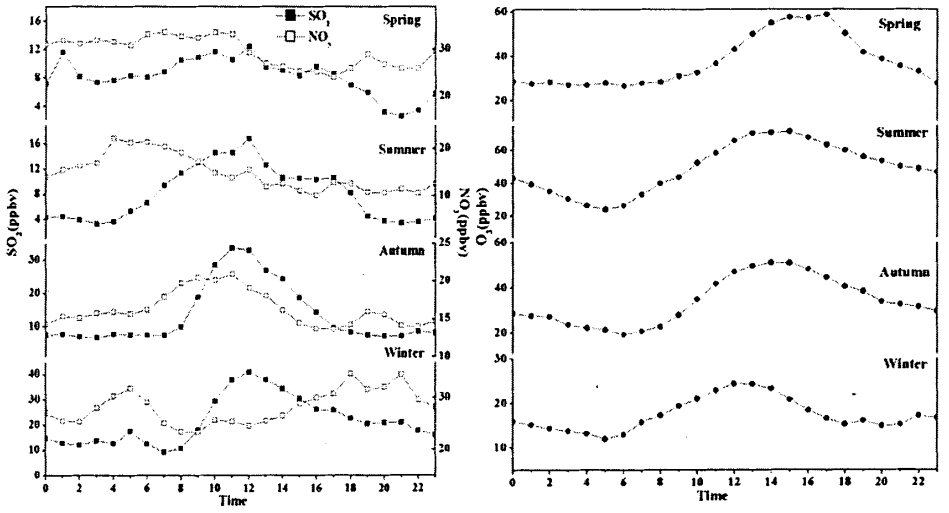

图 3-5 黄河三角洲地区观测期间不同季节 $PM_{2.5}$ 中 SO_4^{2-}、NO_3^-和 NH_4^+的质量浓度、气态污染物（SO_2、NO_y、O_3）以及气象参数（温度、相对湿度）日变化图

3.1.3 $PM_{2.5}$水溶性离子浓度季节变化

SO_4^{2-}是所有水溶性离子中年均浓度最高的一种离子，质量浓度年平均值为 22.48±25.18 μg/m^3，浓度最大值为 153.24 μg/m^3，夏季 SO_4^{2-}浓度最高（30.32 μg/m^3），其次分别是秋季（23.95 μg/m^3）、冬季（19.62 μg/m^3）和春季（8.19 μg/m^3）。SO_4^{2-}夏季浓度较高的原因可能是夏季光化学氧化剂（O_3）浓度较高，同时强的太阳辐射以及高温高湿都有利于硫酸盐通过光化学反应产生。秋季浓度较高可能是因为观测期间秋季的湿度也较高，同时气团的长距离传输也可能对当地的硫酸盐浓度有一定贡献。冬季的气象条件较差，易出现逆温现象，大气扩散系数较低，不利于污染物的扩散，同时冬季燃煤取暖也会排放较高浓度的 SO_2，导致冬季的 SO_4^{2-}浓度也较高。

NO_3^-质量浓度年平均值为 11.21±11.68 μg/m^3，浓度最大值为 63.70 μg/m^3，秋季 NO_3^-浓度最高（18.72 μg/m^3），其次分别是夏季（12.10 μg/m^3）、冬季（7.28 μg/m^3）和春季（7.25 μg/m^3）。NO_3^-的形成主要受到热力学平衡反应的影响，夏季高温，使得不稳定的 NH_4NO_3 容易分解，形成挥发性的 NH_3 和 HNO_3 气体，而使得夏季硝酸盐浓度有一定程度的降低。

NH_4^+质量浓度年平均值为 12.77±14.49 μg/m^3，浓度最大值为 77.35 μg/m^3，夏季 NH_4^+浓度最高（15.06 μg/m^3），其次分别是秋季（12.03 μg/m^3）、冬季（7.13 μg/m^3）和春季（5.31 μg/m^3），这与 SO_4^{2-}的季节变化趋势相同。夏季气温较高，

从而导致动植物尸体腐烂以及土壤微生物的排放加剧，同时由图 3-6 和 3-7 所示，SO_4^{2-}、NO_3^-与 NH_4^+的质量浓度观测期间具有很好的相关性，相关系数分别为 0.92 和 0.88，因此夏季高浓度的 SO_4^{2-}有利于 NH_4^+以颗粒物形态的$(NH_4)_2SO_4$形式存在，秋季高浓度的 NO_3^-有利于 NH_4^+以颗粒物形态的 NH_4NO_3 形式存在。夏季 NH_4^+出现浓度高值另一原因是由于采样期间夏季雾、霾等污染现象频发，研究证明，雾霾天气下 NH_3 的二次转化反应会加剧[226]，从而导致 NH_4^+质量浓度的升高。

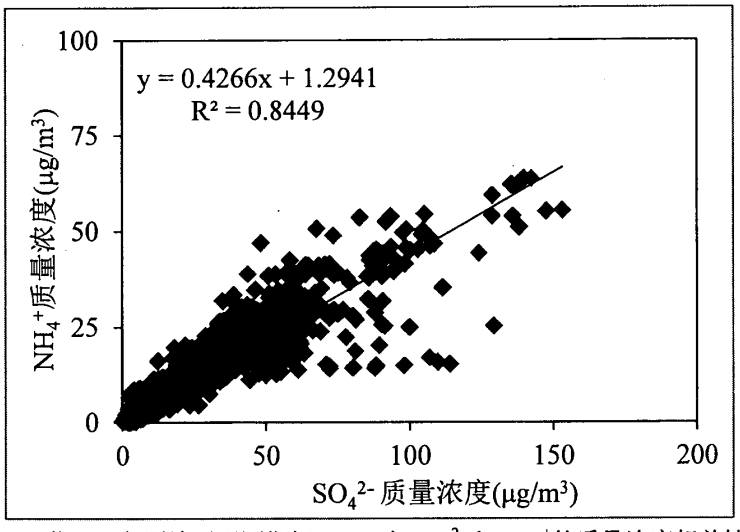

图 3-6 黄河三角洲地区观测期间 $PM_{2.5}$ 中 SO_4^{2-}和 NH_4^+的质量浓度相关性图

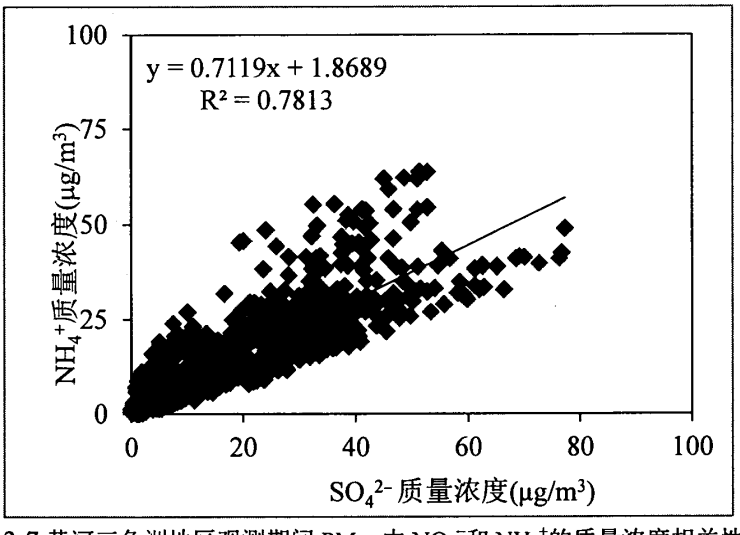

图 3-7 黄河三角洲地区观测期间 $PM_{2.5}$ 中 NO_3^-和 NH_4^+的质量浓度相关性图

3.2 $PM_{2.5}$酸度变化特征

本研究经过数据筛选，共有 1450 个小时的数据用来研究颗粒物酸度，使用中和度（Neutralization degree，$F = [NH_4^+]/(2\times[SO_4^{2-}]+[NO_3^-])$）用来表示气溶胶中 SO_4^{2-}和 NO_3^-被 NH_4^+的中和程度并绘于图 3-8 中。本研究将 F≤0.9 的颗粒物定义为酸性颗粒物，F≤0.75 的颗粒物定为强酸性颗粒物。通过计算结果显示黄河三角洲地区观测期间颗粒物中和度 F 年平均值为 0.89，说明该地区大气颗粒物具有一定酸性。在春季和夏季分别有 35.4%和 45.6%的颗粒物为酸性颗粒物（F≤0.9），其中仅有 11.1%和 8.9%的颗粒物为强酸性颗粒物（F≤0.75）。而在秋季和冬季酸性颗粒物的比重升高明显，分别有 50.1%和 62.4%的颗粒物是酸性颗粒物，其中有 22.5%和 32.1%的颗粒物为强酸性颗粒物。

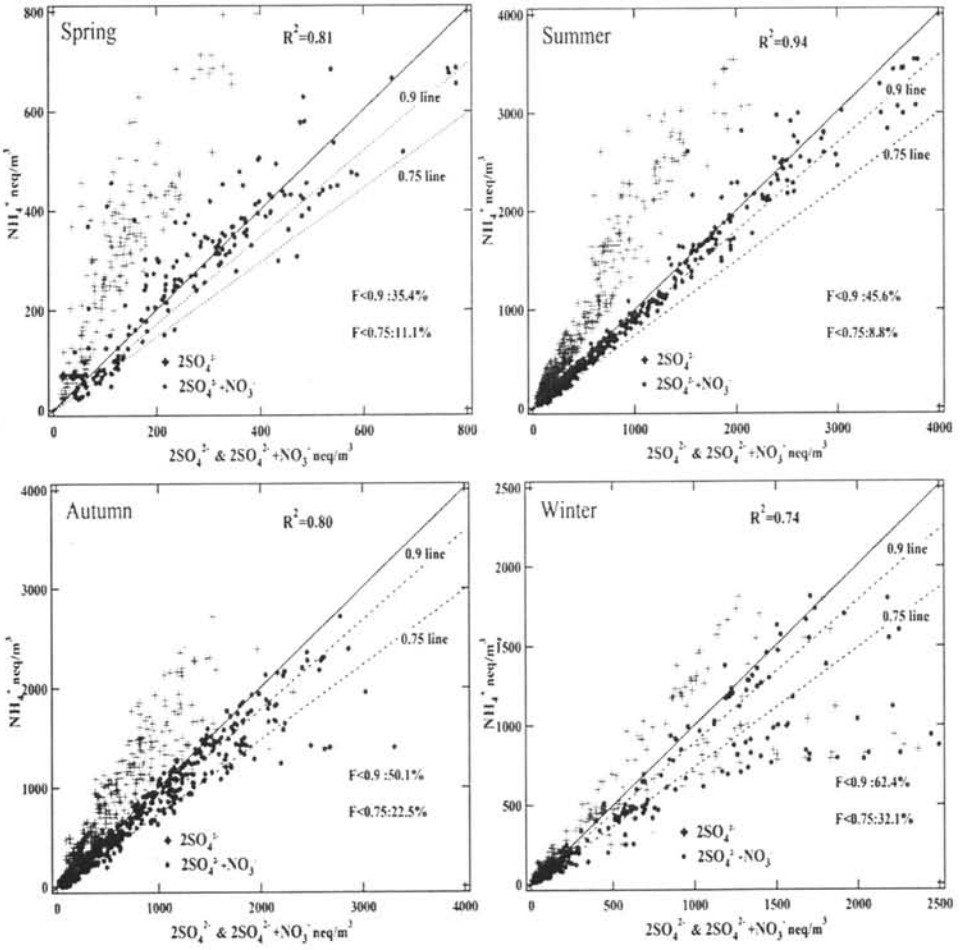

图 3-8 黄河三角洲地区不同季节 $PM_{2.5}$中和度分布图

通过 AIM-II 模型计算得到黄河三角洲地区观测期间酸性颗粒物（共有 850 小时的数据）的 PH、强酸度（H^+_{strong}），自由酸度(H^+_{air})、水含量（water content）的浓度汇总在表 3-3 中。黄河三角洲地区酸性颗粒物的强酸度（H^+_{strong}）、自由酸度(H^+_{air})和水含量（water content）的年均浓度为 125.28nmol/m^3、25.55 nmol/m^3 和 60.80 μg/m^3。冬季酸性颗粒物的强酸度（H^+_{strong}）和自由酸度(H^+_{air})浓度最高，分别为 251.24 nmol/m^3 和 76.03 nmol/m^3，分别是秋季的 2 倍和 3 倍、夏季的 3 倍和 7 倍以及春季的 4 倍和 12 倍。而夏季酸性颗粒物的水含量浓度最高，为 91.79 μg/m^3。和国内其他站点的颗粒物酸度结果对比显示，黄河三角洲地区的酸性颗粒物酸度低于泰山、北京和上海等地，而高于衡山、兰州和广州。

表 3-3 黄河三角洲地区 $PM_{2.5}$ 酸度及与国内外观测结果的对比

Location	Season	H_{air}^+ (nmol/m^3)	H_{strong}^+ (nmol/m^3)	HSO_4^- (nmol/m^3)	Water content (μg/m^3)	Reference
Yellow River Delta	Spring	6.60±6.37	60.10±50.72	41.07±40.67	7.70±8.45	This study
	Summer	11.37±11.36	81.48±96.83	64.49±83.27	91.79±128.92	
	Autumn	24.31±49.86	132.93±183.07	96.32±130.40	48.50±58.88	
	Winter	76.03±149.37	251.24±358.83	155.43±217.48	24.69±34.39	
	Annual	25.55±68.34	125.28±197.14	89.09±131.96	60.80±95.42	
Mt.Tai, China	Spring 2007	25.25±32.23	64.82±75.07	-	47.89±77.14	Zhou et al., 2012[20]
Mt.Tai, China	Summer 2007	35.27±30.38	142.65±115.23	-	78.57±136.99	
Mt.Heng, China	Spring 2009	13.3±15.4	53.4±38.7	-	67.7±143.3	Gao et al., 2012[227]
Beijing, China	Summer 2004-2006	-	326±421	-	66±89	Pathak et al., 2011[228]
Shanghai, China		-	196±201	-	27±24	
Lanzhou, China		-	59±49	-	9±12	
Guangzhou, China		-	90±60	-	60±80	
Hongkong, China	Spring 2000	-	49	-	-	Pathak et al., 2003[83]
	Summer 2000	-	27	-	-	
Pittsburgh, USA	Sept 2002	-	28	-	-	Zhang et al., 2007[65]

"-" 表示无数据

另外，NH_4^+和 SO_4^{2-}的摩尔浓度比值[NH_4^+]/[SO_4^{2-}]通常用来研究颗粒物中硫酸铵以及硝酸铵的存在，当该比值大于 1.5 时，认为处于富铵状态（ammonium-rich），NO_3^-经过气态均相反应生成 NH_4NO_3 的过程会明显存在[41]。以[NH_4^+]/[SO_4^{2-}]的摩尔比值和[NO_3^-]/[SO_4^{2-}]的摩尔比值作图 3-9，结果显示，黄河三角洲地区观测期间在春季、夏季和秋季 90%以上的样品，冬季 80%的样品的[NH_4^+]/[SO_4^{2-}]比值高于 1.5，且 NO_3^-与 NH_4^+质量浓度的相关系数均高于 0.9，这说明在观测期间 NO_3^-主要来自气态 NH_3 和 HNO_3 的均相反应。而冬季 20%的样品是处于贫铵状态，[NH_4^+]/[SO_4^{2-}]比值低于 1.5。冬季 NH_4^+的质量浓度为 7.13 $\mu g/m^3$, 远低于夏季的浓度(15.06 $\mu g/m^3$)，冬季 NH_4^+浓度较低主要是由于冬季低温环境下 NH_3 的低排放[229]，由图 3-8 可知，冬季贫铵状态下[NO_3^-]/[SO_4^{2-}]的摩尔比值也较低，说明冬季贫铵时 SO_4^{2-}在中和 NH_4^+中起主导作用。如图 3-8 所示，秋季贫铵状态下，仍有部分样品[NO_3^-]/[SO_4^{2-}]的摩尔比值接近 1（图中红色椭圆形框内显示的点位）。

有资料显示，夜晚在气溶胶潮湿表面 N_2O_5 的非均相水解反应对于在贫铵状态下高浓度的硝酸盐有重要贡献，实验室研究表明，气溶胶吸湿性和表面积越大，酸度越高，越有利于促进 N_2O_5 的非均相水解反应[230-231]。其他实验室研究也表明，在较高的湿度条件下，N_2O_5 的吸收系数也会升高[232]。水在气溶胶表面通过复杂的方式对 N_2O_5 的非均相水解反应起到至关重要的作用。一方面较高的湿度会使气溶胶具有更高的水含量以及更大的表面积，这就促进了气溶胶表面对 N_2O_5 的吸收。另一方面，气溶胶水含量的提高也会是气溶胶的自由酸度降低，从而降低 N_2O_5 的吸收。从图 3-10 中可以看出，在秋季贫铵环境下样品中，有三个样品的湿度更高，水含量浓度较高，同时这些样品的气溶胶酸度较高，从而有利于 N_2O_5 的水解，促进硝酸盐的生成。从硝酸盐和 NO_y（NO_y=NO_x + HNO_3 + PAN + HONO + NO_3+ HO_2NO_2 +N_2O_5）的散点图中可以看出，高浓度的硝酸盐和高浓度的气溶胶水含量以及较高浓度的 NO_y 有关，这说明非均相水解反应在这些样品中硝酸盐形成中起到的重要作用，同时气态前体物浓度的高低也会直接影响硝酸盐的浓度。

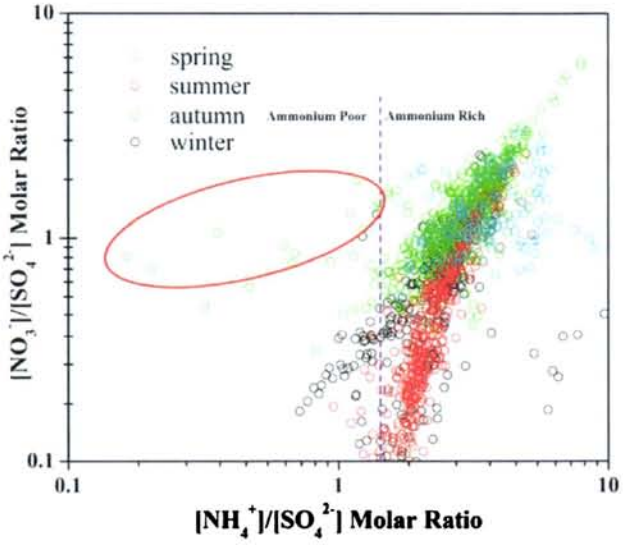

图 3-9 黄河三角洲地区不同季节 $PM_{2.5}$ 的$[NH_4^+]/[SO_4^{2-}]$和$[NO_3^-]/[SO_4^{2-}]$的摩尔比值散点图

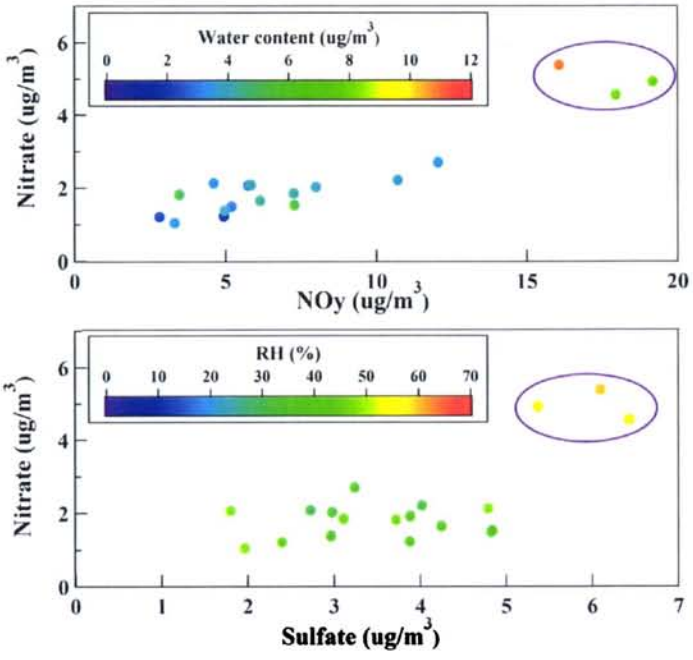

图3-10 黄河三角洲地区秋季贫铵状态下$PM_{2.5}$中NO_3^-浓度与SO_4^{2-}及NOy浓度在不同湿度和不同颗粒物水含量条件下的散点图

本研究将$[HSO_4^-]/[H^+_{air}]$的摩尔质量比与 RH 做散点图（图 3-11），结果发现当 RH 低于 60%时，$[HSO_4^-]/[H^+_{air}]$的摩尔质量比会随着 RH 的增大而增大，当 RH 高于 65%时，$[HSO_4^-]/[H^+_{air}]$的摩尔质量比整体趋势会随着 RH 的增大而减小。

同时从图中可以看出，RH 的增加会导致颗粒物水含量的升高，因此在当颗粒物水存在且浓度升高的时候，有利于 HSO_4^-发生水解，从而释放出更多的自由 H^+。

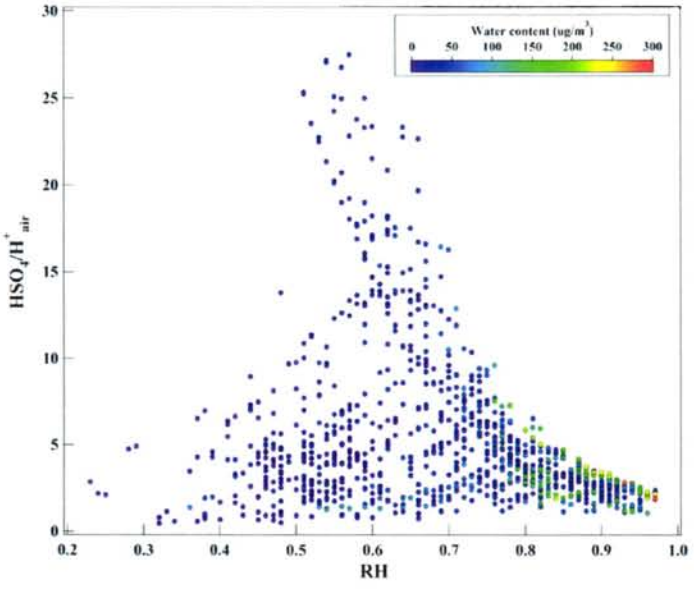

图 3-11 黄河三角洲地区观测期间 $PM_{2.5}$ 中$[HSO_4^-]/[H^+_{air}]$比值与 RH 的关系图

(颜色代表 $PM_{2.5}$ 水含量)

3.3 长距离传输对 $PM_{2.5}$ 水溶性离子浓度的影响

气团传输也是影响黄河三角洲地区的水溶性离子浓度的主要因素之一，为了解气团的来源与传输路径，我们利用 HYSPLIT 模型计算了观测期间的后推 3 天（72h）气流轨迹，然后将所得所有轨迹根据轨迹所经过的地区的经纬度以及气团的高度等进行聚类分析。聚类分析所得的主要气流轨迹以及每条轨迹对应的主要水溶性离子的浓度均绘于图 3-12 中。

春季的气流轨迹可分为 2 大类，一类气团（cluster 1）是源自北部西伯利亚，约占春季总气流轨迹的 63%，传输距离长，高度较高；另一类气团（cluster 2）源自渤海，约占总轨迹的 37%，传输距离较短，高度较低。源自北部西伯利亚的气团经过长距离传输，分别经过西伯利亚、蒙古、内蒙古、京津地区以及渤海，最终到达黄河三角洲地区。源自渤海的气团则是经过烟台、青岛、潍坊。由于传输距离短，气团的运动速度较低，同时气团高度也较低，使得气团更容易将所经过的城市地区排放的污染物融合并携带至黄河三角洲地区，因此 cluster 2 所对应的总水溶性离子浓度（39.22 μg/m^3）更高，约是北部长距离气团的 2 倍（19.22

μg/m^3）。

夏季的气流轨迹可分为4大类。最主要的气团（cluster 2）占夏季总轨迹的39%，其次为来自东部黄海的cluster 4（37%）、来自西部的cluster 1（17%）以及来自东南部东海的cluster 3（7%）。气团2从江苏起源，经过淄博抵达黄河三角洲地区。淄博是山东省重要的工业城市，分布众多的冶金、化工等，空气污染较严重。因此，从这个方向的气流将大量污染物带至黄河三角洲地区，导致较高的离子浓度（91.25 μg/m^3）。

秋季的气流轨迹也可分为2大类，一类气团（cluster 1）是源自北部西伯利亚，约占秋季总气流轨迹的33%，传输距离长，高度较高；另一类气团（cluster 2）源自河北唐山，约占总轨迹的67%，传输距离较短，高度较低。源自北部西伯利亚的气团经过长距离传输，分别经过西伯利亚、蒙古、内蒙古、辽宁以及渤海，最终到达黄河三角洲地区。源自河北唐山的气团则是经过烟台，青岛，潍坊，这三个城市属于蓝色半岛经济区，经济的快速发展和当地的污染对气团的离子贡献较高。同时由于传输距离短，气团的运动速度较低，气团高度也较低，使得气团更容易将所经过的城市地区排放的污染物融合并携带至黄河三角洲地区，因此cluster 2所对应的总水溶性离子浓度（75.19 μg/m^3）约是北部长距离气团的5倍（14.30 μg/m^3）。

冬季黄河三角洲地区的气团均来自北方，一类气团（cluster1）传输距离较长，来自西伯利亚，经过蒙古，河北，最后经过渤海，占冬季总轨迹的68%。另一类气团（cluster 2）传输距离较短，从内蒙古出发经过京津冀地区到达采样点，该类气团的离子贡献率远高于cluster 1。同时冬季气团2的Cl^-浓度也远高于观测期间其他气流轨迹对应的Cl^-浓度，这可能是由于冬季京津冀地区燃煤供暖排放大量的Cl^-。

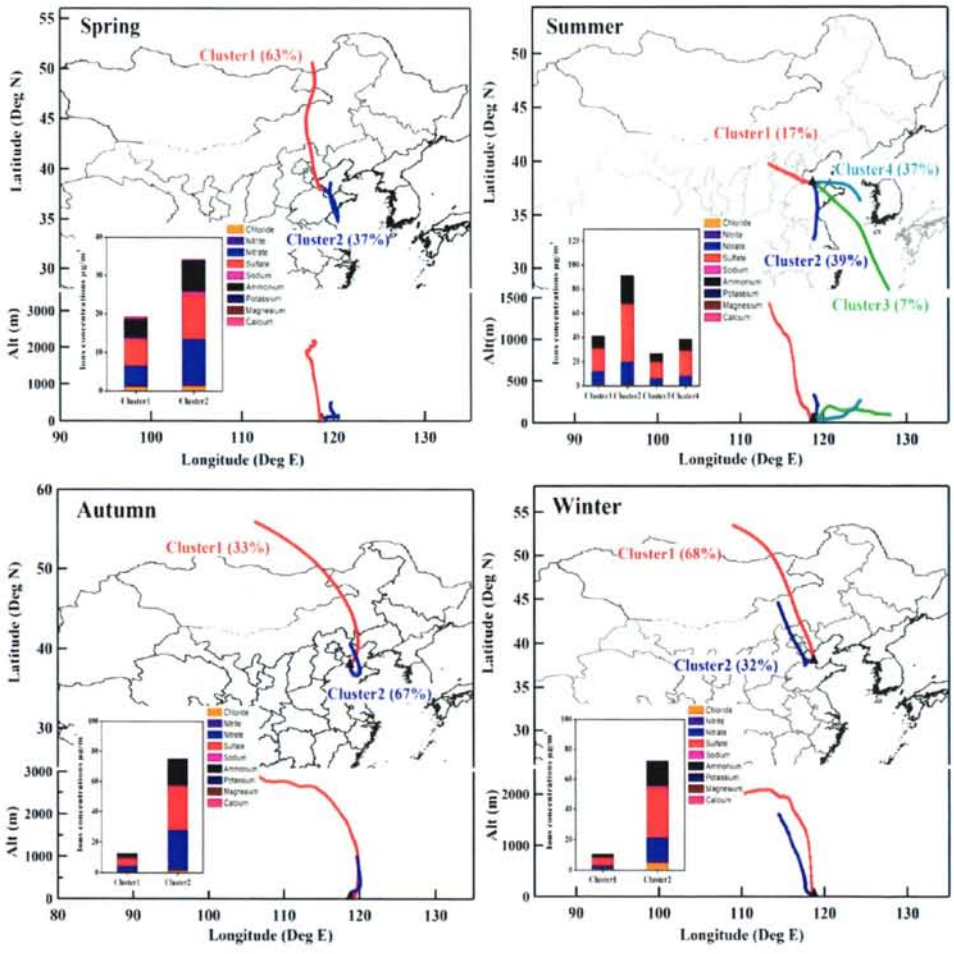

图3-12 黄河三角洲地区观测期间不同季节后推气流轨迹及每条轨迹所对应的离子浓度图

3.4 $PM_{2.5}$水溶性离子来源解析

为研究黄河三角洲地区大气 $PM_{2.5}$ 中水溶性离子变化的影响因素，我们对主要水溶性离子组分及气态污染物（包括 Cl^-、NO_3^-、SO_4^{2-}、Na^+、NH_4^+、K^+、Mg^{2+}、Ca^{2+}、SO_2、NO_y、O_3）进行了主因子分析，利用主因子法提取特征值大于 1 的主因子，利用正交旋转法（Varimax）对因子载荷进行旋转。表 3-4 给出了黄河三角洲地区观测期间全年平均影响大气 $PM_{2.5}$ 中水溶性离子变化的 3 个主要因子载荷结果。

第一主因子对 Cl^-、NO_y、K^+和 SO_2 有较大的正载荷系数，相关性分析结果表明 Cl^-、NO_y、K^+和 SO_2 之间均有较好的正相关性，该因子代表与燃烧有关的

因子，Cl^-和 SO_2 主要与燃煤有关，K^+主要与生物质燃烧有关，NO_y 主要与汽柴油燃烧后的机动车排放有关，因此第一主因子代表燃烧源，该因子方差贡献率最大，占总方差的 46.2%。

第二主因子具有高载荷系数的是 NO_3^-、SO_4^{2-}和 NH_4^+，这些离子成分主要是通过二次转化形成的，通过前文结果分析，NO_3^-、SO_4^{2-}和 NH_4^+具有很好的相关性，说明 NH_4^+主要以硫酸铵和硝酸铵的形式存在，因此该因子代表二次气溶胶，方差贡献率为 16.1%。

第三主因子对 Mg^{2+}、Ca^{2+}和 Na^+有较高的正载荷系数，Mg^{2+}和 Ca^{2+}主要与扬尘有关，Na^+主要来自土壤源，因此该因子代表扬尘和土壤源，方差贡献率为 13.4%。

综上所述，通过主因子分析得出的三个最主要因子的累积方差贡献率为 75.7%，接近 80%，能够较好的表征黄河三角洲地区地区主要的影响因素，从组分分析结果得出燃烧源、二次生成及扬尘和土壤是影响当地气溶胶水溶性离子的主要因素。

表 3-4 影响黄河三角洲地区观测期间 $PM_{2.5}$ 浓度的主要因子

变量	因子载荷		
	1	2	3
Cl^-	**0.86**	0.28	0.09
NO_3^-	0.38	**0.80**	0.09
SO_4^{2-}	0.29	**0.89**	−0.02
Na^+	0.51	0.20	**0.53**
NH_4^+	0.28	**0.93**	0.01
K^+	**0.68**	0.53	0.27
Mg^{2+}	−0.02	0.05	**0.86**
Ca^{2+}	0.04	−0.05	**0.74**
SO_2	**0.68**	0.33	−0.01
NO_y	**0.84**	0.33	0.04
O_3	−0.68	0.59	0.06
贡献率（%）	46.2%	16.1%	13.4%

3.5 不同天气条件下 $PM_{2.5}$ 水溶性离子浓度变化特征

3.5.1 雾霾和清洁天气下气态污染物和气象参数特征

本次研究按能见度将观测期间天气分为清洁天、雾霾天。其中清洁天定义为能见度高于 10 km 的时段，雾霾天则是能见度低于 10 km 且未发生雨雪沙尘等天气的时段。经过统计，黄河三角洲地区观测期间春季清洁天 23 天，雾霾天 9 天，另有 2 天发生沙尘现象；夏季清洁天 6 天，雾霾天 16 天，另有 8 天有降雨发生；秋季清洁天 12 天，雾霾天 14 天，另有 3 天有降雨发生；冬季清洁天 17 天，雾霾天 12 天，另有 2 天发生降雪现象。

表 3-5 给出了黄河三角洲地区观测期间在雾霾和清洁天气下气态污染物（SO_2、O_3 和 NO_y）以及气象参数（WS、T 和 RH）的均值对比，可以看出在雾霾发生时气态污染物浓度远高于清洁天气时，从全年平均值来看，SO_2 和 NO_y 在雾霾天浓度增加明显，分别是清洁天的 2.18 倍和 2.29 倍，而臭氧则变化不大，雾霾天是清洁天的 1.14 倍。从季节变化来看，SO_2 在冬季明显高于其他季节，雾霾天更是高达 31.39 ppbv，是春季清洁天的 15 倍，这可能与冬季当地燃煤取暖有关。O_3 夏季浓度最高，且夏秋季节雾霾天浓度高于清洁天，而春季和冬季则是清洁天浓度更高。NO_y 在冬季浓度最高，且雾霾天浓度高达 53.57 ppbv，是夏季清洁天的 12 倍，这可能与冬季气团传输有一定关系。

从气象条件来看，清洁天具有更高的风速，这有利于污染物的扩散，夏秋季节风速最低，这可能是导致夏秋季节污染物浓度特别是水溶性离子浓度较高的原因之一；温度雾霾天和清洁天差别不大，雾霾天温度略高于清洁天，这说明温度对于黄河三角洲地区雾霾的形成影响不大；相对湿度则是在雾霾天明显升高，湿度对雾霾的形成及污染物浓度的升高有直接的关系。

表 3-5 黄河三角洲雾霾与清洁天气气态污染物及气象参数均值

季节	天气	SO_2 (ppbv)	O_3 (ppbv)	NO_y (ppbv)	WS (m/s)	T (℃)	RH (%)
春	雾霾	15.94	37.86	36.58	3.19	18.11	53.04
	清洁	2.03	39.38	23.93	4.04	13.67	41.19
夏	雾霾	10.99	55.20	20.31	0.57	27.54	79.10
	清洁	3.96	47.70	4.47	0.79	27.85	70.07
秋	雾霾	19.19	34.51	21.95	0.74	13.53	72.50
	清洁	5.30	31.50	7.52	0.91	12.94	58.91
冬	雾霾	31.39	7.47	53.57	0.89	−1.22	62.27
	清洁	15.91	21.81	16.21	1.16	−2.55	54.12
全年平均	雾霾	17.30	38.72	26.60	1.00	17.57	71.76
	清洁	7.94	33.91	11.64	1.56	12.60	60.51

3.5.2 雾霾和清洁天气下 $PM_{2.5}$ 水溶性离子浓度特征

表 3-6 给出了黄河三角洲地区观测期间不同季节的雾霾与清洁天气条件下 $PM_{2.5}$ 中水溶性离子的质量浓度。结果显示，观测期间总水溶性离子质量浓度在雾霾天明显高于清洁天，四季（春、夏、秋、冬）雾霾天与清洁天的总水溶性离子浓度比依次为 1.83、3.97、4.73、4.79，全年平均浓度比为 4.29。冬季比值最高可能是由于冬季采暖期燃煤排放大量的一次污染物，同时冬季大气边界层较低，容易形成逆温层，不利于污染物的扩散，从而造成冬季雾霾发生时污染较严重，浓度比清洁天升高明显。总水溶性离子质量浓度在雾霾天季节变化依次为夏季>冬季>秋季>春季，其中夏、冬、秋三季总水溶性离子的质量浓度接近，远高于春季的浓度。

雾霾天气下 SO_4^{2-} 的质量浓度季节变化依次为冬季>夏季>秋季>春季，SO_4^{2-} 浓度雾霾天气与清洁天气的比值高低依次为冬、秋、夏、春，分别为 5.72、4.41、3.36、2.38，全年平均比值为 4.18，冬秋夏三季增加明显，表 3-5 给出了黄河三角洲地区雾霾天与清洁天的气态污染物以及气象参数的季节变化，可以看出，雾霾天气下的相对湿度在四季均高于清洁天气下的相对湿度，有利于 SO_2 的转化，而且冬季雾霾天气下 SO_2 排放量远高于其他季节，因此冬季雾霾天气下硫酸盐浓度较高。

雾霾天气下 NO_3^- 浓度季节变化依次为秋季>夏季>冬季>春季，NO_3^- 浓度雾霾天气与清洁天气的比值高低依次为夏、秋、冬、春，分别为 7.43、5.97、4.43、

1.64，全年平均比值为 5.64，雾霾天气下 NH_4^+浓度季节变化依次为夏季>秋季>冬季>春季，NH_4^+浓度雾霾天气与清洁天气的比值高低依次为秋、冬、夏、春，分别为 5.56、4.72、4.33、1.54，全年平均比值为 4.72，NO_3^-和 NH_4^+的变化幅度均高于 SO_4^{2-}，通过图 3-13 也可以看出，NO_3^-和 NH_4^+质量浓度占所测总无机水溶性离子质量浓度的百分比雾霾天气高于清洁天气，而硫酸盐变化不大，这均说明黄河三角洲地区气溶胶中硝酸盐和铵盐对雾霾形成的贡献更高。Cl^-冬季雾霾天质量浓度最高，且高于其他季节雾霾天气下的2-3倍，这与冬季燃煤排放有关。

表 3-6 黄河三角洲雾霾与清洁天气 $PM_{2.5}$ 水溶性离子质量浓度四季均值（$\mu g/m^3$）

季节	天气	Cl^-	NO_2^-	NO_3^-	SO_4^{2-}	Na^+	NH_4^+	K^+	Mg^{2+}	Ca^{2+}	总水溶性离子
春	雾霾	1.33	0.48	8.76	11.94	0.90	6.64	0.83	0.17	0.51	31.56
	清洁	0.68	0.36	5.34	5.02	0.74	4.32	0.44	0.09	0.20	17.21
夏	雾霾	1.34	0.28	19.09	44.01	0.60	21.13	0.66	0.10	0.10	87.31
	清洁	0.27	0.14	2.57	13.10	0.51	4.88	0.37	0.08	0.09	22.01
秋	雾霾	1.78	0.36	28.30	31.12	0.73	17.67	0.98	0.18	0.20	81.31
	清洁	0.64	0.25	4.74	7.05	0.64	3.18	0.52	0.09	0.07	17.18
冬	雾霾	4.10	0.73	15.86	46.35	0.94	15.35	1.18	0.08	0.23	84.80
	清洁	1.43	0.28	3.58	8.10	0.58	3.25	0.40	0.04	0.04	17.69
全年平均	雾霾	1.86	0.38	21.67	36.95	0.71	18.00	0.87	0.12	0.24	80.79
	清洁	0.78	0.29	3.84	8.84	0.60	3.81	0.43	0.09	0.15	18.85

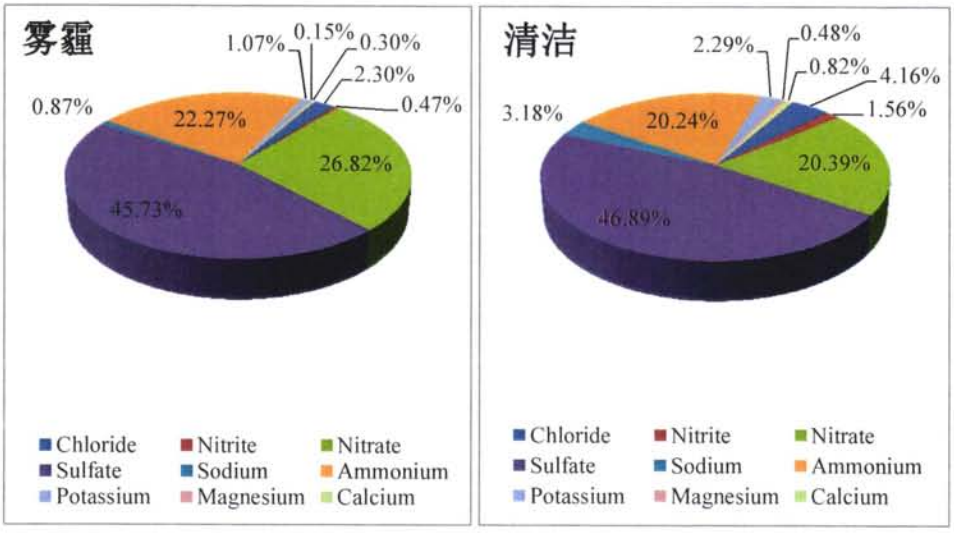

图 3-13 黄河三角洲地区雾霾与清洁天气水溶性离子百分比组成图

图 3-14 给出了黄河三角洲地区不同季节雾霾天气与清洁天气硫酸盐和硝酸盐转化率（SOR 和 NOR）。从图中可以看出雾霾天气下 SOR 和 NOR 均大于清洁天气，说明雾霾期间 SO_2 和 NOx 的二次转化率高于清洁期间。SOR 在冬季雾霾期间增长最明显，这主要是由于冬季燃煤取暖排放大量的 SO_2 且冬季大气结构比较稳定使得燃煤排放的污染物容易积累，而 NOR 在秋季增长最明显，在夏秋季节高于春冬季节，这主要是由于秋季相对湿度在雾霾天增长最明显，且夏秋季节相对湿度较高，更有利于 NO_3^- 的生成和积累。

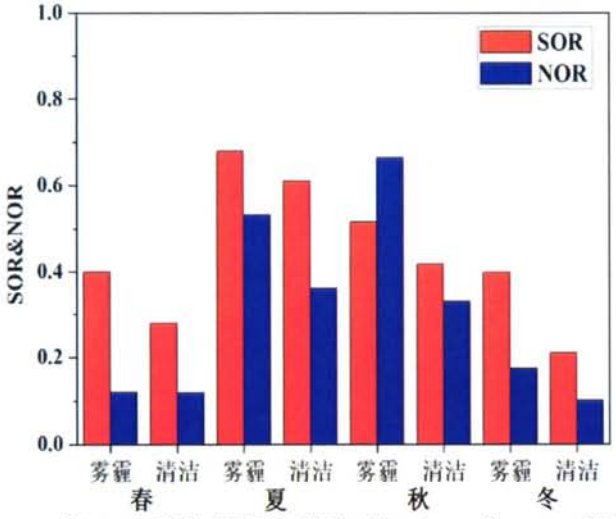

图 3-14 黄河三角洲地区雾霾与清洁天气下 SOR 与 NOR 对比图

3.5.3 雾霾和清洁天气下 $PM_{2.5}$ 酸度特征

表 3-7 给出了黄河三角洲地区雾霾与清洁天气 $PM_{2.5}$ 水溶性离子酸度四季均值，结果发现雾霾天气下黄河三角洲地区的气溶胶酸性更高，在冬季雾霾发生时气溶胶酸性升高更加明显，自由酸度（H_{air}^+）在冬季雾霾天是冬季清洁天的 10.4 倍，是春季清洁天的 116 倍，强酸度（H_{strong}^+）在冬季雾霾天是冬季清洁天的 5.6 倍，是春季清洁天的 31.8 倍。冬季雾霾发生时气溶胶的强酸性一方面是由于冬季气溶胶中高浓度的 HSO_4^-，可以产生更多的 H^+，同时冬季气溶胶水含量比夏季和秋季低，颗粒物水对 H^+ 的稀释作用较弱。由于夏季雾霾发生时相对湿度最高，因此夏季雾霾天颗粒物水含量浓度最高，为 138.41 $\mu g/m^3$，对 H^+ 具有较强的稀释作用，因此夏季酸度明显低于冬季。

表 3-7 黄河三角洲地区雾霾与清洁天气 $PM_{2.5}$ 水溶性离子酸度四季均值

季节	天气	H_{air}^+ (nmol/m^3)	H_{strong}^+ (nmol/m^3)	HSO_4^- (nmol/m^3)	Water content (μg/m^3)
春	雾霾	6.77	86.77	50.93	11.30
	清洁	1.37	15.01	13.64	3.10
夏	雾霾	14.92	112.50	92.59	138.41
	清洁	7.59	53.07	38.04	20.05
秋	雾霾	27.58	171.47	126.36	73.34
	清洁	20.26	74.76	48.21	9.98
冬	雾霾	159.09	476.60	305.15	51.51
	清洁	15.36	85.37	45.26	5.13
全年平均	雾霾	37.77	182.30	132.62	97.15
	清洁	13.65	66.27	42.50	13.14

3.6 本章小结

本章分析了黄河三角洲地区 $PM_{2.5}$ 中水溶性离子质量的季节和日变化特征，研究了气溶胶的酸度，并利用气流轨迹方法和主成分分析法分析了黄河三角洲地区气溶胶的可能来源。主要结论如下:

1、通过对黄河三角洲地区观测期间春、夏、秋、冬四季 $PM_{2.5}$ 水溶性离子的分析发现 SO_4^{2-}是 $PM_{2.5}$ 中含量最高的水溶性离子，约占总水溶性离子的 45.2%，其次为 NO_3^-和 NH_4^+，SO_4^{2-}、NO_3^-和 NH_4^+的质量浓度除了低于国内的济南和西安以及印度的赖普尔，远高于美国、日本和韩国的城市及郊区站点，与国内一些大城市相当，说明黄河三角洲地区面临严重的二次无机气溶胶污染。

2、夏季高温以及较强的辐射有利于非均相气粒转化，而较高的湿度以及较高的 O_3 浓度则有利于液相反应，因此夏季的光化学反应较强，从而使硫酸盐的转化率（SOR）远高于其它三个季节，导致夏季 SO_4^{2-}浓度最高。

3、SO_4^{2-}的质量浓度在夏、秋和冬三个季节均表现出昼高夜低的日变化特征，NO_3^-在春夏秋三个季节均表现出上午高下午低的日变化特征，NH_4^+的质量浓度日变化与 SO_4^{2-}有相似的日变化特征。太阳辐射和 O_3 浓度是影响 SO_4^{2-}日变化的主要因素，而太阳辐射和温度是影响 SO_4^{2-}日变化的主要因素。

4、冬季黄河三角洲地区酸性颗粒物的比重最高，约有 62.4%的颗粒物是酸性颗粒物，其中 32.1%的颗粒物为强酸性颗粒物。黄河三角洲地区的酸性颗粒物酸度低于泰山、北京和上海等地，而高于衡山、兰州和广州。观测期间 NO_3^-主

要来自气态 NH_3 和 HNO_3 的均相反应。

5、主因子分析结果表明影响黄河三角洲地区水溶性离子的主要因素是燃烧源、二次生成及扬尘和土壤。

6、利用后推气流轨迹法对黄河三角洲地区 $PM_{2.5}$ 水溶性离子的主要来源进行分析，结果表明春季、秋季和冬季黄河三角洲地区主要受来自北方西伯利亚的长距离传输以及山东省内和京津冀地区的短距离输送气团的影响，而夏季主要受山东省和河北省短距离传输气团以及东部海洋气团的影响。其中来自山东省内及京津冀的短距离输送气团对黄河三角洲地区的离子贡献率最高。

7、雾霾天气下污染物浓度明显高于清洁天，且雾霾天气下的相对湿度在四季均高于清洁天气下的相对湿度，有利于 SO_2 的转化，而且冬季雾霾天气下 SO_2 排放量远高于其他季节，导致冬季雾霾天气下硫酸盐浓度较高。

8、雾霾天气下气溶胶酸度更强，且冬季气溶胶酸度明显高于其他三个季节，这主要是由于冬季高浓度的 HSO_4^-，可以产生更多的 H^+，同时冬季气溶胶水含量比夏季和秋季低，颗粒物水对 H^+ 的稀释作用较弱。

第四章 黄河三角洲地区颗粒物数浓度及粒径分布特征

4.1 颗粒物数浓度时间变化特征

4.1.1 颗粒物数浓度日变化特征

图 4-1-图 4-4 表明黄河三角洲地区观测期间凝结核模态和爱根模态颗粒物在新颗粒物生成事件（NPF）发生的观测时段数浓度日变化特征明显，而未发生新颗粒物生成事件（non-NPF）的观测时段则没有明显的日变化。NPF 期间，凝结核模态颗粒物的数浓度在四个季节均呈现单峰分布，从早上 7:00 左右开始上升，一直持续增长到正午前后，这主要是新颗粒物生成事件造成的数浓度的爆发。其中春季的峰值最大（26797 #/cm^3），冬季的峰值最小(2298 #/cm^3)。夏季出峰时间最早，在 8:00 前后出现峰值，春季和冬季出峰时间最晚，在 13:00 前后出现峰值，这可能是由于夏季日出时间早，温度较高，导致新颗粒物生成事件发生时间较早，而冬春季节日出时间晚，上午温度较低，光化学反应较弱，直至正午前后才会增强。而未发生新颗粒物生成事件（non-NPF）的观测时段，凝结核模态的颗粒物昼夜没有明显变化，这就导致凝结核模态颗粒物在 non-NPF 时段数浓度明显低于 NPF 发生的时段。在 NPF 发生时段，凝结核模态颗粒物数浓度的升高是伴随温度及 SO_2 浓度的升高，这反应了高温低湿环境下有利于硫酸气的成核反应，从而导致凝结核模态颗粒物的数浓度升高[233-234]。而在 non-NPF 时段凝结核模态颗粒物数浓度明显低于爱根模态和积聚模态，这可能是由于凝结核模态颗粒物在大气中不稳定，易与大颗粒发生碰并增长，粒径增大至爱根模态。因此在 NPF 时段爱根模态颗粒物有明显的爆发峰值，就是由于凝结核模态颗粒物的长大，而由于颗粒物增长需要一定时间，因此爱根模特颗粒物的数浓度峰值出现时间比凝结核模态滞后几个小时。

积聚模态的颗粒物在观测期间 NPF 时段相比凝结核模态和爱根模态没有明显变化特征，一方面是由于积聚模态颗粒物粒径较大，不容易受颗粒物增长的影响，另一方面黄河三角洲地区一次排放较小，积聚模态颗粒物可能主要是受区域气团传输的影响。Wu 等[103]研究表明高浓度的积聚模态颗粒物对凝结蒸汽具有较

强的吸附能力从而抑制凝结核模态颗粒物的生成，因此在夜间积聚模态颗粒物浓度较高时凝结核模态颗粒物浓度较低。而在下午积聚模态颗粒物数浓度有明显的降低可能是受边界层的升高从而有利于颗粒物的扩散而引起的。

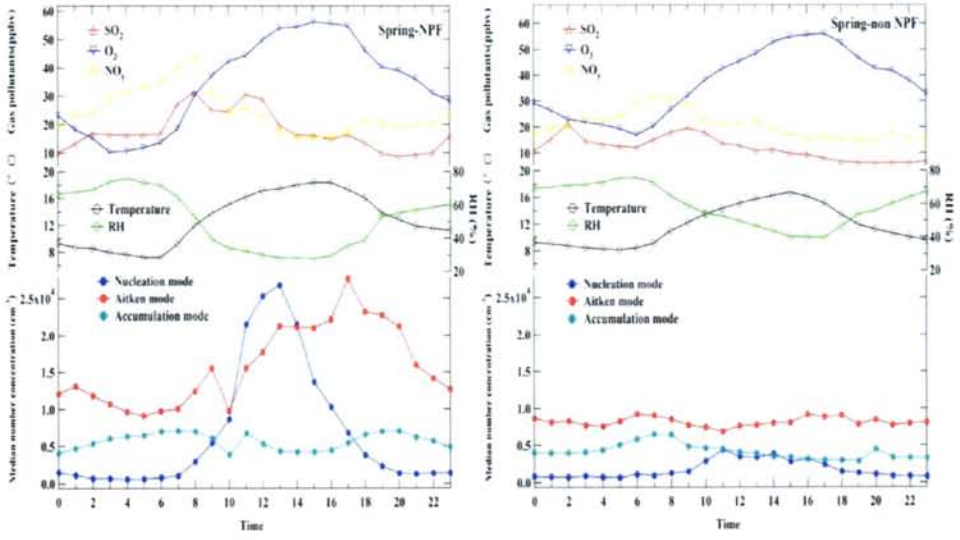

图 4-1 黄河三角洲地区春季发生新颗粒物生成事件（NPF）和不发生新颗粒物生成事件（non-NPF）的不同时段，不同粒径段的颗粒物数浓度中位值以及气体污染物、温度、相对湿度的日变化图

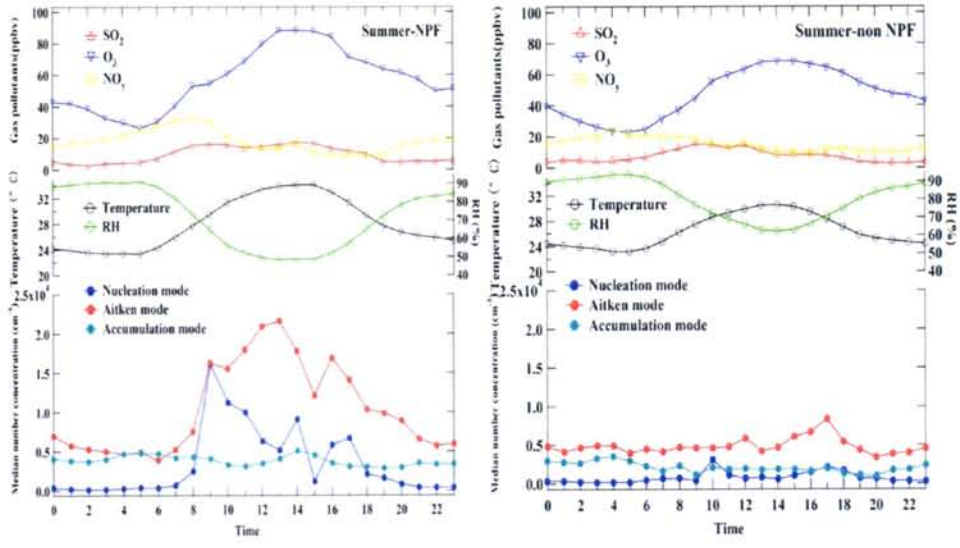

图 4-2 黄河三角洲地区夏季发生新颗粒物生成事件（NPF）和不发生新颗粒物生成事件（non-NPF）的不同时段，不同粒径段的颗粒物数浓度中位值以及气体污染物、温度、相对湿度的日变化图

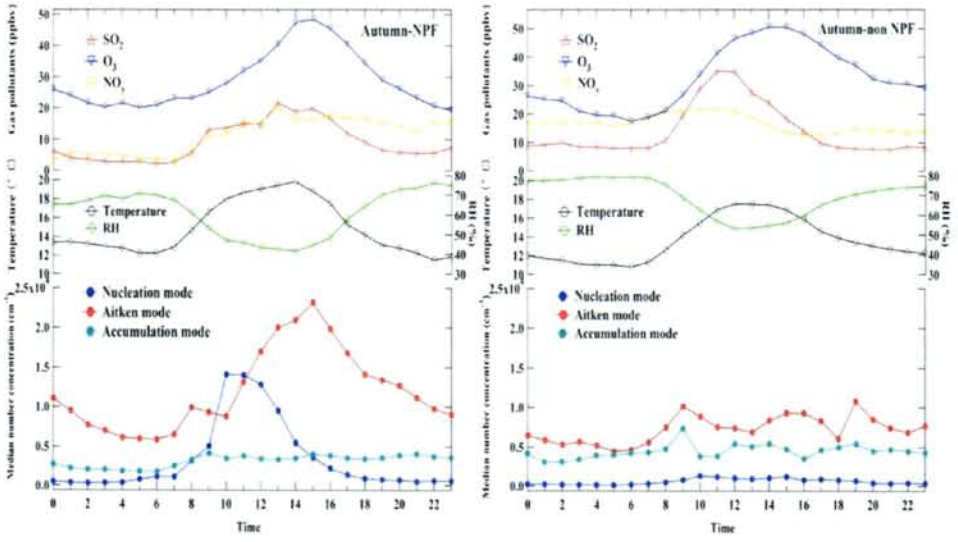

图 4-3 黄河三角洲地区秋季发生新颗粒物生成事件（NPF）和不发生新颗粒物生成事件（non-NPF）的不同时段，不同粒径段的颗粒物数浓度中位值以及气体污染物、温度、相对湿度的日变化图

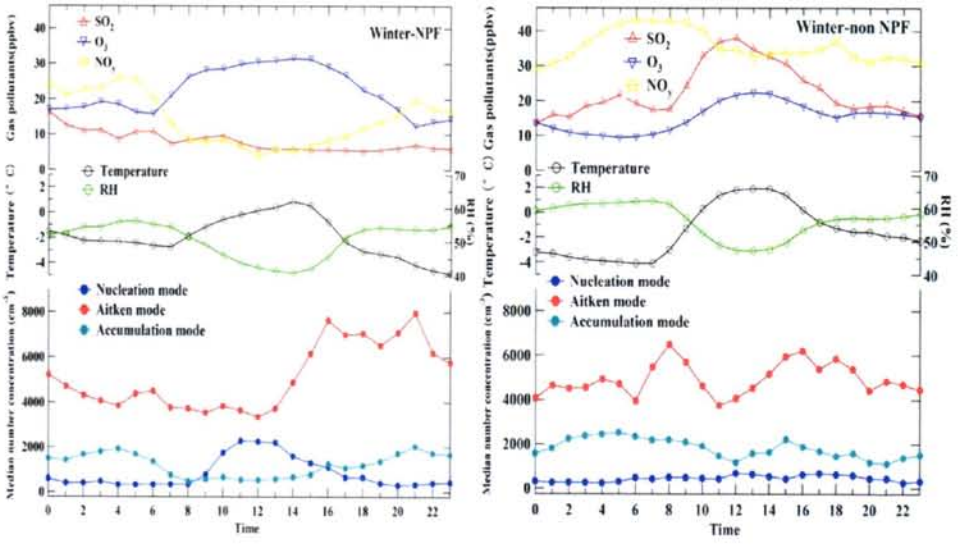

图 4-4 黄河三角洲地区冬季发生新颗粒物生成事件（NPF）和不发生新颗粒物生成事件（non-NPF）的不同时段，不同粒径段的颗粒物数浓度中位值以及气体污染物、温度、相对湿度的日变化图

4.1.2 颗粒物数浓度季节变化特征

气溶胶颗粒物的数浓度可以提供气溶胶颗粒物来源的信息，颗粒物的粒径大小则会影响气溶胶颗粒物在大气中的寿命、理化性质等。为了更清晰的了解黄河三角洲地区颗粒物的数浓度，我们将颗粒物粒径具体分为凝结核模态（5-20 nm）；爱根模态(20-50 nm、50-100 nm)；积聚模态（100-200 nm、200-500 nm、500-1000 nm）以及粗粒子模态（1000-10000 nm）等。表 4-1 所示为黄河三角洲地区不同季节观测到的不同粒径范围内的颗粒物个数浓度小时平均值。结果显示黄河三角洲地区观测期间 5-10000nm 粒径范围内总颗粒物平均数浓度为 12838 #/cm^3。其中秋季（15516 #/cm^3）颗粒物数浓度最高，其次为春季（15488 #/cm^3），夏季（12510 #/cm^3）和冬季（7966 #/cm^3）。数浓度最高值（104907 #/cm^3）和最低值（327 #/cm^3）均出现在夏季。

从不同粒径范围来看，黄河三角洲地区气溶胶中爱根模态颗粒物数浓度最高，全年平均占总颗粒物数浓度的 60.7%，其次为积聚模态（25.2%）和凝结核模态（14.1%）。凝结核模态颗粒物在春季和夏季数浓度最高，爱根模态则是在春季和秋季最高，积聚模态秋季最高。由于新颗粒物生成事件的粒径在凝结核模态，因此春季和夏季较强光化学作用下，新颗粒物生成是 5-20nm 粒径范围内的颗粒物浓度较高的主要贡献因素。20-50 nm 和 50-100 nm 的粒径段颗粒物对爱根模态颗粒物的数浓度贡献在春夏冬三季均为 50%左右，在秋季 20-50 nm 粒径段贡献率约为 59%，略高于其他三个季节。积聚模态颗粒物数浓度的约 75%集中在 100-200 nm 粒径段，其次为 200-500 nm（23%），500-1000 nm 粒径段的颗粒物仅占积聚模态的 2%。积聚模态颗粒物在秋季的数浓度较高可能是由于秋季发生的重污染天气较多（14 个雾霾日），胡敏等[92]研究发现在重污染情况下，积聚模态颗粒物数浓度会不断升高，虽然夏季雾霾发生频率也较高，但夏季降雨频繁，雨水对于气溶胶粗颗粒的冲刷作用使得夏季积聚模态颗粒物浓度低于秋季。

表 4-1 黄河三角洲地区各季节不同颗粒物粒径范围数浓度统计结果（1h 均值，单位：#/cm^3）

季节	统计项目/粒径范围	凝结核模态	爱根模态			积聚模态				
	（nm）	5-20	20-50	50-100	20-100	100-200	200-500	500-1000	100-1000	5-10000
春	平均值	2376	4575	4609	9184	3190	695	39	3924	15488
	最小值	2.1	64	149	259	103	50	1.8	299	1987
	最大值	52405	26224	35921	57582	14606	3252	316	16156	94654
	标准差	5893	3869	3199	5930	2380	583	42	2935	11143
夏	平均值	2238	3968	3626	7594	1978	532	177	2687	12510
	最小值	10	35	43	78	61	20	1.4	106	327
	最大值	46504	50118	28726	57830	12003	2018	837	13547	104907
	标准差	5310	5766	3488	8148	1516	426	190	1957	12670
秋	平均值	1829	5390	3821	9211	2833	1560	79	4472	15516
	最小值	5.8	526	337	1466	130	79	2.1	357	3200
	最大值	37997	24858	10876	28555	9083	5674	439	13935	50498
	标准差	3868	4660	2208	5584	1802	1398	95	3067	7881
冬	平均值	814	2515	2711	5226	1603	318	3	1924	7966
	最小值	16	235	369	689	163	20	0.4	183	1948
	最大值	13768	19284	9359	23757	5535	2782	393	8322	34219
	标准差	1250	1659	1463	2544	1136	344	30	1423	3753
全年	平均值	1817	4082	3716	7798	2421	751	70	3242	12838

与国内外其它站点的研究结果相比（表 4-2），黄河三角洲地区大气颗粒物中，凝结核模态颗粒物的数浓度高于北京和瓦里关，但远低于兰州，太仓，济南以及同是背景站点的上甸子和 Pittsburgh，这说明虽然有新颗粒物生成事件发生，但由于没有机动车等交通源排放，凝结核模态颗粒物数浓度会低于城市站点。而爱根模态的数浓度高于兰州和北京，积聚模态的颗粒物数浓度也高于兰州、北京和济南，说明黄河三角洲地区作为区域背景点，大气颗粒物受气团长距离输送影响，气溶胶老化现象明显。

表 4-2 黄河三角洲地区以及其他站点不同粒径段（凝结核模态、爱根模态、积聚模态）颗粒物数浓度（单位：#/cm^3）

Sites	Types	Season	Nucleation mode 5-20 nm	Aitken mode 20-100 nm	Accumulation mode 100-1000 nm	Reference
YRD	Rural/ Coastal	Spring	2376	9184	3924	本研究
		Summer	2238	7594	2687	
		Autumn	1829	9211	4472	
		winter	814	5226	1924	
		Annual average	1817	7798	3242	
Lanzhou	Urban	Summer 2006	4540*	3550	501	Gao et al., 2011[108]
Beijing	Urban	Jul.-Sept. 2008	434*	3978	1854	Gao et al., 2012[33]
Jinan	Urban	Summer 2006	7374*	2927	481	Gao et al.,2007[235]
		Winter 2006	3839*	11751	1817	
Taicang	Urban	Summer 2005	15521*	12990	1744	Gao et al., 2009[88]
Nanjing	Urban			11581	7543	Kang,2013[236]
Shangdianzi	Rural	May 2008-Aug. 2009	3610 (3-25 nm)	4430 (25-100 nm)	3470	Shen et al., 2011[257]
Yufa	Rural	2006	2000 (3-20 nm)	9000	5000	Yue et al., 2009[258]
Waliguan	Rural	Sept. 2005-May 2007	570 (12-21 nm)	1060 (21-95 nm)	430 (95-570 nm)	Kivekäs et al., 2009[259]
Pittsburgh	Rural	Jul. 2001-Jul. 2002	4100*	10100	2188	Stanier et al., 2004[98]

*表示粒径范围为 10-20nm。

4.2 颗粒物数浓度粒径分布特征

图 4-5 给出了黄河三角洲地区观测期间大气气溶胶数浓度粒径分布图，从图中看出，春季和秋季的颗粒物数浓度明显高于夏季和冬季，黄河三角洲地区观测期间春季、夏季和秋季的颗粒物的粒径分布均呈单峰分布，峰值均出现在爱根模态，具体分别在 90 nm、55 nm、40 nm 附近出现，而冬季呈双峰分布，两个峰值均位于爱根模态，分别在 60 nm 和 80 nm 附近，这进一步说明黄河三角洲地区大气气溶胶主要是爱根模态颗粒物占主导。春季峰值最大可能是由于春季颗粒物增长速率最高且持续时间较长，使得凝结核模态颗粒物增长到更大的粒径范围，而秋季峰值所在位置粒径最小，这可能与秋季积聚模态颗粒物数浓度较大有关，从图中可以看出秋季 110 nm-1000 nm 范围内颗粒物数浓度最高，这就导致新颗粒物生成之后由于大颗粒物的碰并消除，颗粒物增长持续时间较短。

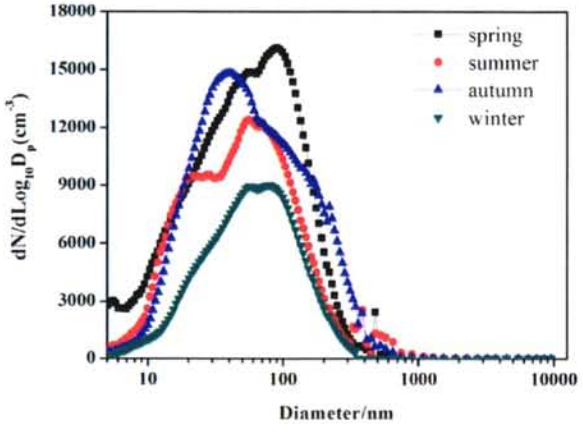

图 4-5 黄河三角洲地区观测期间不同季节颗粒物的粒径分布图

4.3 风向风速对颗粒物数浓度的影响

研究表明，风向风速是影响颗粒物数浓度最主要的气象因素[235]，本次研究为了分析风向对于大气颗粒物的数浓度的影响，将颗粒物总数浓度（TPNC，total particle number concentration，5-10000 nm）和风向一同绘制成风玫瑰图（图4-6），图中不同颜色代表颗粒物的不同数浓度，红色代表数浓度最低(0-10000 #/cm^3)，粉色代表最高的数浓度（>50000 #/cm^3）。将360°风向分为36份，每一个扇形代

表10°，扇形区域的长短代表该风向所占的比例。如图4-6所示，观测期间夏秋季节主要盛行东南风，而春季和冬季盛行西北风和东南风。总体来说，偏南风时颗粒物的数浓度要高于偏北风时，而最高数浓度(104907 #/cm^3)发生于风向为南风（176°）时，这说明南部城市比北部海洋对黄河三角洲地区的颗粒物数浓度贡献更大。从不同数浓度来看，冬季颗粒物数浓度集中于0-10000 #/cm^{3}范围内（红色区域），而其他季节则主要集中于10000-20000 #/cm^{3}范围内（绿色区域）。

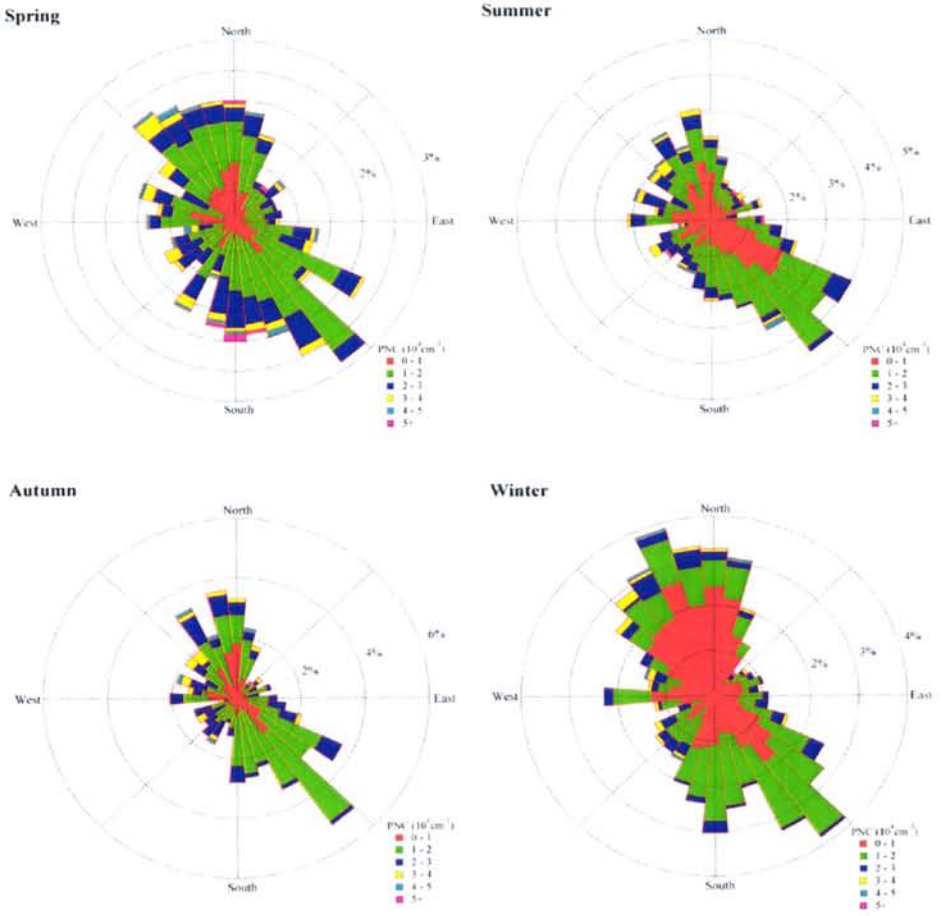

图 4-6 黄河三角洲地区观测期间四季总颗粒物数浓度风玫瑰图

风速也是影响颗粒物数浓度及粒径分布的重要因素之一[96]，为了更清晰的分析风速的影响，本研究将风速分为3部分：WS≤2 m/s，4 m/s >WS>2 m/s，WS≥4 m/s。从图4-7可以看出，当风速增加时，颗粒物总数浓度也会增加：12434 #/cm^3 (WS≤2 m/s) 、13880 #/cm^3 (4 m/s >WS>2 m/s) 、16949 #/cm^3(WS≥4 m/s)。凝结核模态的颗粒物数浓度也会随着风速的增加而迅速增加，这可能是由于风速越大，

环境越干洁，而新颗粒物生成事件越容易在这样的环境下发生[237]。随着风速的提高，爱根模态和积聚模态颗粒物的数浓度会明显降低，这可能是由于风速增大，有利于较大颗粒物的扩散[235]。不同风速下，颗粒物的粒径分布也不同，当风速低于2 m/s，dN/dLogDp峰值在50 nm，随着风速的提高到4 m/s以上时，峰值所在位置移动到更小的粒径（15 nm）。这可能是由于在低风速时大粒径的积聚模态颗粒物的浓度较高，通过强烈的碰并作用消除了部分凝结核模态的颗粒物。

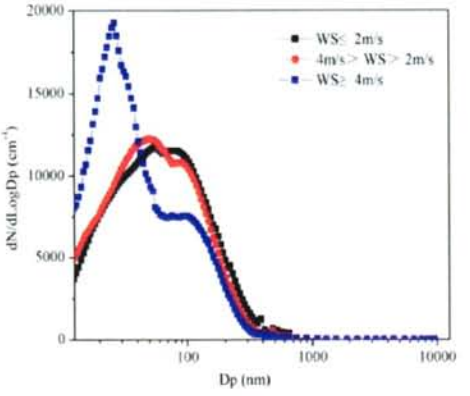

图 4-7 黄河三角洲地区观测期间不同风速条件下颗粒物数浓度粒径分布图

4.4 长距离传输对颗粒物数浓度的影响

气团传输也是影响黄河三角洲地区颗粒物粒径分布的重要因素之一，为了解气团的来源与传输路径，我们利用 HYSPLIT 模型计算了观测期间的后推 3 天（72h）气流轨迹，然后将所得所有轨迹根据轨迹所经过的地区的经纬度以及气团的高度等进行聚类分析。聚类分析所得的主要气流轨迹以及每条轨迹对应的颗粒物粒径分布特征均绘于图 4-8 中。

总体来说，气团可分为三类：1）北方长距离输送气团（春季、秋季和冬季的 cluster 1），这类气团传输距离较长，来自西伯利亚，经过蒙古，京津冀地区，最后经过渤海到达黄河三角洲地区，在春季和冬季占比较高；2）东部或北部海洋性气团（夏季 cluster 3，秋季 cluster 2），这类气团起源于黄海或渤海，经过渤海到达黄河三角洲地区，未经过陆地城市地区；3）来自南部和西部的短距离传输气团（春季 cluster 2，夏季 cluster 1、2，冬季 cluster 2），这类气团传输路径较

短，且沿途均经过陆地且污染较重的区域。

经过统计，第 3 类短距离陆地气团具有更高数浓度的颗粒物，平均为 14903 #/cm^3，而北部长距离传输的气团(春季、秋季和冬季的 cluster 1)的颗粒物数浓度最低，平均为 11462 #/cm^3，这可能是第 3 类气团传输距离短，气团的运动速度较低，气团高度也较低，使得气团更容易将所经过的城市地区排放的污染物融合并携带至黄河三角洲地区。由于北部长距离传输的气团的颗粒物粒径分布均为单峰分布，峰值均在爱根模态，春季峰值在 45 nm，夏季在 30 nm，冬季在 50 nm。而南部和东部短距离传输的气团粒径分布在更大粒径位置（100 nm 附近）出现峰值，这可能是由于这些气团传输路径短，气团运动速度较慢，并且经过一些经济高速发展的城市，城市建设蓬勃兴起，从而带来大量的建筑扬尘，较大粒径的颗粒物更容易随气团传输到达黄河三角洲地区。

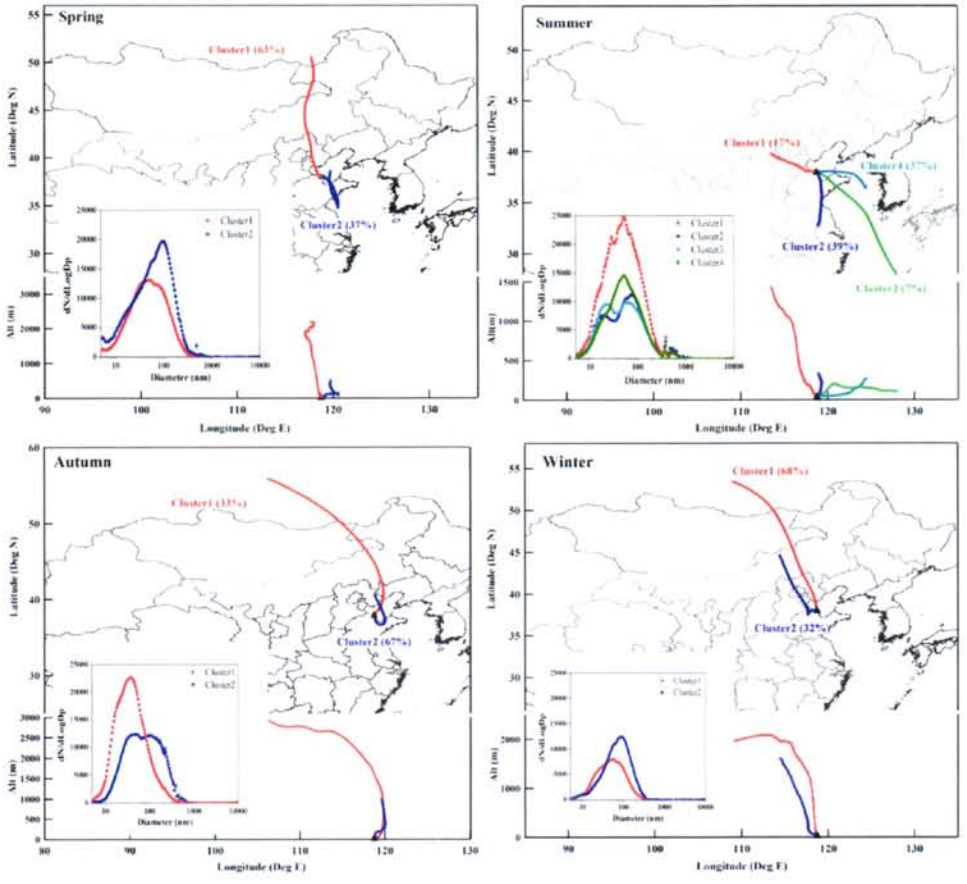

图 4-8 黄河三角洲地区观测期间不同季节后推气流轨迹及轨迹所对应的颗粒物粒径分布图

4.5 新颗粒物生成及粒径增长特征分析

新颗粒物生成事件（New particle Formation event, NPF）是研究颗粒物数浓度变化的重要事件，目前一般使用比较主观方法来判定一天中是否发生了新颗粒物生成事件，即：凝结核模态颗粒物数浓度突然爆发，且持续增加一段时间，之后会伴有颗粒物的长大过程[140]。颗粒物的生成速率(Formation Rate, FR)和颗粒物的增长速率(Growth Rate, GR)是在研究NPF事件的重要参数。为了有效地计算这些参数，我们将WPS每个样品的采样时间周期定为8分钟，从而获得较高的时间分辨率的个数浓度数据。

在观测期间，共有 26 天发生了新颗粒物生成事件（NPF），其中春季 7 天，夏季 7 天，秋季 6 天，冬季 6 天，约占总观测时间的 22%，该发生频率低于国内的如北京（42.7%），珠江三角洲地区（26%）和兰州（33%）等[33,107,108]。这些 NPF 事件中凝结核模态颗粒物的生成速率和增长速率以及相对应的 O_3 和 SO_2 浓度列于表中。经过统计凝结核模态颗粒物的平均成核速率（Formation Rate, $FR_{5\text{-}20}$）为 6.6 #/(cm^3·s)，最低值为 0.3 #/(cm^3·s)，最大值为 31.9 #/(cm^3·s)，凝结核模态颗粒物的平均增长速率(Growth Rate, $GR_{5\text{-}20}$)为 5.3 nm/h，最低值为 2.3 nm/h，最大值为 12.7 nm/h。黄河三角洲地区颗粒物的成核速率低于北京(3.3-81.4 #/(cm^3·s))[131]，Akrotiri(13 #/(cm^3·s))[93]和亚特兰大(30-70 #/(cm^3·s))[121]等地，高于广州(2.4-4.0 #/(cm^3·s))[104]。图 4-9 显示在秋季观测期间一个典型的新颗粒物生成及增长事件（10 月 12 日），从图中可以看出，凝结核模态的颗粒物数浓度从早上 7：00 左右开始增加，在正午前后有个一个爆发，同时凝结核模态的数浓度峰值都会伴随 O_3 及 SO_2 的峰值，O_3 和 SO_2 的小时平均浓度与凝结核模态的颗粒物有较好的相关性（R=0.62 和 0.64），说明较高的 O_3 和 SO_2 的浓度有利于凝结核模态颗粒物的生成。10 月 12 日和 7 月 31 日的颗粒物增长速率（$GR_{5\text{-}20}$）均明显高于其他 NPF 时段（大于 10 nm/h），这可能主要是由于这两天颗粒物的碰汇（coagulation sink）明显高于其他时段（6.5×10^{-4} /s 和 6.3×10^{-4} /s），高的碰并汇有利于凝结核模态颗粒物迅速碰并长大[97]。从表中可以看出冬季的颗粒物平均成核速率（1.0 #/(cm^3·s)）明显低于其他季节（春季 10.0 #/(cm^3·s)、夏季 9.0 #/(cm^3·s)、秋季 5.2 #/(cm^3·s)），这主要是由于冬季低温以及较低的 O_3 和 SO_2 浓度。

表4-3 黄河三角洲地区观测期间新颗粒物生成事件（NPF）相关参数表

（FR_{5-20}、GR_{5-20}、T、RH、SO_2、O_3）

	Date	GR_{5-20} (nm/h)	FR_{5-20} (#/(cm^3·s))	T (℃)	RH (%)	O_3 (ppbv)	SO_2 (ppbv)
spring	2011-4-1	2.9	3.3	5.4	52.7	47.2	2.4
	2011-4-2	4.1	8.0	6.9	40.9	43.9	2.3
	2011-4-4	3.7	2.4	14.7	34.7	60.9	15.7
	2011-4-8	4.7	4.8	15.5	37.6	45.2	2.9
	2011-4-9	5.8	17.2	18.6	22.2	39.8	25.4
	2011-4-12	7.2	31.9	17.1	37.1	44.3	27.0
	2011-4-20	3.1	2.6	22.1	33.4	41.6	41.2
	Avg.	4.5	10.0	14.3	36.9	46.1	16.7
summer	2011-7-5	9.5	22.7	30.6	51.7	86.6	18.4
	2011-7-9	2.7	5.3	31.6	41.2	59.0	4.9
	2011-7-14	3.2	17.6	31.4	59.2	50.3	8.0
	2011-7-16	4.0	3.0	32.7	54.8	85.8	11.0
	2011-7-21	7.8	3.9	30.3	70.2	37.5	19.7
	2011-7-23	8.3	5.4	32.3	66.4	93.7	27.0
	2011-7-31	12.7	5.2	31.9	60.0	50.4	11.6
	Avg.	7.7	9.0	31.5	57.6	66.2	14.4
autumn	2011-10-12	10.3	4.8	20.8	57.6	55.4	59.3
	2011-10-15	4.6	3.3	16.9	43.9	32.8	3.1
	2011-10-16	4.6	8.1	19.4	45.6	33.5	7.2
	2011-10-17	3.0	5.4	14.8	61.3	30.2	0.9
	2011-10-25	3.8	6.6	12.7	42.9	25.6	5.2
	2011-11-07	3.9	2.8	12.8	50.7	40.5	1.6
	Avg.	5.0	5.2	16.2	50.3	36.3	12.9
winter	2011-12-12	2.3	2.6	5.0	50.8	25.4	0.8
	2011-12-14	2.5	0.3	0.7	49.3	27.5	7.5
	2011-12-16	4.6	0.9	-3.4	47.7	27.8	4.3
	2011-12-22	3.9	0.9	-0.8	44.7	28.6	5.5
	2011-12-24	4.1	0.8	1.1	43.8	26.6	8.1
	2012-1-4	3.4	0.7	-3.1	50.5	26.4	6.8
	Avg.	3.5	1.0	-0.1	47.8	27.1	5.5

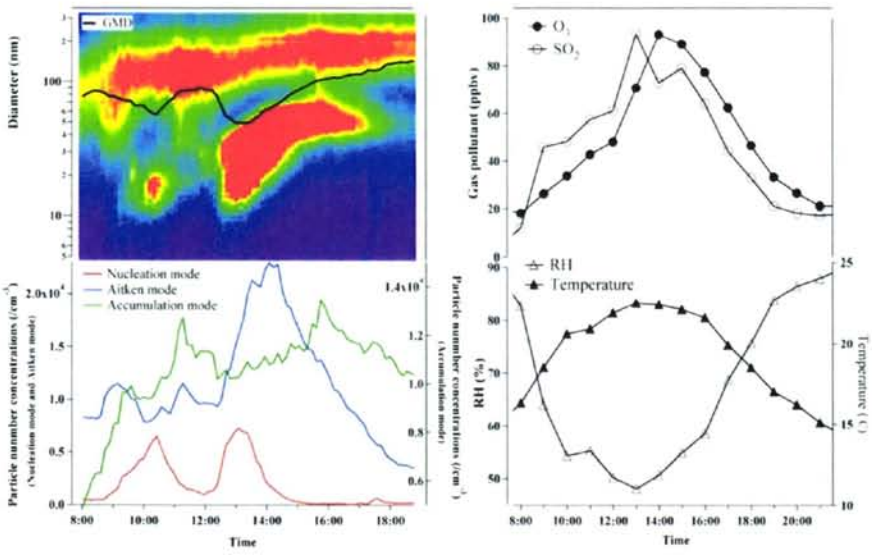

图 4-9 黄河三角洲地区秋季典型新颗粒物生成及事件图（2011/10/12）

本次研究选取黄河三角洲地区夏季 7 月 16 日的另一次典型新颗粒物生成及增长事件进行分析，如图 4-10 所示，凝结核模态颗粒物数浓度在 12:00 左右开始明显增加，并且以 4 nm/h 的颗粒物增长速率（$GR_{5\text{-}20}$）持续长大至 14:30。由图中可以看出，SO_4^{2-}的质量浓度伴随凝结核模态颗粒物数浓度的爆发而明显增加，这说明在 NPF 事件中，光化学反应以及硫酸气的均相成核过程是凝结核模态的颗粒物增加重要的贡献因素。同时从颜色图中看出，老化气团的输送对于爱根模态的增加也有重要的贡献。

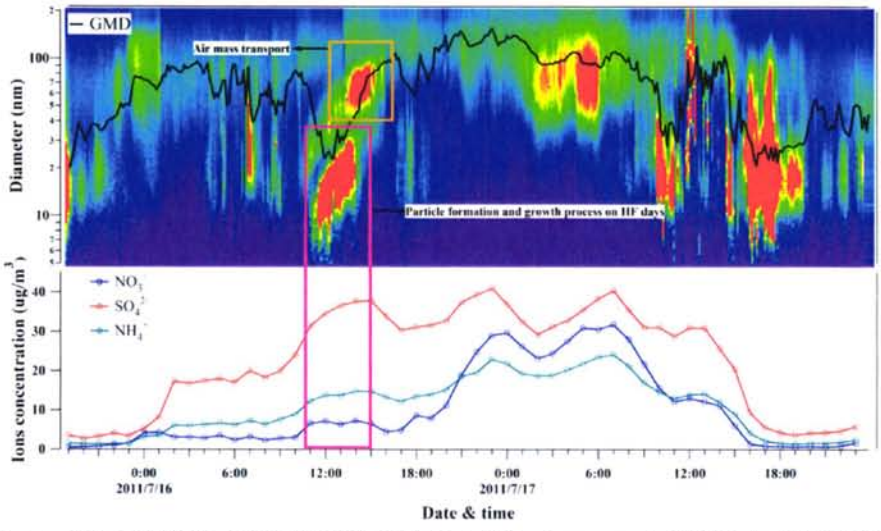

图 4-10 黄河三角洲地区夏季典型新颗粒物生成事件（2011/7/11）颗粒物生成增长颜色图以及对应的主要水溶性离子变化图

4.6 不同天气条件下颗粒物数浓度特征对比

4.6.1 雾霾和清洁天气下颗粒物数浓度及粒径分布对比

为了探讨黄河三角洲地区雾霾发生期间气溶胶颗粒物数浓度及粒径分布与雾霾的关系，我们分别研究了黄河三角洲地区不同季节雾霾与清洁天气下颗粒物的数浓度及粒径分布特征。

表 4-4 列出了各季节雾霾与清洁天气下不同粒径段数浓度的统计结果。由表 4-4 可知，黄河三角洲地区四个季节均表现出为雾霾天气下 5 nm<D_p<20 nm、20 nm<D_p<50 nm、50 nm<D_p<100 nm 三个超细气溶胶粒径段数浓度明显低于清洁天气，而 100 nm<D_p<200 nm、200 nm<D_p<500 nm、500 nm<D_p<1000 nm 三个较大粒径气溶胶粒径段数浓度则高于清洁天气时。其中凝结核模态（5-20 nm）颗粒物数浓度清洁天气下在春季、秋季、夏季和冬季分别是雾霾天气的 6 倍、5.7 倍、2.3 倍和 2.3 倍。如图 4-11 所示，清洁天气条件下，5-100 nm 粒径段的颗粒物所占百分比高于雾霾天气下，而雾霾天气下 100 nm<D_p<500 nm 段颗粒物数浓度所占百分比较高，特别是秋季这种现象更为明显。这在一定程度上说明了 100 nm<D_p<500 nm 粒径段气溶胶在黄河三角洲地区雾霾天气的形成过程中起了关键的作用，而 5 nm<D_p<20 nm、20 nm<D_p<50 nm、50 nm<D_p<100 nm 等超细气溶胶数浓度的降低也说明雾霾天气的大气环境不利于超细粒子的生成与存在。

表 4-4 黄河三角洲地区各季节不同颗粒物粒径范围数浓度统计（1h 均值，单位：#/cm^3）

季节	统计项目/粒径范围	凝结核模态	爱根模态			积聚模态				
	（nm）	5-20	20-50	50-100	20-100	100-200	200-500	500-1000	100-1000	5-10000
春	雾霾	581	3312	4072	7384	3725	791	47	4563	12531
	清洁	3487	5418	5771	11189	1674	312	13	2000	16678
夏	雾霾	1346	2604	3043	5647	2557	622	267	3446	10451
	清洁	3084	4398	4153	8551	1105	248	56	1410	13046
秋	雾霾	546	3106	3234	6340	4345	2563	145	7153	14049
	清洁	3096	7175	4520	11695	1721	589	17	2327	17120
冬	雾霾	507	2383	2508	4891	2007	453	19	2779	7882
	清洁	1153	3187	2905	6092	919	149	1	1069	8314
全年平均	雾霾	819	3114	3140	6254	2761	1115	154	4030	11105
	清洁	2374	4584	4118	8702	1809	329	18	2156	13235

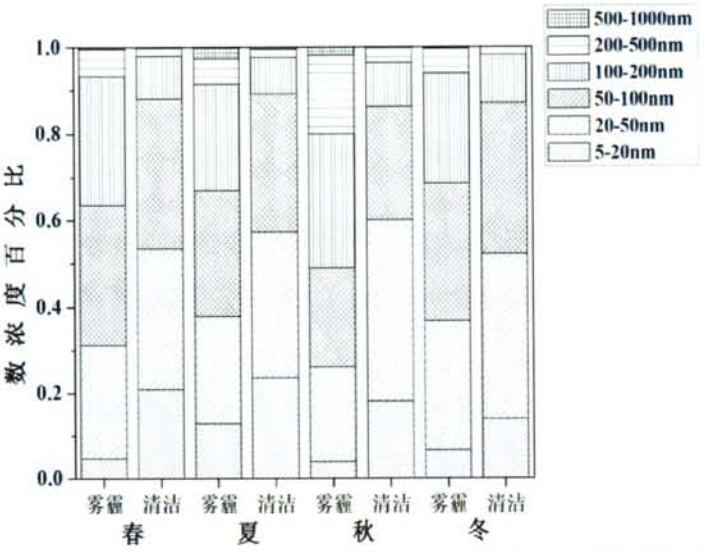

图 4-11 不同大气污染状况下各粒径范围气溶胶数浓度百分比的季节对比图

如图 4-12 所示，雾霾和清洁天气下，大气气溶胶数浓度粒径分布对比特征基本相似，表现为单峰型且雾霾天气下颗粒物的粒径分布曲线向大粒径方向移动，清洁天气下粒径分布曲线的峰值出现在 30 nm 附近，而雾霾天峰值出现 100 nm 附近，这说明爱根模态和积聚模态等粒径较大的颗粒物对雾霾的形成贡献高于凝结核模态的颗粒物。

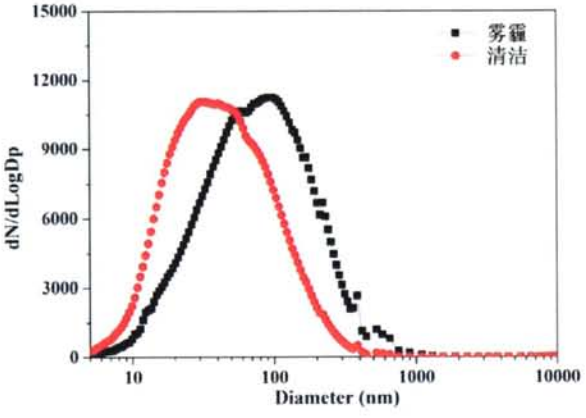

图 4-12 雾霾和清洁天气下颗粒物粒径分布特征图

4.6.2 典型雾霾和清洁天气新颗粒物生成个例分析

新颗粒物生成事件一般发生在清洁天气，但是在雾霾天气下也会有新颗粒物生成及增长现象发生，在观测期间共有 5 次新颗粒物生成事件发生在雾霾天气下，

其中 4 次集中在夏季（7/9，7/16，7/21，7/23），1 次发生在冬季（12/14）。

从表 4-5 对比结果看出，雾霾天与清洁天颗粒物的增长速率接近，但清洁天的成核速率是雾霾天的两倍，同时图 4-14 中显示，雾霾天积聚模态颗粒物数浓度在总颗粒物数浓度中的比例（26%）高于清洁天（11%），这说明雾霾天的天气条件适合爱根模态颗粒物通过碰并和凝结作用长大成为积聚模态颗粒物(Gao et al., 2009; Kang et al., 2013)，而更多较大粒径颗粒物的存在则在一定程度上抑制了颗粒物的生成。凝结核模态颗粒物数浓度在清洁天和雾霾天都是在 12:00 左右开始增加，这可能是由于正午的高温以及较强的太阳辐射，有利于发生光化学反应。

表4-5 黄河三角洲地区观测期间雾霾和清洁天气下新颗粒物生成事件（NPF）相关参数（FR_{5-20}、GR_{5-20}、RH、SO_2、O_3）均值表

天气	GR_{5-20} (nm/h)	FR_{5-20} (#/(cm^3·s))	RH (%)	O_3 (ppbv)	SO_2 (ppbv)
雾霾	5.06	3.4	56.4	60.7	14.0
清洁	5.02	7.3	46.1	41.1	12.3

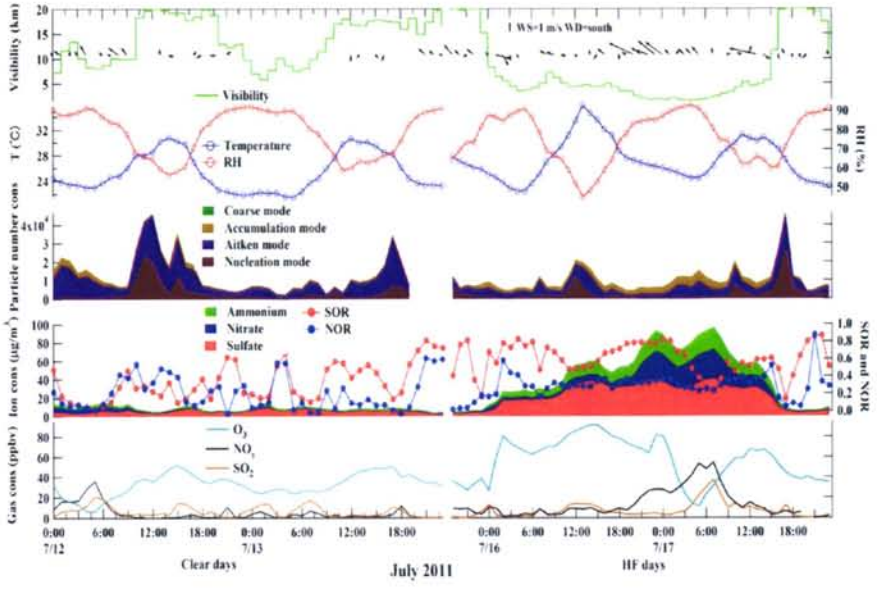

图 4-14 典型雾霾天(7/15 19:00 - 7/17 23:00) 和清洁天(7/12 0:00 - 7/13 23:00)气态污染物(SO_2, O_3, NO_y)、主要水溶性离子(SO_4^{2-}, NH_4^+, and NO_3^-)、SOR、NOR、颗粒物数浓度及气象因素（温度、湿度、风向风速和能见度）小时变化图

4.7 本章小结

本章分析了黄河三角洲地区大气颗粒物数浓度的季节变化及日变化特征，研究了风向风速以及气流轨迹对颗粒物数浓度和粒径分布的影响，并计算了不同季节典型新颗粒物生成事件的成核和增长速率。主要结论如下:

1、黄河三角洲地区观测期间 5-10000 nm 粒径范围内总颗粒物平均数浓度为 12838 #/cm^3，春季数浓度最高，冬季最低。从不同粒径范围来看，黄河三角洲地区气溶胶中爱根模态颗粒物数浓度最高，全年平均占总颗粒物数浓度的 60.7%，其次为积聚模态（25.2%）和凝结核模态（14.1%）。凝结核模态颗粒物在春季和夏季数浓度最高，爱根模态则是在春季和秋季最高，积聚模态秋季最高。

2、黄河三角洲地区观测期间凝结核模态和爱根模态颗粒物在新颗粒物生成事件（NPF）发生的观测时段数浓度日变化特征明显，而未发生新颗粒物生成事件（non-NPF）的观测时段则没有明显的日变化，这说明 NPF 事件对凝结核模态和爱根模态颗粒物数浓度日变化有明显影响。

3、观测期间夏秋季节主要盛行东南风，而春季和冬季盛行西北风和东南风。总体来说，偏南风时颗粒物的数浓度要高于偏北风时。南部及东部短距离传输的气团具有更高浓度的颗粒物，平均为 14903 #/cm^3，而北部长距离传输的气团的颗粒物数浓度较低，平均为 11462 #/cm^3。北部长距离传输的气团的颗粒物粒径分布均为单峰分布，峰值均在爱根模态，而南部和东部短距离传输的气团粒径分布在更大粒径位置（100 nm 附近）出现峰值。

4、在观测期间，共有 26 天发生了新颗粒物生成事件（NPF），其中春季 7 天，夏季 7 天，秋季 6 天，冬季 6 天，约占总观测时间的 22%。凝结核模态颗粒物的平均成核速率为 6.6 #/(cm^3·s)，最低值为 0.3 #/(cm^3·s)，最大值为 31.9 #/(cm^3·s)，颗粒物的平均增长速率为 5.3 nm/h，最低值为 2.3 nm/h，最大值为 12.7 nm/h。

5、100 nm<D_p<500 nm 粒径段气溶胶在黄河三角洲地区雾霾天气的形成过程中起了关键的作用，而 5 nm<D_p<20 nm、20 nm<D_p<50 nm、50 nm<D_p<100 nm 等超细气溶胶数浓度的降低也说明雾霾天气的大气环境不利于超细粒子的生成与存在。

第五章 黄河三角洲地区单颗粒气溶胶特征

前文利用现场连续观测方法研究了黄河三角洲地区 $PM_{2.5}$ 中水溶性离子以及不同粒径颗粒物的数浓度等，本章节根据现场连续观测结果，从单颗粒表征手段对单颗粒成分、形态及混合状态进行了深入分析。

5.1 单颗粒采样期间主要污染物浓度特征

本次单颗粒采样时间集中在2011年春季和夏季，其中春季选取6个雾霾天、2个清洁天和2个沙尘天采样，夏季选取5个雾霾天和3个清洁天采样。本次研究共分析了5724个单颗粒，其中春季雾霾天分析2366个单颗粒，夏季雾霾天分析988个单颗粒，春季清洁天分析403个单颗粒，夏季清洁天分析518个单颗粒样品。采样期间 $PM_{2.5}$ 及其中主要水溶性离子质量浓度、气态污染物浓度以及不同粒径范围的颗粒物数浓度列于表5-1中。

结果显示在单颗粒采样期间 $PM_{2.5}$ 的平均质量浓度高低水平分别为沙尘天（131 $\mu g/m^3$）>雾霾天（81 $\mu g/m^3$）>清洁天（27 $\mu g/m^3$），沙尘天和雾霾天 $PM_{2.5}$ 质量浓度超过了我国空气质量标准的 $PM_{2.5}$ 日均浓度值(75 $\mu g/m^3$)。$PM_{2.5}$ 中主要水溶性离子（NO_3^-、SO_4^{2-}、NH_4^+）雾霾天的平均质量浓度约为清洁天和沙尘天的4-5倍，清洁天和沙尘天的浓度类似，且雾霾天主要水溶性离子在 $PM_{2.5}$ 的比例也明显升高，约占 $PM_{2.5}$ 的53.1%，高于清洁天（35.2%）和沙尘天（7.8%），这说明雾霾天有利于二次离子的生成，而沙尘天则对细粒子中二次离子的生成有抑制作用。SO_2 和 O_3 浓度也是在雾霾天明显高于清洁天和沙尘天，NO_y 则是清洁天较低，雾霾天和沙尘天浓度接近。5-10000 nm 粒径范围的颗粒物总数浓度高低水平为雾霾天(15335 #/m^3)>清洁天(13588 #/m^3)>沙尘天(6456 #/m^3)，清洁天凝结核模态颗粒物数浓度最高，这可能是由于清洁天新颗粒物生成事件发生频率较高，导致凝结核模态颗粒物数浓度的上升；而爱根模态和积聚模态颗粒物则是在雾霾天数浓度最高，沙尘天气下积聚模态颗粒物数浓度比例也较高。爱根模态在黄河三角洲地区大气颗粒物数浓度中占主导地位，不同天气下均占总颗粒物数浓度的60%以上。

表 5-1 黄河三角洲地区春季和夏季单颗粒采样期间不同天气条件下主要理化性质参数浓度表

	Date	Episode	$PM_{2.5}$	NO_3^-	SO_4^{2-}	NH_4^+	Sum proportion in $PM_{2.5}$	SO_2	O_3	NO_y	Nucleation mode (5-20 nm)		Aitken mode (20-100 nm)		Accumulation mode (100-1000 nm)	
			($\mu g/m^3$)	($\mu g/m^3$)	($\mu g/m^3$)	($\mu g/m^3$)	(%)	(ppbv)	(ppbv)	(ppbv)	(#/cm^3)	(%)	(#/cm^3)	(%)	(#/cm^3)	(%)
spring	04/14	HF	183	44.9	35.0	25.0	57.31	20	36	28	621	5.98	5359	51.6	4405	42.42
	04/17	Clear	15	0.8	2.7	0.9	29.33	7	26	9	2566	25.02	6338	61.81	1350	13.17
	04/20	HF	101	3.8	15.2	9.9	28.55	34	38	35	1968	7.03	19745	70.53	6283	22.44
	04/23	Clear	52	1.5	3.9	3.9	17.88	2	40	24	794	8.38	6682	70.57	1991	21.03
	04/25	HF	47	11.4	8.9	11.1	66.75	31	13	42	589	4.25	9424	68.00	3843	27.73
	04/28	HF	69	9.9	12.5	6.8	42.29	19	65	33	110	1.09	7123	70.52	2865	28.36
	04/29	HF	78	18.4	18.0	10.9	60.59	20	48	36	16	0.16	6324	62.71	3743	37.12
	04/30	dust	162	3.8	5.8	3.7	8.21	4	31	26	95	1.84	3334	64.35	1740	33.59
	05/01	After dust	100	2.2	3.5	1.6	7.29	5	29	29	91	1.18	6163	79.42	1488	19.18
	05/02	HF	62	7.7	11.4	6.5	41.12	18	33	40	51	0.42	8645	70.18	3620	29.39
summer	07/05	HF	67	6	18.4	8.8	49.55	14	65	30	6614	17.24	25850	67.39	5884	15.34
	07/07	HF	91	14.9	26.8	13.6	60.77	13	42	23	973	9.18	6499	61.32	3107	29.31
	07/11	HF	51	6	13.3	6.7	50.98	4	36	9	4045	28.06	8262	57.31	2105	14.61
	07/12	Clear	30	1.8	6.5	2.9	37.33	7	30	8	4033	24.18	10749	64.44	1898	11.38
	07/13	Clear	14	1.4	4.1	1.9	52.86	5	34	3	1581	16.39	7211	74.77	852	8.83
	07/14	Clear	23	1.7	5.1	2.1	38.70	6	38	6	8836	40.36	10190	46.54	2867	13.10
	07/16	HF	103	15.7	33.1	16.1	63.01	6	73	9	1610	19.13	4212	50.05	2577	30.62
	07/17	HF	37	2.4	14.7	6.4	63.51	9	45	20	3161	25.83	6181	50.51	2868	23.44
Mean	11 days	HF	81	12.8	18.8	11.1	53.13	17	45	28	1796	10.76	9784	61.83	3754	27.34
	5 days	Clear	27	1.5	4.5	2.3	35.22	6	34	10	3562	22.87	8234	63.63	1792	13.50
	2 days	Dust	131	3.0	4.7	2.6	7.75	5	30	27	93	1.51	4749	71.89	1614	26.38

5.2 单颗粒采样期间气流轨迹分析

气团传输也是影响黄河三角洲地区单颗粒类型及混合状态的重要因素之一，我们利用 HYSPLIT 模型计算了观测期间的后推 3 天（72h）气流轨迹，然后将单颗粒采样期间每一天的平均轨迹绘于图 5-1 中。

从图中可以看出，黄河三角洲地区在单颗粒采样期间雾霾发生时的气团轨迹（图 5-1 中红色线条表示）一般传输距离较短，海拔高度较低，且多来自西部和南部，多经过京津冀地区以及山东省内污染较重城市，将大量污染物带到采样点。清洁天的气团主要来自北部和东部，且传输距离一般较远，气团移动速度较快，气团的海拔高度较高。4 月 30 日 12:00 之后采样点发生了一次严重的沙尘暴现象，MODIS 卫星图片显示沙尘暴从中国的西北部移动到山东半岛区域，后推气流轨迹分析也发现黄河三角洲地区的沙尘来自蒙古和内蒙古，经过京津冀地区和渤海，最后到达黄河三角洲地区。

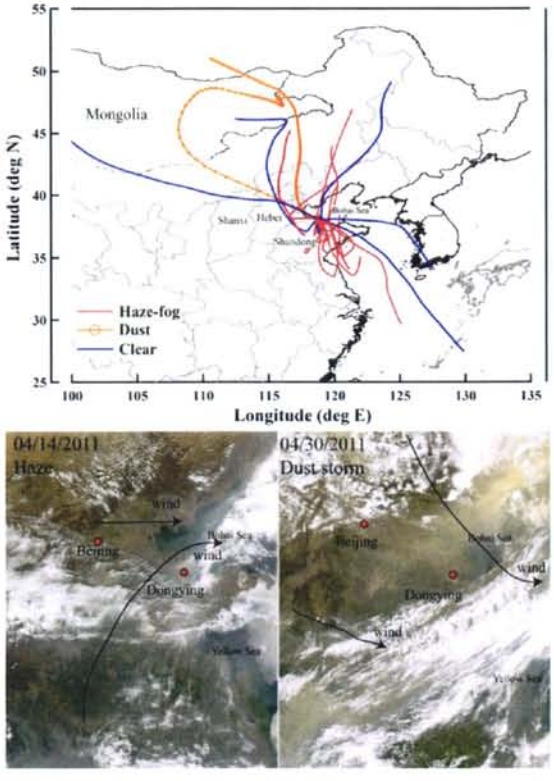

图 5-1 黄河三角洲地区单颗粒采样期间后推 3 天气流轨迹图

及典型雾霾和沙尘天气下的 MODIS 图片

5.3 春季单颗粒气溶胶的主要类型及不同天气条件下单颗粒混合状态

5.3.1 春季单颗粒气溶胶主要类型及颗粒物粒径分布

春季分析的单颗粒样品数量较多，因此颗粒物的类型也较丰富，归纳总结主要分为 9 种：矿物颗粒（mineral particle）、富钾颗粒（K-rich particle）、富钠/镁颗粒（Na/Mg-rich particle）、金属/飞灰颗粒（metal/fly ash particle）、钙盐颗粒（$CaSO_4$/$Ca(NO_3)_2$particle）、富硫颗粒（S-rich particle）、烟尘颗粒（soot particle）、有机颗粒（organic matter particle）和海盐颗粒（NaCl particle）。颗粒物分类的原则是基于在每一个颗粒物中占总成分 60%以上的的成分来确定具体是哪种颗粒。在大多数情况下单颗粒的来源可以通过颗粒物的形貌和成分来确定[238]。主要元素的组成、颗粒物的特征、以及不同类型颗粒物的来源都在表 5-2 中归纳出来，这些信息可以帮助我们更好的理清黄河三角洲地区颗粒物的理化性质及混合状态。

透射电镜图片显示飞灰颗粒为圆形，主要成分为氧、硅、铝和金属，主要来源是燃煤和工业排放，且通常内混于富硫颗粒和富钾颗粒等。烟尘型颗粒是化石燃料(如石油、煤和生物质)不完全燃烧排放出的细颗粒，烟尘颗粒内部往往伴随着一定量的有机组分，主要元素为碳和氧，呈现多个碳球连接的复杂链状，烟尘颗粒粒径通常在 1 μm 以下，在大气中存留时间比较长，并且有强吸光性，对大气起到增温效应[239]。

矿物颗粒具有不规则形状，主要元素为硅、铝、钙、镁等，一般矿物颗粒外层会包裹一层可见的外壳，外壳的元素主要是氮、氧、少量的硫和氯等。金属颗粒呈现球形，主要内混于富硫颗粒和富钾颗粒内部。有机颗粒主要成分为有机碳，也是具有不规则形状，常常与其它颗粒混合。

表 5-2 黄河三角洲地区观测期间不同类型颗粒物的判别标准、形貌特点及主要来源

颗粒物类型	主要元素	颗粒物形貌特点	来源
矿物颗粒	Si, Al, Ca	不规则形状的黏土、石英、长石以及少量的方解石、白云石等	沙漠及土壤扬尘等自然源和建筑扬尘、道路扬尘、燃煤电厂、水泥工业等人为源
富钾颗粒	K, S, Si	不规则形状的硫酸钾和硝酸钾等	生物质燃烧
富钠/镁颗粒	Na, S, Mg	无固定形状的硫酸镁和硫酸钠等	海盐颗粒的老化颗粒
金属/飞灰颗粒	Zn, Fe, S Si, Al, Fe	金属: Fe_2O_3、MnO_2、 ZnO、PbO 等 飞灰: 无固定形状的硅酸盐	燃煤电厂、重工业及石油化工行业排放
钙盐颗粒	Ca, S, Si	规则形状的硫酸钙或附着于其他颗粒表面的硝酸钙等	碳酸钙、氧化钙等颗粒的老化颗粒
富硫颗粒	S, K, Si	硫酸铵等，电镜下多呈泡沫状	气态污染物 SO_2、NO_x 等通过二次转化生成的颗粒
烟尘颗粒	C, O, S	石墨球组成的链状颗粒或者无固定形状的有机颗粒	化石燃料及生物质燃烧
有机颗粒	C, O, Si	圆形或不规则形的有机颗粒	化石燃料及生物质燃烧
海盐颗粒	Na, Cl	立方体状的氯化钠颗粒	海洋（渤海或黄海）

5.3.2 春季雾霾天单颗粒混合状态

雾霾颗粒的混合状态可以帮助追踪颗粒物的来源以及评估颗粒物的气候效应[135,143]。本次研究通过透射电镜分析发现，春季雾霾天气颗粒物主要以二次颗粒和含碳颗粒为主，且老化程度明显，说明颗粒物在大气传输过程中经过了复杂的化学变化过程，颗粒物的混合程度强烈，且多从外部混合转变为内部混合。而清洁天气主要以二次颗粒、海盐颗粒和含碳颗粒为主，二次颗粒的混合程度与污染天气相比有显著降低且二次颗粒的质量浓度较低，这说明污染天气条件下更有利于酸性气体向颗粒物转化，并且二次颗粒物发生的聚集造成进一步的内部混合。

通过对雾霾天气和清洁天气下单个气溶胶颗粒比较发现，不同天气条件下颗粒的形貌和混合程度显示出较大的区别。硫酸或者硫酸铵在硫酸钾或者硝酸钾颗粒物(图 5-2b)中的比例增加时，富钾颗粒可能会转化为含有一定钾元素的富硫颗粒(图 5-2e)。一些碱性颗粒物（如方解石和白云石）(图 5-2a)通过和 SO_2 或 HNO_3 的非均相反应生成 $CaSO_4$/$Ca(NO_3)_2$ 等钙盐或者富镁颗粒（Mg-rich）(图 5-2c\f\g)。氯化钠颗粒通过 SO_2 或 HNO_3 的非均相反应生成可以转化为富钠颗粒(如 Na_2SO_4 和 $NaNO_3$)。因此这些颗粒物在传输过程中通过化学反应和物理凝结发生老化现象，从而可以诱导使一种颗粒物转化为另一种颗粒物。另外，TEM 图片显示可溶性的硫酸盐和富钾颗粒趋向于与难熔的新鲜排放的颗粒物包括烟尘颗粒(图 5-2h\i)、金属/飞灰颗粒(图 5-2b\d\e)、有机颗粒(图 5-2j\k)和矿物颗粒等发生融合。黄河三角洲地区雾霾颗粒的混合状态要比 Adachi 和 Buseck（2008）[240]报道过的重污染的墨西哥城的颗粒物内混状态更复杂，在该报道中只发现了烟尘颗粒、硫酸盐颗粒和有机颗粒的内混现象。

外部混合的有机颗粒，通常表现出圆形或椭圆形，（图 5-2d\k），另外一些由于完全内部混合于硫酸盐而不能够直接通过形貌区分（图 5-2i）。Li 等[241]认为当能够通过形貌来区分有机颗粒时，这些有机颗粒可能是来自一次排放，通常不溶于水；而无法从形貌来区分出的有机颗粒可能是被氧化或在硫酸盐颗粒表面生成的二次有机组分，这种有机组分可溶于水。众多实验证据表明透射电镜能够直接观察到的有机颗粒的吸湿性主要受其混合的硫酸铵影响，而完全混合于硫酸盐而无法辨认的可溶性有机物则会降低硫酸铵的潮解点[242]。

在老化气团中，大多数的富硫颗粒通常会被有机薄膜包裹(图 5-2k)，这些薄膜可能是初级有机物的氧化或者二次有机物的浓缩形成[241]。最近研究表明挥发性和半挥发性的有机物会参与新颗粒物的生成及增长现象[243],因此我们推测在这层薄膜中的有机物质是和硫酸盐在大气中生成开始就一直共存的。另外其他研究也表明，有机物和硫酸盐、硝酸盐大部分时候都是共存在一个颗粒物中[244]。因此我们可以得出这样的结论，通过长距离输送的雾霾颗粒会通过有机和无机的气态凝结（包括在颗粒物表面的非均相反应）和物理凝聚而发生老化现象。样品中部分矿物颗粒表面覆盖有一层似胶体状的物质，Li 等[238]已经证实这是碱性矿物颗粒输送过程中和酸性气体发生非均相反应生成的硝酸钙颗粒。当矿物颗粒表面生成硝酸盐之后，颗粒的粒径会增加，表面吸附更多水或有机组分，因此这种颗粒也会有很强散光特性。

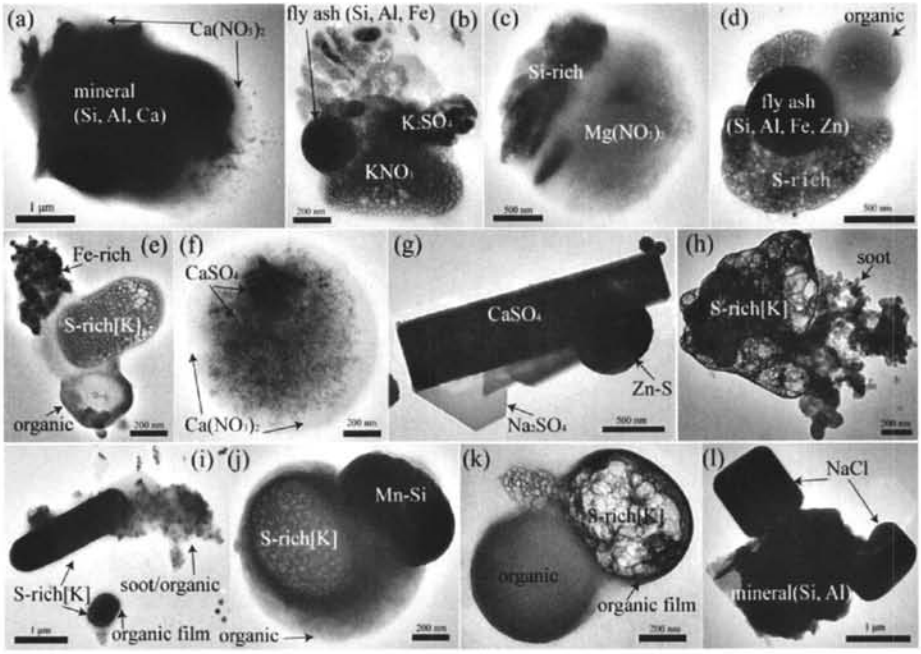

图 5-2 黄河三角洲地区春季不同类型颗粒物典型的混合状态：(a)矿物颗粒，外层包裹 $Ca(NO_3)_2$；(b)富钾颗粒(KNO_3 和 K_2SO_4)与飞灰颗粒的混合颗粒，(c)矿物颗粒，外层包裹 $Mg(NO_3)_2$；(d)硫酸铵、飞灰和有机颗粒的混合颗粒；(e)富硫颗粒、有机颗粒和富铁颗粒的混合颗粒；(f)发生老化反应的颗粒，内部含有或外层包裹有 $CaSO_4$ and $Ca(NO_3)_2$；(g)规则形状的硫酸钠颗粒以及圆形的硫化锌颗粒附着于矩形的 $CaSO_4$ 颗粒；(h)富硫颗粒与烟尘颗粒的混合颗粒；(i)椭圆形富硫颗粒与烟尘颗粒的混合，外层包裹有机物；(j)Mn-Si 颗粒附着于内含富硫颗粒的有机颗粒；(k)圆形的有机颗粒与富硫颗粒的粘合，富硫颗粒外层包裹有机物；(l)两个方形的 NaCl 颗粒附着于不规则的矿物颗粒上。

透射电镜及能谱分析（TEM/EDS）不仅能够提供颗粒物的形貌、组分和混

合状态，还能提供颗粒物的粒径信息。由于不同来源和不同形成过程的大气气溶胶颗粒的粒径不同，所以研究它们的粒径分布特征具有重要的意义。图 5-3 显示了不同类型颗粒物的粒径分布特征，春季雾霾期间，2366 个颗粒物的粒径范围为 40 nm - 5 μm，其中 87%的富硫颗粒粒径小于 1 μm，占所有颗粒物的 64%(图 5-3a)，在雾霾期间约 63%的矿物颗粒和钙盐（$CaSO_4$/$Ca(NO_3)_2$）颗粒粒径大于 1 μm，尽管 TEM 经常会观测到大量的细颗粒物，但只有一小部分的富钾颗粒，金属/飞灰颗粒，烟尘颗粒和有机颗粒粒径小于 1 μm。这可能是由于大部分难熔的细颗粒物通常是内混于硫酸盐颗粒中(图 5-2b\d\e\i)，而这部分并没有显示在图 5-3 中，换句话说，气团的老化会导致内混颗粒物数量的增加，外混的一次排放的颗粒数量会相应降低，而这种颗粒物老化过程会改变颗粒物的光学和吸湿特性[135]。

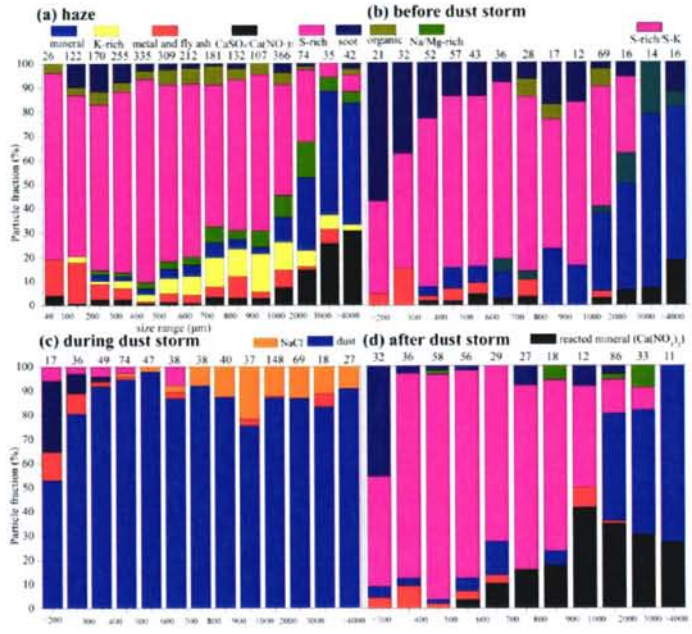

图 5-3 黄河三角洲地区春季雾霾和沙尘前中后期不同粒径段颗粒物的数量百分比图

5.3.3 春季沙尘天颗粒物老化研究

在黄河三角洲地区 4 月 30 日 12:00 开始有沙尘现象发生，一直持续到 4 月 30 日晚 23:00。我们采集了沙尘前、中、后期单颗粒样品，图 5-4-5-6 显示在三个时间段不同类型的颗粒物。

沙尘暴发生之前：观测期间沙尘与灰霾的混合在 4 月 30 日 5:00 开始，在 12:00

结束，这段时间有大量的沙尘颗粒，但由于粒径较小，并不能称为沙尘暴，因此这段时间我定义为沙尘暴前段。TEM 显示有些典型的外混颗粒出现在沙尘暴爆发之前如外混的有机颗粒、矿物颗粒和烟尘颗粒(图 5-4a-b)。图 5-3a-b 显示了沙尘暴发生之前硫酸盐的粒径分布和灰霾期间比较接近，主要是集中在 1 μm 以下，富硫颗粒占总颗粒物的 56%，低于灰霾期间的 64%，但是外混于烟尘颗粒的比例为 16%，高于灰霾期间的 4%。图 5-3a-b 还显示大粒径的矿物颗粒在沙尘暴前段比例明显高于灰霾期间的比例，这些变化主要是由于 4 月 30 日从河北北部、山东西部、以及京津地区传输来的气团(图 5-1)使得扬尘的侵入，降低了黄河三角洲地区内混颗粒及老化颗粒的比例。TEM/EDS 分析结果进一步显示在沙尘暴爆发之前主要存在的颗粒物是含有钾、烟尘、有机物的富硫颗粒以及硫酸钾颗粒(图 5-4)，这表明生物质燃烧可能对传输气团中的颗粒物有一定贡献，而根据省级环境保护部门的报到，3 月份之后就会出现玉米秆燃烧现象。

沙尘暴发生时：4 月 30 日 11:00 之后风速开始增加，严重的沙尘暴现象在 12:00 之后开始出现。由于黄河三角洲地区主要以湿地为主，因此当地的沙尘对此次沙尘暴贡献可以忽略。TEM 图片观测结果显示沙尘期间 87%的颗粒是不规则的沙尘颗粒(图 5-5a)。TEM/EDS 分析结果显示伊利石和石英是最常见的矿物颗粒，而沙尘颗粒对这段时间的颗粒物粒径起主导作用(图 5-3c)。另外，在沙尘颗粒表面能观测到微小的烟尘颗粒，图 5-3c 显示外混的烟尘、金属/飞灰、硫酸颗粒的粒径均小于 200 nm，这表明超过 4.5%的人为源排放的细颗粒混合在了沙尘颗粒中。这些分析证明沙尘颗粒通过长距离输送与人为排放的颗粒物发生了混合现象，Itahashi 等[245]指出在低对流层中沙尘颗粒与污染物的混合是亚洲沙尘暴的典型特点之一。

另外，在雾霾期间发现的包裹钙盐（$Ca(NO_3)_2$）的矿物颗粒没有在沙尘期间发现，同时 TEM/EDS 会经常发现在沙尘颗粒中有少量的硫存在，SO_2 的浓度在沙尘期间降低明显。我们推测在干燥环境下（RH<35%）沙尘颗粒物表面发生非均相反应从而有效吸收 SO_2，同样的现象也在北京沙尘暴期间发现[246]。

在观测中还发现有些沙尘颗粒会和海盐颗粒混合(图 5-21 和图 5-5b)，而这种类型的颗粒物在北京沙尘观测期间未观测到，这种混合现象可能是由于气团传输到达黄河三角洲地区之前会经过渤海从而带来更多的海盐气溶胶。沙尘颗粒与海

盐气溶胶的混合也在中国下风向的韩国和日本观测到[247-249]。令人惊讶的是这种沙尘颗粒和海盐颗粒混合的现象在从北向南经过渤海的冷锋过境时发现的，这可能是由于沙尘暴期间伴随的高风速从而从渤海带来大量的海盐气溶胶。而考虑到我们的观测点是在地面站点，大部分自由对流层的沙尘颗粒则没有和海盐发生混合。

沙尘暴发生之后：沙尘暴过后这段时间持续了 8-10 个小时，能见度逐渐升高，而风速略有下降，温度、湿度和气流轨迹则没有明显的变化。表 5-1 结果显示滞留的悬浮沙尘颗粒依然对 5 月 1 日的空气质量有所影响，$PM_{2.5}$ 浓度仍然高于 100 μg/m^3，同时有 85%的成分是不溶的沙尘成分。图 5-3d 显示硫酸盐颗粒的百分比在这段时间迅速升高到 52%，同时矿物颗粒也通过长距离输送发生了一系列混合现象。图 5-6 显示发生反应后被钙盐包裹的矿物颗粒成为了圆形，不同于他们最初的不规则形状，这表明在这些矿物颗粒表面发生了大量的化学反应。这种现象也在日韩等国家被观测到[247,248,250]。而我们的观测结果则是首次揭示了矿物颗粒与酸性气体(如 SO_2、HNO_3、NO_2 等)的非均相化学反应可以发生在伴随着沙尘烟羽的冷锋过境过程中。

总得来说单颗粒分析清晰的揭示了在沙尘暴发生前、发生中和发生后不同时期的颗粒物类型、含量及成分的不同，这表明不同类型颗粒物的混合以及沙尘矿物颗粒与酸性气体的非均相反应取决于气象因素和混合的过程。

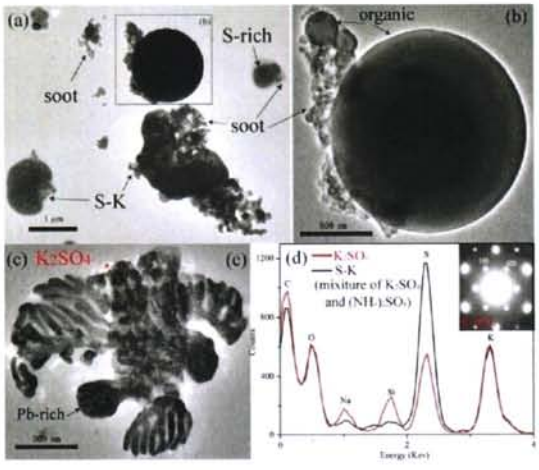

图 5-4 沙尘之前的单颗粒气溶胶：(a)外混的烟尘颗粒以及硫化钾颗粒；(b)圆形有机颗粒表面附着的有机颗粒和烟尘颗粒；(c)硫酸钾与富铅颗粒的混合颗粒；(d)硫化钾以及不同类型硫酸钾的能谱分析

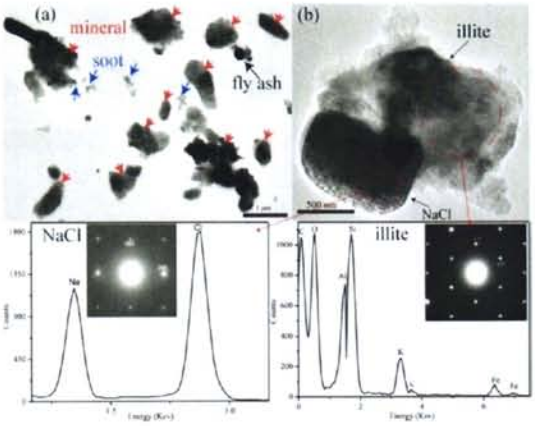

图 5-5 沙尘期间的沙尘单颗粒气溶胶：(a)沙尘颗粒（红色箭头指示）以及烟尘颗粒（黑色箭头指示）；(b)伊利石和海盐的混合颗粒

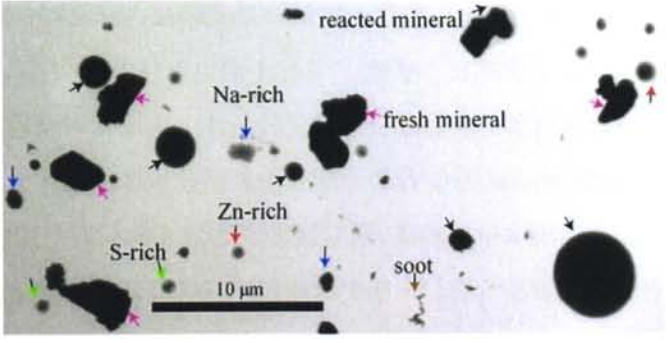

图 5-6 沙尘过后的单颗粒气溶胶：被 $Ca(NO_3)_2$ 包裹的反应后的沙尘颗粒（黑色箭头指示）；新鲜排放的矿物颗粒(紫色色箭头指示)；富钠颗粒(蓝色箭头指示)；烟尘颗粒(深黄色箭头指示)；富硫颗粒(绿色箭头指示)；富锌颗粒(红色箭头指示)

5.4 夏季单颗粒气溶胶的主要类型及雾霾天富硫颗粒混合状态

5.4.1 夏季单颗粒气溶胶主要类型

黄河三角洲地区夏季观测期间颗粒物类型较春季减少，主要有 6 个主要类型：富硫颗粒（S-rich particle）、烟尘颗粒（soot particle）、矿物颗粒（mineral particle）、金属颗粒（metal particle）、飞灰颗粒（fly-ash particle）以及有机颗粒（organic particle）。

通过在线离子色谱监测结果显示黄河三角洲地区硫酸盐在 $PM_{2.5}$ 中占到约 30-50%，而透射电镜结果也显示黄河三角洲地区富硫颗粒在大气中是最丰富的一种颗粒类型。能谱结果显示富硫颗粒颗粒主要含有硫、氧和氮元素，很可能为

硫酸铵或硫酸氢铵。水溶性离子分析结果显示，这种硫酸盐颗粒最有可能是硫酸铵颗粒。在电镜图片中富硫颗粒一般为泡沫状（图 5-7），这主要是由于硫酸铵颗粒在电子束的照射下发生弱分解，留下了剩下富硫的残余物以及其他的内含物呈现泡沫状。

5.4.2 夏季雾霾天富硫颗粒混合状态

富硫颗粒是本研究含量最丰富的颗粒，约占颗粒物总数的 86.8%，这与离子分析中硫酸盐是细颗粒物中最主要的化学组分的结果相对应，水溶性离子分析结果显示这种富硫颗粒最有可能是硫酸铵颗粒。而在本次观测中，富硫颗粒在清洁天多数时候会单独存在，而在雾霾天大部分富硫颗粒内部则混合有其它 1 个或多个气溶胶颗粒，如金属颗粒、矿物、飞灰和烟尘颗粒(图 5-7)等，它的混合程度要远远高于清洁天气的。这是由于雾霾天气条件下风速相对比较小，大气中各种污染物的浓度都较高，这不仅有利于颗粒物表面发生非均相化学反应，而且颗粒物之间相互混合的机率也比较高。通常湿度能达到 80%时固态的硫酸铵发生潮解，并转变为液相的气溶胶颗粒。一旦变成液相的气溶胶，它们能容易地吸收和吸附其周围的 VOC、固体和液态细颗粒。

图 5-7d 显示出烟尘颗粒和硫酸铵的内部混合，这种内部混合现象在过去的研究中经常被发现[251]，这说明烟尘颗粒容易通过与大气中的硫酸盐、硝酸盐、有机物等二次气溶胶相互混合而出现老化现象。随着全球经济快速发展以及能源的急剧消耗，越来越多的烟尘颗粒排放到大气中，而当硫酸铵与烟尘颗粒混合时，它们对光的散射和吸收强度将增加到原来的 10 和 2 倍[252]，因此对全球大气的增温也会起到非常重要的作用。大部分观察的烟尘颗粒表面都有硫酸铵或有机组分，说明烟尘颗粒在大气中具有较快的老化速度。这些老化的烟尘颗粒也由非吸湿性变为吸湿性。随着这些颗粒在大气中进一步扩散并抬升，它们极有可能成为云结核并在区域尺度上影响降雨和雨水的酸碱性。

如图 5-7d 和 5-7e 显示飞灰颗粒混合于硫酸铵，这种混合能促进飞灰表面的一些重金属元素（Fe、Zn 等）变成水溶性的金属离子[253]，加重硫酸铵颗粒对人体的危害。不同物质在透射电镜中对电子的透射能力不同，因此不同组分的颗粒也会显示出不同的黑白比例。图 5-7d 和 5-7e 显示出飞灰颗粒比富硫颗粒颜色更

黑，在强电子束下能够稳定存在。

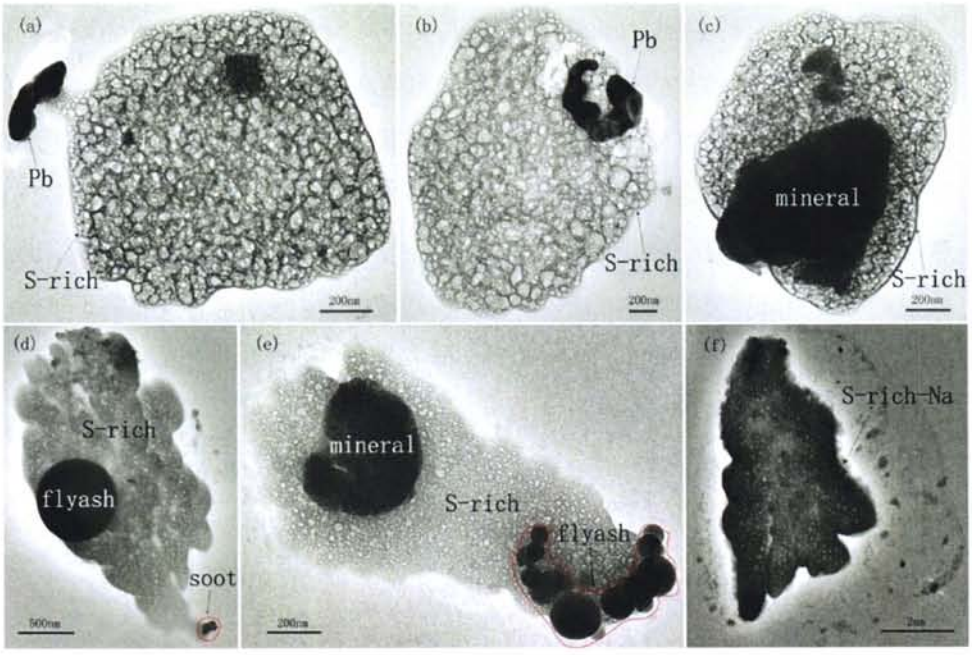

图 5-7 黄河三角洲地区夏季发生混合现象的富硫颗粒: (a)铅与富硫颗粒的外混颗粒；(b)铅与富硫颗粒的内混颗粒；(c)内混矿物的富硫颗粒；(d) 内混飞灰和烟尘的富硫颗粒；(e)内混矿物和飞灰的富硫颗粒；(f)硫酸钠颗粒。

5.4.3 夏季富硫颗粒粒径分布

图 5-8 显示夏季不同天气条件下不同粒径段范围内的颗粒物（特别是富硫颗粒）在每一粒径段数量百分比，由图可知在同一粒径段，雾霾天气条件下收集的颗粒物的绝对数量高于清洁天气中颗粒物数量，500 nm 以上粒径段该现象更明显，这与第四章颗粒物数浓度分析结果相对应（即雾霾天积聚模态颗粒物数浓度明显高于清洁天气下的颗粒物数浓度）。在每个颗粒类型中，雾霾天 S-rich/fly ash 和 S-rich/metal 颗粒物分别占总颗粒物的 8.7%和 13%，这一比例在清洁天则降至 0.9%和 9.8%，这是由于雾霾天有利于污染物的积累。Na_2SO_4 颗粒物在清洁天的比例比在雾霾天高 3 倍，这与离子分析中 Na^+的结果相对应。

夏季雾霾天 51%的富硫颗粒存在内混现象，而在清洁天这一比例仅有 20%，这说明雾霾天颗粒物老化现象明显。富硫颗粒是含量最多的颗粒物，在雾霾天气下其平均粒径为 1.1 μm，粒径范围为 0.4 μm-7 μm，在清洁天气下其平均粒径为 0.8 μm，粒径范围为 0.1 μm-4 μm。富硫颗粒的混合度较高，这可能是由于气团

传输过程中，气团的运动轨迹较短，移动速度较慢，硫酸盐颗粒能有充分的时间与其他类型的颗粒物发生较强的混合反应。由于与硫酸盐的混合使得煤烟型颗粒、飞灰颗粒以及金属颗粒的吸湿性改变[254]，而且这些颗粒物的光学性质也会发生改变[255]。这些改变会直接或者间接影响气候及能见度，并对人体健康有更大的影响[256]。另外富硫颗粒的内混现象也会使颗粒物的粒径增大，对于雾霾天气下颗粒物的增长过程有一定的贡献。雾霾天经常发现有大粒径的硫酸铵颗粒，而这样的颗粒很少清洁天观测到，这表明雾霾天湿度较大，特别是雾天有利于气体的SO_2向硫酸盐的转化并增长。清洁天气条件下仅发现少量的粗硫酸铵颗粒，这表明清洁天气比较好的扩散条件是不利于硫酸铵颗粒增长。

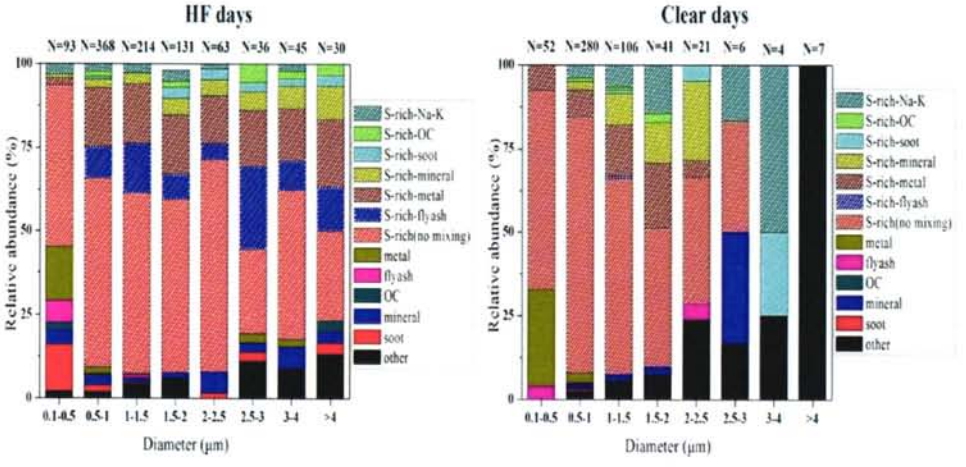

图 5-8 黄河三角洲地区夏季雾霾天和清洁天不同类型颗粒物
在不同粒径范围内的数浓度百分比图

图 5-9 显示了在 100 nm 至 10 μm 之间不同天气条件下富硫颗粒数浓度的粒径分布，雾霾天和清洁天均呈现单峰分布，峰值出现在 1 μm 附近；雾霾天在 2-3 μm 处有个缓冲区，且 1 μm 以上粒径段雾霾天的富硫颗粒数量明显增加。这可能主要是由两个原因造成：一是雾天中大部分颗粒是以雾滴形式存在，雾滴有利于硫酸铵颗粒颗粒的增大，并达到 2 μm。二是其它类型的颗粒物如有机物、飞灰、烟尘或矿物等作为硫酸铵的核，从而增加了它们的粒径。

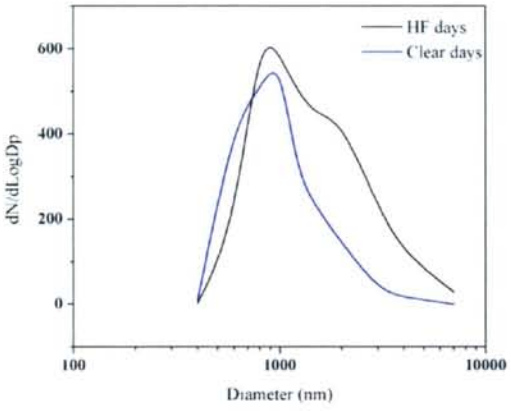

图 5-9 黄河三角洲地区夏季雾霾天和清洁天富硫颗粒个数浓度粒径分布图

5.5 本章小结

1、通过透射电镜及能谱分析相结合的方法研究了不同天气条件下单个气溶胶颗粒，根据它们的形貌和成分，分为以下 9 大类：矿物颗粒、富钾颗粒、富钠/镁颗粒、金属/飞灰颗粒、钙盐颗粒、富硫颗粒、烟尘颗粒、有机颗粒和海盐颗粒。

2、雾霾天气颗粒物老化程度明显，通过长距离输送的雾霾颗粒会通过有机和无机的气态凝结（包括在颗粒物表面的非均相反应）和物理凝聚而发生老化现象。

3、雾霾天颗粒物的混合程度强烈，且多从外部混合转变为内部混合。在雾霾天可溶性的硫酸盐和富钾颗粒趋向于与难熔的新鲜排放的颗粒物包括烟尘颗粒、金属/飞灰颗粒、有机颗粒和矿物颗粒等发生融合。

4、在沙尘暴发生前、发生中和发生后不同时期的颗粒物类型、含量及成分的不同，这表明不同类型颗粒物的混合以及沙尘矿物颗粒与酸性气体的非均相反应取决于气象因素和混合的过程。

5、富硫颗粒是本研究含量最丰富的颗粒，约占颗粒物总数的 86.8%，500 nm 以上粒径段的富硫颗粒数量在雾霾天明显增加。雾天中大部分颗粒是以雾滴形式存在，雾滴有利于硫酸铵颗粒颗粒的增大，同时颗粒物之间强烈的混合作用增加了雾霾天富硫颗粒的粒径。

第六章 结论与展望

6.1 结论

本论文利用在线监测和离线分析相结合的手段全面了解我国典型背景地区气溶胶颗粒物在不同季节及不同天气下的理化性质，并利用后推气流轨迹分析了污染气团的来源，并利用透射电镜分析了单颗粒的类型及混合状态，为全面阐释背景地区雾霾形成机制提供了有效的数据支持，全文的主要结论如下：

1、 $PM_{2.5}$ 水溶性离子

(1) 黄河三角洲地区观测期间总水溶性离子年均浓度为 49.72±49.89 μg/m^3，SO_4^{2-} 是占比最高的水溶性离子，约占总水溶性离子的 45.2%，其次为 NO_3^-和 NH_4^+，SO_4^{2-}、NO_3^-和 NH_4^+的质量浓度除了低于国内的济南和西安以及印度的赖普尔，远高于美国、日本和韩国的城市及郊区站点，与国内一些大城市相当，说明黄河三角洲地区面临严重的二次无机气溶胶污染。

(2) SO_4^{2-}的质量浓度在夏、秋和冬三个季节均表现出昼高夜低的日变化特征，NO_3^-在春夏秋三个季节均表现出上午高下午低的日变化特征，NH_4^+的质量浓度日变化与 SO_4^{2-}有相似的日变化特征。太阳辐射和 O_3 浓度是影响 SO_4^{2-}日变化的主要因素，而太阳辐射和温度是影响 NO_3^-日变化的主要因素。

(3) 冬季黄河三角洲地区酸性颗粒物的比重最高，约有 62.4%的颗粒物是酸性颗粒物，其中 32.1%的颗粒物为强酸性颗粒物。黄河三角洲地区的酸性颗粒物酸度低于泰山、北京和上海等地，而高于衡山、兰州和广州。观测期间 NO_3^-主要来自气态 NH_3 和 HNO_3 的反应。

(4) 主因子分析结果表明影响黄河三角洲地区水溶性离子的主要因素是燃料燃烧、二次生成及扬尘和土壤。

(5) 利用后推气流轨迹分析发现春季、秋季和冬季黄河三角洲地区主要受来自北方西伯利亚的长距离传输以及山东省内和京津冀地区的短距离输送气团的影响，而夏季主要受山东省和河北省短距离传输气团以及东部海洋气团的影响。其中来自山东省内及京津冀的短距离输送气团对黄河三角洲地区的离子贡献率最高。

(6) 雾霾天气下污染物浓度明显高于清洁天，且雾霾天气下的相对湿度在四季均高于清洁天气下的相对湿度，有利于 SO_2 的转化，而且冬季雾霾天气下 SO_2 排放量远高于其他季节，导致冬季雾霾天气下硫酸盐浓度较高。雾霾天气下气溶胶酸度更强，且冬季气溶胶酸度明显高于其他三个季节，这主要是由于冬季高浓度的 HSO_4^-，可以产生更多的 H^+，同时冬季气溶胶水含量比夏季和秋季低，颗粒物水对 H^+的稀释作用较弱。

2、**颗粒物个数浓度及粒径分布**

(7) 黄河三角洲地区观测期间 5-10000 nm 粒径范围内总颗粒物平均数浓度为 12838 #/cm^3，春季数浓度最高，冬季最低。从不同粒径范围来看，黄河三角洲地区气溶胶中爱根模态颗粒物数浓度最高，全年平均占总颗粒物数浓度的 60.7%，其次积聚模态（25.2%）和凝结核模态（14.1%）。凝结核模态颗粒物在春季和夏季数浓度最高，爱根模态则是在春季和秋季最高，积聚模态秋季最高。

(8) 黄河三角洲地区观测期间凝结核模态和爱根模态颗粒物在新颗粒物生成事件（NPF）发生的观测时段数浓度日变化特征明显，而未发生新颗粒物生成事件（non-NPF）的观测时段则没有明显的日变化，这说明 NPF 事件对凝结核模态和爱根模态颗粒物数浓度日变化有明显影响。

(9) 观测期间夏秋季节主要盛行东南风，而春季和冬季盛行西北风和东南风。总体来说，偏南风时颗粒物的数浓度要高于偏北风时。南部及东部短距离传输的气团具有更高浓度的颗粒物，平均为 14903 #/cm^3，而北部长距离传输的气团的颗粒物数浓度较低，平均为 11462 #/cm^3。北部长距离传输的气团的颗粒物粒径分布均为单峰分布，峰值均在爱根模态，而南部和东部短距离传输的气团粒径分布在更大粒径位置（100 nm 附近）出现峰值。

(10) 在观测期间，共有 26 天发生了新颗粒物生成事件（NPF），其中春季 7 天，夏季 7 天，秋季 6 天，冬季 6 天，约占总观测时间的 22%。凝结核模态颗粒物的平均成核速率为 6.6 #/(cm^3·s)，最低值为 0.3 #/(cm^3·s)，最大值为 31.9 #/(cm^3·s)，颗粒物的平均增长速率为 5.3 nm/h，最低值为 2.3 nm/h，最大值为 12.7 nm/h。

(11) 100 nm<D_p<500 nm 粒径段气溶胶在黄河三角洲地区雾霾天气的形成过程中

起了关键的作用，而 5 nm<D_p<20 nm、20 nm<D_p<50 nm、50 nm<D_p<100 nm 等超细气溶胶数浓度的降低也说明雾霾天气的大气环境不利于超细粒子的生成与存在。

3、单颗粒形貌及混合状态

(12) 通过透射电镜及能谱分析相结合的方法研究了不同天气条件下单个气溶胶颗粒，根据它们的形貌和成分，分为以下 9 大类：矿物颗粒、富钾颗粒、富钠/镁颗粒、金属/飞灰颗粒、钙盐颗粒、富硫颗粒、烟尘颗粒、有机颗粒和海盐颗粒。

(13) 雾霾天气颗粒物老化程度明显，通过长距离输送的雾霾颗粒会通过有机和无机的气态凝结（包括在颗粒物表面的非均相反应）和物理凝聚而发生老化现象。

(14) 雾霾天颗粒物的混合程度强烈，且多从外部混合转变为内部混合。在雾霾天可溶性的硫酸盐和富钾颗粒趋向于与难熔的新鲜排放的颗粒物包括烟尘颗粒、金属/飞灰颗粒、有机颗粒和矿物颗粒等发生融合。

(15) 在沙尘暴发生前、发生中和发生后不同时期的颗粒物类型、含量及成分的不同，这表明不同类型颗粒物的混合以及沙尘矿物颗粒与酸性气体的非均相反应取决于气象因素和混合的过程。

(16) 富硫颗粒是本研究含量最丰富的颗粒，约占颗粒物总数的 86.8%，500 nm 以上粒径段的富硫颗粒数量在雾霾天明显增加。雾天中大部分颗粒是以雾滴形式存在，雾滴有利于硫酸铵颗粒颗粒的增大，同时颗粒物之间强烈的混合作用增加了雾霾天富硫颗粒的粒径。

6.2 展望

本研究致力于环渤海地区区域背景点的$PM_{2.5}$水溶性离子特征、颗粒物数浓度粒径分布特征及单颗粒混合状态的研究，获得了黄河三角洲地区污染物的季节变化、日变化、来源及影响因素等，然而目前仅是初步的研究结果，作者未来将从以下几个方面进行进一步的深入研究和完善：

(1) 本文欠缺对硫酸盐、硝酸盐和铵盐形成机制的深入研究，未来将尽可能利用氧化剂（如OH、O_3和金属氧化剂），并且尝试利用大气化学模式，对其形成机

制开展研究；

(2) 本研究获取了$PM_{2.5}$的酸度特征，但未对当地的雨水特别是酸雨进行研究，未来可以尝试将$PM_{2.5}$酸度与酸雨结合，进一步获得酸度对酸雨的影响机制；

(3) 未来需要进一步加强对单颗粒气溶胶分析与全样分析的结合研究。

参考文献

[1] 唐孝炎，张远航，邵敏. 大气环境化学. 北京:高等教育出版社, 2006.

[2] 王明星. 大气化学（第二版）[M]. 北京:气相出版社, 1999.

[3] Jiang F., Liu Q., Huang X., Wang T., Zhuang B., and Xie M. Regional modeling of secondary organic aerosol over China using WRF/Chem. Journal of Aerosol Science, 2006, 43: 57-73.

[4] Iinuma Y., Boge O., Miao Y., Sierau B., Gnauk T., Herrmann H. Laboratory studies on secondary organic aerosol formation from terpenes. Faraday Discussion, 2005, 130: 279-294.

[5] Russell A.G., McRae G.J., Cass G.R. Mathematical modeling of the formation and transport of ammonium nitrate aerosol. Atmospheric Environment, 1983, 17: 949-964.

[6] Stieb D.M., Judek S., Burnett R.T. Meta-analysis of time-series studies of air pollution and mortality: effects of gases and particles and the influence of cause of death, age, and season. Journal of the Air & Waste Management Association, 2002, 52: 470-484.

[7] Borja-Aburto V.H., Castillejos M., Gold D.R., Bierzwinski S., Loomis D. Mortality and ambient fine particles in southwest Mexico City, 1993-1995. Environment Health Perspect, 1998, 106: 849-855.

[8] Ramanathan V., Crutzen P., Kiehl J., Rosenfeld D. Aerosols, climate, and the hydrological cycle. Science, 2001, 294: 2119-2124.

[9] Ramanathan V., Carmichael G. Global and regional climate changes due to black carbon. Nature geosciences, 2008, 1: 221-227.

[10] Pope C.A.I., Thun M.J., Namboodiri M.M., Dockery D.W., Evans J.S., Speizer F.E., HeathJr C.W. Particulate air pollution as a predictor of mortality in a prospective study of US adults[J]. American Journal of Respiratory and Criticial CareMedicine, 1995, 151: 669-674.

[11] 肖晗，李子健，韩启德，张幼怡. 大气污染颗粒物质与心血管疾病[J]. 中国病理生理杂志，2005，4: 822-825.

[12] Kim Y.J., Kim K.W., Kim S.D., Lee B.K., Han J.S. Fine particulate matter characteristics and its impact on visibility impairment at two urban sites in Korea: Seoul and Incheon. Atmospheric Environment, 2006, 40:593-605.

[13] Ramanathan V., Carmichael G. Global and regional climate changes due to black carbon [J]. Nature Geoscience, 2008, 1(4): 221.

[14] 秦瑜，赵春生.大气化学基础[M]. 北京：气象出版社，2003.

[15] 戴树桂. 环境化学[M]. 北京: 高等教育出版社, 2008.

[16] 邵龙义，杨书申，李卫军，等. 大气颗粒物单颗粒分析方法的应用现状及展望[J]. 古地

理学报, 2005,7(4): 535-548.

[17] Fu Q., Zhuang G., Wang J., Xu C., Huang K., Li J., et al. Mechanism of formation of the heaviest pollution episode ever recorded in the Yangtze River Delta, China. Atmospheric Environment, 2008, 42: 2023-2036.

[18] Jung J., Lee H., Kim Y.J., Liu X., Zhang Y., Gu J., et al. Aerosol chemistry and the effect of aerosol water content on visibility impairment and radiative forcing in Guangzhou during the 2006 Pearl River Delta campaign. Journal of Environmental Management, 2009, 90: 3231-3244.

[19] Ocskay R., Salma I., Wang W., Maenhaut W. Characterization and diurnal variation of size-resolved inorganic water-soluble ions at a rural background site. Journal of Environmental Monitoring, 2006, 8: 300-306.

[20] Zhou Y., Xue L., Wang T., Gao X., Wang Z., Wang W., et al. Characterization of aerosol acidity at a high mountain site in central eastern China. Atmospheric Environment, 2012, 51: 11-20.

[21] Wichmann H.E., Peters A. Epidemiological evidence of the effects of ultrafine particle exposure. Philosophical Transactions of the Royal Society of London (A), 2000, 358: 2751-2769.

[22] Kulmala M., Vehkamäki H., Petäjä T., Dal Maso M., Lauri A., Kerminen V.M., Birmili W., McMurry P.H. Formation and growth rates of ultrafine atmospheric particles: a review of observations. Journal of Aerosol Science, 2004, 35:143-176.

[23] Zhang Q., Streets D.G., Carmichael G.R., He K., Huo H., Kannari A., et al. Asian emissions in 2006 for the NASA INTEX-B mission. Atmospheric Chemistry and Physics, 2009, 9: 5131-5153.

[24] Ohara T., Akimoto H., Kurokawa J., Horii N., Yamaji K., Yan X., Hayasaka T. An Asian emission inventory of anthropogenic emission sources for the period 1980-2020[J]. Atmospheric Chemistry and Physics, 2007, 7(16): 4419-4444.

[25] van Donkelaar A., Martin R.V., Brauer M., Kahn R., Levy R., Verduzco C., Villeneuve P.J. Global estimates of ambient fine particulate matter concentrations from satellite-based aerosol optical depth: development and application. Environmental Health Perspectives, 2010, 118(6): 847-855.

[26] Che H., Zhang X., Li Y., Zhou Z., Qu J., Hao X. Haze trends over the capital cities of 31 provinces in China, 1981–2005. Theoreticaland Applied Climatology, 2009, 97 (3): 235-242.

[27] Zhao P., Zhang X., Xu X., Zhao X. Long-term visibility trends and characteristics in the region of Beijing, Tianjin, and Hebei, China. Atmospheric Research, 2011, 101: 711-718.

[28] Arimoto R., Zhang X., Huebert B., Kang C., Savoie D., Prospero J., Sage S., Schloesslin C., Khaing H., Oh S. Chemical composition of atmospheric aerosols from Zhenbeitai, China, and Gosan, South Korea, during ACE-Asia. Journal of Geophysical Research-Atmospheres,

2004, 109: D19.

[29] Jaffe D., Anderson T., Covert D., Kotchenruther R., Trost B., Danielson J., Simpson W., Berntsen T., Karlsdottir S., Blake D., Harris J., Carmichael G., and Uno I. Transport of Asian air pollution to North America. Geophysical Research Letters, 1999, 26: 711-714.

[30] Kahn R., et al. Environmental snapshots from ACE-Asia. Journal of Geophysical Research, 2004, 109, DOI:10.1029/2003JD004339.

[31] Gao X., Yang L., Cheng S., Gao R., Zhou Y., Xue L., Shou Y., Wang J., Wang X., Nie W. Semi-continuous measurement of water-soluble ions in $PM_{2.5}$ in Jinan, China: Temporal variations and source apportionments. Atmospheric Environment, 2011, 45: 6048-6056.

[32] Zhao X., Zhang X., Xu X., Xu J., Meng W., Pu W. Seasonal and diurnal variations of ambient $PM_{2.5}$ concentration in urban and rural environments in Beijing. Atmospheric Environment, 2009, 43: 2893-2900.

[33] Gao J., Chai F., Wang T., Wang S., Wang W. Particle number size distribution and new particle formation: New characteristics during the special pollution control period in Beijing. Journal of Environmental Science, 2012, 24:14-21.

[34] Yang L., Zhou X., Wang Z., Zhou Y., Cheng S., Xu P., Gao X., Nie W., Wang X., Wang W. Airborne fine particulate pollution in Jinan, China: Concentrations, chemical compositions and influence on visibility impairment. Atmospheric Environment,2012, 55: 506-514.

[35] Li W., Shao L., Shi Z., Chen J., Yang L., Yuan Q., Yan C., Zhang X., Wang Y., Sun J., Zhang Y., Shen X., Wang Z., Wang W. Mixing state and hygroscopicity of dust and haze particles before leaving Asian continent. Journal of Geophysical Research-Atmospheres, 2014, 119, DOI: 10.1002/2013JD021003.

[36] Seinfeld J., Pandis S. Atmospheric chemistry and physics: From air pollution to climate change[M]. John Wiley, New York, 2006.

[37] Textor C., Schulz M., Guibert S., Kinne S., Balkanski Y., Bauer S., Berntsen T., Berglen T., Boucher O., Chin M., Dentener F., Diehl T., Feichter J., Fillmore D., Ginoux P., Gong S., Grini A., Hendricks J., Horowitz L., Huang P., Isaksen I. S. A., Iversen T., Kloster S., Koch D., Kirkevag A., Kristjansson J. E., Krol M., Lauer A., Lamarque J. F., Liu X., Montanaro V., Myhre G., Penner J. E., Pitari G., Reddy M. S., Seland O., Stier P., Takemura T., Tie X. The effect of harmonized emissions on aerosol properties in global models - an AeroCom experiment[J]. Atmospheric Chemistry and Physics, 2007 (17): 4489-4501.

[38] Acker K., Mertes S., Möller D., et al. Case study of cloud physical and chemical processes in low clouds at Mt. Brocken. Atmospheric Research, 2002, 64(1-4): 41-51.

[39] Hering S.V., Friedlander S.K. Origins of aerosol sulfur size distributions in the Ls Angel Basin. Atmospheric Environment, 1982, 16: 2647-2656.

[40] Meng Z., Seinfeld J.H. On the source of the sub-micrometer droplet mode of urban and regional aerosols. Aerosol Science Technology, 1994, 20 (3): 253-265.

[41] Pathak P. K., Wu W. S., Wang T. Summertime $PM_{2.5}$ ionic species in four major cities of

China: nitrate formation in an ammonia-deficient atmosphere. Atmospheric Chemistry and Physics, 2009, 9: 1711-1722.

[42] Anttila T., Kiendler-Scharr A., Tillmann R., Mentel T.F. On the reactive uptake of gaseous compounds by organic-coated aqueous aerosols: Theoretical analysis and application to the heterogeneous hydrolysis of N_2O_5. Journal of Physical Chemistry, 2006, 110A: 10435-10443.

[43] Hallquist M., Stewart D.J., Stephenson S.K., Cox R.A. Hydrolysis of N_2O_5 on sub-micron sulfate aerosols. Physical Chemistry Chemical Physics, 2003, 5: 3453-3463.

[44] Sloane C.S., Watson J.G., Chow J., Pritchett L., Richards L.W. Size-segregated fine particle measurements by chemical species and their impact on visibility impairment in Denver. Atmospheric Environment, 1991, 25: 1013-1024.

[45] Kang C.M., Lee H.S., Kang B.W., Lee S.K., Sunwoo Y. Chemical characteristics of acidic gas pollutants and $PM_{2.5}$ species during hazy episodes in Seoul, South Korea. Atmospheric Environment, 2004, 38: 4749-4760.

[46] 栾玉荣. 我国多站点主要水溶性气溶胶的空间分布和时间变化特征[D]. 北京:中国气象科学研究院, 2008.

[47] Misra C., Geller M.D., Shah P., Sioutas C., Solomon P.A. Development and Evaluation of a Continuous Coarse (PM_{10}-$PM_{2.5}$) Particle Monitor[J]. Journal of the Air &Waste Management Association, 2001 (9): 1309-1317.

[48] Chakrabarti B., Sioutas C., Singh M. Development of a near-continuous monitor for measurement of the sub-150 nm PM mass concentration[J]. Aerosol Science Technology, 2004: 239-252.

[49] Meyer M.B., Patashnick H., Ambs J.L., Rupprecht E. Development of a sample equilibration system for the TEOM continuous PM monitor[J]. Journal of the Air &Waste Management Association, 2000 (8): 1345-1349.

[50] Patashnick H., Rupprecht G., Ambs J.L., Meyer M.B. Development of a reference standard for particulate matter mass in ambient air[J]. Aerosol Science Technology, 2001 (1): 42-45.

[51] McMurry P.H., Wang X., Park K., Ehara K. The relationship between mass and mobility for atmospheric particles: A new technique for measuring particle density[J]. Aerosol Science Technology, 2002 (2): 227-238.

[52] Geller M., Biswas S., Sioutas C. Determination of particle effective density in urban environments with a differential mobility analyzer and aerosol particle mass analyzer[J]. Aerosol Science Technology, 2006 (9): 709-723.

[53] Ristimäki J., Virtanen A., Marjamäki M., Rostedt A., Keskinen J. On-line measurement of size distribution and effective density of submicron aerosol particles[J]. Journal of Aerosol Science, 2002 (11): 1541-1557.

[54] Khlystov A., Stanier C., Pandis S. An Algorithm for Combining Electrical Mobility and Aerodynamic Size Distributions Data when Measuring Ambient Aerosol Special Issue of

Aerosol Science and Technology on Findings from the Fine Particulate Matter Supersites Program[J]. Aerosol Science Technology, 2004 (S1): 229-238.

[55] Rattigan O.V., Hogrefe O., Felton H.D., Schwab J.J., Roychowdhury U.K., Husain L., Dutkiewicz V.A., Demerjian K.L. Multi-year urban and rural semi-continuous $PM_{2.5}$ sulfate and nitrate measurements in New York State: Evaluation and comparison with filter based measurements. Atmospheric Environment, 2006, 40: S192-S205.

[56] Hazenkamp-von Arx M. E., Gotschi T., Ackermann-Liebrich U., Bono R., Burney P., Cyrys J., Jarvis D., Lillienberg L., Luczynska C., Maldonado J. A. $PM_{2.5}$ and NO_2 assessment in 21 European study centres of ECRHS II: annual means and seasonal differences[J]. Atmospheric Environment, 2004 (13): 1943-1953.

[57] Sillanpaa M., Hillamo R., Saarikoski S., Frey A., Pennanen A., Makkonen U., Spolnik Z., Van Grieken R., Branis M., Brunekreef B. Chemical composition and mass closure of particulate matter at six urban sites in Europe[J]. Atmospheric Environment, 2006: 212-223.

[58] Huebert B.J., Bates T., Russell P.B., Shi G., Kim Y.J., Kawamura K., Carmichael G., Nakajima T. An overview of ACE-Asia: Strategies for quantifying the relationships between Asian aerosols and their climatic impacts. Journal of Geophysical Research-Atmospheres, 2003, D23: 8633-8653.

[59] Oanh N.T.K., Upadhyaya N., Zhuang Y.H., Hao Z.P., Murthy D.V.S., Lestari P., Villarin J.T., Chengchua K., Co H.X., Dung N.T., Lindgren E.S. Particulate air pollution in six Asian cities: Spatial and temporal distributions, and associated sources. Atmospheric Environment, 2006, 40: 3367-3380.

[60] Chen, Z., Ge, S., Zhang, J. Measurement and analysis for atmospheric aerosol particulates in Beijing. Research of Environmental Sciences, 1994, 7 (3): 1-9.

[61] Zhang D., Iwasaka Y. Nitrate and sulphate in individual Asian dust-storm particles in Beijing, China in spring of 1995 and 1996. Atmospheric Environment, 1999, 33: 3213-3223.

[62] Wei F., Teng E., Wu G., Hu W., Wilson W.E., Chanpman R.S., Pau J.C., Zhang J. Ambient concentrations and elemental compositions of PM_{10} and $PM_{2.5}$ in four Chinese cities. Environmental Science and Technology , 1999, 33: 4188-4193.

[63] Yao X.H., Chan C.K., Fang M., Cadle S., Chan T., Mulawa P., He K.B., Ye B.M. The water-soluble ionic composition of $PM_{2.5}$ in Shanghai and Beijing, China. Atmospheric Environment, 2002, 36: 4223-4234.

[64] YangL., Wang D., Cheng S., Wang Z., ZhouY., Zhou X., Wang W. Influence of meteorological conditions and particulate matter on visual range impairment in Jinan, China. Science of the Total Environment, 2007, 383, 164-173.

[65] Zhang Q., Jimenez J.L., Canagaratna M.R., Allan J.D., Coe H., Ulbrich I., Alfarra M.R., Takami A., Middlebrook A.M., Sun Y.L., Dzepina K., Dunlea E., Docherty K., DeCarlo P.F.,

Salcedo D., Onasch T., Jayne J.T., Miyoshi T., Shimono A., Hatakeyama S., Takegawa N., Kondo Y., Schneider J., Drewnick F., Borrmann S., Weimer S., Demerjian K., Williams P., Bower K., Bahreini R., Cottrell L., Griffin R.J., Rautiainen J., Sun J.Y., Zhang Y.M., Worsnop D. R. Ubiquity and dominance of oxygenated species in organic aerosols in anthropogenically-influenced Northern Hemisphere midlatitudes[J]. Geophysical Research Letters, 2007 (13),DOI: 10.1029/2007GL029979.

[66] Chan C.K., Yao X.H. Air pollution in mega cities in China. Atmospheric Environment, 2008, 42: 1-42.

[67] Yang F., Tan J., Zhao Q., Du Z., He K., Ma Y., Duan F., Chen G., Zhao Q. Characteristics of $PM_{2.5}$ speciation in representative megacities and across China. Atmospheric Chemistry and Physics, 2011, 11: 5207-5219.

[68] 冯宗炜. 中国酸雨对陆地生态系统的影响和防治对策[J]. 中国工程科学，2000，2(9)：5-11.

[69] Takahama S., Davidson C.I., PandisS.N. Semi-continuous measurements of organic carbon and acidity during the Pittsburgh air quality study: implications for acid-catalyzed organic aerosol formation. Environmental Science and Technology, 2006, 40: 2191-2199.

[70] Iinuma Y., Boge O., Miao Y., Sierau B., Gnauk T., Herrmann H. Laboratory studies on secondary organic aerosol formation from terpenes. Faraday Discussion, 2005, 130: 279-294.

[71] Raizenne M., Neas L.M., Damokosh A.I., Dockery D.W., Spengler J.D., Koutrakis P., Ware J.H., Speizer F.E. Health effects of acid aerosols on North American children: pulmonary function[J]. Environmentdal Health Perspectives, 1996, 104(5): 506-514.

[72] 王峰威，李红，柴发合，钱枫，王宗爽，邓利群. 大气气溶胶酸度的研究进展. 环境污染与防治，2010，1: 67-72.

[73] Pathak R.K., Louie P.K.K., Chan C.K. Characteristics of aerosol acidityin Hong Kong. Atmospheric Environment, 2004, 38: 2965-2974.

[74] Zhang Q., Jimenez J.L., Worsnop D.R. and Canagaratna M. A case study of urban particle acidity and its influence on secondary organic aerosol. Environmental Science and Technology , 2007, 41: 3213-3219.

[75] Yao X.H., Ling T.Y., Fang M., Chan C.K. Comparison of thermodynamic predictions for in situ pH in $PM_{2.5}$. Atmospheric Environment, 2006, 16: 2835-2844.

[76] Keene W.C., Sander R., Pszenny A.A.P., Vogt R., Crutzen P.J., Galloway J.N. Aerosol pH in the marine boundary layer A review and model evaluation. Journal of Aerosol Science, 1998, 3: 339-356.

[77] Jang M.S., Czoschke N.M., Sangdon L., Kamens R.M. Heterogeneous atmospheric aerosol production by acid catalyzed particle-phase reactions. Science, 2002, 298:814-817.

[78] Tanner, R.L., Olszyna, K.J., Edgerton, E.S., Knipping, E., Shaw, S.L. Searching for evidence of acid-catalyzed enhancement of secondary organic aerosol formation using

ambient aerosol data. Atmospheric Environment, 2009, 43: 3440-3444.

[79] Ren L.H., Wang W., Wang Q.Y., Yang X.Y., Tang D.G. Comparison and trend study on acidity and acidic buffering capacity of particulate matter in China. Atmospheric Environment, 2011, 45: 7503-7519.

[80] Brook J.R., Wiebe A.H., Woodhouse S.A., Audette C.V., Dann T.F., Callaghan S., Piechowski M., Dabek-Zlotorzynska E., Dloughy J.F. Temporal and spatial relationships in fine particle strong acidity, sulphate, PM_{10}, and $PM_{2.5}$ across multiple canadian locations[J]. Atmospheric Environment, 1997, 31: 4223-4236.

[81] Hazi Y., Heikkinen M., Cohen B. Size distribution of acidic sulfate ions in fine ambient particulate matter and assessment of source region effect[J]. Atmospheric Environment, 2003, 37: 5403-5413.

[82] 王玮，王英，苏红梅，潘志，岳欣，刘红杰，汤大钢.北京市沙尘暴天气大气气溶胶酸度和酸化缓冲能力[J].环境科学，2001 (5): 25-28.

[83] Pathak R.K., Yao X., Lau A.K.H., Chan C.K. Acidity and concentrations of ionic species of $PM_{2.5}$ in Hong Kong[J]. Atmospheric Environment, 2003, 37: 1113-1124.

[84] Dusek U., Frank G.P., Hildebrandt L., et al. Size Matters More Than Chemistry for cloud nucleating ability of aerosol particles. Science, 2006, 312: 1375-1378.

[85] Seinfeld J.H., Pandis S.N. Atmospheric Chemistry and Physics from Air Pollution to Climate Change. Wiley, 1998, New York.

[86] Aitken J. Some Nulei of Cloudy Condensation [J]. Monthly Weather Review, 1917, 45: 452.

[87] Hussein T. Indoor and outdoor aerosol particle size characterization in Helsinki [J]. Report Series in Aerosol Science, 2005, 74:1-53.

[88] Gao J., Wang T., Zhou X., Wu W., Wang W. Measurement of aerosol number size distributions in the Yangtze River delta in China: Formation and growth of particles under polluted conditions. Atmospheric Environment, 2009, 43: 829-836.

[89] Harris S.J. MaricqM.M. Signature size distributions for diesel and gasoline engine exhaust particulate matter [J]. Journal of Aerosol Science, 2001, 32(6): 749-764.

[90] Ristovski Z.D., Morawska L.,Hitchins J., et al. Particle emissions from compressed natural gas engines [J]. Journal of Aerosol Science, 2000, 57(4): 403-413.

[91] Kittelson D.B. Engines and nanopaiticles: a review [J]. Journal of Aerosol Science, 1998, 29:575-588.

[92] 胡敏，何凌燕，黄晓峰等.北京大气细粒子和超细粒子理化特征、来源及形成机制[M]. 科学出版社，2009.

[93] Kopanakis I., Chatoutsidou S., Torseth K., Glytsos T., Lazaridis M. Particle number size distribution in the Eastern Mediterranean: Formation and growth rates of ultrafine airborne atmospheric particles. Atmospheric Environment, 2013, 77:790-802.

[94] Hussein T., Kukkonen J., Korhonen H., Pohjola M., Pirjola L., Wraith D., Härkonen J.,

Teinilä K., Koponen I.K., Karppinen A., Hillamo R., Kulmala M. Evaluation and modeling of the size fractionated aerosol particle number concentration measurements nearby a major road in Helsinki – Part II: Aerosol measurements within the SAPPHIRE project. Atmospheric Chemistry and Physics, 2007, 7: 4081-4094.

[95] Kulmala M., Petäjä T., Mönkkönen P., Koponen I.K., Dal Maso M., Aalto P.P., Lehtinen K.E.J., Kerminen V.M. On the growth of nucleation mode particles: source rates of condensable vapor in polluted and clean environments. Atmospheric Chemistry and Physics, 2005, 5: 409-416.

[96] Agus E.L., Young D.T., Lingard J.J., Smalley R.J., Tate J.E., Goodman P.S., Tomlin A.S. Factors influencing particle number concentrations, size distributions and modal parameters at a roof-level and roadside site in Leicester, UK. Science of the Total Environment, 2007, 386:65-82.

[97] Kerminen V.M., Pirjola L., Kulmala M. How significantly does coagulational scavenging limit atmospheric particle production? Journal of Geophysical Research-Atmospheres, 2001, 106:24119-24125.

[98] Stanier, C.O., Khlystov, A.Y., Pandis, S.N. Ambient aerosol size distributions and number concentrations measured during the Pittsburgh Air Quality Study (PAQS). Atmospheric Environment,2004, 38:3275-3284.

[99] Laakso L., Hussein T., Aarnio P., Komppula M., Hitunen V., Viisanen Y., Kulmala M. Diurnal and annual characteristics of Particle mass and number concentrations in urban,rural and Arctic environments In Finland [J]. Atmospheric Environment, 2003, 37:2629-2641.

[100] 王文兴，杨沛源，任阵海，吕黄生. 太原地区大气环境综合观测总研究报告, 1984.

[101] 许黎，冈田菊夫，张鹏等. 北京地区春末-秋初气溶胶理化特性的观测研究，大气科学，2002，26(3): 401-411.

[102] 胡敏，刘尚，吴志军，张静，赵云良. 北京夏季高温高湿和降水过程对大气颗粒物谱分布的影响. 环境科学，2006，27(11): 2293-2298.

[103] Wu Z., Hu M., Lin P., Liu S., Wehner B., Wiedensohler A. Particle number size distribution in the urban atmosphere of Beijing, China. Atmospheric Environment, 2008, 42:7967-7980.

[104] Yue D., Hu M., Wang Z., Wen M., Guo S., Zhong L., Wiedensohler A., Zhang Y. Comparison of particle number size distributions and new particle formation between the urban and rural sites in the PRD region, China. Atmospheric Environment, 2013, 76:181-188.

[105] Guo H., Wang D.W., Cheung K., Ling Z.H., Chan C.K., Yao X.H. Observation of aerosol size distribution and new particle formation at a mountain site in subtropical Hong Kong. Atmospheric Chemistry and Physics, 2012, 12: 9923-9939.

[106] Wehner B., Wiedensohler A., Tuch T.M., Wu Z.J., Hu M., Slanina J., and Kiang C.S. Variability of the aerosol number size distribution in Beijing, China: New particle

formation, dust storms, and high continental background. Geophysical Research Letters, 2004, 31, L22108, DOI:10.1029/ 2004GL021596.

[107] Liu S., Hu M., Wu Z., Wehner B., Wiedensohler A., Cheng Y. Aerosol number size distribution and new particle formation at a rural/coastal site in Pearl River Delta (PRD) of China. Atmospheric Environment, 2008, 42:6275-6283.

[108] Gao J., Chai F., Wang T., Wang W. Particle number size distribution and new particle formation (NPF) in Lanzhou, Western China. Particuology, 2011, 9:611-618.

[109] Li X.L., Wang J.S., Tu X.D., Liu W., Huang Z. Vertical variations of particle number concentration and size distribution in a street canyon in Shanghai, China. Science of the Total Environment, 2007, 378: 306-316.

[110] 牛生杰，孙照渤. 春末中国西北沙漠地区沙尘气溶胶物理特征的飞机观测，高原气象，2005，24：604-610.

[111] Wang W., Liu H.J., Yue X., Li H., Chen J.H., Tang D.G. Study on size distributions of airborne particles by aircraft observation in spring over eastern coastal areas of China. Advances in Atmospheric Sciences, 2005, 22: 328-336.

[112] Kivekäs N., Kulmala M., Zhang X. Long term particle size distribution measurements at Mount Waliguan, a high-altitude site in inland China. Atmospheric Chemistry and Physics, 2009, 9: 5461-5474.

[113] Kulmala M. How Particles Nucleate and Grow. Science, 2003, 302: 1000-1001.

[114] Kulmala M., Laaksonen A., Pirjola L. Parameterizations for sulfuric acid/water nucleation rates.Journal of Geophysical Research-Atmospheres, 1998, 103 (D7): 8301-8307.

[115] Weber R.J., McMurry P.H., Mauldin L., Tanner D.J., Eisele F.L., Brechtel F.J., Kreidenweis S.M., Kok G.L., Schillawski R.D., Baumgardner D. A study of new particle formation and growth involving biogenic and trace gas species measured during ACE1. Journal of Geophysical Research-Atmospheres, 1998, 103: 16385-16396.

[116] O'Dowd C.D., Becker E., et al. Aerosol physico-chemical characteristics over a boreal forest determined by volatility analysis. Boreal Environmental Research, 2000, 5(4): 337-348.

[117] Yu F., Turco R.P.Ultrafine aerosol formation via ion-mediated nucleation.Geophysical Research Letters, 2000, 27: 883-886.

[118] Kulmala M., Toivonen A., et al. Analysis of the growth of nucleation mode particles observed in Boreal forest. Tellus Series B—Chemical and Physical Meteorology, 1998, 50 (5): 449-462.

[119] O'Dowd C.D., Hämeri K., Mäkelä J.M., Pirjola L., Kulmala M., Jennings S.G., BerresheimH., Hansson H.C., de Leeuw G., Kunz G.J. A dedicated study of New Particle Formation and Fate in the Coastal Environment (PARFORCE): Overview of objectives and achievements. Journal of Geophysical Research, 2002, 107:PAR 1-1-PAR 1-16.

[120] Asmi E., Frey A., Virkkula A., Ehn M., Manninen H.E., Timonen H., Tolonen-Kivimäki O.,

Aurela M., Hillamo R., Kulmala M. Hygroscopicity and chemical composition of Antactic sub-micrometre aerosol particles and observations of new particle formation [J]. Atmospheric Chemistry and Physics, 2010, 10(9): 4253-4271.

[121] Kulmala M., Laakso L., Lehtinen K., Riipinen I., Dal Maso M., Anttila T., Kerminen V.M., Horrak U., Vana M., and Tammet H. Initial steps of aerosol growth.Atmospheric Chemistry and Physics, 2004, 4: 2553-2560.

[122] Vehkamäki H., Dal Maso M., Hussein T., Flanagan R., Hyvärinen A., LaurosJ., Merikanto J., Mönkkönen P.,Pihlatie M., Salminen K. Atmospheric particle formation events at Värriö measurement station in Finnish Lapland 1998-2002. Atmospheric Chemistry and Physics Discussions, 2004, 4: 3535-3563.

[123] Laaksonen A., Hamed A., Joutsensaari J., Hiltunen L., Cavalli F., Junkermann W., Asmi A., Fuzzi S., Facchini M.C. Cloud condensation nucleus production from nucleation events at a highly polluted region. Geophysical Research Letters, 2005, 32 (6): DOI:10.1029/2004GL022092.

[124] Laakso L., Makela J.M., Pirjola L., Kulmala M. Model studies on ion-induced nucleation in the atmosphere [J]. Journal of Geophysical Research-Atmospheres, 2002, 107(D20):4427.

[125] O'DowdC., YoonY., JunkermanW., AaltoP., KulmalaM., LihavainenH., ViisanenY., Airborne measurements of nucleation mode particles I: coastal nucleation and growth rates. Atmospheric Chemistry and Physics, 2007, 7: 1491-1501.

[126] BirmiliW.,WiedensohlerA. New particle formation in the continentalboundary layer: Meteorological and gas phase parameter influence.Geophysical Research Letters, 2000, 27: 3325-3328.

[127] DalMasoM., Kulmala M., Riipinen I., Wagner R., Hussein T., Aalto P.P., Lehtinen K.E. Formation and growth of fresh atmospheric aerosols: eight years of aerosol size distribution data from SMEAR II, Hyytiala. Finland. Boreal Environ Res, 2005, 10:323-336.

[128] HamedA., JoutsensaariJ., MikkonenS., SogachevaL., Dal MasoM., KulmalaM., CavalliF., FuzziS., FacchiniM., DecesariS.Nucleation and growth of new particles in Po Valley, Italy. Atmospheric Chemistry and Physics, 2007, 7:355-376.

[129] Yue D.L.,Hu M.,Zhang R.Y.,Wang Z.B.,Zheng J.,Wu Z.J., Wiedensohler A.,He L.Y., Huang X.F., Zhu T. The roles of sulfuric acid in new particle formation and growth in the mega-city of Beijing [J]. Atmospheric Chemistry and Physics, 2010,10(10): 4953-4960.

[130] GuoH., DingA.J., MorawskaL., HeC.R., AyokoG., Li Y., HungW. Size distribution and new particle formation in subtropical eastern Australia. Environmentalproblems-Chemical approaches, 2008, 5: 382-390.

[131] Wu Z., Hu M., Liu S., Wehner B., Bauer S., Ma Bling A., et al. New particle formation in Beijing, China: Statistical analysis of a 1-year data set. Journal of Geophysical Research-Atmospheres, 2007, 112, D09209. DOI:10.1029/2006JD007406.

[132] Lee S.H., Young L.H.,Benson D.R.,Suni T., Kulmala M., Junninen H., CamposT.L., Rogers

D.C., Jensen J. Observations of nighttime new particle formation inthe troposphere [J]. Journal of Geophysical Research-Atmospheres, 2008, 113(D10), DOI:10.1029/2007JD009351.

[133] Li J., Anderson J.R., Buseck P.R. TEM study of aerosol particles from clean and polluted marine boundary layers over the North Atlantic[J]. Journal of Geophysical Research-Atmospheres, 2003, 108(D6),DOI:10.1029/2002JD002106.

[134] Li W.J.,Shi Z.B., Yan C., Yang L.X., Dong C., Wang W.X. Individual metal-bearing particles in a regional haze caused by firecracker and firework emissions.Science of the Total Environment, 2013, 443: 464-469.

[135] Pósfai M., Buseck P.R. Nature and Climate Effects of Individual Tropospheric Aerosol Particles. Annual Reviews Earth and Planetary Science, 2010, 38 (1): 17-43.

[136] Giere R., Blackford M.,Smith K. TEM study of $PM_{2.5}$ emitted from coal and tire combustion in a thermal power station.Environmental Science and Technology, 2006, 40, 6235-6240.

[137] Zhang D., IwasakaY., ShiG. Soot particles and their impacts on the mass cycle in the Tibetan atmosphere. Atmospheric Environment, 2001, 35(34): 5883-5894.

[138] Twohy C.H., AndersonJ.R., CrozierP.A.Nitrogenated organic aerosols as cloud condensation nuclei. Geophysical Research Letters, 2005, 32, DOI:10.1029/2005GL023605.

[139] Li W.J.,Wang Y., Collett J.L., Chen J.M., Zhang X.Y., Wang Z.F., Wang W.X. Microscopic evaluation of trace metals in cloud droplets in an acid precipitation region.Environmental Science and Technology, 2013, 47(9): 4172-4180.

[140] Matsuki A., QuennehenB., SchwarzenboeckA., CrumeyrolleS., VenzacH., LajP., Gomes L. Temporal and vertical variations of aerosol physical and chemical properties over West Africa: AMMA aircraft campaign in summer 2006.Atmospheric Chemistry and Physics, 2010, 10(17): 8437-8451.

[141] Freney E.J., AdachiK., Buseck P.R.Internally mixed atmospheric aerosol particles: Hygroscopic growth and light scattering.Journal of Geophysical Research-Atmospheres, 2010, 115, DOI:10.1029/2009JD013558.

[142] Niu H., ShaoL.,ZhangD. Aged status of soot particles during the passage of a weak cyclone in Beijing.Atmospheric Environment, 2011,45(16): 2699-2703.

[143] Adachi K., ChungS.H., Buseck P.R. Shapes of soot aerosol particles and implications for their effects on climate.Journal of Geophysical Research-Atmospheres, 2010, 115, D15206, DOI:10.1029/2009JD012868.

[144] Pratt K.A., Prather K.A. Aircraft measurements of vertical profiles of aerosol mixing states[J]. Journal of Geophysical Research, 2010, 115,DOI:10.1029/2009JD013150.

[145] Laskin A., Moffet R.C., Gilles M.K., et al. Tropospheric chemistry of internally mixed sea salt and organic particles: Surprising reactivity of NaCl with weak organic acids[J]. Journal

of Geophysical Research-Atmospheres, 2012, 117,DOI:10.1029/2012JD017743.

[146] Kocbach A., Johansen B.V., Schwarze P.E., Namork E. Analytical electron microscopy of combustion particles: a comparison of vehicle exhaust and residential wood smoke.Science of the Total Environment, 2005, 346: 231-243.

[147] Niemi J.V., Saarikoski S., Tervahattu H., Mäkelä T., Hillamo R., Vehkamäki H., Sogacheva L., Kulmala M.Changes in background aerosol composition in Finland during polluted and clean periods studied by TEM/EDX individual particle analysis. Atmospheric Chemistry and Physic, 2006, 6: 5049-5066.

[148] Li J., Pósfai M., Hobbs P.V., Buseck P.R. Individual aerosol particles from biomass burning in southern Africa: 2, Compositions and aging of inorganic particles. Journal of Geophysical Research-Atmospheres, 2003, 108, DOI:10.1029/2002JD002310.

[149] Kaegi R., Holzer L.Transfer of a single particle for combined ESEM and TEM analyses.Atmospheric Environment,2003,(37):4353-4359.

[150] Okada K., IkegamiM., ZaizenY., TsutsumiY., MakinoY., JensenJ.B., GrasJ.L. Submicrometer sulfur-rich particles in the middle troposphere: Aircraft observations from Australia to Japan. Atmospheric Research, 2008, 88: 185-198.

[151] Ueda S., Osada K.Mixing states of cloud interstitial particles between water-soluble and insoluble materials at Mt. Tateyama, Japan: Effects of meteorological conditions. Atmospheric Research,2011, 99 (2): 325-336.

[152] Gen H., KangS., JungH.J., ChoelM., KimH., RoC.U. Characterization of individual submicrometer aerosol particles collectedin Incheon, Korea, by quantitative transmission electron microscopyenergy - dispersive X - ray spectrometry.Journal of Geophysical Research-Atmospheres, 2010, 115, DOI:10.1029/2009JD013486.

[153] Coz E., Leck C. Morphology and state of mixture of atmospheric soot aggregates during the winter season over Southern Asia–A quantitative approach. Tellus, Ser. B 2011, 63 (1): 107-116.

[154] 李卫军，邵龙义．雾霾和沙尘污染天气气溶胶单颗粒研究(中英文)．北京：科学出版社，2013.

[155] Liu X., Zhu J., Van E.P., et al. Single particle characterization of spring and summer aerosols in Beijing: Formation of composite sulfate of calcium and potassium[J]. Atmospheric Environment, 2005, 39(36): 6909-6918.

[156] Zhou S.Z., Yuan Q., Li W.J., Lu Y.L., Zhang Y.M., Wang W.X. Trace metals in atmospheric fine particles in one industrial urban city: Spatial variations, sources, and health implications. Journal of Environmental Sciences, 2014, 26: 205-213.

[157] Shao L.Y., Li J.J., Zhao H.Y., et al. Associations between particle physicochemical characteristics and oxidative capacity: An indoor PM_{10} study in Beijing, China[J]. Atmospheric Environment, 2007, 41(26): 5316-5326.

[158] Zhang D.Z., Shi G.Y., Iwasaka Y., et al. Mixture of sulfate and nitrate in coastal

atmospheric aerosols: individual particle studies in Qingdao, China[J]. Atmospheric Environment, 2000, 34(17): 2669-2679.

[159] Shi Z.B., Shao L.Y., Jones T.P., et al. Characterization of airborne individual particles collected in an urban area, a satellite city and a clean air area in Beijing, 2001[J]. Atmospheric Environment, 2003, 37(29): 4097-4108.

[160] Li W.J., Shao L.Y. Characterization of mineral particles in winter fog of Beijing analyzed by TEM and SEM.Environmental Monitoringand Assessment, 2010, 161:565-573.

[161] Zhang R.Y., Khalizov A.F., Pagels J., Zhang D., Xue H.X., McMurry P.H.Variability in morphology, hygroscopicity, and optical properties of soot aerosols during atmospheric processing. Proceedings of the National Academy of Sciences of the United States of America, 2008, 105, 30: 10291-10296.

[162] Adachi K.,Buseck P.R. Internally mixed soot, sulfates, and organic matter in aerosol particles from Mexico City [J]. Atmospheric Chemistry and Physics, 2008,8(3): 9179-9207.

[163] Li W.J.,Chi J.W., Shi Z.B, Wang X.F., Chen B., Wang Y., Li T., Chen J.M., Zhang D.Z., Wang Z.F., Shi C., Liu L., WangW.X. Composition and hygroscopicity of aerosol particles at Mt. Lu in South China: Implications for acid precipitation. Atmospheric Environment, 2014, 94: 626-636.

[164] Pósfai M., Anderson J.R., Buseck P.R. Sievering H. Soot and sulfate aerosol particles in the remote marine troposphere [J]. Journal of Geophysical Research-Atmospheres, 1999,104: 21685-21693.

[165] Moffet R.C., Furutani H., Rödel T.C.; Henn T.R., Sprau P.O., Laskin A., Uematsu M., Gilles M.K. Iron speciation and mixingin single aerosol particles from the Asian continental outflow. Journal of Geophysical Research-Atmospheres, 2012,117(D7), DOI:10.1029/2011JD016746.

[166] Bauer S.E., Koch D. Impact of heterogeneous sulfate formation at mineral dust surfaces on aerosol loads and radiative forcing in the Goddard Institute for Space Studies general circulation model [J]. Journal of Geophysical Research-Atmospheres, 2005,110: 1-15.

[167] Li W.J.,Wang T.,Zhou S.Z.,Lee S.C, Huang Y.,Gao Y., Wang W.X. Microscopic Observation of Metal-Containing Particles from Chinese Continental Outflow Observed from a Non-Industrial Site [J]. Environmental Science and Technology, 2013,47(16): 9124-9131.

[168] Wu D., Wu X., Zhu X., 2009. Fog and haze. China Meteorological Press.

[169] Metzger S., LelieveldJ.Reformulating atmospheric aerosol thermodynamics and hygroscopic growth into fog haze and clouds. Atmospheric Chemistry and Physics, 2007, 7: 3163-3193.

[170] Seinfeld J.H. Atmospheric chemistry and physics of air pollution. New York: Wiley, 1986.

[171] Wyzga R.E., Folinsbee L.J. Health effects of acid aerosols. Water, Air, and Soil Pollution, 1995, 85(1): 177-188.

[172] Trijonis J. Visibility in the southwest: An exploration of the historical data base. Atmospheric Environment, 1979, 13: 833-843.

[173] Chen L.W.A., Chow J.C., Doddridge B.G., Dickerson R.R., Ryan W.F., Mueller P.K. Analysis of a summertime $PM_{2.5}$ and haze episode in the mid-Atlantic region. Journal of Air Waste Management Association, 2003, 53: 946-956.

[174] Chan Y.C., Simpson R.W., Mctainsh G.H., Vowles P.D., Cohen D.D., Bailey G.M. Source apportionment of visibility degradation problems in Brishane (Australia) using the multiple linear regression techniques. Atmospheric Environment, 1999, 33: 3237-3250.

[175] Nemery B., Hoet P.H.M., Nemmar A. The Meuse Valley fog of 1930: An air pollution disaster. Lancet, 2001, 357(9257): 704-708.

[176] Wu D. Hazy weather research in China in the last decade: A review. Acta Science Circumstance, 2012, 32: 257-269.

[177] Quan J., Zhang Q., He H., Liu J., Huang M., Jin H. Analysis of the formation of fog and haze in North China Plain (NCP). Atmospheric Chemistry and Physics, 2011, 11: 8205-8214.

[178] Che H., Zhang X., Li Y., Zhou Z., Qu J., Hao X. Haze trends over the capital cities of 31 provinces in China, 1981-2005. Theoretical and Applied Climatology, 2009, 97 (3): 235-242.

[179] Li W.J.,Shao L.Y., Buseck P.R. Haze types in Beijing and the influence of agricultural biomass burning.Atmospheric Chemistry and Physics, 2010, 10(17): 8119-8130.

[180] Li Z., et al. East Asian Studies of Tropospheric Aerosols and theirImpact on Regional Climate (EAST-AIRC): An overview.Journal of Geophysical Research-Atmospheres, 2011, 116, DOI:10.1029/2010JD015257.

[181] Zheng J., et al. Measurements of gaseous H2SO4 by AP-ID-CIMS during CAREBeijing 2008 Campaign.Atmospheric Chemistry and Physics, 2011, 11(15), 7755-7765.

[182] Liu P., ZhaoC., ZhangQ., DengZ., Huang M., MaX., TieX. Aircraft study of aerosol vertical distributions over Beijing and their optical properties. Tellus, Ser. B, 2009, 61, 756-767.

[183] Zhao X., Zhao P., Xu J., Meng W., Pu W., Dong F., He D., Shi Q. Analysis of a winter regional haze event and its formation mechanism in the North China Plain. Atmospheric Chemistry and Physics,2013, 13: 5685-5696.

[184] Cheng Z., Wang S., Jiang J., Fu Q., Chen C., Xu B., Yu J., Fu X., Hao J.Long-term trend of haze pollution and impact of particulate matter in the Yangtze River Delta, China. Environmental Pollution, 2013, 182: 101-110.

[185] Ma J., ChenY., WangW., Yan P., LiuH., YangS., HuZ., LelieveldJ. Strong air pollution causes widespread haze-clouds over China.Journal of Geophysical Research-Atmospheres, 2010, 115, doi:10.1029/2009JD013065.

[186] Zhang Y., Tao S., Shen H., Ma J.Inhalation exposure to ambient polycyclic aromatic

hydrocarbons and lung cancer risk of Chinese population. Proceedings of the NationalAcademy of Science of the United States of America,2009, 106 (50): 21063-21067.

[187] Liu X., Li J., Qu Y., Han T., Hou L., Gu J., Chen C., Yang Y., Liu X., Yang T., Zhang Y., Tian H., Hu M. Formation and evolution mechanism of regional haze: a case study in the megacity Beijing, China. Atmospheric Chemistry and Physics, 2013, 13: 4501-4514.

[188] Huang W., Cao J., Tao Y., Dai L., Lu S., Hou B., Wang Z., Zhu T. Seasonal Variation of Chemical Species Associated With Short-Term Mortality Effects of $PM_{2.5}$ in Xi'an, a Central City in China. American Journal of Epidemiology, 2012, DOI: 10.1093/aje/kwr1342.

[189] Sun Y.L., Zhuang G.S., Tang A.H., Wang Y. and An Z.S. Chemical characteristics of $PM_{2.5}$ and PM_{10} in haze-fog episodes in Beijing. Environmental Science and Technology, 2006, 40(10): 3148-3155.

[190] Wang H.C., John W. Characteristics of the berner impactor for sampling inorganic ions. Aerosol Science and Technology, 1988, 8: 157-172.

[191] Tsai C.J., Perng S.N. Artifacts of ionic species for hi-vol PM_{10} and PM_{10} dichotomous samplers. Atmospheric Environment, 1998, 32: 1605-1613.

[192] Appel B.R., Wall S.M., Tokiwa Y., Haik M. Interference effects in sampling particulate nitrate in ambient air. Atmospheric Environment, 1979, 13: 319-325.

[193] Okada K.,Hitzenberger R.M. Mixing properties of individual submicrometer aerosol particles in Vienna. Atmospheric Environment, 2001, 35: 5617-5628.

[194] Kojima T., Buseck P.R., Iwasaka Y., Matsuki A., Trochkine D. Sulfate-coated dust particles in the free troposphere over Japan. Atmospheric Research, 2006, 82: 698-708.

[195] Harris J., Dlugokencky E., Oltmans S., Tans P., Conway T., Novelli P., Thoning K., Kahl J. An interpretation of trace gas correlations during Barrow, Alaska, winter dark periods, 1986-1997[J]. Journal of Geophysical Research-Atmospheres, 2000, 105, DOI: 10.1029/2000JD900167.

[196] Wotawa G., Kröger H., Stohl A. Transport of ozone towards the Alps-results from trajectory analyses and photochemical model studies[J]. Atmospheric Environment, 2000 9: 1367-1377.

[197] Lam K., Wang T., Chan L., Wang T., Harris J. Flow patterns influencing the seasonal behavior of surface ozone and carbon monoxide at a coastal site near Hong Kong[J]. Atmospheric Environment, 2001 (18): 3121-3135.

[198] Taylor A.D. Conformal map transformations for meteorological modelers[J]. Computers & Geosciences, 1997 (1): 63-75.

[199] Draxler R.R. Trajectory optimization for balloon flight planning[J]. Weather and Forecasting, 1996 (1): 114-114.

[200] Draxler R., Stunder B., Rolph G., Stein A., Taylor A.Hysplit4 User-Guide. National

Oceanic and Atmospheric Administration, 2009.

[201] Zhou Y., Wang T., Gao X.M., Xue L.K., Wang X.F., Wang Z., Gao J.A., Zhang Q.Z., Wang W.X. Continuous observations of water-soluble ions in $PM_{2.5}$ at Mount Tai (1534 ma.s.l.) in central-eastern China. Journal of Atmospheric Chemistry, 2010, 64: 107-127.

[202] Kulmala M., Petäjä T., Nieminen T., Sipilä M., Manninen H.E., Lehtipalo K., Dal Maso M., Aalto P.P., Junninen H., Paasonen P. Measurement of the nucleation of atmospheric aerosol particles. Nature Protocols, 2012, 7:1651-1667.

[203] Wang Y., Zhuang G., Zhang X., Huang K., Xu C., Tang A., Chen J., An Z. The ion chemistry, seasonal cycle, and sources of $PM_{2.5}$ and TSP aerosol in Shanghai[J]. Atmospheric Environment, 2006 (16): 2935-2952.

[204] Wang Y., Zhuang G., Tang A.H., Yuan H., Sun Y.L., Chen S.A., Zheng A.H. The ion chemistry and the source of $PM_{2.5}$ aerosol in Beijing[J]. Atmospheric Environment, 2005 (21): 3771-3784.

[205] Zhang T., Cao J., Tie X., Shen Z., Liu S., Ding H., et al. Water-soluble ions in atmospheric aerosols measured in Xi'an, China: Seasonal variations and sources. Atmospheric Research, 2011, 102: 110-119.

[206] Xu L., Chen X., Chen J., Zhang F., He C., Zhao J., et al. Seasonal variations and chemical compositions of $PM_{2.5}$ aerosol in the urban area of Fuzhou, China. Atmospheric Research, 2012, 104: 264-272.

[207] Hagler G.S., Bergin M.H., Salmon L.G., Yu J.Z., Wan E.C.H., Zheng M., Zeng L.M., Kiang C.S., Zhang Y.H., Lau A.K.H., Schauer J.J. Source areas and chemical composition of fine particulate matter in the Pearl River Delta region of China[J]. Atmospheric Environment., 2006 (20): 3802-3815.

[208] Fang G.C., Chang C.N., Wu Y.S., Wang N.P., Wang V., Fu P.P.C., Yang D.G., Chen S.C. Comparison of particulate mass, chemical species for urban, suburban and rural areas in central Taiwan, Taichung[J]. Chemosphere, 2000 (9): 1349-1359.

[209] Seinfeld J.H., Pandis S.N. Atmospheric chemistry and physics-from air pollution to climate change. 2nd ed. New York: JohnWiley & Sons, Inc., 2006.

[210] Dlugi R., Jordan S., Lindemann E. Theheterogeneous formation of sulfate aerosols in the atmosphere. Journal of Aerosol Science, 1981, 12: 185-197.

[211] Tao J., Ho K.F., Chen L., Zhu L., Han J., Xu Z. Effect of chemical composition of PM2.5 on visibility in Guangzhou, China, 2007 spring. Particuology, 2009, 7: 68-75.

[212] Sun Y., Wang Z., Dong H., Yang T., Li J., Pan X., et al. Characterization of summer organic and inorganic aerosols in Beijing, China with an Aerosol Chemical Speciation Monitor. Atmospheric Environment, 2012, 51: 250-259.

[213] Zhang M., Chen J.M., Chen X.Y., et al. Urban Aerosol Characteristics during the World Expo 2010 in Shanghai[J]. Aerosol and Air Quality Research, 2013, 13: 36-48.

[214] 古金霞，吴丽萍，霍光耀等.天津市 $PM_{2.5}$ 中水溶性无机离子污染特征及来源分析[J].

中国环境监测， 2013，29(3): 30-35.

[215] Hu M., He L.Y., Zhang Y.H., Wang M., Pyo Kim Y., Moon K. Seasonal variation of ionic species in fine particles at Qingdao, China. Atmospheric Environment, 2002, 36: 5853-5859.

[216] Hu M., Wu Z., Slanina J., Lin P., Liu S., Zeng L. Acidic gases, ammonia and water-soluble ions in $PM_{2.5}$ at a coastal site in the Pearl River Delta, China. Atmospheric Environment, 2008, 42: 6310-6320.

[217] Li L., Wang W., Feng J., Zhang D., Li H., Gu Z., et al. Composition, source, mass closure of $PM_{2.5}$ aerosols for four forests in eastern China. Journal of Environmental Science, 2010, 22: 405-412.

[218] Chang S.Y., Lee C.T., Chou C.C.K., Liu S.C., Wen T.X. The continuous field measurements of soluble aerosol compositions at the Taipei Aerosol Supersite, Taiwan. Atmospheric Environment, 2007, 41: 1936-1949.

[219] Hong S., Kim D., Ryu S., Kim Y., Lee J. Chemical characteristics of $PM_{2.5}$ ions measured by a semi-continuous measurement system during the fall season at a suburban site, Gwangju, Korea. Atmospheric Research, 2008, 89: 62-75.

[220] Kim K.H., Sekiguchi K., Furuuchi M., Sakamoto K. Seasonal variation of carbonaceous and ionic components in ultrafine and fine particles in an urban area of Japan. Atmospheric Environment, 2011, 45: 1581-1590.

[221] Favez O., Cachier H., Sciare J., Alfaro S.C., El-Araby T.M., Harhash M.A., et al. Seasonality of major aerosol species and their transformations in Cairo megacity. Atmospheric Environment, 2008, 42: 1503-1516.

[222] Verma S.K., Deb M.K., Suzuki Y., Tsai Y.I. Ion chemistry and source identification of coarse and fine aerosols in an urban area of eastern central India. Atmospheric Research, 2010, 95: 65-76.

[223] Pancras J.P., Landis M.S., Norris G.A., Vedantham R., Dvonch J.T. Source apportionment of ambient fine particulate matter in Dearborn, Michigan, using hourly resolved PM chemical composition data. Science of the Total Environment, 2013, 448:2-13.

[224] Lee T., Yu X.Y., Kreidenweis S.M., Malm W.C., Collett J.L. Semi-continuous measurement of $PM_{2.5}$ ionic composition at several rural locations in the United States. Atmospheric Environment, 2008, 42: 6655-6669.

[225] Querol X., Perez N., Pey J., Alastuey A., Lopez J.M., Viana Partitioning of major and trace components in PM_{10}-$PM_{2.5}$-PM_1 at an urban site in Southern Europe[J]. Atmospheric Environment, 2008 (8):1677-1691.

[226] Aikawa M., Hiraki T., Suzuki M., et al. Separate chemical characterizations of fog water, aerosol, and gas before, during, and after fog events near an industrialized area in Japan [J]. Atmospheric Environment, 2007, 41 : 1950-1959.

[227] Gao X., Xue L., Wang X., Wang T., Yuan C., Gao R., et al. Aerosol ionic components at Mt.

Heng in central southern China: Abundances, size distribution, and impacts of long-range transport. Science of the Total Environment, 2012, 433: 498-506.

[228] Pathak R.K., Wang T., Ho K., Lee S. Characteristics of summertime $PM_{2.5}$ organic and elemental carbon in four major Chinese cities: Implications of high acidity for water-soluble organic carbon (WSOC). Atmospheric Environment, 2011, 45: 318-325.

[229] Stelson A., Seinfeld J. Relative humidity and temperature dependence of the ammonium nitrate dissociation constant. Atmospheric Environment, 1982, 16: 983-992.

[230] Anttila T., Kiendler-Scharr A., Tillmann R., Mentel T.F. On the reactive uptake of gaseous compounds by organic-coated aqueous aerosols: Theoretical analysis and application to the heterogeneous hydrolysis of N_2O_5. The Journal of Physical Chemistry, 2006 110: 10435-10443.

[231] McLaren R., Salmon R.A., John-Liggio J., Hayden K.L, Anlauf K.G., Leaitch W.R. Nighttime chemistry at a rural site in the Lower Fraser Valley. Atmospheric Environment, 2004, 38: 5837-5848.

[232] Hallquist M., Stewart D.J., Stephenson S.K.,Cox R.A. Hydrolysis of N_2O_5 on sub-micron sulfate aerosols. Physical Chemistry Chemical Physics, 2003, 5: 3453-3463.

[233] Bismarck-Osten C., Birmili W., Ketzel M., Massling A., Petäjä T., Weber S. Characterization of parameters influencing the spatiotemporalvariability of urban particle number size distributions infour European cities. Atmospheric Environment, 2013, 77:415-429.

[234] Gómez-Moreno F.J., Pujadas M., Plaza J., Rodríguez-Maroto J.J., Martínez-Lozano P., Artíñano B. Influence of seasonal factors on theatmospheric particle number concentration and size distribution inMadrid. Atmospheric Environment, 2011, 45:3169-3180.

[235] Gao J., Wang J., Cheng S.H., Xue L.K., Yan H.Z., Hou L.J., Jiang Y.Q., Wang W.X. Number concentration and size distributions of submicron particles in Jinan urban area: characteristics in summer and winter. Journal of Environmental Science., 2007, 19: 1466-1473.

[236] Kang H., Zhu B., Su J., Wang H., Zhang Q., Wang F. Analysis of a long-lasting haze episode in Nanjing, China. Atmospheric Research, 2013, 120-121: 78-87.

[237] Robinson A.L., Donahue N.M., Shrivastava M.K., Weitkamp E.A., Sage A.M., GrieshopA.P., Lane T.E., Pierce J.R., Pandis S.N. Rethinking organic aerosols: Semivolatile emissions and photochemical aging. Science, 2007, 315:1259-1262.

[238] Li, W.J., Shao, L.Y. Observation of nitrate coatings on atmospheric mineral dust particles. Atmospheric Chemistry and Physics, 2009, 6: 1863-1871.

[239] Bond T.C., Zarzycki C.,Flaimer M.G., Koch D.M. Quantifying immediate radiative forcing by black carbon and organic matter with the Specific Forcing Pulse [J]. Atmospheric Chemistry and Physics Discussions, 2013,10(6): 15713-15753.

[240] Adachi K., Buseck P.R. Internally mixed soot, sulfates, and organic matter in aerosol

particles from Mexico City.Atmospheric Chemistry and Physics, 2008, 8(21), 6469-6481.

[241] Li W.J., ShaoL.Y. Mixing and water-soluble characteristics of particulate organic compounds in individual urban aerosol particles.Journal of Geophysical Research-Atmospheres, 2010, *115*(D02301), DOI:10.1029/2009JD012575.

[242] Gao Y., Yu L.E., Chen S.B. Effects of organics on efflorescence relative humidity of ammonium sulfate or sodium chloride particles. Atmospheric Environment, 42, 19: 4433-4445.

[243] Kulmala M., et al. Direct Observations of Atmospheric Aerosol Nucleation. Science, 2013, 339(6122): 943-946.

[244] Whiteaker J.R., Suess D.T.,Prather K.A. Effects of meteorological conditions on aerosol composition and mixing state in Bakersfield, CA.Environmental Science and Technology, 2002, 36(11): 2345-2353.

[245] Itahashi S., Yumimoto K., Uno I., Eguchi K., Takemura T., Hara Y., Shimizu A., Sugimoto N., Liu Z. Structure of dust and air pollutant outflow over East Asia in the spring.Geophysical Research Letters, 2010, 37, DOI: 10.1029/2010GL044776

[246] Li W.J., Shao L.Y. Chemical Modification of Dust Particles during Different Dust Storm Episodes, Aerosol and Air Quality Research, 2012, 12(6): 1095-1104.

[247] Geng H., Park Y., Hwang H., Kang S., Ro C.U. Elevated nitrogen-containing particles observed in Asian dust aerosol samples collected at the marine boundary layer of the Bohai Sea and the Yellow Sea.Atmospheric Chemistry and Physics, 2009, 9(18), 6933-6947.

[248] Kim, J.S., Park K. Atmospheric Aging of Asian Dust Particles During Long Range Transport, Aerosol Science and Technology., 2012, 46(8): 913-924.

[249] Zhang D.Z., Iwasaka Y. Size change of Asian dust particles caused by sea salt interaction: Measurements in southwestern Japan.Geophysical Research Letters, 2004, 31(15): 15102-15102.

[250] ToboY., Zhang D.Z., Matsuki A., Iwasaka Y. Asian dust particles converted into aqueous droplets under remote marine atmospheric conditions. Proceeding of the National Academy of Science of the United States of America, 2010, 107(42): 17905-17910.

[251] Li W.J., Shao L.Y. Transmission electron microscopy study of aerosol particles from the brown hazes in northern China. Journal of Geophysical Research-Atmospheres,2009, 114, DOI:10.1029/2008JD011285.

[252] Moffet R.C., Prather K.A.In-situ measurements of the mixing state and optical properties of soot with implications for radiative forcing estimates. Proceedings of the National Academy of Sciencesof the United States of America, 2009, 106: 11872-11877.

[253] Desboeufs K. V., Sofikitis A., Losno R., Colin, J.L., Ausset P. Dissolution and solubility of trace metals from natural and anthropogenic aerosol particulate matter. Chemosphere, 2005, 58, 2: 195-203.

[254] Li W.J.,Shao L.Y., ShenR.R., Yang S.S., Wang Z.S., Tang U. Internally mixed sea salt, soot,

and sulfates at Macao: A coastal city in South China.Journal of the Air & Waste Management Association, 2011, 61(11): 1166-1173.

[255] Pan X., Yan P., Tang J., Ma J., Wang Z., Gbaguidi A., Sun Y. Observational study of influence of aerosol hygroscopic growth on scattering coefficient over rural area near Beijing mega-city. Atmospheric Chemistry and Physics, 2009, 9: 7519-7530.

[256] Li W.J., Zhang D.Z., ShaoL.Y., Wang W.X. Individual particle analysis of aerosols collected under haze and non-haze conditions at a high-elevation mountain site in the North China plain. Atmospheric Chemistry and Physics, 2011, 11: 11733-11744.

[257] Shen X.J., Sun J.Y., Zhang Y.M., Wehner B., Nowak A., Tuch T., Zhang X.C., Wang T.T., Zhou H.G., Zhang X.L., Dong F., Birmili W. And WiedensohlerA.First long-term study of particle number size distributionsand new particle formation events of regional aerosol in theNorth China Plain. Atmospheric Chemistry and Physics, 2011,11:1565-1580.

[258] Yue D.L., Hu M., WuZ.J., Wang Z.B., Guo S., Wehner B.,Nowak A., Achtert P., Wiedensohler A., Jung J.S., KimY.J.and Liu S.H. Characteristics of aerosol size distributions andnew particle formation in the summer in Beijing.Journal of Geophysical Research-Atmospheres, 114, D00G12, doi:10.1029/2008JD010894, 2009.

[259] Kivekäs N., Sun J., Zhan M., Kerminen V.M., Hyvärinen A.,Komppula M., Viisanen Y., Hong N., Zhang Y., Kulmala M.,Zhang X.C., Deli-Geer and Lihavainen H. Long term particlesize distributionmeasurements at Mount Waliguan, a highaltitudesite in inland China. Atmospheric Chemistry and Physics, 2009,9: 5461-5474.

致谢

本文的研究工作是在导师王文兴院士和王韬教授的悉心指导下完成的。在硕士和博士六年多的学习时间里，感谢王文兴院士为我提供了宝贵的学习机会，并在学术指导以及学习和生活中所给予的无微不至的关怀和帮助，您渊博的学识、严谨的学术态度、孜孜不倦的科学追求、忘我的工作热情和平易近人的人格魅力深深地影响并激励着我。本论文从选题到完成，每一步都倾注了王文兴院士的大量心血。感谢王韬教授在实验、数据分析和论文写作方面的建议和指导，他严谨的科学态度、对科学的执着追求以及自我严格要求的态度深深地影响着我。在此，谨向两位导师表示最崇高的敬意和最衷心的感谢！

感谢张庆竹教授、胡敬田教授、李卫军教授、杨凌霄教授对我在研究院学习期间给予的关心、指导和帮助。感谢环境研究院的孙孝敏、周学华、谢慧君、孙瑞莲、孙廷利、尹娜等诸位老师对我学习和工作上的帮助。

感谢许鹏举、周杨、王哲、刘晓环、程淑会、薛丽坤、高晓梅、高锐、聂玮、王新锋、袁超、徐政、周声圳、于阳春、马强等师兄师姐以及鄢超、董灿、孟川平、隋潇、姚兰、朱艳红、芦亚玲、杨飞等诸多同学在学习和实验中的热心帮助。

最后，感谢我的父母、爱人对我的无尽关爱和帮助，感谢元宝对我精神上的支持，是你们的爱让我以坚强的信念完成学业。

感谢山东大学环境研究院多年以来对我的培养。

袁琦

2015.5.23 于济南

博士期间发表论文情况

1. **Yuan Q.**, Yang L.X., Dong C., Yan C., Meng C.P., Sui X., Wang W.X. Temporal variations, acidity and transport patterns of $PM_{2.5}$ ionic components at a background site in the Yellow River Delta, China. Air Quality, Atmosphere &Health, 2014, 7: 143-153.
2. **Yuan Q.**,Yang L.X., Dong C., Yan C., Meng C.P.,Sui X., Wang W.X. Particle physical characterization in Yellow River Delta of Eastern China: number size distribution and new particle formation. Air Quality, Atmosphere &Health, DOI: 10.1007/s11869-014-0293-4.
3. **Yuan Q.**, Li W.J, Zhou S.Z., Yang L.X., Chi J.W., Sui X., Wang W.X. Integrated evaluation of aerosols during haze-fog episodes at one regional background site in North China Plain. Atmospheric Research, 2015, 156: 102-110.
4. Zhou S.Z, **Yuan Q.**, Li W.J., Lu Y.L., Zhang Y.M., Wang W.X.Trace Metals in Atmospheric Fine Particles in One Industrial Urban City: Spatial Variations, Sources, and Health Implications. Journal of Environmental Sciences-China, 2014, 26: 205-213.
5. Zhu Y.H., Yang L.X., **Yuan Q.**,Yan C., Dong C., Meng C.P.,Sui X.,Yao L., Yang F., Lu Y.L., Wang W.X. Airborne particulatepolycyclic aromatic hydrocarbons (PAHs) pollution in a background site in the NorthChina plain: concentration, size distribution, toxicity and sources [J]. Science of theTotal Environment, 2014, 466-467: 357-368.
6. Li W.J., Li P.R., Sun G.D., Zhou S.Z., **Yuan, Q.**, Wang W.X. Cloud residues and interstitial aerosols from non-precipitating clouds over an industrial and urban area in northern China. Atmospheric Environment, 2011, 45(15): 2488-2495.
7. Dong C.,Yang L.X., Yan C., **Yuan Q.**, Yu Y.C., Wang W.X.Particle size distributions, $PM_{2.5}$concentrations and water-soluble inorganic ions in different public indoorenvironments: a case study in Jinan, China[J]. Frontiers of Environmental Science & m Engineering, 2013, 7: 55-65.
8. Li W.J., Shao L, Shi Z, Chen J., Yang L., **Yuan Q.**, Yan C., Zhang X., Wang Y., Sun J., Zhang Y., Shen X., Wang Z.F., Wang W.X. Mixing State and Hygroscopicity of Dust and Haze Particles Before Leaving Asian Continent. Journal of Geophysical Research: Atmospheres, 2014, 119, (2), 1044-1059.

9. Li W.J., Shi Z.B., Zhang D.Z., Zhang X.Y., Li P.R., Feng Q.J., **Yuan Q.,** Wang W.X. Haze particles over a coal-burning region in the China Loess Plateau in winter: Three flight missions in December 2010. Journal of Geophysical Research-Atmosphere, 2012, 117, DOI:10.1029/2012JD017720.

10. 孙玉伟,周学华,**袁琦,**马强,周声圳,徐政,马玉洁. 济南市秋末冬初大气颗粒物和气体污染物污染水平及来源. 环境科学研究, 2012, 25: 245-252.

11. 鄢超, 杨凌霄, 董灿, **袁琦**, 高晓梅, 薛丽坤, 王哲, 王文兴. 济南冬季典型商业室内环境颗粒物污染特征[J].中国环境科学,2012,32 (4): 478-484.

12. 孟川平, 杨凌霄, 董灿, 鄢超, **袁琦**, 姚兰, 杨飞, 王文兴. 济南冬春季室内空气$PM_{2.5}$中多环芳烃污染特征及健康风险评价[J]. 环境化学, 2013,5(32), DOI: 10.7524/j.issn.0254-6108.2013.05.

13. 杨飞, 杨凌霄, 孟川平, 朱艳红, 姚兰, 芦亚玲, **袁琦,**隋潇, 王文兴. 济南市 $PM_{2.5}$ 中多环芳烃(PAHs)的季节变化特征及健康风险评价.中国科学院大学学报, 2014,31(3): 389-396.

Atmospheric Research 156 (2015) 102–110

Contents lists available at ScienceDirect

Atmospheric Research

journal homepage: www.elsevier.com/locate/atmos

Integrated evaluation of aerosols during haze-fog episodes at one regional background site in North China Plain

Qi Yuan [a], Weijun Li [a,*], Shengzhen Zhou [a,c], Lingxiao Yang [b], Jianwei Chi [a], Xiao Sui [a], Wenxing Wang [a]

[a] Environment Research Institute, Shandong University, Jinan 250100, China
[b] School of Environmental Science and Engineering, Shandong University, Jinan 250100, China
[c] School of Environmental Science and Engineering, Sun Yat-sen University, Guangzhou, China

ARTICLE INFO

Article history:
Received 9 October 2014
Received in revised form 31 December 2014
Accepted 7 January 2015
Available online 13 January 2015

Keywords:
Regional background site
Haze-fog episode
PM2.5
Mixing state
New particle formation

ABSTRACT

To investigate haze-fog (HF) formation mechanisms and transport, trace gases and aerosols in the aged air masses during regional haze episodes were measured at a regional background site in the North China Plain during 4–19 July, 2011. Mixing state of individual particles, soluble ions of $PM_{2.5}$, and particle number concentrations were studied using transmission electron microscope, ambient ion monitoring, and wide-range particle spectrometer, respectively. Average mass concentration of $PM_{2.5}$ was 3 times higher on HF days (70 μg/m^3) than on clear days (22 μg/m^3). The major soluble ionic components (SO_4^{2-}, NO_3^-, and NH_4^+) in $PM_{2.5}$ were over 4 times higher on HF days (40.6 μg/m^3) than on clear days (9.1 μg/m^3). The high sulfur oxidation ratios (SOR) and nitrogen oxidation ratios (NOR) values during HF days suggest that polluted weather favored transformation of SO_2 and NO_x into sulfates and nitrates compared to clear days. Particle number fraction of the accumulation mode increases from 11% on clear days up to 26% on HF days. Individual particle analysis shows that secondary inorganic particles (e.g., sulfate and nitrate) as the most abundant species likely determine internal mixing of individual particles and almost half of them mixed refractory particles (e.g., metal, fly ash, soot, and mineral) on HF days. These fine refractory particles were likely emitted from coal fired power plants, heavy industries, and urban city in Shandong and Hebei provinces. Our results suggest that aged air masses mostly contain aged particles of long-range transport and some from new particle formation and growth in the regional background atmosphere.

1. Introduction

Haze is defined as a weather phenomenon which leads to atmospheric visibility less than 10 km with relative humidity (RH) less than 80%, while fog is composed of fine water droplets and ice crystals suspended in the air near the Earth's surface (visibility ≤ 10 km and RH > 95%) (Wu et al., 2009). When visibility is lower than 10 km and RH is between 80% and 95%, we call it mist (Wu et al., 2009). Because haze, fog, and mist periods frequently alternate in one day, we call these mixed periods haze-fog (HF) phenomenon.

HF pollution affects climate, reduces visibility, endangers public health, and damages natural and agricultural systems (Kim et al., 2006; Li et al., 2013b); such episodes have been extensively studied (Metzger and Lelieveld, 2007; Quan et al., 2011). Secondary components, combustion species, and transition metals appear most responsible for increased mortality on HF days (Huang et al., 2012). The haze formation may be affected by anti-cyclone synoptic conditions, primary pollutant emissions, and planetary boundary layer (PBL) height (Liu et al., 2013; Zhang et al., 2013). Secondary aerosol formation significantly contributes to regional haze (Zhao et al., 2013).

* Corresponding author.
E-mail address: liweijun@sdu.edu.cn (W. Li).

http://dx.doi.org/10.1016/j.atmosres.2015.01.002
0169-8095/

The long-rang transport and weather conditions are important factors controlling the formation of HF phenomena in Northern China (Ji et al., 2014). The growth processes can be enhanced by the internally mixed particles in haze layers (Li et al., 2011a). In addition, transmission electron microscopy (TEM) is an important technique for investigating the physical and chemical properties and mixing state of individual aerosol particles in HF episode (Li et al., 2011a; Posfai and Buseck, 2010; Ueda et al., 2011).

HF episodes are becoming a major environmental problem in North China and have increased in the past ten years (Che et al., 2009; Zhao et al., 2011). In the Asian monsoon, anthropogenic pollutants in North China not only seriously influence local air quality but also affect downwind regions by long-distance transport, such as South Korea, Japan, and North America (Jaffe et al., 1999; Kahn et al., 2004). Therefore, HF phenomena over North China have been examined by atmosphere scientists throughout the world. The Bohai Bay city-cluster (including Beijing-Tianjin, Hebei and Shandong provinces) is one of the principal economic zones in North China suffering from severe air pollution. Annual average ground-level $PM_{2.5}$ at 60–90 μg/m^3 in Bohai Bay of eastern China is one of the highest $PM_{2.5}$ concentrations in the world (van Donkelaar et al., 2010). Many studies on the chemical and physical characteristics of haze aerosols have been conducted at urban sites with large amounts of pollutant emissions in Bohai Bay such as Beijing, Tianjin, and Jinan (Han et al., 2014; Li et al., 2011b; Ma et al., 2010; Tao et al., 2012). The background area of Bohai Bay is frequently influenced by the regional pollutants of long-range transport from the urban areas, and the aged air masses mainly influenced air quality of the background area. However, the study on chemical and physical properties of aerosol particles in aged air masses is limited in the background area of Bohai Bay (Li et al., 2014).

In this study, one regional background site was selected in the Yellow River Delta (YRD) of North China Plain to investigate the possible formation mechanisms and transport of regional HF through understanding the physical and chemical properties of its aerosol particles. The field study was conducted during 4–19 July, 2011. Online measurements (wide-range particle spectrometer and ambient ion monitor) and individual particle analysis (transmission electron microscope) were used to determine the bulk and microscopic characterizations of aerosols during HF and clear days. Possible pollution sources and transport were evaluated using the backward trajectories cluster method.

2. Experiments

2.1. Sampling site

The sampling site (38°03′N, 118°44′E) was located in the Yellow River Delta (YRD) Nature Reserve Yi Qian Er Management Station in Dongying in Shandong Province. The site is 10 km south of the Bohai Sea and 300 km from the major cities in Shandong Province and in the Beijing–Tianjin–Hebei region. Though there are limited primary sources nearby, such as coal-fired power plants and industrial activities, this site is frequently under the influence of regional air pollution from North China (Li et al., 2013a). The sampling inlet of the instruments was placed on the rooftop of a building 15 m above ground. The sampling period was 4–19 July, 2011.

2.2. Instruments and methods

2.2.1. Online measurements

Particle number size concentrations were measured using a wide-range particle spectrometer (WPS, Model 1000XP, MSP Corporation) in the range of 0.005–10 μm. To verify proper differential mobility analyzer (DMA) and laser particle spectrometer (LPS) transfer function, the DMA was calibrated with NIST SRM 1691 and SRM 1963 PSL spheres (0.269 μm and 0.1007 μm mean diameter) and the LPS was calibrated with four NIST traceable sizes of PSL (0.701 μm, 1.36 μm, 1.6 μm and 4.0 μm). An ambient ion monitor (AIM, Model URG 9000B, URG Corporation) was used to measure hourly concentrations of water-soluble ions in $PM_{2.5}$, including F^-, Cl^-, NO_2^-, NO_3^-, SO_4^{2-}, Na^+, NH_4^+, K^+, Mg^{2+}, and Ca^{2+}. Multi-point calibrations were carried out for the AIM measurement every 4 days and a NaOH solution (5 mmol L^{-1}) was used as the denuder liquid to enhance the absorption of SO_2. SO_2 was measured by a pulsed UV fluorescence analyzer (Thermo Environmental Instruments (TEI), Model 43C); O_3 by a UV photometric analyzer (TEI, Model 49C); and NO_y by a commercial chemiluminescence analyzer (TEI,Model 42CY) fitted with an externally placed molybdenum oxides catalytic converter. The methods used to calibrate these instruments were the same as those reported in previous study (Wang et al., 2001).

2.2.2. Filter sampling and analysis

Daily $PM_{2.5}$ samples were collected on Teflon membranes using a filter-based sampler (Thermo Andersen, Model RAAS 2.5-400). The sampler collector was cleaned by ultrapure water (>18 MΩ) before sampling and field blanks were collected before and after the sampling period. The Teflon filters were put in polyethylene boxes immediately after sampling and stored at −5 °C. The filters were equilibrated at constant temperature (20 ± 0.5 °C) and humidity (50 ± 2%) for over 24 h before being weighed with an electronic microbalance (Sartorius-ME5, ±1 μg). Individual particle samples were collected on copper TEM grids coated with carbon film using a single-stage cascade impactor with a 0.5 mm diameter jet nozzle at a flow rate of 0.5 L/min (Li et al., 2011a). Sampling times varied from 40 s to 80 s, depending on the weather and visibility. Individual particle aerosols were analyzed by a high resolution transmission electron microscope (TEM, JEOL JEM-2100) to get the size and morphology of individual particles, and an energy-dispersive X-ray spectrometer (EDS) was used to determine elemental composition of targeted particles.

2.2.3. Meteorological data

Meteorological data (including temperature, relative humidity (RH), wind speed, wind direction etc.) were obtained from an automatic meteorological station. Visibility was detected by a visibility sensor (PW10, Vaisala). According to the visibility, sampling periods were divided into haze-fog (HF) days (visibility < 10 km) and clear days (visibility ≥ 10 km). Although ambient air temperatures did not vary between HF (25.5 °C) and clear days (24.7 °C), higher RH (81.9%) and lower wind speed (0.32 m/s) were observed on HF days than those on clear days (69.3% and 1.1 m/s). The prevailing wind directions were southeast and east on HF and clear days, respectively.

2.2.4. Back trajectory analysis

Backward trajectories and cluster analyses were applied to identify the origins and transport patterns of air masses during the field study. 72-h backward trajectories beginning at 500 m above ground level were calculated every hour using the Hybrid Single Particle Lagrange Integrated Trajectory model (HYSPLIT) (Draxler and Rolph, 2003). The trajectories were then clustered according to their similarity in spatial distribution using the HYSPLIT software (HYSPLIT 4.9).

3. Results and discussion

3.1. $PM_{2.5}$ concentrations and water soluble ions

Fig. 1 shows the temporal variations of $PM_{2.5}$ mass concentrations and visibility during the observation periods. The black dots in Fig. 1 represent the collection time of individual particle samples. In the individual sampling period, the average daily $PM_{2.5}$ mass concentration in the YRD was 52 μg/m^3, much lower than that in the polluted urban Jinan (129 μg/m^3) in summer of 2006 (Yang et al., 2012) and in urban Beijing (92 μg/m^3) in summer of 2007 (Zhao et al., 2009). However, this value is about 1.5 times higher than the 24h US NAAQS standards of $PM_{2.5}$ (35 μg/m^3). As shown in Table 1, HF phenomena occurred on five days with an average $PM_{2.5}$ mass concentration of 70 μg/m^3, ranging from 37 μg/m^3 (17 July) to 103 μg/m^3 (16 July) and three clear days in 12–14 July with an average $PM_{2.5}$ mass concentration of 22 μg/m^3. More specific pollutants data on HF and clear days will be compared in Sections 3.3 and 3.4.

SO_4^{2-}, NO_3^-, and NH_4^+ were the major soluble inorganic ionic components in $PM_{2.5}$, accounting for an average of 57.6% of $PM_{2.5}$ mass concentration on HF days and 43.4% on clear days. The average concentrations of SO_4^{2-}, NO_3^-, and NH_4^+ on HF days were 21.3 μg/m^3, 9.0 μg/m^3 and 10.3 μg/m^3, respectively, 4 times higher than those on clear days, suggesting that the more pronounced stability on HF days favored secondary aerosol formation and accumulation. Na^+/$PM_{2.5}$ mass ratio was 2.39% on clear days, 4 times higher than that on HF days (0.47%), suggesting that sea salts contributed more to $PM_{2.5}$ on clear days. The mass ratio of Na^+/SO_4^{2-} in the YRD was 0.02 on HF days and 0.09 on clear days, both lower than 3.98 in seawater, suggesting that the sulfates were mainly from the secondary formation of SO_2 in the YRD. Water-soluble inorganic ions are important components of aerosols and are considered to be a significant contributor to the visibility impairment in urban areas (Yang et al., 2007). The correlation coefficients (R) between water soluble inorganic ions (SO_4^{2-}, NO_3^-, and NH_4^+) and visibility were significantly negative ($R = -0.65$, -0.72, -0.72, respectively), indicating that water-soluble ions were a significant contributor to visibility impairment in background area.

SO_4^{2-}, NO_3^-, and NH_4^+ in ambient aerosols are normally considered as the transformation products of their gaseous precursors SO_2, NO_2, and NH_3, respectively. Sulfur oxidation ratios (SOR, defined SOR = $[SO_4^{2-}]/([SO_4^{2-}] + [SO_2])$ and nitrogen oxidation ratios (NOR, defined NOR = $[NO_3^-]/[NO_y]$ reflect the and the extent of conversion from SO_2 to SO_4^{2-} and from NO_x to NO_3^- (Gao et al., 2011). In this study, the SOR and NOR were 0.46 and 0.22 on HF days, which were higher than those on clear days (Table 1). The higher SOR and NOR values during HF episodes suggests that more SO_2 and NO_x can be oxidized into sulfates and nitrates under the stable weather conditions. Correlation coefficients of SO_4^{2-} & NH_4^+ and NO_3^- & NH_4^+ were further calculated through the hourly SO_4^{2-}, NO_3^-, and NH_4^+ concentrations through the AIM (Ambient Ion Monitor). Their high R values on HF days indicate that the main sulfate and nitrate salts are $(NH_4)_2SO_4$, NH_4HSO_4, and NH_4NO_3 at the YRD sampling site, consistent with the results on haze days in Beijing and Shanghai cities (Du et al., 2011; Sun et al., 2006).

3.2. Individual particle classification, size distribution and relative abundance

1506 individual particles were analyzed on HF (988) and clear (518) days through TEM. Based on particle composition

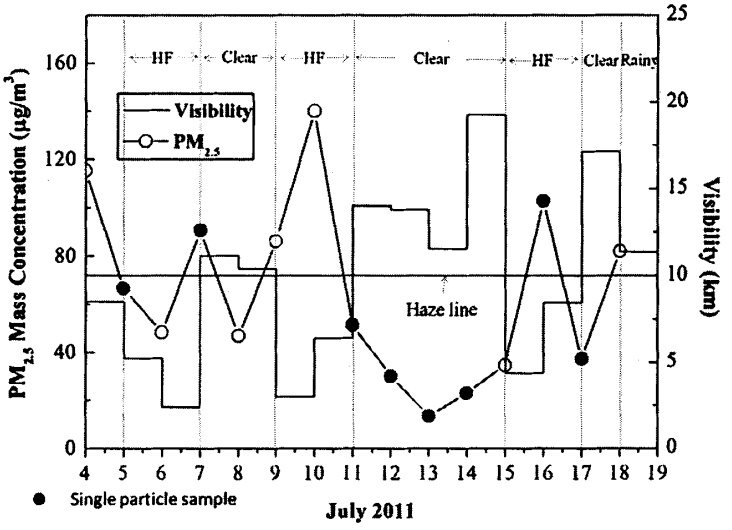

Fig. 1. Daily $PM_{2.5}$ mass concentrations and visibilities during 4–19 July, 2011. HF, clear and rainy days are identified and a visibility lower than 10 km (blue line) is used to define HF and clear episodes.

Table 1
$PM_{2.5}$ mass concentrations (μg/m³) and the major water soluble ions (SO_4^{2-}, NO_3^- and NH_4^+) concentrations (μg/m³), proportion in $PM_{2.5}$, O_3 (ppbv), SOR, NOR and the correlation coefficients (R value) between SO_4^{2-}, NO_3^- and NH_4^+ during HF and clear days in the YRD.

Site	Date	Weather type	$PM_{2.5}$ (μg/m³)	O_3 (ppbv)	Major water soluble ions in $PM_{2.5}$							
					NO_3^- (μg/m³)	SO_4^{2-} (μg/m³)	NH_4^+ (μg/m³)	Sum proportion in $PM_{2.5}$	SOR	NOR	R (SO_4^{2-} & NH_4^+)	R (NO_3^- & NH_4^+)
Yellow River Delta	7/5	HF	67	63	6.0	18.4	8.8	50.0%	0.31	0.08	0.94	0.91
	7/7	HF	91	42	14.9	26.8	13.6	61.0%	0.44	0.26		
	7/11	HF	51	35	6.0	13.3	6.7	50.6%	0.56	0.23		
	7/16	HF	103	73	15.7	33.1	16.1	63.2%	0.68	0.49		
	7/17	HF	37	46	2.4	14.7	6.4	63.0%	0.30	0.04		
	Avg.		70	52	9.0	21.3	10.3	57.6%	0.46	0.22	0.75	0.77
	7/12	Clear	30	34	1.8	6.5	2.9	36.8%	0.29	0.17		
	7/13	Clear	14	38	1.4	4.1	1.9	54.8%	0.33	0.26		
	7/14	Clear	23	38	1.7	5.1	2.1	38.7%	0.24	0.13		
	Avg.		22	37	1.6	5.2	2.3	43.4%	0.29	0.19		

and morphology, we classified individual particles into six types: S-rich, soot, mineral, fly ash, organic matter (OM) and metal (Fig. 2), the same criteria employed in a previous study (Li and Shao, 2009). Because the particle number of Na-rich particles is very low, we defined them as others in Fig. 3. S-rich particles are the most abundant and their sub-rounded shape with S, O, and N is distinctive (Fig. 2a). Fly ash particles are spherical with the principal components being O, Si, Al and minor metals (Fig. 2b). Soot particles are a complex spherical chain containing C and O (Fig. 2c). Mineral particles have irregular shapes and most contain Si and Al (Fig. 2d). Metal particles have a spherical shape (Fig. 2e) and most internally mixed with S-rich and K-rich particles. Stable organic matter (OM) contains organic carbon and has a number of complicated shapes with different mixtures in individual particles (Fig. 2f) (Li and Shao, 2010). The majority of aerosol particles were S-rich particles, accounting for 86.8% on both HF and clear days. Most of S-rich particles are internally mixed with other refractory aerosol particles such as metal, fly ash, soot, and mineral (Fig. 3).

Fig. 4 shows number fractions of different aerosol types in different size ranges on HF and clear days. The particles ranging from 0.1 μm to 2 μm in diameter made up about 82% on HF days and 93% on clear days (Fig. 4). On clear days, the percentages of the coarse particles containing mineral and Na-rich particles increased with increasing particle size, with average 50% of them at the range of 2 μm to 7 μm. On HF days, 51% of S-rich particles were internally mixed and only 20% of S-rich particles were internally mixed on clear days. This result indicated that aerosol particles aged significantly on HF days. S-rich/fly ash and S-rich/metal particles accounted for 8.7% and 13% of all particles on HF days and 0.9% and 9.8% of all particles on clear days. The proportions of externally mixed OM and soot particles in all particles were 3 times and 6 times higher on

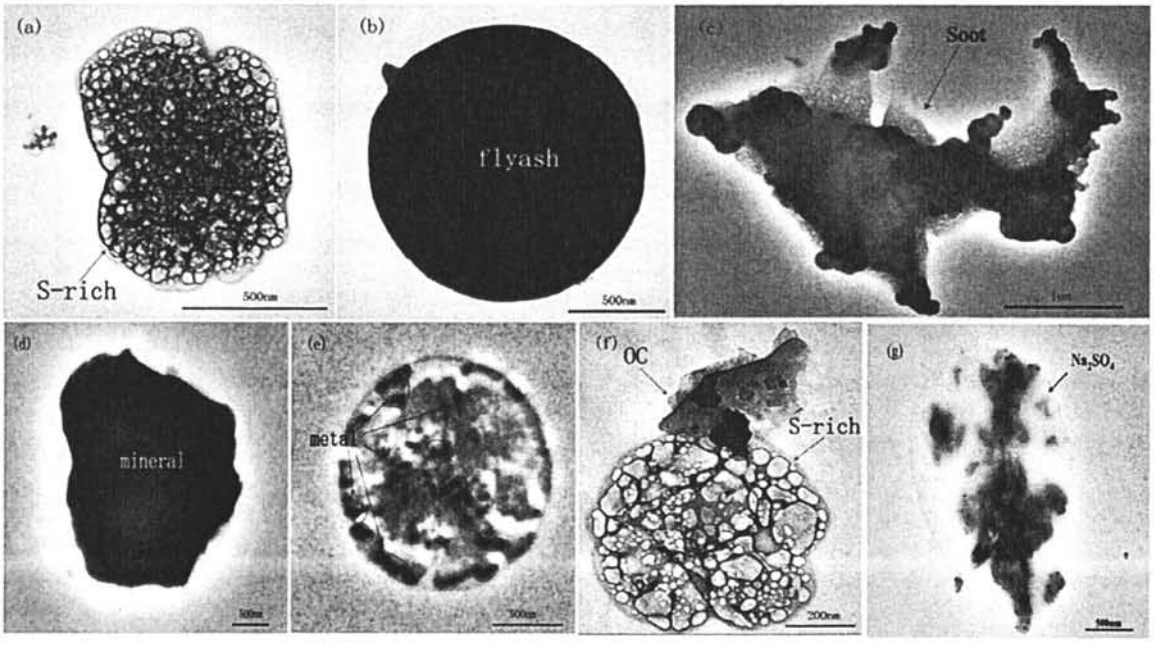

Fig. 2. TEM images of individual particles. a) S-rich, b) fly ash, c) soot particle coated by S-rich, d) mineral particle, e) metal particle, f) S-rich-OC, and g) Na_2SO_4.

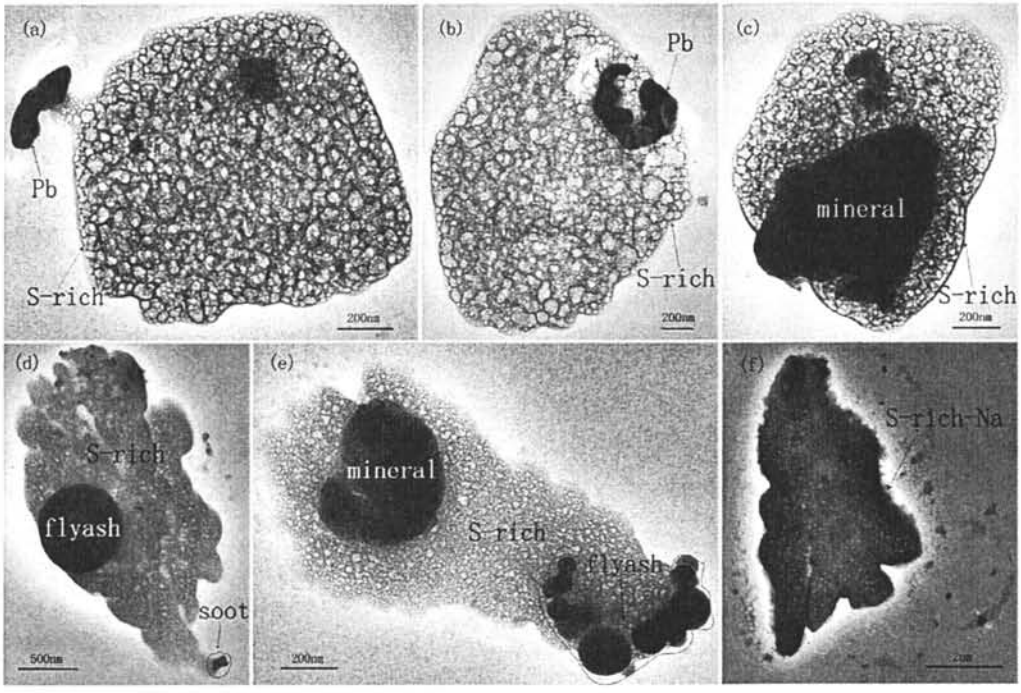

Fig. 3. The mixture of S-rich particles: a) S-rich-Pb (externally mixed), b) S-rich-Pb (internally mixed), c) S-rich-mineral, d) S-rich-fly ash-soot, e) S-rich-mineral-fly ash, and f) S-rich-Na.

HF days than those on clear days. However, Na_2SO_4 particle proportion was 3 times higher on clear days than on HF days, which was consistent with the Na^+ analysis results in chapter 3.1.

3.3. Possible source regions of particulate pollutants

The three-day backward trajectories and gaseous pollutant concentrations corresponding to individual particle sampling durations showed that these air masses arriving at the YRD had been transported from the polluted source areas into the background area on HF days (Fig. 5). These trajectories were generally sorted into two types: 1) marine air masses (e.g., 7/12–13 and 7/14) and 2) continental air masses in Shandong province (e.g., 7/5, 7/7, 7/11, 7/16 and 7/17). In Section 3.4 the blue and green lines represent two distinct cases: air masses on clear days from clean marine, and air masses on HF days from polluted areas in Hebei and Shandong provinces. The gaseous pollutant concentrations (10.3 ppbv for SO_2, 21.3 ppbv for NO_y, and 51.9 ppbv for O_3) from the polluted areas on HF days were 1.5–6 times higher than those from the marine air masses on clear days (5.1 ppbv for SO_2, 4.3 ppbv for NO_y, and 37.0 ppbv for

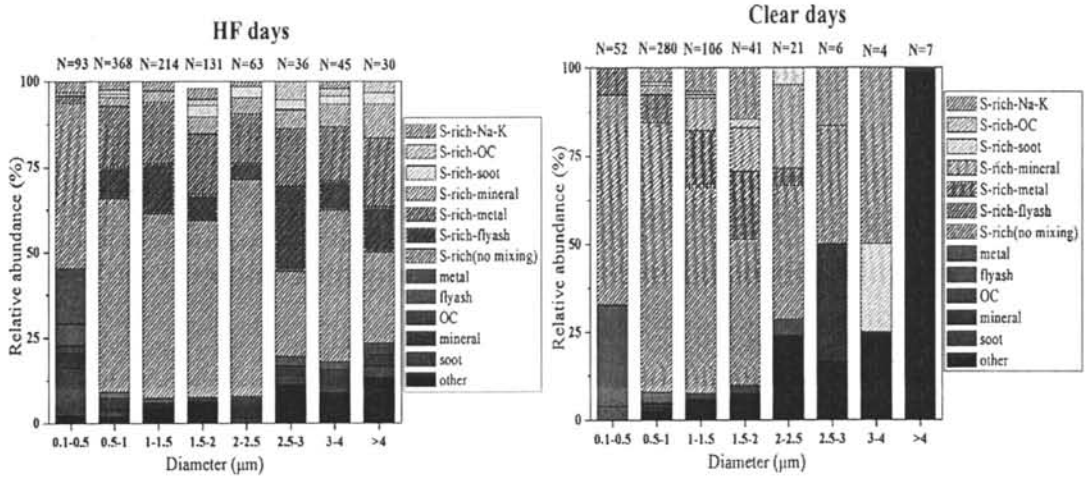

Fig. 4. Proportions of different aerosol particle types in different size ranges on HF and clear days. Other includes Na-rich particles besides the six major types.

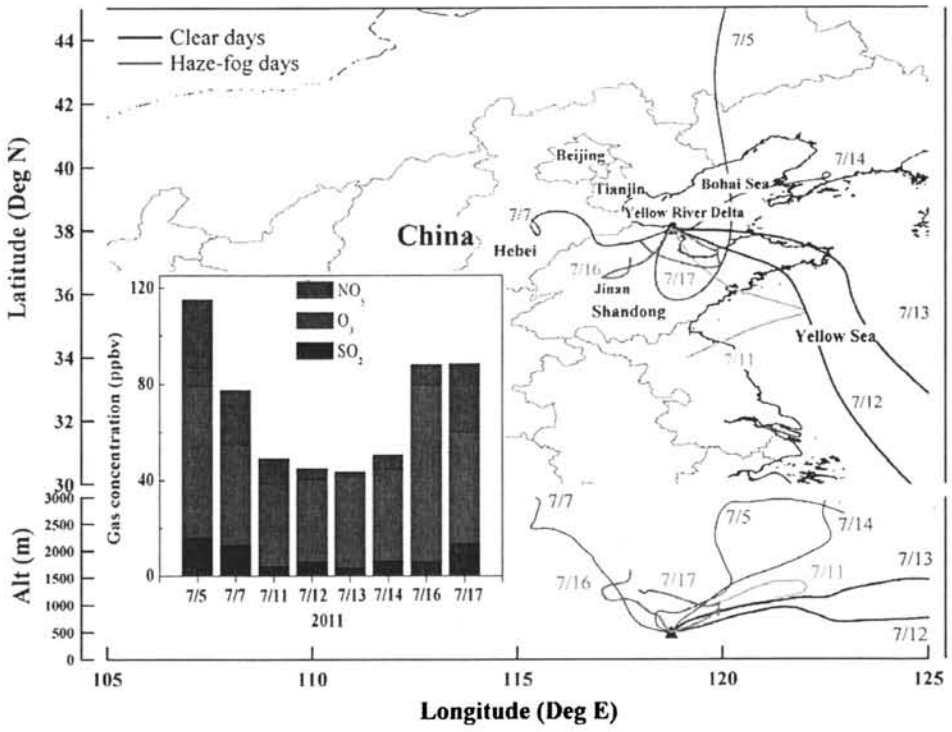

Fig. 5. 72-h backward trajectories in the individual particle sampling period and SO_2, NO_y, and O_3 concentrations on these days. The 72-h backward trajectories were calculated to identify the air mass transport paths before arriving at the Yellow River Delta.

O_3) (Fig. 5). Air quality on HF days was influenced by air masses passing through several heavily polluted areas: northern Hebei and western Shandong provinces, where significant amounts of heavy industrial activities, coal-fired power plant, and cities cluster are located (Zhang et al., 2012). As the results in chapter 3.2, S-rich/fly ash and S-rich/metal particles from the continental air masses accounted for about 10 and 1.5 times higher than those in marine air masses. These results indicate that coal-fired power plants and heavy industrial emissions from the polluted area significantly influenced downwind background area on HF days because abundant nano-sized metal and fly ash particles are good tracer of coal-fired plants and heavy industries (Li et al, 2011b). The air masses that originated in the Yellow Sea on clear days brought abundant sodium salts to the YRD and this contributed to the higher Na^+ concentrations and higher proportion of Na-rich particles on clear days.

3.4. Cases study during HF and clear days

3.4.1. Hourly variations of the major ions and gaseous pollutants on HF and clear day

We compared the physico-chemical properties of aerosols on typical clear days (case 1: 7/12 0:00– 7/13 23:00) and HF days (case 2: 7/15 21:00–7/17 23:00) in the YRD. Fig. 6 shows the hourly variation of major water soluble inorganic ions (SO_4^{2-}, NO_3^-, and NH_4^+), gaseous pollutants (SO_2, NO_y, and O_3), particle number size concentrations, visibility, and meteorology (e.g., temperature and RH) in these two episodes. The visibility was below 10 km starting at 7/16 0:00 and ending at 7/17 14:00 with an average of 7.6 km in the HF episode. Concentrations of sulfate, nitrate, and ammonium were 23.1 μg/m^3, 10.1 μg/m^3, and 10.6 μg/m^3 on HF days, about 4 times higher than those on clear days (5.2 μg/m^3, 1.5 μg/m^3, and 2.1 μg/m^3, respectively). SO_4^{2-} can be either produced from the gas-phase reaction of SO_2 with OH radicals (Seinfeld, 1986), or from heterogeneous or aqueous reaction (H_2O_2/O_3 oxidation or metal catalyzed oxidation) (Dlugi et al., 1981; Wang et al., 2012). The gas-phase reaction between SO_2 and OH radical is influenced strongly by temperature (Seinfeld, 1986) and the temperature was close on HF days and clear days, indicating that heterogeneous reactions was the major factor for the sulfate formation under different weather. The correlation coefficient between O_3 and SO_4^{2-} concentration was 0.75 on clear days and 0.35 on HF days, indicating that the ozone played more important role in heterogeneous reactions for the sulfate formation on clear days. TEM analysis suggested that abundant metal particles were internally mixed with secondary sulfates on HF days (Fig. 4) which totally become liquid phase under RH at 81.9% in the ambient air (Li et al., 2014). The metal-catalyzed oxidation in the aqueous reactions could be a more important factor for the sulfate formation and ozone depletion on HF days. The similar phenomenon has been observed in polluted urban city in North China Plain (Li et al., 2011b).

Fig. 6 shows the temporal variation of the particle number concentrations in different size ranges. The particle number concentrations in nucleation mode (5–20 nm), Aitken mode (20–100 nm), accumulation mode (100–1000 nm) and coarse mode (1–10 μm) were 2392 cm^{-3}, 5112 cm^{-3}, 2595 cm^{-3}, and 19 cm^{-3} on HF days, while those were 2918 cm^{-3}, 9140 cm^{-3}, 1422 cm^{-3}, and 1 cm^{-3} on clear days, respectively. The accumulation mode particles on HF days comprised a higher percentage (26%) of the total particle number concentrations

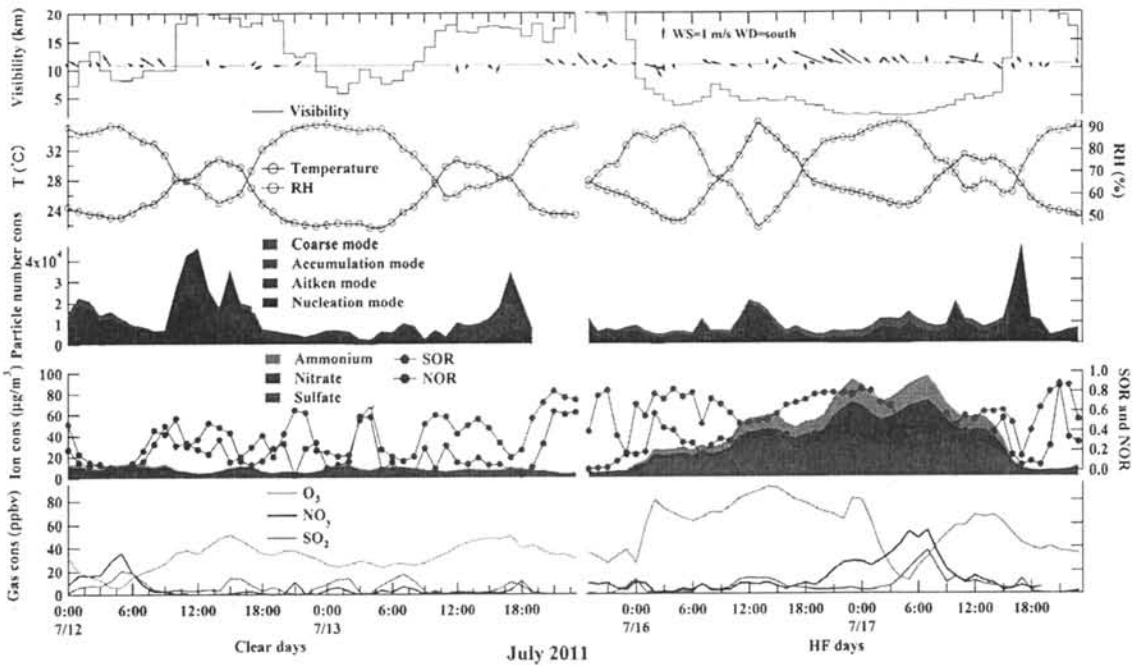

Fig. 6. Temporal variations of gaseous pollutants (SO_2, O_3, NO_y), major ions (SO_4^{2-}, NH_4^+, and NO_3^-), SOR, NOR, particle number size concentrations, temperature, wind speed (WS), wind direction (WD), RH and visibility on clear days (7/12 0:00–7/13 23:00) and HF days (7/15 19:00–7/17 23:00).

(5–10,000 nm) than that on clear days (11%), suggesting that the stable weather condition on HF days was favorable to accumulation mode aerosols through collision and coagulation of Aitken mode particles (Gao et al., 2009; Kang et al., 2013). Nucleation mode particles increased at 12:00 on both clear and HF days, which may be ascribed to the higher temperatures and to the stronger solar radiation, both of which favor photochemical production and homogeneous nucleation of particles. A new particle formation (NPF) process was found at noon of 7/16, when the ultrafine particle number concentrations began to significantly increase at 12:00 and grew up until to 14:30 at a rate of 21 nm/h (Fig. 7). This unusually high growth rate indicated that sufficiently condensable vapors over the YRD region on HF days favored fast growth of the newly formed particles. As shown in Fig. 6, the SO_4^{2-} concentration on NPF process increased with a burst of nucleation mode particles, which suggests that intense photo-chemical activities coincided with this process and the homogeneous nucleation of sulphuric acid and water may be an important factor contributing to the high number concentrations of the nucleation mode particles. The aged air mass with larger particles transported from the polluted area lead to the burst of Aitken mode particles (Fig. 7), which caused the geometric mean diameters to grow further still after 14:30. This observation is consistent with the individual particle analysis in the Section 3.3.

3.4.2. S-rich particles on HF and clear days

As shown in Section 3.2, S-rich particles were the most abundant particles in this study. Size distributions of S-rich particles ranged from 0.4 μm to 7 μm with a median diameter of 1.1 μm on HF days and ranged from 0.1 μm to 4 μm with a median diameter of 0.8 μm on clear days. Both cases displayed a unimodal pattern with a peak at 1 μm (Fig. 8), indicating that these particles were secondary aerosol particles. The high mixing of S-rich particles might be due to the slow air mass transport (as shown in Section 3.3), which would have given the sulfate particles sufficient time to mix strongly with other aerosols after chemical reactions or physical processes. Due to the sulfate formation and the predominance of S-rich particles, the internally mixed particles can completely change hygroscopic properties of hydrophobic soot, fly ash, and metal particles (Zuberi et al., 2005), and had different optical properties (Pan et al., 2009). These physical characteristics could directly and indirectly affect climate and visibility on HF days and can cause adverse effects to human health (Li et al., 2011a; Ramanathan and Carmichael, 2008). Moreover, the internal mixing of S-rich particles probably enlarged particle size and contributed to the particle growth process on HF days in the YRD.

4. Conclusions

The average daily $PM_{2.5}$ mass concentration of the YRD was 52 μg/m³. HF pollution occurred half the time and the average daily $PM_{2.5}$ mass concentration on HF days was 70 μg/m³. SO_4^{2-}, NO_3^-, and NH_4^+ were the major water soluble ions in $PM_{2.5}$, accounting for an average of 57.6% of $PM_{2.5}$ mass concentration on HF days. SO_2 and NO_x were highly oxidized into sulfates and nitrates on HF days due to high SOR and NOR and the metal-catalyzed oxidation in the aqueous reactions was considered as

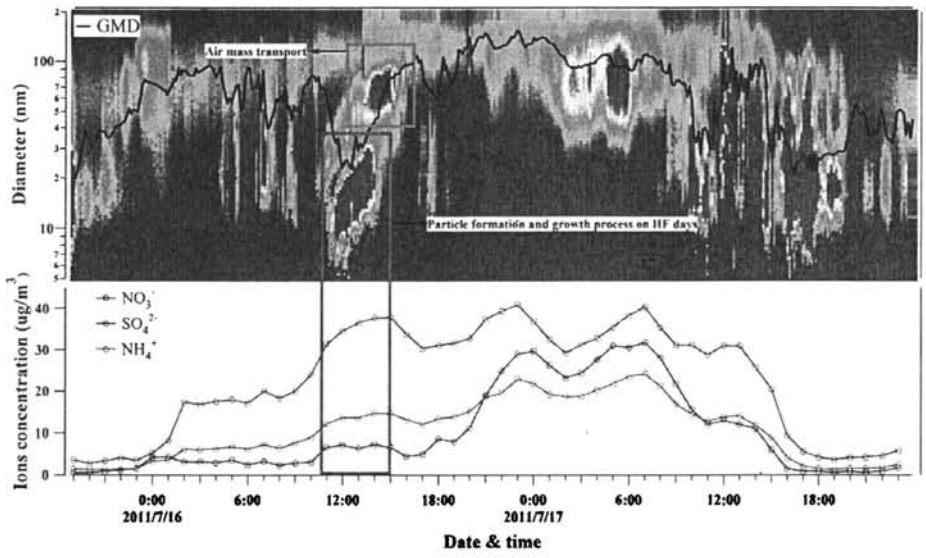

Fig. 7. Particle formation and growth process on 16 July and the major water soluble ions concentrations on 16 and 17 July of 2011.

an important factor for the sulfate formation on humid HF days. Water-soluble ions were a significant attribution to the visibility impairment. The accumulation mode particles displayed a higher percentage (26%) of the total particle number concentrations (5–10,000 nm) on HF days than that (11%) on clear days. The aerosol aged significantly on HF days due to highly mixing state of S-rich particles compared to clear days. Backward trajectory analysis showed that the HF pollution in the YRD originated from some polluted areas (Hebei and Shandong province) and the coal-fired and heavy industry emissions significantly influenced the downwind background area on HF days. New particle formation and growth event and long-range transport internally mixed particles from polluted continental air together contributed to HF formation in the background YRD region.

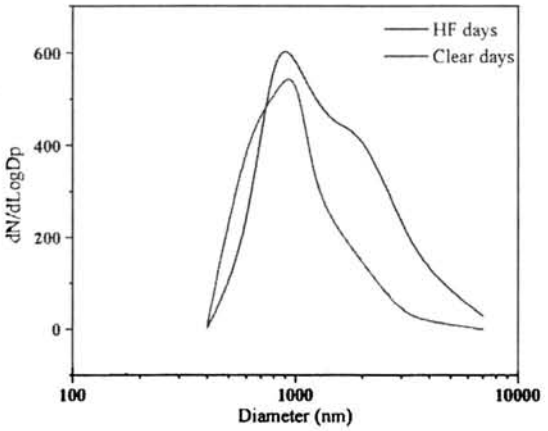

Fig. 8. Number size distribution of S-rich particles during HF days and clear days in YRD.

Acknowledgments

We appreciated Peter Hyde's proofreading. This work was funded by the Shandong Provincial Science Fund for Distinguished Young Scholars (JQ201413), the National Basic Research Program of China (2011CB403401), the National Natural Science Foundation of China (41311140168 and 21307074), the Special Research for Public-Beneficial Environment Protection (201009001-1), and Fundamental Research Funds of Shandong University (2014QY001-02).

References

Che, H., Zhang, X., Li, Y., Zhou, Z., Qu, J., Hao, X., 2009. Haze trends over the capital cities of 31 provinces in China, 1981–2005. Theor. Appl. Climatol. 97 (3), 235–242.

Dlugi, R., Jordan, S., Lindemann, E., 1981. The heterogeneous formation of sulfate aerosols in the atmosphere. J. Aerosol Sci. 12, 185–197.

Draxler, R., Rolph, G., 2003. HYSPLIT (HYbrid Single-Particle Lagrangian Integrated Trajectory) model access via NOAA ARL READY. website (http://www.arl.noaa.gov/ready/hysplit4.html). NOAA Air Resources Laboratory, Silver Spring, Md.

Du, H., Kong, L., Cheng, T., Chen, J., Du, J., Li, L., Xia, X., Leng, C., Huang, G., 2011. Insights into summertime haze pollution events over Shanghai based on online water-soluble ionic composition of aerosols. Atmos. Environ. 45, 5131–5137.

Gao, J., Wang, T., Zhou, X., Wu, W., Wang, W., 2009. Measurement of aerosol number size distributions in the Yangtze River delta in China: formation and growth of particles under polluted conditions. Atmos. Environ. 43, 829–836.

Gao, X., Yang, L., Cheng, S., Gao, R., Zhou, Y., Xue, L., Shou, Y., Wang, J., Wang, X., Nie, W., 2011. Semi-continuous measurement of water-soluble ions in $PM_{2.5}$ in Jinan, China: temporal variations and source apportionments. Atmos. Environ. 45, 6048–6056.

Han, S., Wu, J., Zhang, Y., Cai, Z., Feng, Y., Yao, Q., Li, X., Liu, Y., Zhang, M., 2014. Characteristics and formation mechanism of a winter haze-fog episode in Tianjin, China. Atmos. Res. 98, 323–330.

Huang, W., Cao, J., Tao, Y., Dai, L., Lu, S., Hou, B., Wang, Z., Zhu, T., 2012. Seasonal variation of chemical species associated with short-term mortality effects of PM2.5 in Xi'an, a central city in China. Am. J. Epidemiol. http://dx.doi.org/10.1093/aje/kwr1342.

Jaffe, D., Anderson, T., Covert, D., Kotchenruther, R., Trost, B., Danielson, J., Simpson, W., Berntsen, T., Karlsdottir, S., Blake, D., Harris, J., Carmichael, G.,

Uno, I., 1999. Transport of Asian air pollution to North America. Geophys. Res. Lett. 26, 711–714.
Ji, D., Li, L., Wang, Y., Zhang, J., Cheng, M., Sun, Y., Liu, Z., Wang, L., Tang, G., Hu, B., Chao, N., Wen, T., Miao, H., 2014. The heaviest particulate air-pollution episodes occurred in northern China in January, 2013: insights gained from observation. Atmos. Environ. 92, 546–556.
Kahn, R., et al., 2004. Environmental snapshots from ACE-Asia. J. Geophys. Res. 109, D19S14. http://dx.doi.org/10.1029/2003JD004339.
Kang, H., Zhu, B., Su, J., Wang, H., Zhang, Q., Wang, F., 2013. Analysis of a long-lasting haze episode in Nanjing, China. Atmos. Res. 120–121, 78–87.
Kim, Y.J., Kim, K.W., Kim, S.D., Lee, B.K., Han, J.S., 2006. Fine particulate matter characteristics and its impact on visibility impairment at two urban sites in Korea: Seoul and Incheon. Atmos. Environ. 40, 593–605.
Li, W., Shao, L., 2009. Transmission electron microscopy study of aerosol particles from the brown hazes in northern China. J. Geophys. Res. 114. http://dx.doi.org/10.1029/2008JD011285.
Li, W., Shao, L., 2010. Mixing and water-soluble characteristics of particulate organic compounds in individual urban aerosol particles. J. Geophys. Res. 115. http://dx.doi.org/10.1029/2009JD012575.
Li, W., Zhang, D., Shao, L., Wang, W., 2011a. Individual particle analysis of aerosols collected under haze and non-haze conditions at a high-elevation mountain site in the North China plain. Atmos. Chem. Phys. 11, 11733–11744.
Li, W., Zhou, S., Wang, X., Xu, Z., Yuan, C., Yu, Y., Zhang, Q., Wang, W., 2011b. Integrated evaluation of aerosols from regional brown hazes over northern China in winter: concentrations, sources, transformation, and mixing states. J. Geophys. Res. 116. http://dx.doi.org/10.1029/2010JD015099.
Li, W., Shi, Z., Yan, C., Yang, L., Dong, C., Wang, W., 2013a. Individual metal-bearing particles in a regional haze caused by firecracker and firework emissions. Sci. Total Environ. 443, 464–469.
Li, W., Wang, T., Zhou, S., Lee, S., Huang, Y., Gao, Y., Wang, W., 2013b. Microscopic observation of metal-containing particles from Chinese continental outflow observed from a non-industrial site. Environ. Sci. Technol. 47, 9124–9131.
Li, W., Shao, L., Shi, Z., Chen, J., Yang, L., Yuan, Q., Yan, C., Zhang, X., Wang, Y., Sun, J., Zhang, Y., Shen, X., Wang, Z., Wang, W., 2014. Mixing state and hygroscopicity of dust and haze particles before leaving Asian continent. J. Geophys. Res. 119. http://dx.doi.org/10.1002/2013JD021003.
Liu, X., Li, J., Qu, Y., Han, T., Hou, L., Gu, J., Chen, C., Yang, Y., Liu, X., Yang, T., Zhang, Y., Tian, H., Hu, M., 2013. Formation and evolution mechanism of regional haze: a case study in the megacity Beijing, China. Atmos. Chem. Phys. 13, 4501–4514.
Ma, J., Chen, Y., Wang, W., Yan, P., Liu, H., Yang, S., Hu, Z., Lelieveld, J., 2010. Strong air pollution causes widespread haze-clouds over China. J. Geophys. Res. 115 (D18). http://dx.doi.org/10.1029/2009JD013065.
Metzger, S., Lelieveld, J., 2007. Reformulating atmospheric aerosol thermodynamics and hygroscopic growth into fog, haze and clouds. Atmos. Chem. Phys. 7, 3163–3193.
Pan, X., Yan, P., Tang, J., Ma, J., Wang, Z., Gbaguidi, A., Sun, Y., 2009. Observational study of influence of aerosol hygroscopic growth on scattering coefficient over rural area near Beijing mega-city. Atmos. Chem. Phys. 9, 7519–7530.
Posfai, M., Buseck, P.R., 2010. Nature and climate effects of individual tropospheric aerosol particles. Annu. Rev. Earth Planet. Sci. 38 (1), 17–43.
Quan, J., Zhang, Q., He, H., Liu, J., Huang, M., Jin, H., 2011. Analysis of the formation of fog and haze in North China Plain (NCP). Atmos. Chem. Phys. 11, 8205–8214.
Ramanathan, V., Carmichael, G., 2008. Global and regional climate changes due to black carbon. Nat. Geosci. 1, 221–227.
Seinfeld, J.H., 1986. Atmospheric Chemistry and Physics of Air Pollution.
Sun, Y., Zhuang, G., Tang, A., Wang, Y., An, Z., 2006. Chemical characteristics of $PM_{2.5}$ and PM_{10} in haze-fog episodes in Beijing. Environ. Sci. Technol. 40, 3148–3155.
Tao, M., Chen, L., Su, L., Tao, J., 2012. Satellite observation of regional haze pollution over the North China Plain. J. Geophys. Res. 117 (D12) D12203.
Ueda, S., Osada, K., Okada, K., 2011. Mixing states of cloud interstitial particles between water-soluble and insoluble materials at Mt. Tateyama, Japan: effects of meteorological conditions. Atmos. Res. 99 (2), 325–336.
van Donkelaar, A., Martin, R.V., Brauer, M., Kahn, R., Levy, R., Verduzco, C., Villeneuve, P.J., 2010. Global estimates of ambient fine particulate matter concentrations from satellite-based aerosol optical depth: development and application. Environ. Health Perspect. 118 (6), 847–855.
Wang, T., Cheung, V.T.F., Anson, M., Li, Y.S., 2001. Ozone and related gaseous pollutants in the boundary layer of eastern China: overview of the recent measurements at a rural site. Geophys. Res. Lett. 28 (12), 2373–2376.
Wang, X., Wang, W., Yang, L., Gao, X., Nie, W., Yu, Y., Xu, P., Zhou, Y., Wang, Z., 2012. The secondary formation of inorganic aerosols in the droplet mode through heterogeneous aqueous reactions under haze conditions. Atmos. Environ. 63, 68–76.
Wu, D., Wu, X., Zhu, X., 2009. Fog and Haze. China Meteorological Press.
Yang, L., Wang, D., Cheng, S., Wang, Z., Zhou, Y., Zhou, X., Wang, W., 2007. Influence of meteorological conditions and particulate matter on visual range impairment in Jinan, China. Sci. Total Environ. 383, 164–173.
Yang, L., Zhou, X., Wang, Z., Zhou, Y., Cheng, S., Xu, P., Gao, X., Nie, W., Wang, X., Wang, W., 2012. Airborne fine particulate pollution in Jinan, China: concentrations, chemical compositions and influence on visibility impairment. Atmos. Environ. 55, 506–514.
Zhang, X., Wang, Y., Niu, T., Zhang, X., Gong, S., Zhang, Y., Sun, J., 2012. Atmospheric aerosol compositions in China: spatial/temporal variability, chemical signature, regional haze distribution and comparisons with global aerosols. Atmos. Chem. Phys. 12, 779–799.
Zhang, X., Huang, Y., Zhu, W., Rao, R., 2013. Aerosol characteristics during summer haze episodes from different source regions over the coast city of North China Plain. J. Quant. Spectrosc. Radiat. Transf. 122, 180–193.
Zhao, X., Zhang, X., Xu, X., Xu, J., Meng, W., Pu, W., 2009. Seasonal and diurnal variations of ambient $PM_{2.5}$ concentration in urban and rural environments in Beijing. Atmos. Environ. 43, 2893–2900.
Zhao, P., Zhang, X., Xu, X., Zhao, X., 2011. Long-term visibility trends and characteristics in the region of Beijing, Tianjin, and Hebei, China. Atmos. Res. 101, 711–718.
Zhao, X., Zhao, P., Xu, J., Meng, W., Pu, W., Dong, F., He, D., Shi, Q., 2013. Analysis of a winter regional haze event and its formation mechanism in the North China Plain. Atmos. Chem. Phys. 13, 5685–5696.
Zuberi, B., Johnson, K.S., Aleks, G.K., Molina, L.T., Molina, M.J., Laskin, A., 2005. Hydrophilic properties of aged soot. Geophys. Res. Lett. 32. http://dx.doi.org/10.1029/2004GL021496.

Air Qual Atmos Health
DOI 10.1007/s11869-014-0293-4

Particle physical characterisation in the Yellow River Delta of Eastern China: number size distribution and new particle formation

Qi Yuan · Lingxiao Yang · Can Dong · Chao Yan · Chuanping Meng · Xiao Sui · Wenxing Wang

Received: 7 June 2014 / Accepted: 21 August 2014

Abstract Particle number concentration was measured in 2011 in the Yellow River Delta (YRD) of eastern China. The objectives were to study the number size distribution characteristics of ambient aerosols and the meteorological effects on the particle physical characterisation, in addition to investigating the new particle formation (NPF) events in the Yellow River Delta. The particle formation rates and growth rates of the newborn particles were evaluated to identify the new particle formation events. The annual median total number concentration (5–10,000 nm) was 10,349 cm^{-3}, with a maximum concentration in autumn and lowest in winter. A higher number concentration was observed for Aitken mode particles than for accumulation and nucleation mode particles. Higher temperature and lower humidity could favour the homogeneous nucleation. With increasing wind speed, the Aitken and accumulation mode particle numbers decreased obviously, and the particle sizes were reduced. Higher particle number concentrations were associated with southeast local air masses which passed from polluted area, and smaller diameter peaks were associated with northern air masses. In total, 26 new particle formation events were recorded during the 120 days of measurements, and this frequency was slightly lower than that observed in other cities in China. The mean growth and formation rates were calculated as 5.3 nm h^{-1} and 6.6 cm^{-3} s^{-1}, respectively. High SO_2 and O_3 concentrations might have contributed to the increase in nucleation mode particles in the NPF events.

Keywords Number size distribution · Wind speed · Backward trajectory · New particle formation · Yellow River Delta

Q. Yuan · L. Yang · C. Dong · C. Yan · C. Meng · X. Sui · W. Wang
Environment Research Institute, Shandong University, Jinan 250100, China

L. Yang (✉)
School of Environmental Science and Engineering, Shandong University, Jinan 250100, China
e-mail: yanglingxiao@sdu.edu.cn

W. Wang
Chinese Research Academy of Environmental Sciences, Beijing 100012, China

Published online: 04 September 2014

Introduction

In recent years, atmospheric environment and air quality have drawn increasing attention, especially aerosol particle pollution. Aerosol particles can affect human health (Ayala et al. 2012; Fann and Risley 2013; Stieb et al. 2002), visibility (Kim et al. 2006) and climate (Ramanathan et al. 2001; Stott et al. 2000), and the physical characteristics of aerosol particles play an important role in these process. Some laboratory studies have also demonstrated that for a given mass concentration, the health effects are more significant for smaller particle sizes (Wichmann and Peters 2000). In addition, the growth of nuclei from a few nanometres to optically active and efficient cloud condensation nuclei has important implications for visibility and climate (Kulmala et al. 2004).

The number size distribution is an important parameter of particle physical characterisation. New particle formation (NPF) and growth are the main sources of aerosol particles and important factors in particle size distribution (Gao et al. 2011; Kulmala et al. 2004). New particle formation events usually occur during daytime when the pre-existing particle mass concentration is low and under sunny and dry conditions (Birmili and Wiedensohler 2000). In different seasons and at different sites, new particle events have different frequencies (Dal Maso et al. 2005). New particle formation events have been detected at many different sites with different atmospheric environments (Kulmala et al. 2004): remote boreal forests (Kulmala et al. 1998) heavily populated urban sites (Mönkkönen et al. 2005), coastal boundary layers (O'Dowd

et al. 2002) and industrialized agricultural regions (Birmili et al. 2003). Consequently, it is important to advance our understanding of the formation and growth processes of new particles in the atmosphere. In China, studies on particle physical characterisation have been conducted in recent years, and the research area mainly covers the large cities of the Bohai Sea Rim (BSR), Yangtze River Delta and Pearl River Delta region (Gao et al. 2009; Leng et al. 2013; Wu et al. 2007).

China is one of the largest coal-, iron- and steel-production countries in the world. The consumption of coal and the rapid increase of motor vehicles in recent decades have led to large amounts of $PM_{2.5}$ emissions (Zhang et al. 2009). The BSR region is an area with the largest amount of pollutants and particulate matter emissions in China. The air quality in this region has worsened, and haze phenomena have occurred more frequently in recent years. The Yellow River Delta (YRD) Nature Reserve is an ecological protection zone near the Bohai Sea, and the environment here, especially the ecosystem, is intact because of the restriction of human activity. Some industrial cities in the BSR have heavy air pollution, and the local transmission may affect the air quality. Because of its positional specificity and environment sensitivity, the environment of the Yellow River Delta Nature Reserve has received great attention. Most studies on pollution have focused on the organic contamination of soil and water, such as PAHs and nitrobenzene's (He et al. 2006; Wang et al. 2011) and only rarely on aerosol and air pollution. Our group has conducted a comprehensive evaluation of aerosols, and the ionic and organic components of $PM_{2.5}$ were reported in a previous study (Yuan et al. 2014; Zhu et al. 2014). In the Yellow River Delta, the potential mechanisms and compounds participating in atmospheric NPF and growth remain unclear. Therefore, it is important to increase the data on particle number size distribution and to investigate the NPF and growth processes in this background area.

The aim of this study was to determine the long-term variation in the physical characteristics of aerosol particles in the Yellow River Delta, such as the particle number concentrations and size distributions, to investigate the meteorological and transmission effects on the particle number size distribution, to gain the particle formation rate (FR) and growth rate (GR) in NPF events for understanding the particle physical characteristics.

Experiment and method

Sampling site

The sampling site was a nature reserve management station of the Yellow River Delta in Dongying, Shandong Province (38° 03′ N, 118° 44′ E, 5 m a.s.l.), (as shown in Fig. 1). This regional background site is located in the east of the North China Plain, 10 km away from the Bohai Sea (Fig. 1). Oil exploration is an important industry of Dongying, and the Shengli Oil Field is one of the largest oil exploration bases. Measurement instruments, including a meteorological station, were set up on the roof of the station building of four floors, which is 15 m above the ground level. Continuous measurements were collected intensively in 2011, in spring (Apr 1–May 4), summer (Jul 1–Jul 31), autumn (Oct 11–Nov 7) and winter (Dec 12 of 2011–Jan 7 of 2012).

Instruments

An aerosol wide-range particle spectrometer (WPS model 1000XP, MSP Corporation, USA) was used to measure the particle number concentration. The Model 1000XP WPS is a general purpose, high-resolution aerosol spectrometer that combines the principles of differential mobility analysis, condensation particle counting and laser light scattering to measure the diameter and number concentration of aerosol particles in the 5- to 10,000-nm particle diameter range. The instrument's differential mobility analyser (DMA) and condensation particle counter (CPC) can measure aerosol size distributions in the 5- to 350-nm particle diameter range in up to 96 channels. The laser particle spectrometer (LPS) covers the 350- to 10,000-nm particle diameter range in 24 additional channels. Overall, the WPS covers three orders of magnitude of particle diameter with a single, easy-to-use, compact and energy-efficient aerosol spectrometer. The CPC has an advanced design that eliminates the traditional problems of water condensation and collection in the saturator. A dual-reservoir design ensures the condensate is collected into a separate reservoir to avoid any mixing of condensed water with the butanol in the working fluid reservoir. The CPC features rapid warm-up and response time for accurate aerosol concentration measurements.

The other instruments used for measuring SO_2 (TEI Model 43C) and O_3 (TEI, Model 49C) have been described previously (Wang et al. 2003, 2006). Meteorological data (including temperature, relative humidity (RH), wind speed, wind direction, etc.) were obtained from the meteorological station.

Methodology

Typically, the sizes of sub-micrometre particles are categorised into three modes: nucleation mode, representing quite newly formed particles, and Aitken and accumulation modes, representing aged particles. In this study, we divided the size distribution into 5–20 nm (nucleation mode), 20–100 nm (Aitken mode), and 100–1,000 nm (accumulation mode). The calculation of the growth rate and formation rate follows the method described by Kulmala et al. 2012 in

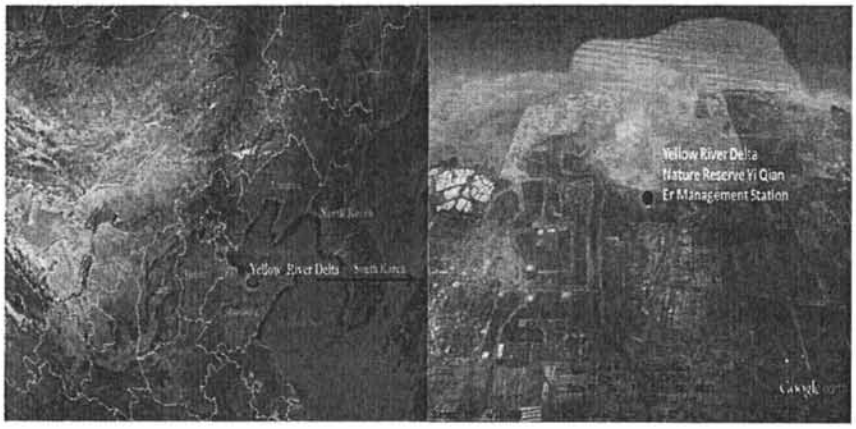

Fig. 1 Location of the sampling site in the Yellow River Delta, Shandong Province, China

Nature Protocols. The growth rate of NPF events can be expressed as follows:

$$GR = \frac{\Delta dp}{\Delta t} = \frac{dp_2 - dp_1}{t_2 - t_1} \quad (1)$$

In the equation, dp_1 and dp_2 are the representative particle geometric mean diameter (GMD) at time t_1 and t_2, respectively. For the calculation, dp_1 and dp_2 are defined as the centre of the size bin and t_1 and t_2 are the times when the concentration of this size bin reaches its maximum.

The formation rate (J_{5-20}) is represented as follows:

$$J_{5-20} = \frac{dN_{5-20}}{dt} + CoagS_{dp=13\ nm} \times N_{5-20} \times \frac{GR_{5-20} \times N_{5-20}}{15\ nm} \quad (2)$$

Where J_{5-20} is the formation rate of new particles in the range of 5 to 20 nm. The second item is the coagulation losses for the nucleated particles (5–20 nm) by large particles, and it is represented by the loss of 13-nm particles (13 nm is the geometric mean of 5–20 nm) in this study. The third item is the growth out of the considered size range.

Backward trajectories and cluster analysis

Backward trajectories and cluster analysis were applied to investigate the air mass transport effects on the particle number size distribution. In this study, the backward trajectories were run using the Hybrid Single Particle Lagrange Integrated Trajectory (HYSPLIT4) model (Draxler et al. 2003) that was developed by the National Oceanic and Atmospheric Administration (NOAA). First, 72-h backward trajectories terminating at 50 m above ground level in the YRD (38° 03′ N, 118° 44′ E) were calculated every 1 h during the sampling period. The trajectories were then clustered according to their similarity in spatial distribution using the HYSPLIT4 software. The clustering principles and processes are described in the user's guide of the software (Draxler et al. 2009).

Results and discussion

Overview of the particle number concentration

Based on the four-season continuous measurements, approximately 120 days of data were available. Table 1 shows some major parameter of particle number concentrations for different sizes: nucleation mode (5–20 nm), Aitken mode (20–100 nm) and accumulation mode (100–1,000 nm) in the four seasons. The annual average median value of the total number concentrations (TNC) for size of 5–10,000 nm was 10,349 cm^{-3} and the annual average number concentrations of 20 and 80 % percentile were 6,123 and 17,825 cm^{-3}, respectively. A higher median number concentration (6,105 cm^{-3}) was observed for Aitken mode particles than accumulation and nucleation mode particles (2,600 and 494 cm^{-3}, respectively). This might be due to oil combustion influencing the Aitken mode particles (Harris and Maricq 2001). The particle number concentration (PNC) exhibited significant seasonal variation with highest median value in autumn (14,161 cm^{-3}) and lowest in winter (7,494 cm^{-3}). The percentage of Aitken mode particles to the TNC increased from 58 % in autumn to 66 % in winter and this could be attributed to the lower boundary layer and domestic heating in winter. The particle number concentrations had significant negative correlation (R=−0.56) with wind speed, indicating that high wind speed lead to low particle concentrations.

According to the comparison with other cities home and abroad shown in Table 2, the particle number concentration in the YRD was larger than that of Lanzhou, but much lower than those in urban and rural sites of China, which is due to strongly local traffic emissions in these stations. Compared to

Table 1 Median, 20 and 80 % percentile, standard deviation (SD) of particle number concentrations in four seasons in different sizes (cm^{-3})

		Spring	Summer	Autumn	Winter	Annual average
Nucleation mode (5–20 nm)	Median	609	479	549	441	494
	20 % Percentile	69	157	198	206	152
	80 % Percentile	2,521	2,142	2,112	1,069	1,843
	SD	5,893	5,310	3,868	1,250	4,539
Aitken mode (20–100 nm)	Median	7,703	5,135	7,687	4,805	6,105
	20 % Percentile	4,669	2,593	4,344	3,188	3,600
	80 % Percentile	12,828	10,135	13,895	7,070	11,018
	SD	5,930	8,147	5,584	2,544	6,056
Accumulation mode (100–1,000 nm)	Median	3,157	2,375	3,385	1,516	2,600
	20 % percentile	1,523	937	1,758	598	990
	80 % Percentile	6,098	4,083	7,329	3,262	4,835
	SD	2,935	1,959	3,067	1,423	2,640
TNC (5–10,000 nm)	Median	12,717	9,037	14,161	7,494	10,349
	20 % Percentile	7,511	5,165	9,146	4,780	6,123
	80 % Percentile	20,909	15,951	21,139	10,657	17,825
	SD	11,143	12,591	7,758	3,753	9,951

the rural sites in Europe and USA, the measured value in the YRD was 2 to 12 times higher and this may be because the sampling site in this research was affected by transmission from the nearby industrial areas. A much higher concentration of accumulation mode particles in the YRD was observed compared with other sites. Considering that the sampling site was a regional background area, the polluted air masses from nearby industrial and urban cities had a significant impact on the accumulation mode particles in the atmosphere of the YRD. In addition, agricultural biomass burning in autumn might have influenced the accumulation mode particles (Li et al. 2007), and agricultural burning takes place more

Table 2 Comparisons of mean particle number concentrations (cm^{-3}) and GMD (nm) between this study and other studies

	Country	Types	Period	Particle size range	GMD (nm)	TNC (cm^{-3})	Reference
YRD	China	Rural/coastal	Spring	5–10,000	67	15,488	This work
			Summer		80	12,510	
			Autumn		71	15,516	
			winter		67	7,966	
			Annual average		69	12,838	
Jinan		Urban	2,008	10–500		15,700	(Xu et al. 2011)
Lanzhou		Urban	Summer 2006	10–500		8,514	(Gao et al. 2011)
Beijing		Urban	2004–2006	3–10,000		32,800	(Wu et al. 2008)
Taicang		Urban	Summer 2005	10–500		29,990	(Gao et al. 2009)
Guangzhou		Urban	Jul. 2006	20–10,000		29,000	(Yue et al. 2013)
Backgarden of PRD		Rural		20–10,000		17,000	
Xinken		Rural	Oct. 2004	3–10,000		16,000	(Liu et al. 2008)
Pittsburgh	USA	Rural	Jul. 2001–Jul. 2002	3–500	40	22,000	(Stanier et al. 2004)
Barcelona	Spain	Urban	2009	5–1,000		16,847	(Reche et al. 2011)
London urban site	UK	Urban	2008–2010	19–600	45	6,680	(Bismarck-Osten et al. 2013)
London rural site		Rural		19–600	50	3,393	
Helsinki rural site	Finland	Rural		3.4–1,000	78	1,731	
Aspvreten	Sweden	Rural		30–500		1,631	(Asmi et al. 2011)
Mace head	Ireland	Rural		30–500		889	

frequently in fields in Hebei and Shandong provinces close to the YRD in the harvesting seasons with the accompanying production of larger aerosol particles. The pollutants coming from those processes might have been transported to our monitoring site during the sampling period.

Diurnal variations of particle number size distributions

The diurnal variations of the particle number concentrations of different particle modes were investigated during NPF events and non-NPF events. During NPF events, the nucleation modes of particles all displayed a unimodel pattern of particle number size distribution in four seasons. An increase of nucleation mode particles all began at approximately 07:00 a.m. and lasted several hours to noon, which were the result of new particle formation. The peak of nucleation mode particle exhibited the highest number of concentration in spring and the lowest value in winter. However, no significant variation of nucleation mode particle occurred in non-NPF days, leading to much lower number concentrations of nucleated particles in non-NPF days compared to those in NPF events. Due to the nucleated particles growing to larger sizes, the number of the Aitken mode particles also increased by lagging some hours. The diurnal pattern of the accumulation mode particles was possibly affected by transport from the surrounding areas, and the variation was relatively small. The particle number concentrations decreasing in the late afternoon mainly results from the rising of boundary layer height.

During the NPF events, the morning peak of nucleation mode particles coincides with the rise of temperature and polluted gases of SO_2 (as shown in Fig. 2). This finding suggests that higher temperature and lower humidity could favour the homogeneous nucleation of sulphuric acid and water, which may be an important factor contributing to the high number concentrations of the nucleation mode particles (Bismarck-Osten et al. 2013; Gómez-Moreno et al. 2011). The Aitken mode peak tracked well with the O_3 concentration peak, suggesting that the condensational growth of nucleated particles contributed to this peak.

The effects of wind direction and speed on particle number concentration

To understand the function of wind direction on the particle number concentration, we combined total particle number concentration (TNC) with wind direction in a rose plot. Figure 3 shows the wind direction frequency and the mean TNC. During the sampling period, most frequent winds were from the southeast (115–155 °) and northwest (315–355 °), accounting for approximately 28 % of the wind direction; however, when wind blew from the south (135–225 °), higher particle number concentrations (13,965 cm^{-3}) were measured and the maximum concentration (104,907 cm^{-3}) occurred at 176 °. It indicated that south wind correlated with high particle number concentration and this might be due to higher anthropogenic emissions from south of the sampling sites, where the urban area is.

Wind speed (WS) also can affect the particle number concentrations and size distributions (Agus et al. 2007). To analyse the influence of wind speed on the particle size distribution, three conditions were chosen to determine the size distribution variation: (a) wind speed lower than 2 m s^{-1}, (b) wind speed between 2 and 4 m s^{-1} and (c) wind speed higher than 4 m s^{-1} (plots in Fig. 4). Figure 4 shows that as the wind velocity increased, the total particle number concentrations increased, varying from 12,434 cm^{-3} (WS≤2 m s^{-1}) and 13,880 cm^{-3} (4 m s^{-1}>WS>2 m s^{-1}) to 16,949 cm^{-3} (WS≥ 4 m s^{-1}). The number concentration of the nucleation mode particles increased significantly with increasing wind speed. This might be due to the dry and pristine atmospheric conditions under high wind speeds, and new particle formation events could occur to increase the nucleation mode particle number concentration in these conditions (Robinson et al. 2007). The Aitken and accumulation mode particle number concentrations decreased obviously with increasing wind speed, and the possible reason for this number concentration reduction is that the higher wind speeds favoured the dilution and dispersion of the larger particles (Bismarck-Osten et al. 2013). Under different wind speeds, the particle size distribution was also different. When the wind speed was lower than 2 m s^{-1}, the peak of the size distribution in dN/dLogDp occurred at 50 nm. This peak drifted to a smaller diameter (15 nm) with increasing wind speed (above 4 m s^{-1}). The explanation for this phenomenon is that high concentrations of the accumulation mode particles under low wind speed conditions prevented nucleation, and the nucleated particles were scavenged by strong coagulation.

Relation of particle number size distributions with air mass history

A total of 2,402 backward trajectories were work out and a *K*-means cluster approach was then used to classify the trajectories into several different clusters (Salvador et al. 2010). As shown in Fig. 5, the trajectories in spring, autumn and winter can be classified into two main categories, whereas there were three categories in summer based on their origins, paths and latitudes. The air masses generally came from the north, passing through Inner Mongolia, Hebei and Bohai Sea at a high altitude or from local Shandong and the adjacent areas in low altitude before arriving at the YRD in the spring, autumn and winter. In the spring and winter, the northern airflows accounted for 53 and 68 %, respectively, of the total trajectories, and the proportion of northern airflows decreased to 22 % in the autumn, whereas in the summer, 41 % of the air masses came from the south (cluster 2), 36 % of the air masses came

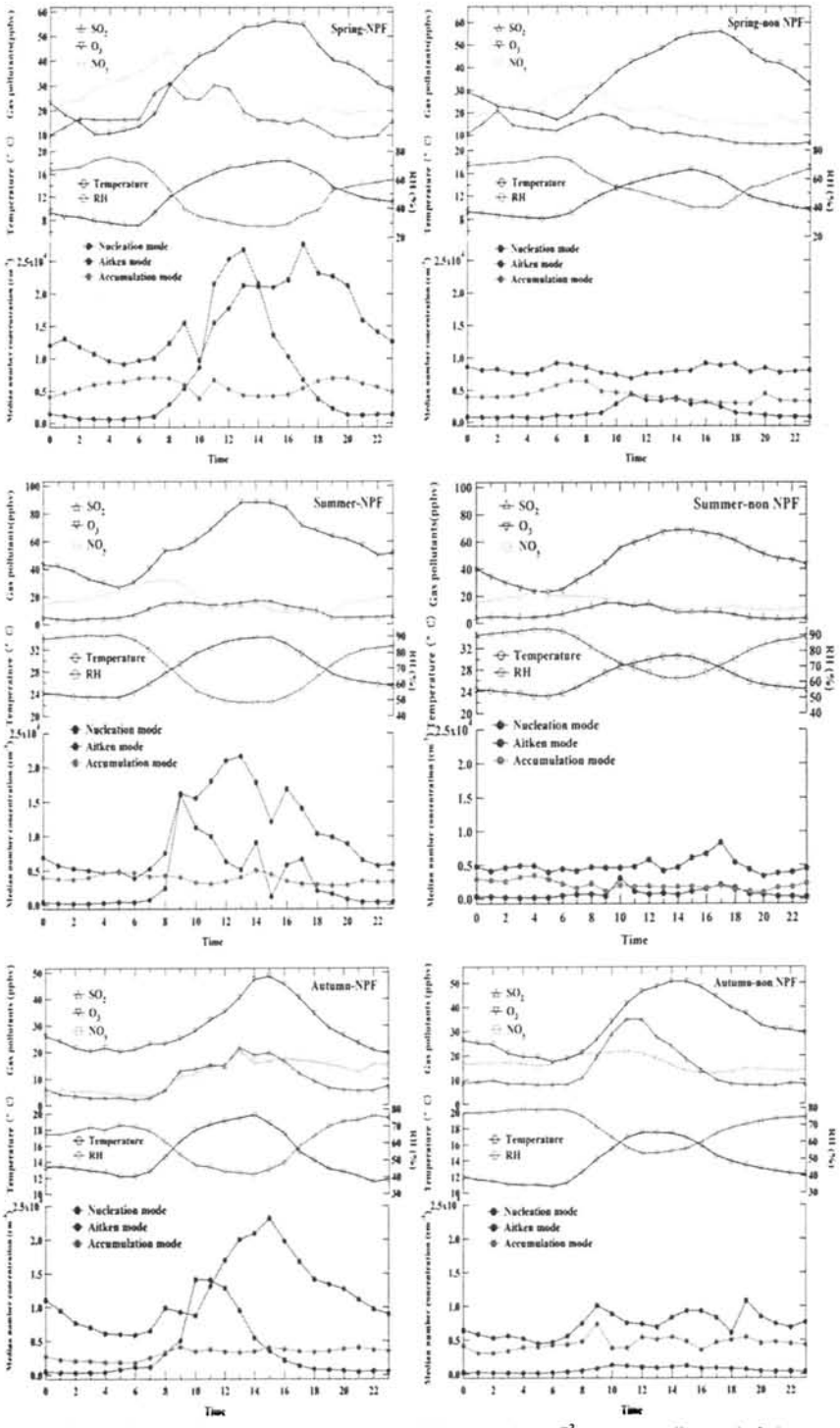

Fig. 2 Diurnal variations of the median particle number concentrations in different mode (cm^{-3}), gaseous pollutants (ppbv), temperature (°C) and RH (%) in NPF events and non-NPF events of four seasons

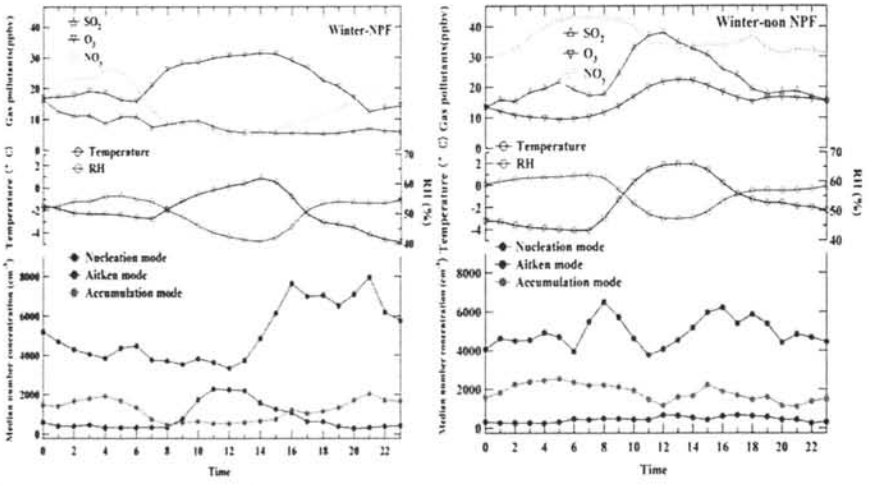

Fig. 2 (continued)

from the east passing the ocean (cluster 3), and only 23 % came from the northwest, passing through Beijing and Tianjin (cluster 1).

As shown in Table 3, air masses from the southern and eastern short distance transport contributed higher particle number concentration (average of being 14,903 cm^{-3}) than those from the northern long-distance transport (cluster 1 in spring, autumn and winter) (average of being 11,462 cm^{-3}). The Aitken mode particles had higher number concentrations than the other two mode particles in all of the trajectories during the sampling period. The particle number size distributions were all unimodal for the northern long-distance air masses with a Aitken mode peak (45 nm of cluster 1 in spring, 30 nm of cluster 1 in autumn and 50 nm of cluster 1 in winter). The particle number size distribution of short distance air masses from the south and east had a shift to the larger size,

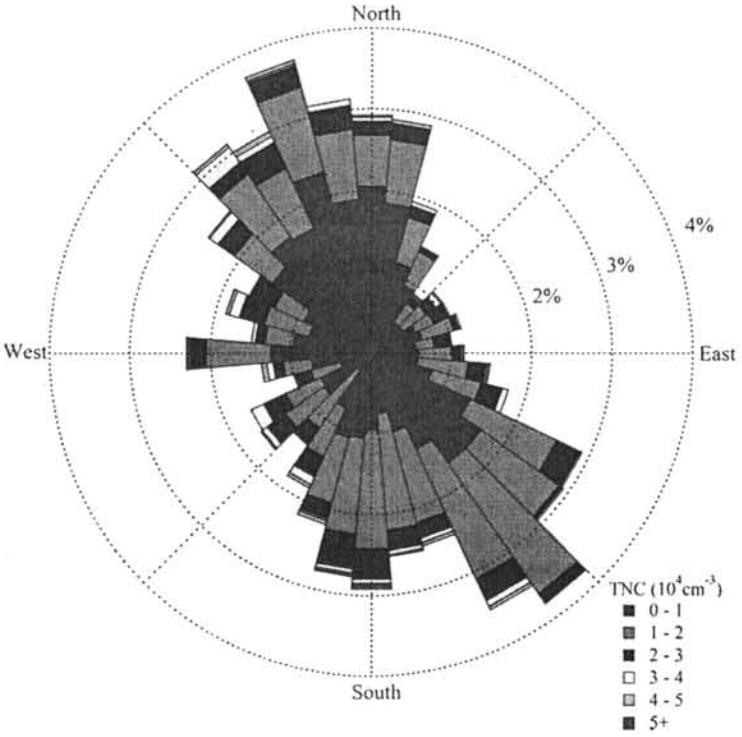

Fig. 3 Total particle number concentrations in the YRD as a function of wind direction, frequency plot. Each *bar* of the frequency plot represents 10 °. The *magnitude of the bars* shows the wind direction frequency, and the *colour of the bars* shows the intensity of TNC for a given wind direction (1-h means)

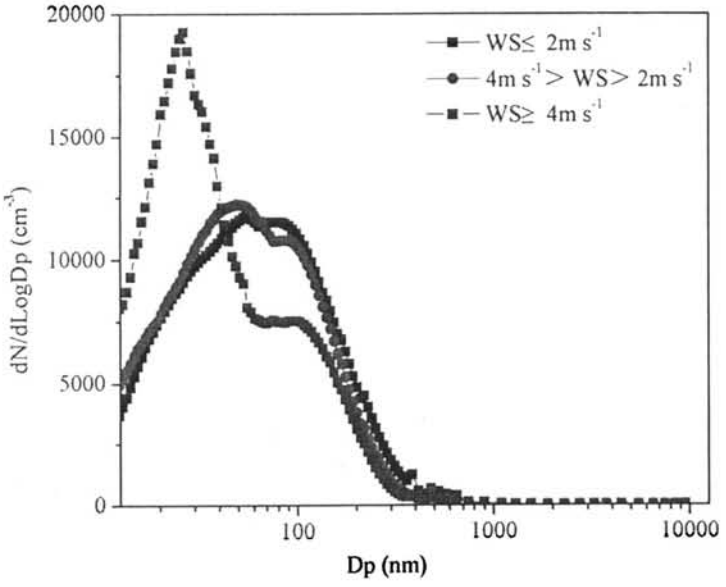

Fig. 4 Mean particle size distributions measured during different wind speeds

and the peak was observed near 100 nm. These local air masses passed through some developing cities (e.g. Weifang and Yantai) with a large number of new buildings and construction projects, leading to building dust emission into the environment air, which brought more coarse particles to the YRD. In addition, these air masses moved slowly and spent much more time over the fast-developing regions in the south and east. The regional transport combined with further growth by condensation may have resulted in the high number concentrations of the accumulation mode particles.

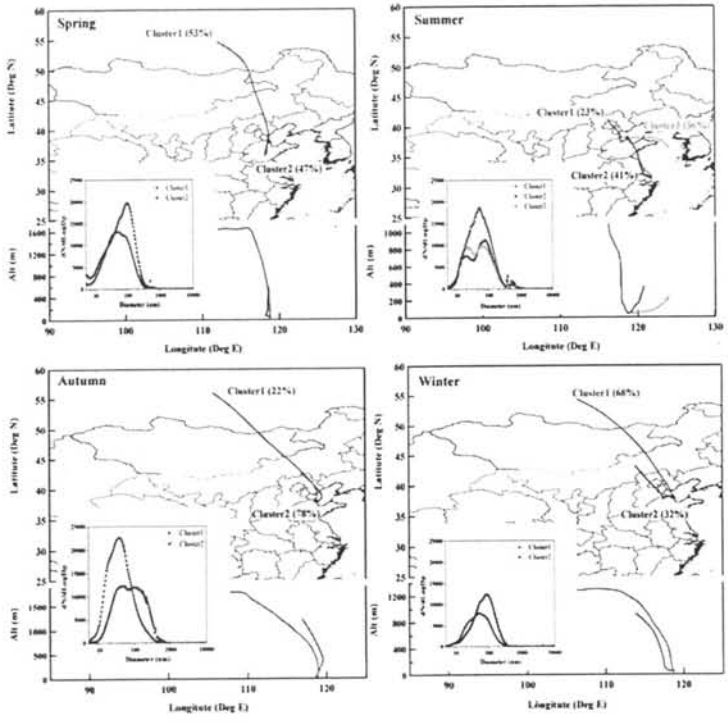

Fig. 5 Backward air mass trajectories of four clusters and the particle number size distribution corresponding to the clusters

Table 3 Mean particle number concentrations in different backward trajectories clusters in the four seasons (cm^{-3})

	Cluster	Nucleation mode	Aitken mode	Accumulation mode	TNC
Spring	1	1,965	8,377	2,588	12,934
	2	2,853	10,050	5,370	18,278
Summer	1	2,006	6,230	2,664	10,923
	2	2,235	6,427	2,228	10,899
	3	2,535	10,915	3,272	16,732
Autumn	1	1,082	7,973	5,344	14,404
	2	4,048	12,929	2,043	19,021
Winter	1	961	4,912	1,173	7,048
	2	629	5,899	3,042	9,585

NPF events

Several previous studies have described the NPF event criteria (Gao et al. 2012; Wu et al. 2007), and, in total, 26 NPF events (accounting for 22 % of 120 days) were observed during the sampling period according to the NPF criteria. This frequency is lower than that for some other sites in China, such as Beijing (42.7 %), PRD of China (26 %) and Lanzhou (33 %) (Gao et al. 2011, 2012; Liu et al. 2008). During all of these NPF events, nucleated particles (5–20 nm) had low concentrations in the early morning and began to increase at 07:00 a.m. in spring and summer, 08:00 a.m. in autumn and 09:00 a.m. in winter. A spontaneous burst occurred before noon, and then subsequently grew into Aitken and accumulation mode particles at a rate of a few nanometres per hour until afternoon. These processes were all new particle formation events displaying a "banana shape", as presented in Fig. 6.

These NPF event parameters are shown in Table 4. The GR at YRD ranged from 2.3 to 12.7 nm h^{-1} with the annual average value being 5.3 nm h^{-1}, and the FR varied in the range of 0.3 to 31.9 cm^{-3} s^{-1} with the annual average value being 6.6 cm^{-3} s^{-1}. The formation rate was much lower than that in urban environments such as Beijing (3.3–81.4 cm^{-3} s^{-1}) (Wu et al. 2007), Akrotiri (13 cm^{-3} s^{-1}) (Kopanakis et al. 2013) and Atlanta (30–70 cm^{-3} s^{-1}) (Kulmala et al. 2004) but higher than in Guangzhou (2.4–4.0 cm^{-3} s^{-1}) (Yue et al. 2013). The GR of the July 31 and Oct 12 NPF event exceeded 10 nm h^{-1}, which was significantly larger than that of other NPF events. The most likely reason for this is the strong interplay between the nuclei growth and their loss by coagulation. The higher the coagulation sink is, the faster small nuclei must grow to survive the coagulational scavenging onto larger pre-existing particles (Kerminen et al. 2001), whereas the coagulation sink on July 31 and Oct 12 was higher than on other NPF days (6.5×10^{-4} s^{-1} and 6.3×

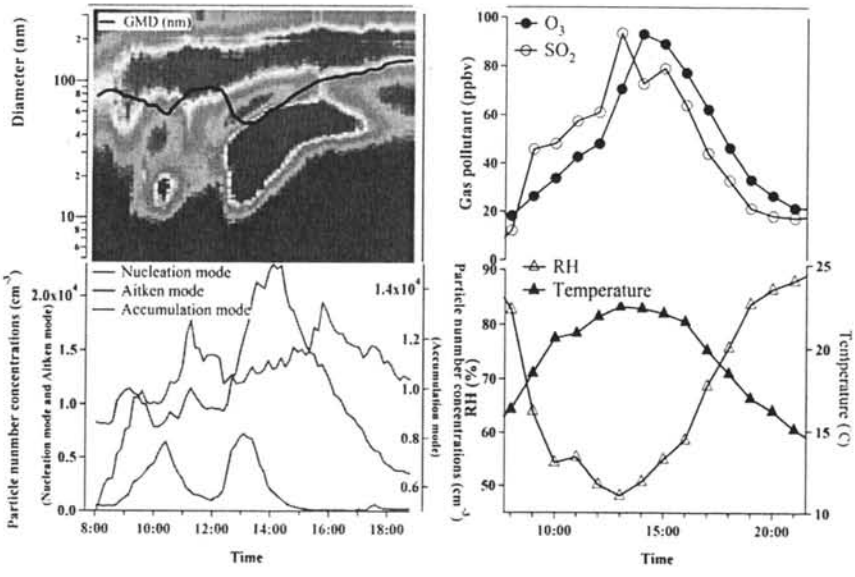

Fig. 6 Diurnal variation of particle number size distribution, GMD (geometric mean diameter, *black line*), gas pollutant concentrations, RH and temperature during a NPF event on Oct 12

Table 4 The relevant parameters of the NPF events

	Dates	Growth rate (nm h^{-1})	Formation rate (cm^{-3} s^{-1})	T (°C)	RH (%)	O_3 (ppbv)	SO_2 (ppbv)
Spring	1 Apr. 2011	2.9	3.3	5.4	52.7	47.2	2.4
	2 Apr. 2011	4.1	8.0	6.9	40.9	43.9	2.3
	4 Apr. 2011	3.7	2.4	14.7	34.7	60.9	15.7
	8 Apr. 2011	4.7	4.8	15.5	37.6	45.2	2.9
	9 Apr. 2011	5.8	17.2	18.6	22.2	39.8	25.4
	12 Apr. 2011	7.2	31.9	17.1	37.1	44.3	27.0
	20 Apr. 2011	3.1	2.6	22.1	33.4	41.6	41.2
	Average	4.5	10.0	14.3	36.9	46.1	16.7
Summer	5 Jul. 2011	9.5	22.7	30.6	51.7	86.6	18.4
	9 Jul. 2011	2.7	5.3	31.6	41.2	59.0	4.9
	14 Jul. 2011	3.2	17.6	31.4	59.2	50.3	8.0
	16 Jul. 2011	4.0	3.0	32.7	54.8	85.8	11.0
	21 Jul. 2011	7.8	3.9	30.3	70.2	37.5	19.7
	23 Jul. 2011	8.3	5.4	32.3	66.4	93.7	27.0
	31 Jul. 2011	12.7	5.2	31.9	60.0	50.4	11.6
	Average	7.7	9.0	31.5	57.6	66.2	14.4
Autumn	12 Oct 2011	10.3	4.8	20.8	57.6	55.4	59.3
	15 Oct. 2011	4.6	3.3	16.9	43.9	32.8	3.1
	16 Oct. 2011	4.6	8.1	19.4	45.6	33.5	7.2
	17 Oct. 2011	3.0	5.4	14.8	61.3	30.2	0.9
	25 Oct. 2011	3.8	6.6	12.7	42.9	25.6	5.2
	Average	5.3	5.6	16.9	50.3	35.5	15.1
	7 Nov. 2011	3.9	2.8	12.8	50.7	40.5	1.6
	Average	5.0	5.2	16.2	50.3	36.3	12.9
Winter	12 Dec. 2011	2.3	2.6	5.0	50.8	25.4	0.8
	14 Dec. 2011	2.5	0.3	0.7	49.3	27.5	7.5
	16 Dec. 2011	4.6	0.9	−3.4	47.7	27.8	4.3
	22 Dec. 2011	3.9	0.9	−0.8	44.7	28.6	5.5
	24 Dec. 2011	4.1	0.8	1.1	43.8	26.6	8.1
	4 Jan. 2012	3.4	0.7	−3.1	50.5	26.4	6.8
	Average	3.5	1.0	−0.1	47.8	27.1	5.5

10^{-4} s^{-1}). The formation rates were much lower in winter (average of 1.0 cm^{-3} s^{-1}) than in other seasons (10.0 cm^{-3} s^{-1} in spring, 9.0 cm^{-3} s^{-1} in summer and 5.2 cm^{-3} s^{-1} in autumn). This might be due to the low temperature and lower SO_2 and O_3 concentrations. The hourly average SO_2 and O_3 concentration on NPF days displayed a good correlation with nucleation mode particle number concentrations (R^2=0.41 and 0.39, respectively), which suggests that high SO_2 and O_3 concentration might contribute to the increasing of nucleation mode particles in the NPF events. As shown in Fig. 6, a significant increase of SO_2 and O_3 concentration was observed during an increase of nucleation mode particle number concentration, which also indicates that intense photo-chemical activities coincided with these events.

Conclusions

Particle number size distributions between 5 nm and 10 μm were measured in 2011 in the Yellow River Delta, China, using a wide-range particle spectrometer. The annual median total number concentration (5 nm to 10 μm) was 10,349 cm^{-3}. The Aitken mode particles had higher number concentrations, and the accumulation mode particles accounted for a larger proportion of the total surface and volume concentrations. The particle number concentration exhibited significant temporal variations, and most of the particle bursts were caused by the sharp increase of the nucleation mode particles. With increasing wind speed, the Aitken and accumulation mode particle number decreased obviously, and the particle size was reduced. Air masses from the southern and eastern short

distance transport contributed higher particle number concentrations than those from the northern long-distance transport. New particle formation events were observed on approximately 22 % of the measurement days and were generally observed under high visibility and sunny conditions. The GR in the YRD ranged from 2.3 to 12.7 nm h^{-1} with an annual average of 5.3 nm h^{-1}, and the FR varied in the range of 0.3 to 31.9 cm^{-3} s^{-1} with an annual average value of 6.6 cm^{-3} s^{-1}. High SO_2 and O_3 concentrations might have contributed to the increase of nucleation mode particles in the NPF events.

Acknowledgment This work was supported by the National Basic Research Programme (973 Programme) of China (2005CB422203), Jiangsu Collaborative Innovation Center for Climate Change, Key Project of Shandong Provincial Environmental Agency (2006045), Promotive Research Fund for Young and Middle-aged Scientists of Shandong Province (BS2010HZ010), Independent Innovation Foundation of Shandong University (2009TS024) and Special Research for Public-Beneficial Environment Protection (201009001–1). The HYSPLIT mode was provided by the NOAA Air Resources Laboratory.

References

Agus EL, Young DT, Lingard JJ, Smalley RJ, Tate JE, Goodman PS, Tomlin AS (2007) Factors influencing particle number concentrations, size distributions and modal parameters at a roof-level and roadside site in Leicester, UK. Sci Total Environ 386:65–82

Asmi A, Wiedensohler A et al (2011) Number size distributions and seasonality of submicron particles in Europe 2008–2009. Atmos Chem Phys 11:5505–5538

Ayala A, Brauer M, Mauderly JL, Samet JM (2012) Air pollutants and sources associated with health effects. Air Qual Atmos Health 5: 151–167

Birmili W, Wiedensohler A (2000) New particle formation in the continental boundary layer: meteorological and gas phase parameter influence. Geophys Res Lett 27:3325–3328

Birmili W, Berresheim H, Plass-Dülmer C, Elste T, Gilge S, Wiedensohler A, Uhrner U (2003) The Hohenpeissenberg aerosol formation experiment (HAFEX): a long-term study including size-resolved aerosol, H_2SO_4, OH, and monoterpenes measurements. Atmos Chem Phys 3:361–376

Bismarck-Osten C, Birmili W, Ketzel M, Massling A, Petäjä T, Weber S (2013) Characterization of parameters influencing the spatio-temporal variability of urban particle number size distributions in four European cities. Atmos Environ 77:415–429

Dal Maso M, Kulmala M, Riipinen I, Wagner R, Hussein T, Aalto PP, Lehtinen KE (2005) Formation and growth of fresh atmospheric aerosols: eight years of aerosol size distribution data from SMEAR II, Hyytiala, Finland. Boreal Environ Res 10:323–336

Draxler R, Rolph GD HYSPLIT (hybrid single-particle Lagrangian integrated trajectory) model access via NOAA ARL READY website. Silver Spring, MD: NOAA Air Resources Laboratory; 2003

Draxler R, Stunder B, Rolph G, Stein A, Taylor A (2009) Hysplit4 user—guide. National Oceanic and Atmospheric Administration

Fann N, Risley D (2013) The public health context for $PM_{2.5}$ and ozone air quality trends. Air Qual Atmos Health 6:1–11

Gao J, Wang T, Zhou X, Wu W, Wang W (2009) Measurement of aerosol number size distributions in the Yangtze River delta in China: formation and growth of particles under polluted conditions. Atmos Environ 43:829–836

Gao J, Chai F, Wang T, Wang W (2011) Particle number size distribution and new particle formation (NPF) in Lanzhou, Western China. Particuology 9:611–618

Gao J, Chai F, Wang T, Wang S, Wang W (2012) Particle number size distribution and new particle formation: new characteristics during the special pollution control period in Beijing. J Environ Sci 24:14–21

Gómez-Moreno FJ, Pujadas M, Plaza J, Rodríguez-Maroto JJ, Martínez-Lozano P, Artiñano B (2011) Influence of seasonal factors on the atmospheric particle number concentration and size distribution in Madrid. Atmos Environ 45:3169–3180

Harris SJ, Maricq MM (2001) Signature size distributions for diesel and gasoline engine exhaust particulate matter. J Aerosol Sci 32:749–764

He M, Sun Y, Li X, Yang Z (2006) Distribution patterns of nitrobenzene's and polychlorinated biphenyls in water, suspended particulate matter and sediment from mid-and down-stream of the Yellow River (China). Chemosphere 65:365–374

Kerminen V-M, Pirjola L, Kulmala M (2001) How significantly does coagulational scavenging limit atmospheric particle production? J Geophys Res. 106:24119-24125

Kim YJ, Kim KW, Kim SD, Lee BK, Han JS (2006) Fine particulate matter characteristics and its impact on visibility impairment at two urban sites in Korea: Seoul and Incheon. Atmos Environ 40:593–605

Kopanakis I, Chatoutsidou SE, Torseth K, Glytsos T, Lazaridis M (2013) Particle number size distribution in the eastern Mediterranean: formation and growth rates of ultrafine airborne atmospheric particles. Atmos Environ 77:790–802

Kulmala M, Toivonen A, Mäkelä JM, Laaksonen A (1998) Analysis of the growth of nucleation mode particles observed in Boreal forest. Tellus B 50:449–462

Kulmala M, Vehkamäki H, Petäjä T, Dal Maso M, Lauri A, Kerminen VM, Birmili W, McMurry PH (2004) Formation and growth rates of ultrafine atmospheric particles: a review of observations. J Aerosol Sci 35:143–176

Kulmala M, Petäjä T, Nieminen T, Sipilä M, Manninen HE, Lehtipalo K, Dal Maso M, Aalto PP, Junninen H, Paasonen P (2012) Measurement of the nucleation of atmospheric aerosol particles. Nat Protoc 7:1651–1667

Leng C, Cheng T, Chen J, Zhang R, Tao J, Huang G, Zha S, Zhang M, Fang W, Li X (2013) Measurements of surface cloud condensation nuclei and aerosol activity in downtown Shanghai. Atmos Environ 69:354–361

Li X, Duan L, Wang S, Duan J, Guo X, Yi H, Hu J, Li C, Hao J (2007) Emission characteristics of particulate matter from rural household biofuel combustion in China. Energy Fuel 21:845–851

Liu S, Hu M, Wu Z, Wehner B, Wiedensohler A, Cheng Y (2008) Aerosol number size distribution and new particle formation at a rural/coastal site in Pearl River Delta (PRD) of China. Atmos Environ 42:6275–6283

Mönkkönen P, Koponen IK, Lehtinen KEJ, Hämeri K, Uma R, Kulmala M (2005) Measurements in a highly polluted Asian mega city: observations of aerosol number size distribution, modal parameters and nucleation events. Atmos Chem Phys 5:57–66

O'Dowd CD, Hämeri K, Mäkelä JM, Pirjola L, Kulmala M, Jennings SG, Berresheim H, Hansson HC, de Leeuw G, Kunz GJ (2002) A dedicated study of New Particle Formation and Fate in the Coastal Environment (PARFORCE): overview of objectives and achievements. J Geophys Res: Atmos (1984–2012) 107: PAR 1.1-PAR 1.16

Ramanathan V, Crutzen P, Kiehl J, Rosenfeld D (2001) Aerosols, climate, and the hydrological cycle. Science 294:2119–2124

Reche C, Querol X, Alastuey A, Viana M, Pey J, Moreno T, Rodríguez S, González Y, Fernández-Camacho R, Sánchez de la Campa AM, De la Rosa J, Dall'Osto M, Prévôt ASH, Hueglin C, Harrison RM,

Quincey P (2011) New considerations for PM, black carbon and particle number concentration for air quality monitoring across different European cities. Atmos Chem Phys 11:6207–6227

Robinson AL, Donahue NM, Shrivastava MK, Weitkamp EA, Sage AM, Grieshop AP, Lane TE, Pierce JR, Pandis SN (2007) Rethinking organic aerosols: semivolatile emissions and photochemical aging. Science 315:1259–1262

Salvador P, Artíñano B, Pio C, Afonso J, Legrand M, Puxbaum H, Hammer S (2010) Evaluation of aerosol sources at European high altitude background sites with trajectory statistical methods. Atmos Environ 44(19):2316–2329

Stanier CO, Khlystov AY, Pandis SN (2004) Ambient aerosol size distributions and number concentrations measured during the Pittsburgh Air quality study (PAQS). Atmos Environ 38:3275–3284

Stieb DM, Judek S, Burnett RT (2002) Meta-analysis of time-series studies of air pollution and mortality: effects of gases and particles and the influence of cause of death, age, and season. J Air Waste Manage Assoc 52:470–484

Stott PA, Tett S, Jones G, Allen M, Mitchell J, Jenkins G (2000) External control of 20th century temperature by natural and anthropogenic forcings. Science 290:2133–2137

Wang T, Poon C, Kwok Y, Li Y (2003) Characterizing the temporal variability and emission patterns of pollution plumes in the Pearl River Delta of China. Atmos Environ 37:3539–3550

Wang T, Wong H, Tang J, Ding A, Wu W, Zhang X (2006) On the origin of surface ozone and reactive nitrogen observed at a remote mountain site in the northeastern Qinghai-Tibetan plateau, Western China. J Geophys Res Atmos 111(D8):D08303. doi:10.1029/2005JD006527

Wang C, Wang W, He S, Du J, Sun Z (2011) Sources and distribution of aliphatic and polycyclic aromatic hydrocarbons in Yellow River Delta Nature Reserve, China. Appl Geochem 26:1330–1336

Wichmann HE, Peters A (2000) Epidemiological evidence of the effects of ultrafine particle exposure. Philosophical transactions of the royal society of London. Ser A: Math Phys Eng Sci 358:2751–2769

Wu Z, Hu M, Liu S, Wehner B, Bauer S, Wiedensohler A, Petäjä T, Dal Maso M, Kulmala M (2007) New particle formation in Beijing, China: statistical analysis of a 1-year data set. J Geophys Res: Atmos (1984–2012) 112: Issue D9, DOI: 10.1029/2006JD007406 DOI: 10.1029%2f2006JD007406%23_blank

Wu Z, Hu M, Lin P, Liu S, Wehner B, Wiedensohler A (2008) Particle number size distribution in the urban atmosphere of Beijing, China. Atmos Environ 42(34):7967–7980

Xu P, Wang W, Yang L, Zhang Q, Gao R, Wang X, Nie W, Gao X (2011) Aerosol size distributions in urban Jinan: seasonal characteristics and variations between weekdays and weekends in a heavily polluted atmosphere. Environ Monit Assess 179:443–456

Yuan Q, Yang L, Dong C, Yan C, Meng C, Sui X, Wang W (2014) Temporal variations, acidity, and transport patterns of $PM_{2.5}$ ionic components at a background site in the Yellow River Delta, China. Air Qual Atmos Health 7:143–153

Yue D, Hu M, Wang Z, Wen M, Guo S, Zhong L, Wiedensohler A, Zhang Y (2013) Comparison of particle number size distributions and new particle formation between the urban and rural sites in the PRD region, China. Atmos Environ 76:181–188

Zhang Q, Streets DG, Carmichael GR, He K, Huo H, Kannari A, Klimont Z, Park I, Reddy S, Fu J (2009) Asian emissions in 2006 for the NASA INTEX-B mission. Atmos Chem Phys 9:5131–5153

Zhu Y, Yang L, Yuan Q, Yan C, Dong C, Meng C, Sui X, Yao L (2014) Airborne particulate polycyclic aromatic hydrocarbon (PAH) pollution in a background site in the North China plain: concentration, size distribution, toxicity and sources. Sci Total Environ 466:357–368

Air Qual Atmos Health (2014) 7:143–153
DOI 10.1007/s11869-014-0236-0

Temporal variations, acidity, and transport patterns of $PM_{2.5}$ ionic components at a background site in the Yellow River Delta, China

Qi Yuan · Lingxiao Yang · Can Dong · Chao Yan · Chuanping Meng · Xiao Sui · Wenxing Wang

Received: 4 November 2013 / Accepted: 6 January 2014 / Published online: 21 January 2014

Abstract To better understand the pollution characteristics and potential sources of $PM_{2.5}$ ionic components at the Yellow River Delta (YRD), a semicontinuous measurement was conducted to observe water-soluble ions in $PM_{2.5}$ at a nature reserve in Dongying of Shandong province, China, in 2011. The results showed that SO_4^{2-}, NO_3^-, and NH_4^+ were the dominant ionic species (constituting 93 % of the total ionic mass) with their annual average concentrations of 22.48, 12.77, and 11.21 μg/m^3, respectively. These three ion concentrations were generally lower than those observed in major cities in China but higher than those in other rural and nature reserve sites. Ion concentrations exhibited large seasonal variations, and maximum values were observed in summer. SO_4^{2-} concentration presented a daytime peak in summer, autumn, and winter, while in spring, a relative flat diurnal cycle was observed. NO_3^- concentration changed with that of SO_4^{2-} during most of measurement period. Transport from surrounding areas contributed to the diurnal cycle of secondary ions. In addition, photochemical reaction and thermodynamic equilibrium played important roles on the diurnal variation of SO_4^{2-} and NO_3^-, respectively. The aerosol at the YRD was weakly acidic, and it was most acidic in winter. A cluster analysis showed that fine particle pollution at the YRD was mainly affected by southwest local emissions and northern middle- to long-distance transport.

Q. Yuan · L. Yang (✉) · C. Dong · C. Yan · C. Meng · X. Sui · W. Wang
Environment Research Institute, Shandong University, Jinan 250100, China
e-mail: yanglingxiao@sdu.edu.cn

L. Yang
School of Environmental Science and Engineering, Shandong University, Jinan 250100, China

W. Wang
Chinese Research Academy of Environmental Sciences, Beijing 100012, China

Keywords Water-soluble ions · High time resolution · Acidity · Transport · Yellow River Delta

Introduction

Atmospheric fine particulate matter ($PM_{2.5}$, with the aerodynamic diameters ≤2.5 μm) is one of the most complex and harmful pollutants in urban atmospheres, and it is the cause of significant public concern (Borja-Aburto et al. 1998; Schwartz et al. 1996). Water-soluble inorganic ions, particularly the secondary ions (e.g., NO_3^-, SO_4^{2-}, and NH_4^+), are the major components of $PM_{2.5}$. They play important roles in reducing atmospheric visibility, altering radiation forcing, changing surface temperatures, and influencing cloud formation and wet deposition (Fu et al. 2008; Jung et al. 2009; Kim et al. 2008; Ocskay et al. 2006). Ionic composition determines the acidity of fine particles, which has potential influences on the ecosystem and environmental materials through deposition (Zhou et al. 2012). Thus, the seasonal and diurnal variations in the water-soluble ion concentrations of $PM_{2.5}$ are important in studying aerosol characteristics.

China is one of the largest coal, iron, and steel producing countries in the world. The consumption of coal and the rapid increase in motor vehicles in recent decades have led to large amounts of SO_2 and NO_x emissions (Zhang et al. 2009). The Bohai Sea rim region generates the largest amount of pollutants, especially for particulate matters in China. However, most previous studies in this area have focused on the aerosol chemical properties of large cities, such as Beijing and Jinan (Gao et al. 2011; Sun et al. 2006; Wang et al. 2006). The Yellow River Delta Nature Reserve is an ecological protection zone near the Bohai Sea and features a unique environment. Because of the restriction of human activity in this reserve, the environment and the ecosystem remain intact. Some industrial cities near the Yellow River Delta (YRD), such as Zibo and

Jinan, have significant local emissions and suffer serious air pollution, which may affect the air quality of the YRD. Because of its geographic positional specificity and environment sensitivity, the YRD Nature Reserve has received a significant amount of attention. Most studies on pollution have focused on the organic contaminants of soil and water, such as PAHs and nitrobenzene (He et al. 2006; Zhang et al. 2011), but rarely on air pollution, especially on chemical composition of $PM_{2.5}$.

The filter-based measurement and online monitor are the two primary methods for measuring chemical particle composition. Traditional filter-based measurement is time-consuming and is unable to provide finer spatial and temporal variations. Online measurement can provide highly time-resolved data for investigating more detailed information, such as temporal variation, process analysis, and source of water-soluble ions (Oms et al. 1996; Stolzenburg and Hering 2000; Trebs et al. 2004). In this study, a semicontinuous ion monitor (URG 9000B) was used for high time-resolution measurement of $PM_{2.5}$ water-soluble ions at a background site in the YRD. This study presents the overall results for $PM_{2.5}$ water-soluble ions, including their seasonal and diurnal variations and the relationships between water-soluble ions and gaseous precursors and meteorological parameters. Additionally, this study investigates the aerosol acidity and source of pollutants using a backward-trajectory cluster analysis.

Experimental

Sampling site

The sampling site was chosen at the YRD Nature Reserve Yi Qian Er Management Station in Dongying, Shandong province (38°03′N, 118°44′E, 5 m a.s.l.). This regional background site is located in the east of North China Plain, 10 km away from the Bohai Sea (Fig. 1) and far away from the major cities in Shandong and Beijing-Tianjin-Hebei region. There are rare coal-fired power plants and industrial activities nearby, and the nearest plant is located in the southwest Dongying district with 58 km away from the sampling site. Measuring instruments including an automatic meteorological station were set up on the fourth floor of the station building, which is 15 m above the ground level. Four series of measurements were collected intensively in 2011, in spring (April 26–May 3), summer (July 8–July 31), autumn (October 16–November 7), and winter (December 30 of 2011 to January 9 of 2012).

Instruments

An ambient ion monitor (AIM, model URG 9000B, URG Corporation) was used to measure hourly concentration of water-soluble ions in $PM_{2.5}$. Some previous research (Gao et al. 2011) has showed excellent correlations (R=0.92–0.97) between AIM and the traditional filter-based measurement for measuring the major water-soluble ions (SO_4^{2-}, NO_3^-, NH_4^+, Cl^-, and K^+). Ambient air samples were drawn into the instrument at a flow rate of 3 L min^{-1}. The particles first entered a denuder that removed acidic and alkaline interfering gases before the particles were collected. An H_2O_2 solution (6 mmol/L) was substituted for the original ultrapure water as the denuder liquid to enhance the absorption of SO_2 and to avoid interference with the SO_4^{2-} measurement from SO_2. The particles were then mixed with supersaturated steam to form water droplets. The droplets passed through a condensing tube, and the condensed solutions were collected into two syringes every hour. The solutions were injected into two ion chromatographs (Dionex, ICs90) to detect the major inorganic ions, which included F^-, Cl^-, NO_2^-, NO_3^-, SO_4^{2-}, Na^+, NH_4^+, K^+, Mg^{2+}, and Ca^{2+}. Multipoint calibration was performed with standard ion solutions ordered from Dionex Corporation. Standard reference materials produced by the National Research Center for Certified Reference Materials (Beijing, China) were analyzed for quality control and assurance purposes.

Other instruments for measuring SO_2 (TEI model 43C), NO_y (TEI model 42CY), and O_3 (TEI model 49C) have been described previously (Gao et al. 2005; Wang et al. 2003). The 43C model is based on the principle that SO_2 molecules absorb ultraviolet (UV) light, become excited at one wavelength, and then decay to a lower energy state, emitting UV light at a different wavelength. NO_y was detected with a modified commercial MoO/chemiluminescence analyzer. Meteorological data (including temperature, relative humidity (RH), wind speed, wind direction, etc.) were obtained from the meteorological station.

In situ acidity

Aerosol acidity plays a particular role in secondary aerosol formation and can promote the formation of secondary inorganic aerosols by catalyzing heterogeneous reactions (Underwood et al. 2001). In this study, we adopted the online version of the aerosol inorganic model (AIM-II) (Clegg et al. 1998) to investigate the acidic characteristics of $PM_{2.5}$ with hourly concentrations of SO_4^{2-}, NO_3^-, and NH_4^+. Hourly measurements of SO_4^{2-}, NO_3^-, NH_4^+, ambient temperature (T), RH, and H^+_{strong} ($H^+_{strong}=2\times[SO_4^{2-}]+[NO_3^-]-[NH_4^+]$) were inputted into the model to obtain the aqueous phase concentrations of free ions including in situ acidity (H^+_{air}), SO_4^{2-}, NO_3^-, NH_4^+, and HSO_4^-, and water content in the aerosol droplets. The pH was predicted by the equation of $pH=-Log[\gamma\times H^+_{air}/(V_{eq}/1000)]$, in which γ and V_{eq} denote the activity coefficient for H^+_{air} and the volume of particle aqueous phase in air (cm^3/m^3).

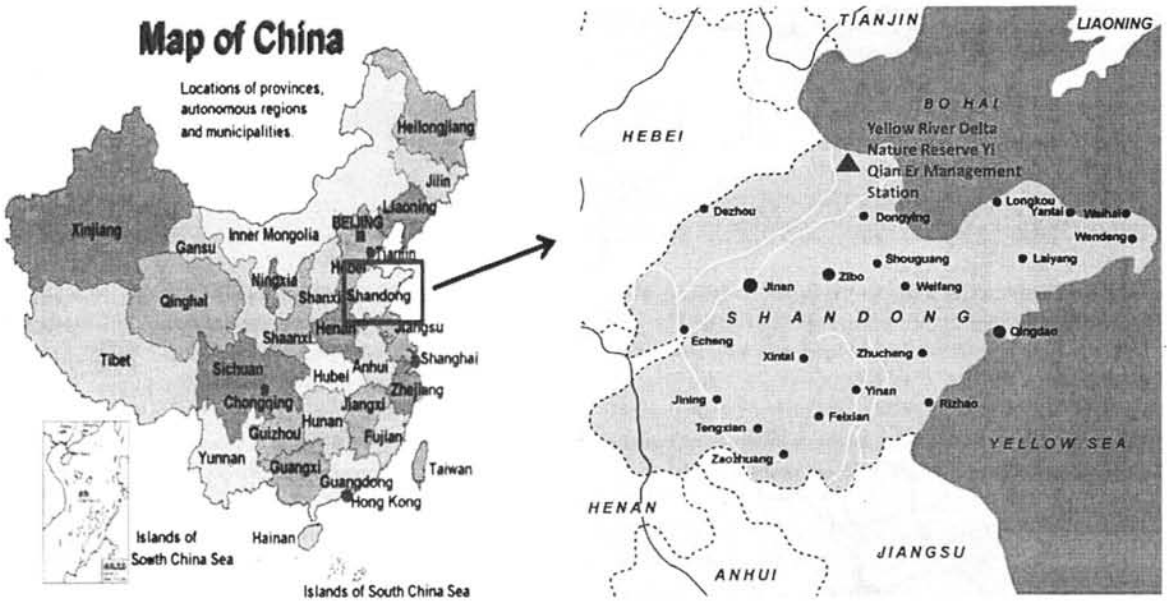

Fig. 1 Location of the sampling site in the Yellow River Delta, Shandong province, China

Backward-trajectory cluster analysis

For a more accurate analysis of the major ion sources, the backward trajectories and cluster analysis were applied. In this study, the backward trajectories were run using the Hybrid Single-Particle Lagrange Integrated Trajectory (HYSPLIT4) model (Draxler and Rolph 2003) that was developed by the National Oceanic and Atmospheric Administration (NOAA). First, 72-h backward trajectories beginning at 50 m above ground level in YRD (38°03′N, 118°44′E) were calculated every 1 h during the sampling period. The trajectories were then clustered according to their similarity in spatial distribution using the HYSPLIT 4 software. The clustering principles and processes are described in the user's guide of the software (Draxler et al. 1999).

Weather conditions

Weather conditions during the sampling period are shown in Table 1. The ambient average annual temperature is 13.0 °C, with the highest monthly average in July at 26.8 °C and the lowest monthly average in January at −1.6 °C. The RH in YRD during the period was somewhat high (at an annual average of 64.4 %), although the largest variations occurred in summer (78.8 %) and lowest in spring (57.7 %). The average annual wind speed was 1.3 m/s, with higher speeds in spring (2.1 m/s) and lower speeds in summer and autumn (0.80 and 0.78 m/s, respectively). The prevailing wind direction in winter was northern, from northwest to northeast; in summer, it was southern and eastern, from southeast to southwest. Dust storm invaded the sampling site on April 30th and May 1st during the spring measurement, when the wind speed increased to 4 m/s.

Results and discussions

Statistics for major water-soluble ions

Concentrations of water-soluble ions over the four seasons are shown in Table 2 and Fig. 2. The annual average TWSI (total water-soluble ions) was 49.72 μg/m^3, with the highest value in summer (59.91 μg/m^3) and the lowest value in spring (24.25 μg/m^3). In autumn and winter, average TWSI concentrations were 58.20 and 38.26 μg/m^3, respectively. SO_4^{2-}, NO_3^-, and NH_4^+ were the dominant ionic species and accounted for approximately 93 % of the total ions. Cl^-, NO_2^-, Na^+, K^+, Mg^{2+}, and Ca^{2+} contributed approximately 7 % of the TWSI on the annual average. The concentration of F^- was always below the limits of detection.

Table 1 Meteorological data from different seasons in the Yellow River Delta during the sampling period

	Temperature (°C)	RH (%)	Wind speed (m/s)
Annual mean	13.0	64.4	1.28
Spring	11.8	57.7	2.11
Summer	26.8	78.8	0.80
Autumn	14.1	68.5	0.78
Winter	−1.6	59.3	0.62

Table 2 Concentrations of water-soluble ions during four seasons in the Yellow River Delta

	Cl^-	NO_2^-	NO_3^-	SO_4^{2-}	Na^+	NH_4^+	K^+	Mg^{2+}	Ca^{2+}	TWSI
Spring	1.12	0.40	7.25	8.19	0.75	5.31	0.63	0.14	0.46	24.25
Summer	0.91	0.23	12.10	30.32	0.57	15.06	0.54	0.09	0.09	59.91
Autumn	1.34	0.34	18.72	23.95	0.71	12.03	0.85	0.13	0.13	58.20
Winter	2.26	0.42	7.28	19.62	0.70	7.13	0.65	0.05	0.05	38.26
Annual mean	1.31	0.33	12.77	22.48	0.66	11.21	0.65	0.10	0.19	49.72

TWSI total water-soluble ions, $\mu g/m^3$

SO_4^{2-} was the most abundant ions, accounting for 50.6 % of the total ion mass. It showed clear seasonal variation with the highest value in summer (30.32 $\mu g/m^3$), lowest concentration in spring (8.19 $\mu g/m^3$). High concentration in summer might be the result of the high RH, abundant photochemical oxidants, and strong solar radiation, while low emissions and good atmospheric diffusion conditions caused low levels in spring. The average NO_3^- concentration in autumn (18.72 $\mu g/m^3$) was much higher than that in the other seasons. The variation of NH_4^+ coincided with that of SO_4^{2-}, indicating that NH_4^+ largely originated from ammonia neutralizing acidic species.

The average concentrations of major ions (NO_3^-, SO_4^{2-}, and NH_4^+) in this research were compared with observations from other world cities (shown in Table 3). Compared with the other cities, these three ion concentrations at YRD were lower than those measured in Jinan, Xi'an, and Raipur, but they were still higher than those in Beijing, Shanghai, and Guangzhou in China and the other major world cities. As a regional background site, the major ion concentrations at YRD were substantially higher than those in other rural sites, indicating serious secondary inorganic aerosol pollution at the YRD. This may be the result of intensive emissions of SO_2, NO_x, NH_3, and particulate matters in the Bohai Sea rim region (Zhang et al. 2009). Effective emission reduction measures are required to address the severe $PM_{2.5}$ pollution in this region.

The mass ratio of NO_3^-/SO_4^{2-} has been used as an indicator to show the relative importance of mobile (e.g., vehicles) versus stationary sources (e.g., power plant) in air pollution (Yao et al. 2002). In this study, the value of NO_3^-/SO_4^{2-} was 0.89 in spring, 0.40 in summer, 0.78 in autumn, and 0.67 in winter, with an annual mean of 0.57. It was substantially higher than 0.44 in Jinan (Gao et al. 2011), 0.46 in Xi'an (Zhang et al. 2011), and 0.41 in Fuzhou (Xu et al. 2012). The high NO_3^-/SO_4^{2-} values were most likely related to less usage of coal because petroleum products and natural gas are the main energy sources in local area, where there are many large oil and gas fields. However, they were significantly lower than that in the NO_3^-/SO_4^{2-} mass ratio of 2 in downtown Los Angeles (Kim et al. 2000), suggesting that stationary source emissions are also very important in the study area. The NO_3^-/SO_4^{2-} exhibited the lowest value in summer, which might hypothetically be the result of higher SO_4^{2-} levels and the evaporative loss of NO_3^- with a higher temperature.

Given that the sampling site is a coastal city, sea salt aerosol is the major source of Cl^- and Na^+. This was verified by the Cl^-/Na^+ molar ratio. The Cl^-/Na^+ ratios were 1.01, 1.06, and

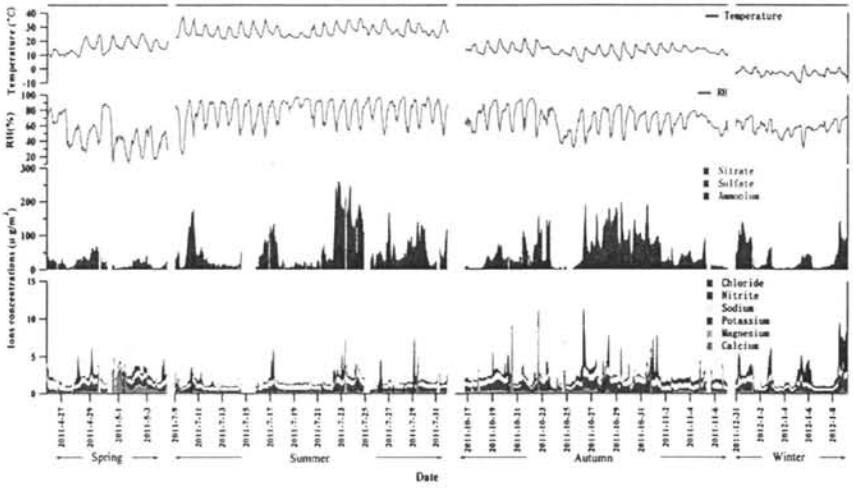

Fig. 2 Temporal variation of SO_4^{2-}, NO_3^-, NH_4^+, and meteorological conditions during the sampling period

Table 3 Mass concentrations of major chemical components in the YRD and other cities in the remainder of the world (μg/m³)

Site	Type	Time	Major ion concentrations (μg/m³)			References
			NO_3^-	SO_4^{2-}	NH_4^+	
Yellow River Delta	Rural/coastal	2011–2012	12.77	22.48	11.21	
Jinan, China	Urban	Dec. 2007–Oct. 2008	15.77	38.33	21.26	(Gao et al. 2011)
Xi'an, China	Urban	Mar. 2006–Mar. 2007	16.4	35.6	11.4	(Zhang et al. 2011)
Guangzhou, China	Urban	Apr. 2007	9.5	21.6	7.3	(Tao et al. 2009)
Beijing, China	Urban	June–August 2011	12.4	9	8	(Sun et al. 2012)
Beijing, China	Urban	June–August 2005	5.5	16.2		(Wu and Wang 2007)
Shanghai, China	Urban	May–June 2005	5.8	23.1		
Qingdao, China	Coastal	1997–2000	3.4	11.94	5.79	(Hu et al. 2002)
Xinken, China	Rural/coastal	Oct.–Nov. 2004	7.2	24.1	9.2	(Hu et al. 2008)
Chongming Island, China	Rural/coastal	Jun. 2006	10.89	23.14	10.28	(Li et al. 2010)
Jianfengling Nature Reserve, China	Rural/coastal	Nov. 2007	0.13	2.17	0.56	
Taibei summer	Urban	Aug. 2003	1.71	3.47	2.04	(Chang et al. 2007)
Taibei winter	Urban	Dec. 2003–Jan. 2004	3.66	12.01	5.67	
Gwangju, Korea	Rural	Oct.–Nov. 2003	2.89	3.86	2.62	(Hong et al. 2008)
Saitama City, Japan	Urban	Jan. 2010	5.67	2.26	2.22	(Kim et al. 2011)
Cario, Egypt	Urban	Nov. 2004–Mar. 2005	6.1	14.2	2.5	(Favez et al. 2008)
Raipur, India	Urban	Apr. 2005–Mar. 2006	8.16	46.5	8.76	(Verma et al. 2010)
Dearborn, USA	Urban	July–Aug. 2007	0.81	3.69		(Pancras et al. 2013)
Brigantine, USA	Rural/coastal	Nov. 2003	1.26	2.27	1.32	(Lee et al. 2008)

1.12 in spring, summer, and autumn, respectively, and 1.96 in winter, while the Cl^-/Na^+ molar ratio is 1.17 in seawater. The ratio was highest in winter, indicating that more part of Cl^- was related to nonmarine sources such as coal-fired emission. Cl^- levels decreased during the summer months as a consequence of its volatilization as HCl during the formation of $NaNO_3$ from gaseous HNO_3 and marine NaCl.

Secondary formation of SO_4^{2-} and NO_3^-

To understand the factor that affected the secondary inorganic aerosol formation, the diurnal variations of sulfate, nitrate, temperature, RH, O_3, SO_2, and NO_y are provided in Fig. 3. The average sulfate oxidation ratio (SOR) and the nitrate oxidation ratio (NOR) were used to reflect the secondary formation of the fine sulfate and nitrate. They are defined as $SOR=[SO_4^{2-}]/([SO_4^{2-}]+[SO_2])$ and $NOR=[NO_3^-]/[NO_y]$, respectively, to indicate the process and extent of the formations from SO_2 to SO_4^{2-} and NO_x to NO_3^- (Wang et al. 2006). Higher SOR and NOR levels suggest that more SO_2 and NO_x are oxidized to sulfates and nitrates.

Overall, SO_4^{2-} exhibited similar diurnal cycle with SO_2, with a broad day maximum in summer, autumn, and winter, while in spring with a little diurnal variation. Because the sampling site is located in the YRD Nature Reserve, it is anticipated that local emissions were at low levels. Thus, just like SO_2, SO_4^{2-} diurnal cycle was possibly affected by the transport from the surrounding areas concentrated with coal-fired power plants to this sampling site. In addition, secondary formation may be another factor in affecting diurnal variation of SO_4^{2-}. In summer, autumn, and winter, SO_4^{2-} concentration began to increase with the rising of sun when SO_2 and O_3 concentrations were rapidly elevated. The enhancing of solar radiation and O_3 concentrations promoted photochemical production of SO_4^{2-}. Generally, sulfates were produced from homogeneous oxidation of SO_2 by OH radicals by following subsequent condensation or from heterogeneous reactions of SO_2 on surfaces of aerosols or droplets (Dlugi et al. 1981; Meng and Seinfeld 1994). Thus, secondary formation of SO_4^{2-} depended on SO_2 concentration, and the SO_2 concentration was 12.1, 7.9, 12.7, and 20.0 ppbv in spring, summer, autumn, and winter. Although SO_4^{2-} concentration in the summer was significantly higher than that in the other seasons, SO_2 concentration was lowest. This could be attributed to the higher conversion rate (SOR=0.65) in summer than that in the other seasons (SOR spring=0.31, autumn=0.50, winter=0.27). High RH, temperature, and photochemical oxidants are conducive to the second generation in summer in YRD. The spring diurnal variation of SO_4^{2-} with small fluctuations also may be related with invasion of dust storm from the northwest of China (Wang et al. 2005).

NO_3^- concentration varied with that of SO_4^{2-} and NO_y during most of measurement period except in summer, suggesting that the transport from source areas may be one reason for NO_3^- diurnal cycle (e.g., the urban cities as Jinan and Zibo).

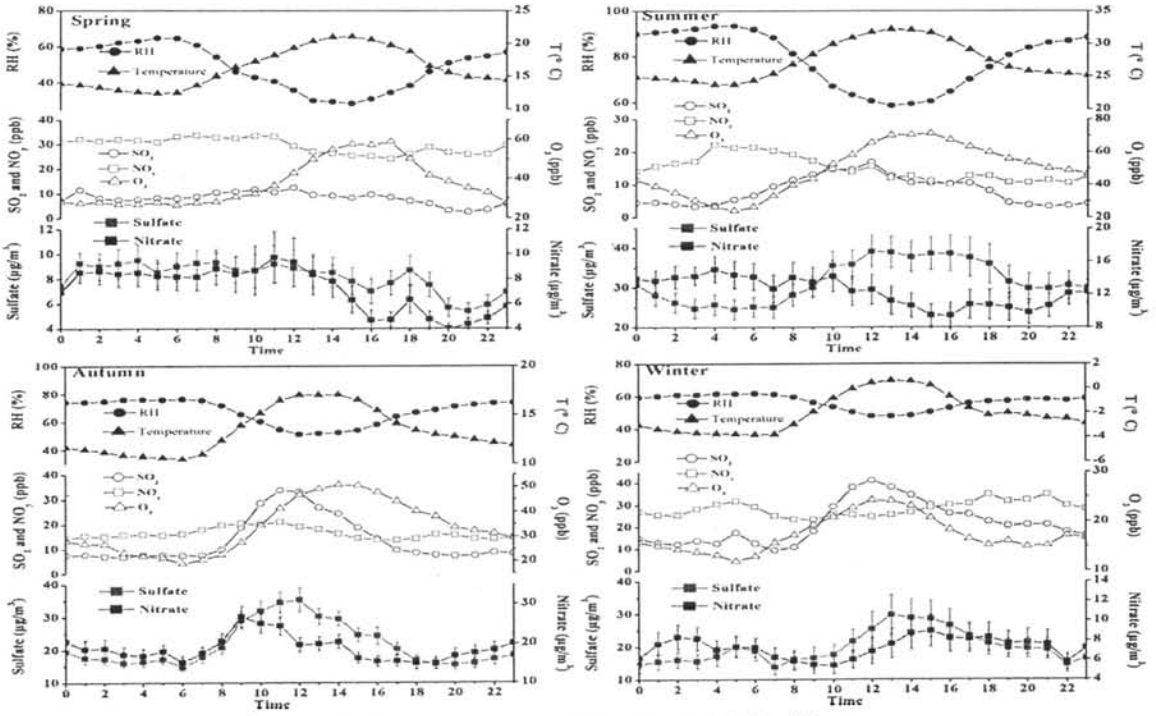

Fig. 3 Diurnal variation of SO_4^{2-} and NO_3^- and related parameters at the Yellow River Delta during different seasons

Besides, in spring, summer, and autumn, NO_3^- showed lowest concentration in the afternoon when the temperature was highest in a day, which was driven by the thermodynamic equilibrium of NO_3^-. It is well known that NH_4NO_3 tends to decompose into gaseous HNO_3 and NH_3 in hot and dry conditions. In winter, due to low temperature, thermodynamic equilibrium had small influence on NO_3^- concentration variation, while NO_3^- was mainly affected by transport in the afternoon and accumulation during the night. Thus, there were two peaks, which appeared in the afternoon and early in the morning. In addition, the nitrate concentrations varied with NO_y during most of measurement period except in spring with high correlation coefficient (average of 0.83 in summer, autumn, and winter, 0.45 in spring), suggesting that the NO_3^- could be mainly formed by the oxidation from NO_x. In our study, NOR values were obviously higher in summer (NOR=0.30) and autumn (NOR=0.29) than those in spring (NOR=0.07) and winter (NOR=0.10). Higher NOR value in summer and autumn led to high concentrations of NO_3^-.

Aerosol acidity

Aerosol acidity is an important parameter for investigating the aerosol phase reactions, acidity-dependent heterogeneous formation of secondary aerosols (Jang et al. 2002; Surratt et al. 2007). The neutralization degree ($F=NH_4^+/(2SO_4^{2-}+NO_3^-)$) was defined as the extent to which acidic aerosol is neutralized. In this study, the samples with F lower than 0.9 and 0.75 are regarded as acidic and more acidic aerosols (Zhou et al. 2012). It is noted that this method was not adapted while mineral ions (e.g., Ca^{2+}, Mg^{2+}, Na^+) contributed to a large proportion of $PM_{2.5}$, and these data were excluded from this analysis. Finally, a total of 1,450 sets of hourly data were used to calculate the neutralization degree, which accounted for approximately 95 % of the total measurements. Figure 4 shows the neutralization degree ($F=NH_4^+/(2SO_4^{2-}+NO_3^-)$). In this study, the aerosol at YRD presented as weakly acidic (annual average F of being 0.89). In spring and summer, acidic aerosols (F<0.9) accounted for 35.4 and 45.6 % of all samples, respectively, and only 11.1 and 8.8 %, respectively, of $PM_{2.5}$ samples presented strongly acidic (F<0.75). In autumn and winter, more than 50 % of $PM_{2.5}$ samples showed acidic (F<0.9), with 22.5 and 32.1 % being strongly acidic (F<0.75). These results indicated higher acidities in autumn and winter than those in spring and summer. Strong acidity (H^+_{strong}) and in situ acidity (H^+_{air}) were further modeled for acidic aerosols with F<1, and a total of 850 sets of hourly data were used to model the aerosol acidity. The pH, strong acidity (H^+_{strong}), in situ acidity (H^+_{air}), and water content of $PM_{2.5}$ obtained from AIM-II model at YRD and the other sites of China are provided in Table 4. The average concentrations of H^+_{strong} and H^+_{air} in winter were 251.24 and 76.03 nmol/m^3,

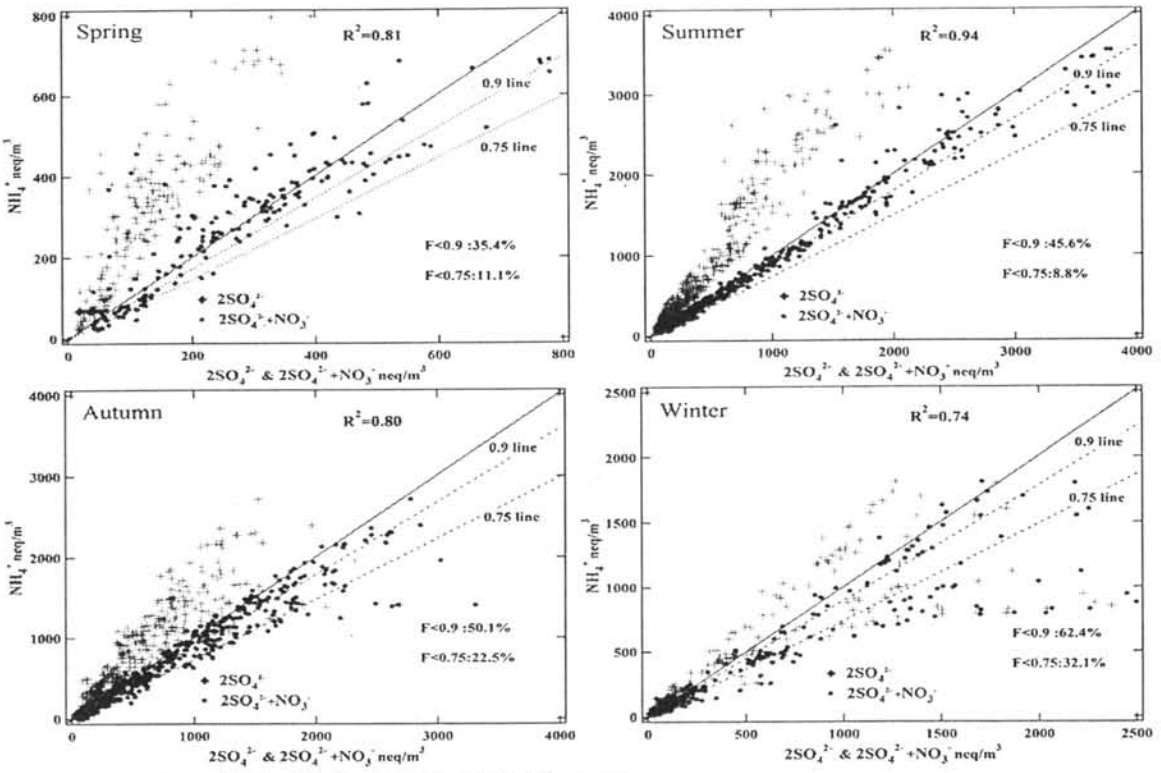

Fig. 4 The extent of neutralization of SO_4^{2-} and NO_3^- by NH_4^+ in $PM_{2.5}$ in different seasons

which were much higher than those in the other seasons. Compared with the other sites in China, the aerosol acidity at YRD was medium level, i.e., lower than that of Mt. Tai, Beijing, and Shanghai and higher than that of Mt. Heng, Lanzhou, and Guangzhou.

In addition, the molar ratio of $[NH_4^+]/[SO_4^{2-}]$ was also used to identify the ammonium sulfate and the reaction between nitrate and ammonia (Pathak et al. 2009). When the ratio is >1.5, the homogenous gas-phase formation of nitrate was significant by forming nitrate or the nitrate–sulfate salts of ammonium. After statistical analysis, the molar ratios of $[NH_4^+]/[SO_4^{2-}]$ in most samples were larger than 1.5 in spring, summer, and autumn, which suggested that NO_3^- was mainly formed by homogeneous reaction between the

Table 4 Aerosol acidity of $PM_{2.5}$ modeled by AIM-II at the YRD and other sites in China

Location	Season	pH	H_{air}^+ (nmol/m³)	H_{strong}^+ (nmol/m³)	Water content (μg/m³)	Reference
Yellow River Delta	Spring	−0.41±1.14	6.60±6.37	60.10±50.72	7.70±8.45	This study
	Summer	1.01±0.87	11.37±11.36	81.48±96.83	91.79±128.92	
	Autumn	0.23±1.15	24.31±49.86	132.93±183.07	48.50±58.88	
	Winter	−0.98±0.60	76.03±149.37	251.24±358.83	24.69±34.39	
	Annual	0.34±1.19	25.55±68.34	125.28±197.14	60.80±95.42	
Mt. Tai	Spring	−0.32±1.38	25.25±32.23	64.82±75.07	47.89±77.14	(Zhou et al. 2012)
Mt. Tai	Summer	−0.04±1.01	35.27±30.38	142.65±115.23	78.57±136.99	
Mt. Heng	Spring	0.64±0.96	13.3±15.4	53.4±38.7	67.7±143.3	(Gao et al. 2012)
Beijing	Summer	–	–	326±421	66±89	(Pathak et al. 2011)
Shanghai	Summer	–	–	196±201	27±24	
Lanzhou	Summer	–	–	59±49	9±12	
Guangzhou	Summer	–	–	90±60	60±80	

"–" indicates no data

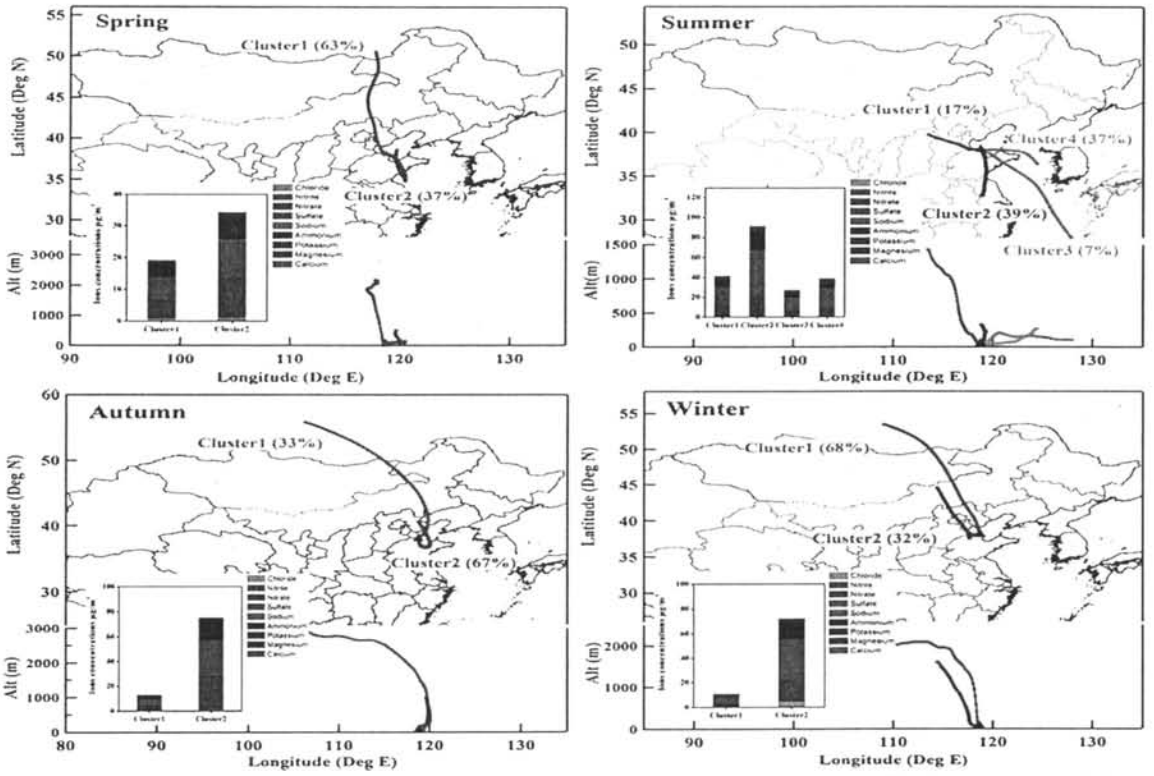

Fig. 5 Three-day backward trajectories of air mass and corresponding ion concentrations of the clusters at the Yellow River Delta during different seasons

ambient ammonia and nitric acid. While about 30 % of samples were ammonium poor in winter with their $[NH_4^+]/[SO_4^{2-}]$ molar ratios of below 1.5. In winter, the concentration of NH_4^+ was 7.13 μg/m^3, which is much lower than that in summer (15.06 μg/m^3). The low level of NH_4^+ was attributed to low emissions of NH_3 (Stelson and Seinfeld 1982), and NH_3 played an important role in the fine aerosol acidity in the Bohai Sea rim region. Therefore, under poor-ammonium conditions,

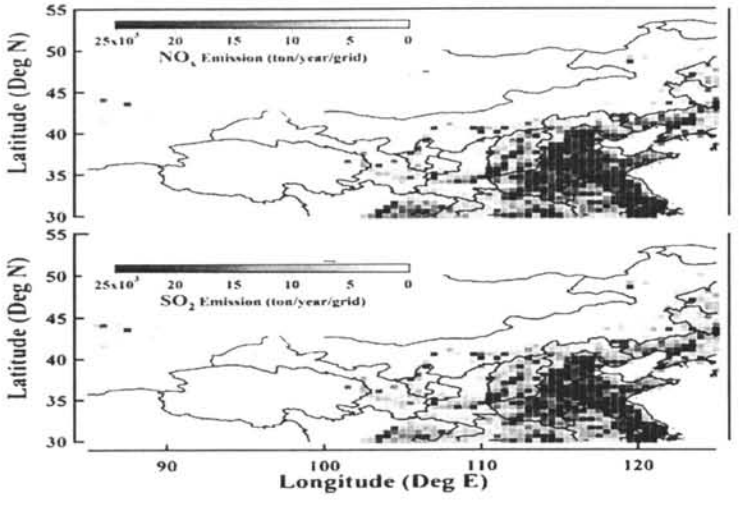

Fig. 6 SO_2 and NO_x emissions in China in 2006 (Zhang et al. 2009)

heterogeneous hydrolysis of N_2O_5 on the moist surface of the preexisting aerosols to form fine nitrate was very possible (Pathak et al. 2009).

Air mass transport

Apart from its secondary formation from gaseous precursors in local area, the concentration of major inorganic ions (SO_4^{2-}, NO_3^-, and NH_4^+) might be significantly influenced by air mass transport. Figure 5 shows the 3-day mean trajectories for clusters and the corresponding mean concentrations of water-soluble ions during the four seasons. SO_2 and NO_x emissions in 2006 (Zhang et al. 2009) are shown in Fig. 6, and different emission intensities are aslo shown along different paths of the clusters. The trajectories in spring, autumn, and winter can be classified into two main categories, while four categories in summer based on their origins, paths, and latitudes. Air masses generally came from the north passing through Inner Mongolia, Hebei, and Beijing at high altitude or from local Shandong and the adjacent areas in low altitude in spring, autumn, and winter. In spring and winter, the northern airflows accounted for 63 and 68 %, respectively, of the total trajectories, and the proportion of northern airflows decreased to 33 % in autumn (cluster 1 in these three seasons), whereas in summer, 39 % of the air masses came from the south, 44 % of the air masses came from the southeast passing the ocean (clusters 3 and 4), and only 17 % came from the northwest passing through Shanxi and Hebei province (cluster 1).

Generally, the air masses from local areas contained the highest concentrations of TWSI with concentrations being 39.22 μg/m^3 in spring (cluster 2), 75.19 μg/m^3 in autumn (cluster 2), and 91.25 μg/m^3 in summer (cluster 2). SO_4^{2-} levels from the southern air masses were highest in summer (47.53 μg/m^3), and NO_3^- of the southern airflows had the highest concentrations in autumn (25.63 μg/m^3). Compared with the southern airflows, the northern airflows had lower ion contributions, with the TWSI concentrations being 19.22 μg/m^3 in spring, 14.30 μg/m^3 in autumn, and 10.52 μg/m^3 in winter.

Local high TWSI concentrations might be related to two main causes: (1) short distance and low altitude and (2) paths through heavily polluted areas (as shown in Fig. 6). These local airflows were short and low, which indicated that it moved more slowly at lower altitude. This caused the air from these paths to more easily carry pollutant emissions from the cities to the atmosphere. In summer and autumn, the low-altitude air mass accounted for 83 and 67 % of all trajectories, respectively, and it might be an important reason for the high concentrations of sulfate and nitrate. Significant amounts of industrial activities and surface primary emission, such as coal combustion and vehicle emission, led to heavy pollution and contributed to elevated concentrations of secondary inorganic aerosol. The southern air mass in summer originated from Jiangsu and moved over Zibo before arriving at YRD. Zibo has a long history of metallurgy and chemical industry, which has led to heavy air pollution. In winter, the path of cluster 2 was also from the north, but it passed over Hebei province before arriving at the YRD. In 2011, Shandong and Hebei had the highest emission intensity of SO_2 and NO_x in China. Thus, a significant amount of pollutants, particularly NO_x, were emitted into the air and brought to the YRD, leading to high ion concentrations. Because of coal-fired heating, chlorine levels significantly increased to 5 μg/m^3 from cluster 2 in winter, which was more than twice the average value in winter and 3~5 times the value in other seasons. The western cluster in the summer passed through several heavily polluted areas, but because of its high height and low frequency of occurrence, the air mass from this direction contributed little to the YRD. Therefore, the focus for emission reduction of the primary pollutant should be in the Bohai Sea rim region.

Conclusions

A total of 1530 h of samples were measured in the four seasons in the YRD at the YRD Nature Reserve. Overall, the annual average TWSI concentration was 49.72 μg/m^3, and SO_4^{2-}, NO_3^-, and NH_4^+ were the dominant ionic species (accounting for approximately 93 % of TWSI). High humidity, O_3 concentrations, and strong solar radiation in summer and autumn, and high emissions of SO_2 and NO_x from coal combustion in winter led to higher ion concentrations in these three seasons compared with spring. These three major ion concentrations at the YRD were lower compared with the cities in China and abroad; however, as a reserve, the YRD showed a high pollution level compared with the rural sites. Stationary source emissions were more important than vehicle emissions in the source areas, as implied by low ratios of NO_3^-/SO_4^{2-}. SO_4^{2-} concentration varied with SO_2 abundance, exhibited a peak near the noon, and it was significantly higher in the summer than that in the other seasons. Photochemical reaction played important roles on the production of SO_4^{2-}. The nitrate concentration changed with that of SO_4^{2-} and NO_y during most of measurement period except in summer, which is attributed to thermodecomposition of NH_4NO_3 under the condition of high temperature. Transport from surrounding areas contributed to the diurnal cycle of secondary ions. The aerosol in autumn and winter presented as more acidic, although the high NO_3^- and low NH_4^+ levels play major roles in affecting aerosol acidity at the YRD in these two seasons. Compared with other sites in China, the aerosol acidity at YRD was medium. A cluster analysis showed that fine particle pollution in the YRD was mainly affected by southwest local emissions and northern middle-long distance transmission. In the summer and autumn, the higher frequency of southern local and low-altitude air masses led to high concentrations of sulfate and nitrate.

Acknowledgments The authors would like to thank Dong Can, Yan Chao, Meng Chuanping, Sui Xiao, and Yu Yangchun for their help in setting up the instruments. The HYSPLIT mode was provided by the NOAA Air Resources Laboratory. This work was supported by the National Basic Research Program (973 Program) of China (2005CB422203), Key Project of Shandong Provincial Environmental Agency (2006045), Promotive Research Fund for Young and Middle-aged Scientists of Shandong Province (BS2010HZ010), Independent Innovation Foundation of Shandong University (2009TS024), National Natural Science Foundation (21307074), and Special Research for Public-Beneficial Environment Protection (201009001-1).

References

Borja-Aburto VH, Castillejos M, Gold DR, Bierzwinski S, Loomis D (1998) Mortality and ambient fine particles in southwest Mexico City, 1993–1995. Environ Health Perspect 106:849–855

Chang SY, Lee CT, Chou CCK, Liu SC, Wen TX (2007) The continuous field measurements of soluble aerosol compositions at the Taipei Aerosol Supersite, Taiwan. Atmos Environ 41:1936–1949

Clegg SL, Brimblecombe P, Wexler AS (1998) Thermodynamic model of the system H+-NH_4^+-SO_4^{2-}–NO_3–H2O at tropospheric temperatures. J Phys Chem A 102:2137–2154

Dlugi R, Jordan S, Lindemann E (1981) The heterogeneous formation of sulfate aerosols in the atmosphere. J Aerosol Sci 12:185–197

Draxler R, Rolph G (2003) HYSPLIT (HYbrid Single-Particle Lagrangian Integrated Trajectory) model access via NOAA ARL READY website (http://www.arl.noaa.gov/ready/hysplit4.html). NOAA Air Resources Laboratory, Silver Spring

Draxler R, Stunder B, Rolph G, Stein A, Taylor A (1999) Hysplit4 User Guide. National Oceanic and Atmospheric Administration Technical Memorandum ERL ARL-230

Favez O, Cachier H, Sciare J, Alfaro SC, El-Araby TM, Harhash MA et al (2008) Seasonality of major aerosol species and their transformations in Cairo megacity. Atmos Environ 42:1503–1516

Fu Q, Zhuang G, Wang J, Xu C, Huang K, Li J et al (2008) Mechanism of formation of the heaviest pollution episode ever recorded in the Yangtze River Delta, China. Atmos Environ 42:2023–2036

Gao J, Wang T, Ding A, Liu C (2005) Observational study of ozone and carbon monoxide at the summit of mount Tai (1534 m asl) in central-eastern China. Atmos Environ 39:4779–4791

Gao X, Yang L, Cheng S, Gao R, Zhou Y, Xue L et al (2011) Semi-continuous measurement of water-soluble ions in $PM_{2.5}$ in Jinan, China: temporal variations and source apportionments. Atmos Environ 45:6048–6056

Gao X, Xue L, Wang X, Wang T, Yuan C, Gao R et al (2012) Aerosol ionic components at Mt. Heng in central southern China: abundances, size distribution, and impacts of long-range transport. Sci Total Environ 433:498–506

He M, Sun Y, Li X, Yang Z (2006) Distribution patterns of nitrobenzenes and polychlorinated biphenyls in water, suspended particulate matter and sediment from mid-and down-stream of the Yellow River (China). Chemosphere 65:365–374

Hong S, Kim D, Ryu S, Kim Y, Lee J (2008) Chemical characteristics of $PM_{2.5}$ ions measured by a semicontinuous measurement system during the fall season at a suburban site, Gwangju, Korea. Atmos Res 89:62–75

Hu M, He LY, Zhang YH, Wang M, Pyo Kim Y, Moon K (2002) Seasonal variation of ionic species in fine particles at Qingdao, China. Atmos Environ 36:5853–5859

Hu M, Wu Z, Slanina J, Lin P, Liu S, Zeng L (2008) Acidic gases, ammonia and water-soluble ions in PM2.5 at a coastal site in the Pearl River Delta, China. Atmos Environ 42:6310–6320

Jang M, Czoschke NM, Lee S, Kamens RM (2002) Heterogeneous atmospheric aerosol production by acid-catalyzed particle-phase reactions. Science 298:814–817

Jung J, Lee H, Kim YJ, Liu X, Zhang Y, Gu J et al (2009) Aerosol chemistry and the effect of aerosol water content on visibility impairment and radiative forcing in Guangzhou during the 2006 Pearl River Delta campaign. J Environ Manage 90:3231–3244

Kim BM, Teffera S, Zeldin MD (2000) Characterization of PM2. 5 and PM10 in the south coast air basin of southern California: Part 1-Spatial variations. J Air Waste Manag Assoc 50:2034–2044

Kim KW, Kim YJ, Bang SY (2008) Summer time haze characteristics of the urban atmosphere of Gwangju and the rural atmosphere of Anmyon, Korea. Environ Monit Assess 141:189–199

Kim KH, Sekiguchi K, Furuuchi M, Sakamoto K (2011) Seasonal variation of carbonaceous and ionic components in ultrafine and fine particles in an urban area of Japan. Atmos Environ 45:1581–1590

Lee T, Yu XY, Kreidenweis SM, Malm WC, Collett JL (2008) Semi-continuous measurement of PM2. 5 ionic composition at several rural locations in the United States. Atmos Environ 42:6655–6669

Li L, Wang W, Feng J, Zhang D, Li H, Gu Z et al (2010) Composition, source, mass closure of $PM_{2.5}$ aerosols for four forests in eastern China. J Environ Sci 22:405–412

Meng Z, Seinfeld JH (1994) On the source of the submicrometer droplet mode of urban and regional aerosols. Aerosol Sci Technol 20:253–265

Ocskay R, Salma I, Wang W, Maenhaut W (2006) Characterization and diurnal variation of size-resolved inorganic water-soluble ions at a rural background site. J Environ Monit 8:300–306

Oms M, Jongejan P, Veltkamp A, Wyers G, Slanina J (1996) Continuous monitoring of atmospheric HCl, HNO2, HNO3 and SO2 by wet-annular denuder air sampling with on-line chromatographic analysis. Int J Environ Anal Chem 62:207–218

Pancras JP, Landis MS, Norris GA, Vedantham R, Dvonch JT (2013) Source apportionment of ambient fine particulate matter in Dearborn, Michigan, using hourly resolved PM chemical composition data. Sci Total Environ 448:2–13

Pathak RK, Wu W, Wang T (2009) Summertime PM 2.5 ionic species in four major cities of China: nitrate formation in an ammonia-deficient atmosphere. Atmos Chem Phys 9:1711–1722

Pathak RK, Wang T, Ho K, Lee S (2011) Characteristics of summertime $PM_{2.5}$ organic and elemental carbon in four major Chinese cities: Implications of high acidity for water-soluble organic carbon (WSOC). Atmos Environ 45:318–325

Schwartz J, Dockery DW, Neas LM (1996) Is daily mortality associated specifically with fine particles? J Air Waste Manage Assoc 46:927–939

Stelson A, Seinfeld J (1982) Relative humidity and temperature dependence of the ammonium nitrate dissociation constant. Atmos Environ 16:983–992, 1967

Stolzenburg MR, Hering SV (2000) Method for the automated measurement of fine particle nitrate in the atmosphere. Environ Sci Technol 34:907–914

Sun Y, Zhuang G, Tang A, Wang Y, An Z (2006) Chemical characteristics of PM2.5 and PM10 in haze-fog episodes in Beijing. Environ Sci Technol 40:3148–3155

Sun Y, Wang Z, Dong H, Yang T, Li J, Pan X et al (2012) Characterization of summer organic and inorganic aerosols in Beijing, China with an Aerosol Chemical Speciation Monitor. Atmos Environ 51:250–259

Surratt JD, Kroll JH, Kleindienst TE, Edney EO, Claeys M, Sorooshian A, Ng NL, Offenberg JH, Lewandowski M, Jaoui M (2007) Evidence for organosulfates in secondary organic aerosol. Environ Sci Technol 41:517–527

Tao J, Ho KF, Chen L, Zhu L, Han J, Xu Z (2009) Effect of chemical composition of PM2.5 on visibility in Guangzhou, China, 2007 spring. Particuology 7:68–75

Trebs I, Meixner F, Slanina J, Otjes R, Jongejan P, Andreae M (2004) Real-time measurements of ammonia, acidic trace gases and water-

soluble inorganic aerosol species at a rural site in the Amazon Basin. Atmos Chem Phys 4:967–987

Underwood G, Song C, Phadnis M, Carmichael G, Grassian V (2001) Heterogeneous reactions of NO2 and HNO3 on oxides and mineral dust: A combined laboratory and modeling study. J Geophys Res 106:18055–18066

Verma SK, Deb MK, Suzuki Y, Tsai YI (2010) Ion chemistry and source identification of coarse and fine aerosols in an urban area of eastern central India. Atmos Res 95:65–76

Wang T, Poon C, Kwok Y, Li Y (2003) Characterizing the temporal variability and emission patterns of pollution plumes in the Pearl River Delta of China. Atmos Environ 37:3539–3550

Wang Y, Zhuang G, Tang A, Yuan H, Sun Y, Chen S, Zheng A (2005) The ion chemistry and the source of $PM_{2.5}$ aerosol in Beijing. Atmos Environ 39:3771–3784

Wang Y, Zhuang G, Zhang X, Huang K, Xu C, Tang A et al (2006) The ion chemistry, seasonal cycle, and sources of $PM_{2.5}$ and TSP aerosol in Shanghai. Atmos Environ 40:2935–2952

Wu WS, Wang T (2007) On the performance of a semi-continuous $PM_{2.5}$ sulphate and nitrate instrument under high loadings of particulate and sulphur dioxide. Atmos Environ 41:5442–5451

Xu L, Chen X, Chen J, Zhang F, He C, Zhao J et al (2012) Seasonal variations and chemical compositions of $PM_{2.5}$ aerosol in the urban area of Fuzhou, China. Atmos Res 104:264–272

Yao X, Chan CK, Fang M, Cadle S, Chan T, Mulawa P et al (2002) The water-soluble ionic composition of PM2.5 in Shanghai and Beijing, China. Atmos Environ 36:4223–4234

Zhang Q, Streets DG, Carmichael GR, He K, Huo H, Kannari A et al (2009) Asian emissions in 2006 for the NASA INTEX-B mission. Atmos Chem Phys 9:5131–5153

Zhang T, Cao J, Tie X, Shen Z, Liu S, Ding H et al (2011) Water-soluble ions in atmospheric aerosols measured in Xi'an, China: Seasonal variations and sources. Atmos Res 102:110–119

Zhou Y, Xue L, Wang T, Gao X, Wang Z, Wang X et al (2012) Characterization of aerosol acidity at a high mountain site in central eastern China. Atmos Environ 51:11–20

学位论文评阅及答辩情况表

论文评阅人	姓名	专业技术职务	是否博导（硕导）	所在单位	总体评价※
	匿名评阅	教授	是		A
	匿名评阅	教授	是		A
	薛丽坤	教授	是	山东大学环境研究院	A

答辩委员会成员	姓名		专业技术职务	是否博导（硕导）	所在单位
	主席	申大忠	教授	博导	山东师范大学
	委员	魏琴	教授	博导	济南大学
		侯万国	教授	博导	山东大学
		张庆竹	教授	博导	山东大学
		胡敬田	教授	博导	山东大学

答辩委员会对论文的总体评价※		答辩秘书	王新锋	答辩日期	2015年5月24日
备注					

※优秀为“A”；良好为“B”；合格为“C”；不合格为“D”。